Universidade de São Paulo

Instituto de Física

"Espectroscopia Nuclear com Íons Leves: aspectos microscópicos e macroscópicos da região de $A \sim 100$"

Thereza Borello-Lewin

Apresentado ao Instituto de Física da Universidade de São Paulo como parte dos requisitos para obtenção do título de Livre Docente.

São Paulo

2001

Resumo

Informações espectroscópicas de estrutura nuclear foram acessadas, na região de $A \sim 100$, por intermédio de reações de transferência de um nêutron (d,p) e (d,t) e espalhamentos inelásticos provocados por dêuterons e/ou partículas alfa. Dados de altíssima qualidade foram obtidos com a utilização principalmente do sistema Pelletron-Espectrógrafo Magnético de São Paulo. A interpretação das intensidades espectroscópicas de partícula e/ou buraco de nêutron experimentais associadas aos vários orbitais do modelo de camadas, salientou nos ^{99,101,103}Ru aspectos microscópicos de estrutura nuclear que demonstraram não ser aparente uma sistemática de preenchimento dos orbitais, revelaram a existência de excitações de $\ell = 3$ (não de valência) a baixa energia de excitação e diagnosticaram coexistência de forma também a baixa energia. Na excitação de estados coletivos por espalhamento inelástico com projéteis isoescalares, o método de análise da interferência coulombiana-nuclear permite, na descrição DWBA-DOMP, quantificar aspectos macroscópicos com a extração simultânea da probabilidade reduzida de transição isoescalar $B(ISL)$ e da razão $B(EL)/B(ISL)$. Nos núcleos de ^{90,92}Zr, ^{94,98}Mo e ^{100,102,104}Ru, a aplicação da metodologia desenvolvida possibilitou o acompanhamento do caráter de isospin, principalmente da primeira excitação quadrupolar. Destaca-se o ^{92}Zr, para o qual a razão dos momentos quadrupolares de nêutrons e prótons obtida ultrapassa em mais do que $\sim 50\%$ o valor N/Z previsto pelo modelo coletivo homogêneo, que é detectado no ^{90}Zr. Muito semelhantes entre si, os dois isótopos ^{94}Mo (isótono do ^{92}Zr) e ^{98}Mo, revelaram também aspectos não homogêneos, embora menos intensos e com predominância da contribuição dos prótons. No ^{100}Ru, isótono do ^{98}Mo, a predominância de prótons é bem mais leve, intensificando-se na seqüência dos isótopos ^{102}Ru e ^{104}Ru.

Abstract

Nuclear structure information for the $A \sim 100$ transition region was extracted from the analysis of (d,p) and (d,t), one neutron transfer reactions and inelastic scattering by deuterons and alpha particles. High quality data were obtained mainly using the Pelletron-Magnetic Spectrograph facility of São Paulo. The measured particle and hole neutron strengths in the nuclei ^{99,101,103}Ru revealed microscopic aspects of nuclear structure associated with the various shell model orbitals. The results showed that all of the spherical valence orbitals are filling regardless of the neutron number, as well as indicating the existence of low energy $\ell = 3$ (non valence) excitations and low energy shape coexistence. The excitation of collective states by inelastic scattering of isoscalar projectiles was analyzed by the Coulomb-nuclear interference method in the DWBA-DOMP description to permit the simultaneous extraction of the isoscalar reduced transition probability $B(ISL)$ and of the ratio $B(EL)/B(ISL)$, thus quantifying macroscopic aspects of nuclear structure. This methodology allowed the assessment of the isospin character, mainly of the first quadrupolar excitations, in ^{90,92}Zr, ^{94,98}Mo and ^{100,102,104}Ru. The extracted ratio of the neutron to proton quadrupole moments for ^{92}Zr exceeds by more than $\sim 50\%$ the predicted value of N/Z even though ^{90}Zr is in good agreement with the N/Z prediction. In contrast, both ^{94}Mo (isotone of ^{92}Zr) and ^{98}Mo demostrate a non homogeneous behavior but with predominance of the protons in their quadrupolar excitations. The predominance of the protons is very slight in ^{100}Ru (isotone of ^{98}Mo) with an enhancement of this tendency for ^{102}Ru – ^{104}Ru.

Índice

Capítulo 1

Introdução

Uma das questões mais instigantes, nos estudos de estrutura nuclear, está relacionada com a compreensão das chamadas regiões de transição de forma com número de massa intermediário. Nessas regiões, prótons e/ou nêutrons não são suficientes em número, com respeito a um *"core"*, para produzir, por exemplo, efeitos coletivos mais facilmente previsíveis, nem são tão poucos para permitir considerações individuais simples. Por outro lado, a adição de um ou poucos pares de núcleons, em particular de nêutrons, é frequentemente responsável por uma apreciável mudança de comportamento [Eb88, Zh95]. Regiões de transição têm sido a arena de interesse na evolução da pesquisa em São Paulo, explorando as potencialidades da Espectroscopia Nuclear com Íons Leves, segundo duas vertentes principais: (i) o exame de reações de transferência, na caracterização experimental de aspectos microscópicos de estrutura nuclear, e (ii) de interferência coulombiana-nuclear (ICN), em espalhamentos inelásticos com projéteis de interação isoescalar, salientando aspectos macroscópicos.

Reações de transferência de um núcleon, *"pick-up"* e *"stripping"*, têm sido tradicionalmente empregadas para salientar aspectos de buraco e partícula únicos nos estados do núcleo residual, na caracterização microscópica destes com respeito a um caroço, neste caso o estado fundamental do núcleo alvo. A informação assim obtida pode e deve, entretanto, ser analisada de uma forma sistemática, observando o comportamento evolutivo em cadeias de isótopos e/ou isótonos, através dos conceitos de ocupação e vacância, que revelam como uma certa região de massa pode ser representada em termos dos núcleons, nos orbitais do modelo de camadas. Os trabalhos associados à pesquisa em Espec-

troscopia Nuclear com Íons Leves demonstram a tradição, em São Paulo, na investigação da estrutura nuclear através de reações de *"pick-up"* (d,t) e *"stripping"* (d,p), em particular na região de transição $A \sim 100$, sempre perseguindo o objetivo de entender a estrutura global que se delineia a partir da análise crítica dos resultados [Du88, Du94, Bo94, Bo97a, Ba97, Bo98, Ba98]. Estados a baixa energia de excitação associados a orbitais não de valência foram detectados [Du88, Du94] e coexistência de forma foi diagnosticada em isótopos de Ru à baixa energia de excitação [Bo98, Ba98].

Especialmente em regiões de transição, não é razoável considerar que, como é feito usualmente, os valores de $B(EL)$ reflitam toda a coletividade que caracteriza a transição entre estados do núcleo, pois, são em princípio relacionados somente à contribuição de prótons. Fica claro que para quantificar as contribuições dos nêutrons, de importância primordial no aspecto coletivo, medidas complementares devem ser obtidas. Foi feito, nos últimos anos, um grande esforço para dominar aspectos teóricos e experimentais relacionados à extração, na excitação de estados coletivos, dos valores das probabilidades reduzidas de transição $B(ISL)$, que fornecem informações referentes à contribuição da massa (prótons + nêutrons) para as transições. O método de análise da ICN em espalhamentos inelásticos, com projéteis isoescalares [Du97], é especialmente vantajoso para esse propósito, pois, permite a extração simultânea de $B(ISL)$ e das razões $B(EL)/B(ISL)$, levando estas ao cancelamento de algumas incertezas sistemáticas associadas à escala da seção de choque absoluta e ao modelo de reação adotado. As publicações, segundo essa vertente, enfocam estudos de ICN com dêuterons e partículas alfa em núcleos par-par, na região de $A \sim 100$ (isótopos de Zr, Mo, Ru) [Du97, Ho89, Go96, Bo97b, Uk97, Uk01].

As características do sistema Pelletron-Espectrógrafo Magnético de Enge, conjuntamente com a técnica de detecção em emulsões nucleares, em particular quando é utilizado o feixe de dêuterons, são em grande parte responsáveis pela qualidade dos dados de São Paulo. Estes, tratados no Laboratório de Emulsões Nucleares e Outras Técnicas, tem merecido o reconhecimento da comunidade científica da área, tanto no seu aspecto precisão (com citações por extenso dos resultados na compilação Nuclear Data Sheets [Si90, Mu90, Bl91, Ba92], que assim costuma destacar os trabalhos mais precisos e completos de cada reação), quanto de inserção na temática da área. Estes trabalhos só puderam

ser realizados porque contei com a colaboração de pesquisadores interessados, originais e lutadores e com o reforço contínuo representado pelos estudantes que se formaram junto ao Grupo de Espectroscopia Nuclear com Íons Leves. A cada um deles o merecido crédito.

A metodologia experimental utilizada é delineada no Capítulo 2. Na resenha que apresento, dois conjuntos de trabalhos que desenvolvi ilustram a evolução dos estudos de espectroscopia nuclear com íons leves, na caracterização microscópica e macroscópica da estrutura nuclear da região de $A \sim 100$, conforme pode ser acompanhado nos Capítulos 3 e 4, respectivamente. Comentários finais e perspectivas são apresentados no Capítulo 5.

Os trabalhos publicados relacionados a esta resenha, e encontrados em anexo, são:

1) Caracterização Microscópica

- *"Level structure of ^{101}Ru from the ^{100}Ru(d,p) reaction"*, J. L. M. Duarte, L. B. Horodynski-Matsushigue, T. Borello-Lewin, and O. Dietzsch, Phys. Rev. C **38** (1988) 664-672. (Anexo 1.1)

- *"Neutron-spectroscopic strength in Ru isotopes"*, J. L. M. Duarte, L. B. Horodynski-Matsushigue, and T. Borello-Lewin, Phys. Rev. C **50** (1994) 666-681. (Anexo 1.2)

- *"Systematics of yrast levels in odd Ru isotopes: Do they point to coexistence at low excitation?"*, T. Borello-Lewin, J. L. M. Duarte, L. B. Horodynski-Matsushigue, and M. D. L. Barbosa, Phys. Rev. C **57** (1998) 967-970. (Anexo 1.3)

- *"Single particle strength in ^{103}Ru with the ^{102}Ru(d,p) reaction"*, M. D. L. Barbosa, T. Borello-Lewin, L. B. Horodynski-Matsushigue, J. L. M. Duarte, G. M. Ukita, and L. C. Gomes, Phys. Rev. C **58** (1998) 2689-2702. (Anexo 1.4)

2) Caracterização Macroscópica

- *"Collective aspects of ^{91}Zr by (d,d') scattering at 17 MeV"*, L. B. Horodynski-Matsushigue, T. Borello-Lewin, and O. Dietzsch, Phys. Rev. C **33** (1986) 1594-1605. (Anexo 2.1)

- *"Coulomb-Nuclear Interference in Inelastic Scattering of 21 MeV Alpha-Particles on $^{90,92}Zr$"*, L. B. Horodynski-Matsushigue, T. Borello-Lewin, and J. L. M. Duarte, in *Proceedings of the International Nuclear Physics Conference - IUPAP* (São Paulo, Brazil). Contributed Papers, Vol. **1** (1989) 307. (Anexo 2.2)

- *"Coulomb-nuclear interference with α particles in the excitation of the 2_1^+ states in $^{100,102,104}Ru$"*, L. C. Gomes, L. B. Horodynski-Matsushigue, T. Borello-Lewin, J. L. M. Duarte, J. Hirata, S. Salém Vasconcelos, and O. Dietzsch, Phys. Rev. C **54** (1996) 2296-2303. (Anexo 2.3)

- *"Inelastic deuteron scattering in the Coulomb nuclear interference region: Procedures for estimating the precision of the extracted $B(E2)$ and $B(IS2)$ values"*, J. L. M. Duarte, G. M. Ukita, T. Borello-Lewin, L. B. Horodynski-Matsushigue, and L. C. Gomes, Phys. Rev. C **56** (1997) 1855-1865. (Anexo 2.4)

- *"5^- excitations in the $40 \leq Z \leq 50$ region"*, L. B. Horodynski-Matsushigue, G. M. Ukita, T. Borello-Lewin, and J. L. M. Duarte, Phys. Rev. C **60** (1999) 047301, 1-4. (Anexo 2.5)

- *"Coulomb-nuclear interference with deuterons: Isospin character of the 2_1^+ and 3_1^- excitations in $^{94,98}Mo$"*, G. M. Ukita, T. Borello-Lewin, L. B. Horodynski-Matsushigue, J. L. M. Duarte, and L. C. Gomes, Phys. Rev. C **64** (2001) 014316, 1-10. (Anexo 2.6)

Capítulo 2

Metodologia Experimental

O estudo experimental da estrutura de núcleos através de reações de transferência é feito com o objetivo de detectar estados fracamente excitados, com ótima resolução em energia, visando obter informações sobre o fracionamento de configurações simples diluídas em estados mais complicados. Aspectos coletivos do núcleo são, por outro lado, analisados por intermédio de espalhamento inelástico, incluindo o exame da Interferência Coulombiana-Nuclear (ICN). Nesse caso, também é importante a obtenção de ótima resolução em energia, não apenas para separar picos associados a estados nucleares de energias próximas, mas também, para salientar esses picos em relação ao fundo proveniente da cauda do pico elástico. Em vista dos objetivos postos, a opção por reações induzidas por íons leves se fundamenta em dois aspectos: (i) as informações de estrutura nuclear extraídas são quantitativas e mais confiáveis, pois tais reações têm mecanismos de reação melhor conhecidos e (ii) a resolução obtida experimentalmente é melhor, em cerca de uma ordem de grandeza, do que a típica para reações com íons pesados.

A boa resolução em energia que a metodologia empregada permite alcançar é essencial ao êxito do estudo. A utilização experiente do Espectrógrafo Enge, do tipo polo partido, proporciona condições de competir com vantagem a nível mundial. O quadro se complementa pelas características de energia do feixe fornecido pelo acelerador Pelletron, de excelente perfil, e com cuidados adicionais de focalização do feixe, além da utilização de alvos de qualidade. As partículas carregadas emergentes da reação, associadas a cada ângulo de espalhamento admitidas no espectrógrafo, são analisadas pelo campo do ímã e

detectadas no plano focal em emulsões nucleares ou detetores sensíveis à posição de barreira de superfície.

2.1 Espectrógrafo Magnético

O espectrógrafo magnético Enge, de polo partido, de São Paulo é constituído por dois dipolos e tem características excelentes discutidas no artigo de J. E. Spencer e H. A. Enge [Sp67]. Os efeitos de borda do campo permitem que íons associados à mesma razão p/q (módulo do momento sobre a carga) convirjam para uma mesma região na câmara de detecção, mesmo que os momentos não sejam paralelos, possibilitando focalização bidirecional (horizontal e vertical) e escolha, para detecção, da posição de melhor foco, levando em conta efeitos do alargamento cinemático da reação em exame. É amplo o espectro das energias, para um mesmo íon, que podem ser analisadas simultaneamente; a limitação geométrica proveniente dos raios de curvatura efetivos máximo e mínimo das trajetórias corresponde à uma razão E_{max}/E_{min} de $\sim 7,3$. O valor máximo de campo é de 17 KG e o maior ângulo sólido de admitância, que tem sido utilizado com boa compensação, é de 2,68 msr.

Dispersão, magnificação e poder de resolução são propriedades importantes dos ímãs analisadores e serão quantificados para o ímã de São Paulo [Sp67, Cr78]. O valor da dispersão, próximo de 1,9, informa o deslocamento da imagem em função da variação da curvatura efetiva da trajetória do íon, devido à variação do momento. Os valores para as magnificações vertical e horizontal são 2,7 e 0,34, respectivamente, e referem-se à dimensão da imagem em relação à dimensão do objeto. O poder de resolução permite distinguir, para mesma carga, diferentes momentos correspondendo ao valor $E/\Delta E$ aproximadamente 2750.

A calibração do espectrógrafo foi obtida através de uma ampla análise de raios de curvatura efetivos, utilizando principalmente a reação ^{90}Zr(α,α') e o exame de estados do ^{90}Zr, núcleo detalhadamente estudado até 5,9 MeV de excitação [Ho87]. A investigação das superfícies focais associadas a uma larga gama de alargamentos cinemáticos foi essencial para permitir exposições seguras de placas de emulsão nuclear, com as quais não é possível o controle

da qualidade dos dados durante a aquisição, e medir espectros de altíssima qualidade com resoluções de 0,5 – 0,6 mm (largura à meia altura).

2.2 Emulsões Nucleares

A detecção através de emulsões nucleares aproveita ao máximo as características do espectrógrafo e garante a redução drástica do fundo associado ao feixe de íons leves. Por outro lado, apresenta algumas desvantagens como: o não controle da qualidade dos dados durante a aquisição e a demora na obtenção definitiva desses dados. Detetores de silício, conhecidos como detetores de "estado sólido", têm resolução em posição normalmente pior, são fornecidos em tamanhos que não ultrapassam uma dezena de cm, são sujeitos a deterioração por bombardeio de nêutrons e são extremamente dispendiosos. Em vista destas características, poucos laboratórios [Ro84] os utilizam atualmente, em trabalho rotineiro. Detetores a gás têm sido desenvolvidos em vários laboratórios [Ma75b, St75, Op78, Ko83, He87, Cu85, Ch83, Fa85], sendo a leitura de posição feita basicamente por três métodos diferentes: fio resistivo, linha de atraso capacitivo-indutiva e multifios posicionadores. A dificuldade na utilização de detetores a gás com íons leves vem de dois fatos: (i) sendo estas partículas pouco ionizantes deixam pouca carga na região do detetor de posição, levando a sinais baixos, facilmente confundíveis com o *"background"*; e (ii) os feixes de íons leves, em particular os de dêuterons e de prótons, especialmente interessantes do ponto de vista de estudos de estrutura nuclear, vêm acompanhados de alta produção de nêutrons, raios γ e X, o que, associado à grande quantidade do material presente no ímã e mesmo nas paredes do detetor, leva a um *"background"* importante de pulsos baixos no detetor. A imposição de correlação entre os vários parâmetros que podem ser medidos em alguns detetores (ΔE, E, posição, ângulo de entrada e até tempo de vôo) tem sido essencial [Op78, Ma75b] na utilização dos mesmos nestas condições. A complexidade envolvida na utilização dos detetores a gás e a necessidade de resolução máxima em energia têm, na verdade, feito com que também em alguns outros laboratórios se voltasse a utilizar emulsões nucleares na detecção de íons leves nos planos focais de espectrógrafos [Mu88, Cl80, Bu87, Bu90, Wa92, Ga92, Ch92, Ro92],

especialmente quando são de média dispersão, como é o do tipo Enge de polo partido da Universidade de São Paulo.

Emulsões nucleares são essenciais quando, além da alta resolução, a estabilidade da calibração em posição é importante. A emulsão é então usada como indicador de posição dos grupos de íons ao longo do plano focal. A camada de emulsão, normalmente com $\sim$ 50 μm de espessura, é usada sobre placas de vidro para definir sua estabilidade mecânica. É interessante lembrar que duas placas de emulsão, que têm sido utilizadas lado a lado, cobrem 50 cm ao longo da superfície focal e permitem medidas de três espectros. São também utilizados absorvedores, em geral de alumínio, para cobrir as emulsões com duas finalidades: (i) ajustar a energia do íon que chega na emulsão para ter a melhor qualidade dos traços e (ii) absorver se possível produtos de reações que não são de interesse. O elemento detetor em emulsões nucleares é um pequeno cristal de brometo de prata (grão). Nas emulsões utilizadas, os grãos têm cerca de 0,25 μm de diâmetro e estão dispersos de forma aleatória em gelatina, com um espaçamento médio de diversas vezes o seu diâmetro. Uma partícula nuclear que penetra na emulsão atravessa vários grãos. A teoria do processo é complexa. Os cristais de brometo de prata atingidos constituem-se em centros que são catalizadores da redução de íons de prata em prata metálica. A imagem latente consiste de alguns até algumas centenas de átomos de prata, concentrados em posições especiais do cristal denominadas posições sensíveis. A energia perdida pela radiação ionizante promove, por exemplo, a passagem de elétrons ligados a íons de bromo à banda de condução do brometo de prata. Esses elétrons movem-se livremente até encontrarem impurezas no cristal, sendo então capturados. O campo elétrico criado atrai íons de prata da vizinhança, dando origem aos aglomerados. No processo de revelação, somente os cristais atingidos transformam-se em aglomerados de prata metálica e que, no conjunto, formam um traço de grãos de prata ao longo da trajetória da partícula [Ba73, Er79].

As emulsões nucleares expostas, após reveladas no Laboratório de Emulsões Nucleares e Outras Técnicas, são examinadas ao microscópio e o número de traços produzidos pelas partículas ionizantes é registrado em função da posição ao longo do plano focal (espectro). A contagem dos traços é feita com um aumento em geral de 500 vezes, em retângulos de 0,19 $\times$ 10 mm^2, em função

da distância medida ao longo da emulsão, em passos de 0,20 mm. Essas condições foram estabelecidas levando em conta a dimensão do objeto para o espectrógrafo, normalmente 3 mm de altura e 1 mm de largura e as características do espectrógrafo, em particular as magnificações vertical e horizontal. Os trabalhos de leitura das emulsões e digitação destes dados são feitos por técnica-microscopista, treinada para este fim. Critérios bem definidos na identificação e contagem dos traços, principalmente em regiões com alta densidade de traços, desenvolvidos em São Paulo, incrementaram a precisão nos espectros obtidos com as características inerentes à detecção em plano focal de espectrógrafo magnético. No esforço para aumentar a velocidade de obtenção dos espectros, dois projetos estão sendo desenvolvidos. Um deles trata da transferência automática dos dados lidos ao microscópio para um microcomputador dedicado e está atualmente em fase de montagem da interface. O outro projeto refere-se à própria leitura automática das emulsões em microscópio. Pretende-se, desta forma, ter inicialmente uma leitura de todo o espectro, embora nas regiões deste com picos muito intensos ou com outras características críticas, para a precisão pretendida a leitura manual (humana) ainda seja indispensável. São parte deste projeto: (a) adaptar ao microscópio uma câmera digitalizadora de imagem; (b) desenvolver o algoritmo de processamento de imagens para identificar a trajetória tridimensional de uma partícula ionizante - pelo menos dois planos da emulsão devem ter sua imagem tratada: o de entrada e o de saída da partícula; (c) adaptar um sistema de motores de passo, comandados por microcomputador, para movimentar a platina do microscópio nas direções X e Y (plano da platina) e o prato na direção Z; e (d) construir uma interface de comunicação entre o sistema mecânico e o microcomputador.

2.3 Preparação do Feixe e do Alvo

Para um adequado aproveitamento das potencialidades do espectrógrafo, não deve ser esquecida também a importância da fabricação de alvos de boa qualidade: uniformes e limpos. Evita-se a possível deterioração da resolução e a perda de largos trechos nos espectros medidos, perdas essas provenientes de reações com contaminantes, cujas condições de foco são muito distantes das da

reação em exame. As condições extremamente restritivas impostas às características dos alvos levaram ao desenvolvimento, com sucesso, de metodologia especial para fabricação de filmes finos auto-sustentados ou não, a partir da evaporação por bombardeamento eletrônico de materiais de altas temperaturas de evaporação a baixas pressões [Pu91]. Foram também fabricados alvos em que o material isotopicamente enriquecido é depositado sobre o substrato, apenas em região retangular centrada, que permitem eliminar as fendas de definição, reduzindo o fundo nos espectros.

Outro ponto que merece destaque diz respeito à qualidade do feixe de íons que, em especial, em estudos de espalhamentos inelásticos em ângulos dianteiros, tem papel preponderante na qualidade dos espectros. Assim, a dificuldade experimental em medidas de interferência coulombiana-nuclear com dêuterons advém do fato do padrão de interferência situar-se numa faixa angular nas distribuições angulares, em que os espectros correspondentes, obtidos da maneira usual, sem cuidados adicionais, são obscurecidos pela cauda do pico elástico. Esses cuidados estão atualmente controlados e referem-se principalmente ao adequado transporte do feixe ao longo do acelerador e, em especial, na linha do espectrógrafo e a definição das dimensões do objeto para o ímã. Razões entre as intensidades de corrente de fendas e de feixe de 1:30 e 1:100 são recomendadas, respectivamente, para as fendas de definição antes do alvo (em geral, 1,0 $\times$ 3,0 mm^2) e na fenda circular de $\sim$ 6 mm (corta-halo) situada a aproximadamente 1,5 m do centro da câmara de espalhamento.

Capítulo 3

Aspectos Microscópicos

Os padrões das distribuições das intensidades espectroscópicas de partícula e buraco, ao longo de cadeias de isótopos e isótonos, são ferramentas potentes para evidenciar transições de estrutura nuclear [Sa83, Bo75]. No modelo de camadas esférico, a configuração de uma partícula independente ou de um buraco independente está concentrada em uma única energia de excitação, correlações tendem a diluirem essa feição. Mudanças abruptas nas distribuições espectroscópicas de partícula e buraco são indicadores seguros de transições repentinas.

Reações de transferência de um núcleon são reconhecidamente importantes como pontas de prova espectroscópicas no confronto entre informações experimentais e o modelamento teórico que contenha ingredientes microscópicos. Também o modelo de bósons interatuantes (bosônico), na descrição, por exemplo, de núcleos de número de massa ímpar ou ímpar-ímpar, são severamente testados nesse confronto.

A informação detalhada da intensidade de partícula e buraco de nêutron associada aos vários orbitais do modelo de camadas, medida em São Paulo através de reações (d,p) e (d,t), em vários isótopos de Rutênio ao redor de $A \sim 100$, foi extraída da comparação das distribuições angulares experimentais com previsões de cálculos DWBA, utilizando potenciais ópticos globais, amplamente testados. Essa informação revelou, entre outros aspectos, que não é aparente uma sistemática de preenchimento dos orbitais de valência, independentemente do número de nêutrons, evidenciou a população intensa de excitações de $\ell = 3$ (não de valência) a baixa energia nos ^{101,103}Ru e indicou intensidades de

partícula e buraco no ^{103}Ru significativamente reduzidas em comparação com as do ^{101}Ru, apontando nesse núcleo uma possível coexistência a baixa energia de excitação.

O estudo apontou que o estado fundamental do ^{103}Ru é populado fracamente em ambas as reações de transferência, em desacordo com resultado anteriormente divulgado, e ensejou investigação dos núcleos de massa ímpar da região, evidenciando que na maioria destes existem, a energias de excitação muito baixas, estados $\frac{3}{2}^+$ associados a fatores espectroscópicos de uma partícula pequenos, que podem representar o estado mais baixo da configuração coexistente diagnosticada.

3.1 Procedimento Experimental e Análise

Dêuterons do acelerador Pelletron de São Paulo, com energias incidentes de 12,0 MeV, 15,0 MeV, 15,5 MeV e 16,0 MeV foram focalizados em alvos de Ru, uniformes e isotopicamente enriquecidos, provocando as reações ^{100}Ru(d,p) [Du88], ^{102}Ru(d,p) [Ba98, Bo98], ^{100}Ru(d,t) [Du94] e ^{102,104}Ru(d,t) [Du94], respectivamente. Os ejéteis foram analisados em momento pelo campo do espectrógrafo Enge de São Paulo e detectados em emulsões nucleares (Kodak NTA ou NTB e Fuji G6B, de 50 μm de espessura). Conforme discutido detalhadamente no capítulo anterior, cuidados especiais na preparação do feixe e aquisição de dados, revelação e leitura das emulsões resultaram em espectros com resoluções em energia de 6 a 8 keV nas reações (d,t) e de $\sim$ 10 keV nas reações (d,p), de excelente qualidade. Espectros típicos são mostrados nos artigos [Du88, Du94, Ba98, Bo98].

A normalização relativa dos espectros associados a cada ângulo de espalhamento, foi obtida através da integração da corrente do feixe medida em um copo de Faraday com supressões elétrica e geométrica. Para a normalização absoluta das seções de choque foram consideradas previsões do modelo óptico e realizadas medidas de espalhamento elástico no mesmo alvo e sob as mesmas condições. Para quantificar a incerteza na escala das seções de choque absolutas, previsões do modelo óptico foram calculadas com os parâmetros bem estabelecidos de três famílias de potenciais ópticos: das sistemáticas de Perey e

Perey [Pe74], Lohr e Haeberli [Lo74] e Daenick [Da80]. Na seqüência temporal dos trabalhos, medidas mais detalhadas das distribuições elásticas permitiram uma redução da incerteza na escala associada à seção de choque absoluta de praticamente um fator dois, chegando a 8% no artigo mais recente [Ba98].

Reações (d,p) e (d,t), em que a energia do dêuteron é da ordem de uma dezena de MeV são diretas, isto é, ocorrem em uma única etapa, sem estados intermediários. Consequentemente, as seções de choque experimentais fornecem relações simples entre estados nucleares inicial e final. Processos diretos acontecem na superfície dos núcleos e favorecem a transferência de pequenas quantidades de energia devido ao tempo curto de reação, da ordem do tempo que o projétil leva para passar pelo núcleo alvo. A análise e a interpretação dos dados experimentais é essencialmente feita na aproximação de Born com ondas distorcidas (DWBA). Na DWBA, a premissa é que o processo mais importante, quando um par de núcleos colidem, é o espalhamento elástico. Os demais processos são tratados por teoria de perturbação [Sa83]. Os pares colidente e emergente são representados pelas ondas distorcidas incidentes e emergentes geradas pelos respectivos potenciais ópticos. Nessa aproximação, os estados do núcleo residual são descritos como a superposição dos estados do caroço-alvo acoplados a uma partícula (*"stripping"*) ou a um buraco (*"pick-up"*) no orbital $(n\ell j)$ do modelo de camadas. Se o núcleo alvo é par-par, não são permitidas misturas de (ℓ, j) na população de estados do núcleo residual e os formatos das distribuições angulares experimentais são características do momento angular orbital transferido.

De maneira geral, a amplitude de transição T para a reação $A(a,b)B$ é:

$$T = J \iint \chi^{-}(\vec{k}_b, \vec{r}_b)^* < bB \mid V \mid aA > \chi^{+}(\vec{k}_a, \vec{r}_a)\, d\vec{r}_a\, d\vec{r}_b \ , \qquad (3.1)$$

onde $\chi(\vec{k}, \vec{r})$ são as ondas distorcidas, $\vec{r}_a$ e $\vec{r}_b$ são as coordenadas relativas dos sistemas (a, A) e (b, B), com $\vec{k}_a$ e $\vec{k}_b$ são os momentos relativos, J é o jacobiano da transformação para as coordenadas $\vec{r}_a$ e $\vec{r}_b$.

O elemento de matriz $< bB \mid V \mid aA >$ contém toda a informação de estrutura nuclear e as ondas distorcidas têm a forma assintótica de uma onda plana com momento $\vec{k}$ mais uma onda esférica emergente, ou incidente, isto é:

$$\chi^{(\pm)}(\vec{k}, \vec{r}) \rightarrow e^{i\vec{k}.\vec{r}} + f(\theta)\frac{e^{\pm ikr}}{r} \ . \qquad (3.2)$$

Quando a reação de *"stripping"* está sendo tratada, $a = b+x$ e $B = A+x$ e resulta o seguinte elemento de matriz:

$$< J_B M_B s_b m_b \mid V \mid J_A M_A s_a m_a > = \sum_{j\ell} \sqrt{S_{j\ell}}\, R_{j\ell}(r_{xA})(\ell s m\mu - m \mid j\mu)(s_b s m_b m_a - m_b \mid s_a m_a) (J_A j M_A M_B - M_A \mid J_B M_B)\, D(r_{xb})\, Y_\ell^m(\hat{r}_{xa}) \ , \tag{3.3}$$

sendo $\sqrt{S_{j\ell}}$ a amplitude espectroscópica, $R_{j\ell}(r_{xA})$ a função de onda radial da partícula transferida x para o alvo B, $(\ell s m_\ell m_s | jm)$ os coeficientes de Clebsch-Gordan [Ed57], e $D(r_{xb})$ o produto da função de onda interna do projétil com o potencial de interação entre x e b.

As seções de choque previstas na aproximação DWBA para a transferência de momentos angulares associados a j e ℓ, partindo de alvos par-par, são expressas por:

- Reação (d,p):

$$\sigma_{exp}(\theta) \ = \ 1,55\, S_{\ell j}\, \sigma_{\ell j}^{DW}(\theta) \tag{3.4}$$

onde

$\sigma_{\ell j}^{DW}(\theta)$ é a seção de choque reduzida, calculada na aproximação DWBA;

$S_{\ell j}$ é o fator espectroscópico e tem valor máximo 1; e

1,55 é o fator quando a função de onda de Hulthén para o dêuteron (com dependência radial da forma $(e^{-\alpha r} - e^{-\beta r})/r$) é utilizada.

- Reação (d,t):

$$\sigma_{exp}(\theta) \ = \ 3,33\, C^2\, S_{\ell j}\, \frac{\sigma_{\ell j}^{DW}(\theta)}{(2j+1)} \tag{3.5}$$

onde

$\sigma_{\ell j}^{DW}(\theta)$ é a seção de choque reduzida, calculada na aproximação DWBA;

$C^2\, S_{\ell j}$ é a intensidade espectroscópica e pode ter valor máximo $(2j+1)$;

e

3,33 é o fator quando a função de onda de Irwing-Gunn é utilizada para o tríton e de Hulthén para o dêuteron [Ba66].

Através da comparação entre as seções de choque experimentais absolutas e as previstas, associadas ao ℓ atribuído para cada transição, extraem-se as intensidades espectroscópicas correspondentes.

Os potenciais de Perey e Perey [Pe74] com um termo de spin-órbita sugerido por Lohr e Haeberli [Lo74] foram utilizados para gerar ondas distorcidas incidentes e, nos canais emergentes de próton e de tríton, foram usado os parâmetros de Becchetti e Greenlees [Be69a].

A forma padrão do potencial óptico é:

$$V_{opt} = \vee_C + \vec{\sigma}.\vec{L} \vee_{SO} \tag{3.6}$$

com

$$\vee_C \equiv V_{Coul} - V\, f(x_0) - i\left[W\, f(x_w) - 4\, W_D \frac{d}{dx_D} f(x_D)\right] \tag{3.7}$$

e

$$\vee_{SO} = \left(\frac{\hbar}{m_\pi c}\right)^2 V_{SO} \frac{1}{r} \frac{d}{dr} f(x_{SO}) \tag{3.8}$$

onde V_{Coul} é o potencial coulombiano e $f(x)$ é a função de Woods-Saxon.

Para descrever o potencial do nêutron capturado ou arrancado, foram utilizados os parâmetros geométricos do potencial de Becchetti e Greenlees para o próton [Be69a], com forma de Woods-Saxon mais um termo de spin-órbita. Os cálculos foram realizados com o programa DWUCK4 [Ku74], com a utilização de parâmetros usuais para simular o alcance finito da interação e a não localidade dos potenciais. Com exceção das órbitas $1g_{9/2}$, $3p$ e $2f$, os orbitais considerados foram os da camada $50 - 82$.

A utilização de diferentes conjuntos de parâmetros ópticos globais, embora os cálculos reproduzam os formatos das distribuições angulares para cada ℓ, permitem variações máximas de $\pm$ 15% nas seções de choque previstas, resultando em variações correspondentes das intensidades espectroscópicas.

3.2 Resultados

Os resultados serão comentados de forma global, partindo do ^{99}Ru alcançado através da reação de *"pick-up"* [Du94]. Nesse núcleo, o estudo limitou-se à região até 1,4 MeV de excitação devido à presença nos espectros do pico

elástico e cauda associada. Os desvios padrões nas energias foram tipicamente de 1 keV, tendo sido feitas atribuições claras de transferências de $\ell = 0$, 2, 4 e extraídas as respectivas intensidades espectroscópicas.

O núcleo ^{101}Ru teve suas características de partícula [Du88] e buraco [Du94] independentes mapeadas até 3,2 MeV e 2,2 MeV, respectivamente. O acordo entre as energias de excitação dos dois trabalhos de São Paulo é excelente, também em relação à informação proveniente de transições γ. Há também concordância quanto as energias de excitação de [Du88] com o trabalho de Hollas referente à reação (d,p) [Ho77], que analisou apenas a faixa de até 1,9 MeV, com uma resolução de 25 keV. Por outro lado, há indicação clara de desvios sistemáticos nas energias do estudo da reação (p,d) de Dickey et al. [Di86], recomendando a revisão na compilação Nuclear Data Sheets [Bl91]. Há concordância geral entre as intensidades espectroscópicas de buraco e de partícula de nêutron obtida nos dois estudos de *"pick-up"* [Du94, Di86] e também em ambas as reações (d,p) [Du88, Ho77], neste caso de forma mais restrita, quando a comparação pode ser feita. Um ponto que merece destaque é a transição $\ell = 3$, correspondente a orbital não de valência, com energia de excitação de apenas 597 keV e intensidade espectroscópica de partícula e buraco relativamente intensa, revelada em ambos os trabalhos de São Paulo. De fato, Hollas *et al.* [Ho77], no exame da reação (d,p), preferiram a atribuição de $\ell = 4$, com uma qualidade pobre de ajuste quando comparada com outros ajustes de mesmo ℓ, enquanto que os autores do trabalho (p,d) não publicaram essa transição, provavelmente devido à resolução de seus espectros. Foram detectadas nas análises de *"stripping"* e *"pick-up"* de Duarte *et al.* [Du94, Du88], também com primazia, transições de orbitais não de valência associadas a ℓ igual a 1.

No ^{103}Ru, a investigação dos estados de partícula e buraco independentes estendeu-se até 3,5 MeV [Ba98] e 2,6 MeV [Du94] de excitação, respectivamente. Berg *et al.* [Be82], embora tenham estudado ambas as reações (p,d) e (d,p) populando o ^{103}Ru, não excederam 0,9 MeV de excitação e seus dados são de estatística pobre. Esses autores argumentam que a transição de $\ell = 2$ de menor energia seleciona, na reação de *"pick-up"*, o primeiro estado excitado $\frac{5}{2}^+$ e, na de *"stripping"*, a população preferencial é a do estado fundamental $\frac{3}{2}^+$. Os estudos de São Paulo confirmam a população do estado $\frac{5}{2}^+$ na análise da reação (d,t) [Du94], mas, ao contrário do argumentado por Berg it et al. [Be82],

apontam de forma robusta, na reação (d,p) [Ba98], também a população desse mesmo estado. Essa conclusão é respaldada pela concordância de energias, de cerca de vinte transições intensas, até 2 MeV de excitação, para os quais há correspondência clara com níveis detectados por estudos de γ's. Deve ser mencionado que Niizeki *et al.* [Ni79], na sua análise do ^{103}Ru a partir do decaimento β^- do ^{103}Tc, já tinha argumentado a favor da mesma atribuição, contrariando a adotada pela compilação NDS [Bl91]. Duas ou até três transições foram detectadas na reação (d,p), associadas à energia de 0,553 MeV. Um bom ajuste à distribuição angular integrada foi obtido pela superposição de $\ell = 0$, $\ell = 1$ e $\ell = 2$. Por outro lado, o estudo da reação (d,t) anterior [Du94] revelou três níveis nessa região e a reanálise da distribuição angular integrada publicada apontou contribuições de $\ell = 0$, $\ell = 1$ e $\ell = 4$ [Ba98]. O estado a 2,167 MeV populado pela transferência intensa de $\ell = 4$ na reação (d,t), foi muito pouco excitado na reação (d,p), revelando característica predominantemente de buraco independente e parentesco com o orbital $1g_{9/2}$ do core "fechado" $N = 50$. Há acordo geral entre as intensidades espectroscópicas de partícula independente obtidas na análise de São Paulo [Ba98] e nos trabalhos de Fortune *et al.* [Fo71] e Berg *et al.* [Be82]. A intensidade espectroscópica de $\ell = 3$, relatada por Fortune *et al.* [Fo71], na população do estado a 0,298 MeV, quase um fator 4 maior, torna-se compatível na reanálise supondo transição associada ao orbital $2f_{7/2}$, conforme foi preferido por Barbosa *et al.* [Ba98]. Por outro lado, as intensidades espectroscópicas de buraco independente extraídas por Diehl *et al.* [Di70], através da reação (d,t), mostram concordância geral nos valores relativos, mas não nos valores absolutos, provavelmente devido aos cálculos DWBA realizados por aqueles autores.

3.3 Discussão

3.3.1 Distribuições das Intensidades Espectroscópicas

Na cadeia de isótopos ^{99,100,101}Ru, $A = 101$ [Du88, Du94] e $A = 103$ [Du94, Ba98, Bo98] têm suas distribuições de intensidades espectroscópicas de partícula e buraco mapeadas em detalhes semelhantes. Já para o ^{99}Ru,

apenas a distribuição das intensidades de buraco é conhecida, até 1,4 MeV de excitação [Du94]. A visualização dessas informações costuma ser feita representando as respectivas intensidades espectroscópicas como função da energia de excitação, classificadas de acordo com o ℓ transferido, de forma aditiva e comparativa. Utiliza-se o símbolo $G = G_{pick} + G_{strip}$ para as intensidades espectroscópicas somadas, com $G_{pick} = C^2S(d,t)$ e $G_{strip} = C^2S'(d,p)$ $[S'(d,p) = (2j+1)S(d,p)]$. Concentrando a atenção nos orbitais de valência, as distribuições para os ^{101,103}Ru mostram que, para cada ℓ transferido, os níveis de menor energia de excitação são os mais intensamente populados. Para esses estados, as intensidades somadas (buraco + partícula) no ^{101}Ru, sempre excedem 60% do limite correspondente ao orbital do modelo de camadas, enquanto no ^{103}Ru, embora os níveis detectados a energias mais baixas, ainda preservem seu caráter predominantemente de quase-partícula, as intensidades são apreciavelmente reduzidas. Para o ^{99}Ru como para os outros isótopos, a maior intensidade espectroscópica $\ell = 2$ de buraco está concentrada no primeiro nível $\frac{5}{2}^+$. Transições similares e intensas associadas à transferência de $\ell = 4$ correspondem aos primeiros níveis $\frac{7}{2}^+$ nos três isótopos, com energias de excitação menores de 0,4 MeV.

3.3.2 Intensidades Espectroscópicas Totais

Partindo das informações espectroscópicas obtidas de reações de *"stripping"* e *"pick-up"* complementares, estados específicos do núcleo residual podem ter seu caráter de quase-partícula definido, conforme já foi discutido. Entretanto, globalmente as intensidades espectroscópicas permitem outra interpretação dos dados, pois são associadas com ocupação e vacância dos orbitais do modelo de camadas no núcleo alvo. Foram então calculadas as intensidades espectroscópicas, que puderam ser associadas a cada ℓ transferido, nas reações que partiram dos estados fundamentais dos núcleos ^{100,102}Ru [Du88, Du94, Ba98, Bo98]. Se fossem adicionadas as atribuições tentativas o panorama pincelado não se modificaria. Dados de ocupação ($\Sigma G_{pick} = \Sigma C^2S$) foram obtidos da análise das reações ^{100,102}Ru(d,t)^{99,101}Ru e informações de vacância ($\Sigma G_{strip} = \Sigma C^2S'$) de ^{100,102}Ru(d,p)^{101,103}Ru, considerando apenas orbitais de valência. A soma dos valores de vacância e de ocupação, para cada

orbital, deve ser comparada com $(2j+1)$ ou para $\ell = 2$, à soma dos limites para $2d_{5/2}$ e $2d_{3/2}$. O conjunto das informações extraídas mostra que as reações (d,t) localizaram, nos estados fundamentais dos ^{100}Ru e ^{102}Ru respectivamente, 83% e 93% do número esperado de partículas, estas espalhadas entre os vários orbitais, sem revelar um padrão sequencial de preenchimento. Note-se que na reação ^{100}Ru(d,t)^{99}Ru, apenas foram analisadas energias de excitação menores do que 1,2 MeV, mas a perda de intensidade não se revelou dramática. De forma contrastante, a soma total $(\sum G_{pick} + \sum G_{strip})_{\text{valência}}$ exaure 86% do esperado no ^{100}Ru, mas corresponde a apenas 62% no ^{102}Ru. Há claramente, associada à soma $\sum G_{strip}$, para o ^{102}Ru falta de intensidade experimentalmente verificada, correspondendo à detecção de pouco mais da metade da esperada. O quadro se completa com a também falta de intensidade revelada pela reação ^{104}Ru(d,t)^{103}Ru [Du94], que deixa 37% da intensidade de valência não detectada, até 2,5 MeV de excitação. O diagnóstico experimental aponta a dificuldade de formação do núcleo ^{103}Ru partindo dos isótopos pares vizinhos, sinal interpretado como indicativo do fenômeno de coexistência nesse núcleo. Reforçando o diagnóstico de coexistência, a comparação de dados de transições γ no ^{103}Ru [Ni79, Kl75, Ka86] com as informações de *"pick-up"* e *"stripping"* de São Paulo [Ba98, Bo98], permitiu ainda distinguir nesse núcleo dois conjuntos de níveis. Um dos conjuntos é de estados parentes do fundamental $\frac{3}{2}^+$ e populados pelo decaimento β^- do estado fundamental $\frac{5}{2}^+$ do ^{103}Tc e o outro é de estados parentes do nível *"yrast"* $\frac{5}{2}^+$, populados nas transferências de um nêutron.

3.3.3 Acompanhamento da Informação Espectroscópica

O acompanhamento da informação espectroscópica na cadeia $^{99-103}$Ru, extraída em São Paulo, por intermédio de reações de transferência de um nêutron, mostra globalmente que a intensidade: (i) para cada orbital de valência é fortemente concentrada no estado excitado de menor energia, com exceção do orbital $2d_{3/2}$ e do fracionamento observado nas transições de $\ell = 0$ na reação ^{100}Ru(d,t)^{99}Ru; (ii) é espalhada entre todos os orbitais de valência; e (iii) diagnostica pequena superposição entre os estados fundamentais $\frac{3}{2}^+$ dos núcleos ^{103}Ru e ^{105}Ru e os de seus isótopos pares vizinhos aclopados a uma partícula ou a um buraco de nêutron. Essa situação incomum levou ao levantamento dos

estados de *"yrast"* com $J^\pi = \frac{1}{2}^+$ a $\frac{9}{2}^+$ e $J^\pi = \frac{7}{2}^-$ e $\frac{11}{2}^-$ nos isótopos ímpares $^{97-105}$Ru e nos isótonos dos ^{101,103}Ru (sempre consultando a compilação Nuclear Data Sheets correspondente mais recente). Esse estudo mostrou um estado $\frac{3}{2}^+$ *"yrast"* na maioria dos núcleos a energias de excitação inferiores a 0,3 MeV, valor esse ultrapassado somente no ^{97}Zr e ^{109}Sn, núcleos de características reconhecidamente semi-mágicas. Esse nível *"yrast"* é fracamente populado em reações de transferência de um nêutron, consistentemente em todos os isótopos de Ru mencionados, revelando-se semelhante aos estados fundamentais dos ^{103,105}Ru. Outras regularidades são os níveis *"yrast"* $\frac{7}{2}^+$ e $\frac{9}{2}^+$ a energias quase constantes, respectivamente 0,2 a 0,4 MeV e 0,7 a 0,9 MeV de excitação (com exceção do ^{97}Zr e ^{107}Sn) e evidente nos isótopos de Ru, a energia de excitação do estado $\frac{11}{2}^-$, cuja variação é seguida pelo "companheiro" $\frac{7}{2}^-$. Todos esses estados e também o $\frac{5}{2}^+$ apresentam um caráter importante de quase-partícula nos Ru e, conforme salientado pelas reações de transferência de um nêutron, a intensidade do nível *"yrast"* $\frac{1}{2}^+$ esgota aproximadamente metade da fração esperada para o orbital $3s_{1/2}$ e é praticamente constante na região.

Do ponto de vista teórico, os isótopos de Ru, em particular os ímpares, embora tenham sido objeto de várias interpretações, aparentemente conclusivas, representam ainda um desafio na busca de uma descrição consistente. A interpretação de Whisnant *et al.* [Wh86] do ^{99}Ru utilizando o modelo partícula + rotor simétrico, com aclopamento de Coriolis, foi capaz de reproduzir até mesmo algumas características aparentemente vibracionais. Em particular, caracterizou um multipleto associado à excitação $R = 2$ dominante do core e à partícula $1h_{11/2}$, em que, por exemplo, a energia de excitação obtida do membro $\frac{7}{2}^-$ está em ótimo acordo com a experiência. Uma inspeção mais detalhada do cálculo mostra, entretanto, que para obter o ajuste, esses autores [Wh86] tiveram que reduzir, na descrição do core ^{98}Ru, a deformação quadrupolar a praticamente metade do valor experimental conhecido e empregar o tratamento associado a um momento de inércia variável (VMI). Descrições também tipo rotor + partícula nos núcleos ^{101,103}Ru por Imanishi *et al.* [Im73] e no ^{103}Ru por Rekstad [Re75] recorreram ao mesmo tipo de decréscimo na coletividade dos cores, produzindo mesmo assim resultados pouco animadores em comparação com a experiência. Particularmente, esses modelos não reproduziram, para os estados de paridade positiva e negativa, a mesma escala absoluta de energia.

Cálculos do tipo phonon + quase-partícula também relatados para os estados de paridade positiva do ^{101}Ru, não conseguem explicar, por exemplo, a extensão da faixa de energia de excitação dos níveis, que de acordo com o modelo vibracional deveriam pertencer ao mesmo multipleto [Bh78, Va85]. Um complicador adicional advém da possível importância do grau de liberdade hexadecapolar nesses núcleos, em conexão com o alto valor de β_4, dos maiores ao longo de toda tabela periódica, extraído no ^{100}Ru através do espalhamento inelástico de prótons [Si89], na análise da transição de $L = 4$ em uma etapa, na população do estado a $\sim$ 2,3 MeV de excitação. O modelo de bósons-férmions interatuantes (IBFM) parece mais promissor, na medida em que pode intrinsicamente descrever transições entre simetrias puras e também se necessário aumentar os tipos de bósons considerados, incluir por exemplo bósons g. O cálculo de Arias *et al.* [Ar87] de IBFM2 na região $A \sim 100$, bastante detalhado, considerou uma transição entre as simetrias $U(5)$ (vibracional) e $O(6)$ (γ-soft) e teve a necessidade de incluir contribuições dos orbitais $2f_{7/2}$ e $1h_{9/2}$ no seu espaço de férmions, não de orbitais de valência, para ajustar estados de paridade negativa. A apreciação crítica das previsões no acompanhamento da cadeia dos isótopos de Ru não foi entretanto possível. Os dois estudos de IBFM relatados (Arias e Maino), partem de cores de Ru pares descritos por parâmetros de Van Isacker e Puddu [Is80], utilizam valores ajustados para as interações bóson-férmion, publicando somente fatores espectroscópicos associados a buraco e a orbitais de valência no ^{103}Ru [Ar87] e a buraco e orbitais de paridade positiva no ^{101}Ru [Ma91], ambos abaixo de $\sim$ 1,1 MeV. Esses cálculos, embora reproduzam características gerais das distribuições das intensidades espectroscópicas, não descrevem a extensão do fracionamento, em particular para $\ell = 2$. Para $\ell = 4$, ambos concentram a intensidade nos estados $\frac{7^+}{21}$, tendo ficado prejudicado o confronto das intensidades experimentais e previstas para os estados desafiantes atingidos pela transferência de $\ell = 3$ e $\ell = 1$.

Na região de $A \sim 100$, merece destaque a existência de um nível $\frac{3}{2}^+$, a baixa energia de excitação na maioria dos núcleos ímpar-par, que apresenta, onde medido, uma pequena superposição com os estados fundamentais de seus vizinhos par-par mais uma quase-partícula. Esse estado peculiar $\frac{3}{2}^+$ pode representar a sobrevivência da configuração $(2d_{5/2})^3$ acoplada a $\frac{3}{2}^+$, conforme sugerido no ^{93}Zr$_{53}$ e ^{95}Mo$_{53}$ por Talmi [Ta93], bem como no ^{105}Pd$_{59}$, bem além de

$N = 50$. O ingrediente intrigante nessa hipótese é que a maioria dos estados $(j)^n$ não podem ser quantitativamente explicados pela interação de emparelhamento, devendo ser adicionada uma interação efetiva empírica de longo alcance [Ta93] e que, para $j \geq \frac{5}{2}$, o estado de momento angular $J = j - 1$ tem sua energia de excitação diminuída. Por outro lado, acompanhando Bohr e Mottelson [Bo75], o acoplamento da quase-partícula $d_{5/2}$ com deformações estáticas ou dinâmicas de quadrupolo poderia fornecer uma interpretação alternativa, entretanto, não facilmente reconhecida.

3.4 Conclusões

Do ponto de vista experimental, os isótopos ^{101}Ru e ^{103}Ru tiveram suas propriedades relacionadas às intensidades espectroscópicas de partícula e buraco independentes de nêutron mapeadas, com o mesmo nível de detalhe. Assim é possível argumentar, com segurança, que uma fração considerável dessa intensidade não foi encontrada no ^{103}Ru, de forma significativa principalmente com referência à componente de partícula. O fenômeno de coexistência a baixa energia de excitação nesse núcleo foi assim diagnosticado, apontando um conjunto de níveis no ^{103}Ru não construídos sobre os estados fundamentais de seus isótopos vizinhos. Nos três isótopos ímpares investigados ^{99,101,103}Ru, para cada ℓ transferido, o estado detectado de energia de excitação menor é associado à maior fração da intensidade espectroscópica, com exceção de $\ell = 0$ no ^{99}Ru. Todos os orbitais de valência estão sendo preenchidos independentemente do número de nêutrons e a excitação de $\ell = 3$ a baixa energia de excitação nos ^{101,103}Ru está agora bem documentada.

Faltam ainda alguns ingredientes nas interpretações dos isótopos de Ru, na região de $A \sim 100$. As grandes dificuldades são esperadas provavelmente para os ^{103,105}Ru e são diagnosticadas levando em conta que os cálculos partem dos núcleos pares vizinhos com a adição de uma quase-partícula e que portanto, em vista da coexistência inferida, podem explicar somente uma parte dos espectros nos núcleos ímpares.

Capítulo 4

Aspectos Macroscópicos

As características de excitação dos estados 2_1^+ são na literatura amplamente utilizadas como indicadoras de estrutura nuclear e, em particular, as probabilidades reduzidas de transição elétricas, $B(E2)$, empregadas como medidas da coletividade nessas transições [Bo75]. Em princípio, $B(E2)$ é sensível somente à contribuição das cargas e, embora estudos experimentais e teóricos apontem que nessas excitações efeitos coletivos simples dominem [Ga82, Be77, Be81a], a quantificação da contribuição dos nêutrons se faz necessária, particularmente em regiões de transição, onde estes desempenham um papel essencial no estabelecimento das propriedades coletivas. A região de $A \sim 100$ é especialmente adequada se o objetivo é extrair a contribuição relativa de nêutrons e prótons nessas excitações. Assim, nos isótopos de Zr, para valores entre $N = 50$ e $N = 56$ os prótons se comportam como camada fechada, registrando-se modificação abrupta de comportamento acima de $N = 56$. Cada cadeia isotópica, nessa região, mostra algum tipo de transição ao redor de $N = 56$, sendo essa transição gradualmente menos intensa à medida que Z cresce além de $Z = 40$. A interpretação passa pelos trabalhos de Federman e Pittel [Fe77, Fe79] que apontam a importância da interação $p - n$ entre parceiros spin-órbita (sop - *"spin orbit partners"*): $\pi 1g_{5/2}$ e $\nu 1g_{7/2}$. É, portanto, a adição de nêutrons que, tendo ultrapassado um valor crítico, polariza a distribuição de prótons.

O entendimento de que o espalhamento inelástico de hádrons, no regime em que a interação nuclear predomina, poderia ser utilizado para evidenciar a contribuição dos nêutrons, potencialmente diferente da suposta, no modelo coletivo usual, na razão $\frac{N}{Z}$ em relação à dos prótons, teve início com os tra-

balhos de Bernstein e colaboradores [Ma75a, Be77, Be83]. O campo externo pode ser variado com diferentes projéteis e energias e sua descrição depende da intensidade da interação associada a cada tipo de nucleon [Be81a, Be81b]. A possibilidade de considerar intensidades iguais, aponta a vantagem dos estudos com projéteis de interação isoescalar, com os quais se acessa a probabilidade reduzida de transição isoescalar: para a primeira excitação quadrupolar $B(IS2)$. É importante destacar ainda que, do ponto de vista experimental, são acessíveis, em princípio, as várias regiões, a dominada pela excitação coulombiana pura, a região onde a interferência coulombiana-nuclear é máxima e também a de predominância da interação nuclear, evitando na análise global a influência de alguns erros sistemáticos.

O conjunto de trabalhos de São Paulo refere-se à região de transição de $A \sim 100$, utilizando no exame de espalhamentos inelásticos, dêuterons e partículas alfa, projéteis de interação isoescalar. Medidas de interferência coulombiana-nuclear com dêuterons são primazia de São Paulo, devido principalmente à dificuldade na tomada de dados associadas a esse feixe. A utilização de potenciais ópticos globais, amplamente testados, ajuda a manter parâmetros livres da análise sob controle, o que é especialmente importante na extração de conclusões comparativas no seguimento de cadeias de isótopos ou isótonos. A análise foi feita na aproximação de Born com ondas distorcidas (DWBA), utilizando na descrição do potencial de transição o modelo do potencial óptico-deformado (DOMP). Foram objetos de investigação na busca do caráter de isospin, principalmente a excitação 2_1^+: na desafiante cadeia de isótopos de Zr, o ^{90}Zr [Ho89], com suas propriedades de núcleo semi-mágico e seus vizinhos, o ^{91}Zr [Ho86] e o ^{92}Zr [Ho89]; os isótopos ^{94,98}Mo [Uk01], isótonos do ^{92}Zr e ^{96}Zr, respectivamente, e na cadeia do Ru, os isótopos ^{100,102,104}Ru [Go96], com um comportamento transicional mais suave, onde o ^{100}Ru também é isótono do ^{96}Zr.

4.1 Procedimento Experimental e Análise

Fabricados em São Paulo, alvos enriquecidos em ^{94,98}Mo foram bombardeados por dêuterons com energias de 13,2 MeV e de 16,0 MeV e os en-

riquecidos em ^{90,92}Zr e em ^{100,102,104}Ru, por partículas alfa com energias entre 9 e 22 MeV. As partículas incidentes foram aceleradas pelo Pelletron, tendo sido medidos espalhamentos elásticos e inelásticos. A medida do espalhamento de dêuterons de 17 MeV no ^{91}Zr utilizou o feixe do Van de Graaff, de três estágios, do Laboratório de Física Nuclear da Universidade de Pittsburgh. Em todos os espalhamentos com dêuterons a detecção foi feita em emulsões nucleares (Kodak NTB e Ilford G5, de 50 μm de espessura), expostas na superfície focal de um espectrógrafo magnético tipo Enge. As placas de emulsão foram lidas em faixas de 200 μm em São Paulo. Resoluções de $\sim$ 8 keV e $\sim$ 12 keV foram obtidas nos espalhamentos ^{94,98}Mo(d,d') nas energias incidentes de 13,2 e 16,0 MeV, respectivamente, e no espalhamento ^{91}Zr(d,d'), a resolução experimental foi de $\sim$ 15 keV. Os espalhamentos inelásticos de partículas alfa nos núcleos ^{90,92}Zr também foram medidos no plano focal do espectrógrafo, mas a detecção foi feita quer com placas de emulsão nuclear, quer por intermédio de um detetor a gás sensível à posição [Ko83]. Os alvos utilizados foram de dois tipos: lineares, essenciais nas medidas dos ângulos dianteiros, e alvos auto-sustentados finos e limpos, importantes nas medidas de espectros a ângulos intermediários. Resoluções entre 30 e 40 keV foram obtidas nos espectros de retroespalhamento de partículas alfa nos ^{100,102,104}Ru, em que se utilizou um detetor anular, a 172,8° no sistema de laboratório, com um ângulo sólido de 40,7 msr. A qualidade dos espectros, referentes aos vários espalhamentos, pode ser visualizada através dos exemplos apresentados nos trabalhos: [Ho86], [Go96], [Du97] e [Uk01].

A normalização relativa dos espectros associados a cada ângulo de espalhamento, na obtenção de distribuições angulares, ou a cada energia, no levantamento de funções de excitação, foi obtida a partir do número de partículas espalhadas elasticamente em detetores fixos ou através da medida da corrente de feixe integrada durante cada exposição, sempre monitorando a direção do feixe. A normalização absoluta foi obtida com referência a previsões do modelo óptico para o espalhamento elástico dos projéteis, considerando, as medidas dos picos elásticos, simultâneas às tomadas de dados em monitores, ou as de distribuições angulares elásticas associadas ao mesmo alvo e obtidas em condições semelhantes. As incertezas nos fatores de escala absolutos puderam ser quantificadas nos trabalhos mais recentes ao redor de 5%, levando em conta as previsões de cálculos com várias famílias de potenciais ópticos para as seções de

choque elásticas de alfa [En82, Ry87, Pa71] e dêuterons [Pe76, Da80], e onde necessário, melhor acesso aos ângulos sólidos dos detetores, além de medidas mais detalhadas e com melhor estatística de distribuições angulares elásticas.

O procedimento adotado aplica, na análise dos espalhamentos inelásticos, o modelo de potencial óptico deformado (DOMP) para o potencial de transição nuclear. De fato, na interpretação microscópica, um ponto difícil na descrição do espalhamento inelástico está na densidade de transição a ser utilizada, que carrega necessariamente informação de estrutura entre os dois estados envolvidos, sob severa investigação na região de $A \sim 100$. Por outro lado, a dependência radial na região da cauda do potencial de transição, onde o espalhamento inelástico de dêuterons e alfas de baixa energia acontece, é, para a maioria dos fatores de forma microscópicos calculados até agora, não substancialmente diferente da dos potenciais macroscópicos para excitações predominantemente coletivas.

Com o interesse centrado nos estados fortemente coletivos, em que predomina o processo de excitação em uma etapa na análise da reação, as distribuições angulares e funções de excitação experimentais foram comparadas então com previsões de cálculos na aproximação de Born com ondas distorcidas (DWBA), considerando a descrição macroscópica da excitação no modelo do potencial óptico deformado (DOMP) com parâmetros ópticos globais. Nesse modelo, a principal hipótese é, no processo em uma etapa responsável pela excitação nuclear, a associação do potencial efetivo de interação à não esfericidade do potencial óptico [Sa83]. Na descrição DWBA-DOMP, os mesmos parâmetros do modelo óptico descrevem as ondas distorcidas incidentes e emergentes e o potencial de transição para o estado coletivo, mantendo a análise a mais consistente possível para o acompanhamento comparativo da coletividade ao longo de cadeias de isótopos.

Os fatores de forma [Sa83], para cada L transferido, responsáveis, respectivamente, pelos processos de excitação nuclear $F_L^N(r)$ e coulombiano $F_L^C(r)$ são:

$$F_L^N(r) = -\,\delta_{R,L}^N(U)\,\frac{dV(r)}{dr} - i\,\delta_{I,L}^N(U)\,\frac{dW(r)}{dr} \tag{4.1}$$

onde V e W são, respectivamente, correspondentes às componentes real e ima-

ginária do potencial óptico U e:

$$F_L^C(r) = \begin{cases} \frac{4\pi Z_a e}{2L+1}\,\delta_L^C\,\frac{3\,Z\,R_c^{L-1}}{4\pi}\,e\,\frac{1}{r^{L+1}} & , \text{ para } r \geq R_c \\ 0 & , \text{ para } r < R_c\,, \end{cases} \tag{4.2}$$

onde $R_c = r_c\,A^{1/3}$ é o raio da distribuição de carga de corte abrupto.

Nos espalhamentos inelásticos estudados, as reações procedem perifericamente e os resultados dos cálculos não são afetados anulando o fator de forma coulombiano no interior da distribuição de carga.

A probabilidade de transição elétrica $B(EL)$, partindo do estado fundamental 0^+, é:

$$B(EL) \;=\; (\delta_L^C)^2 \left[\frac{3\,Z\,R_c^{L-1}}{4\pi}\right]^2 e^2 \tag{4.3}$$

onde δ_L^C é o comprimento de deformação de carga, definido por $\delta_L^C = \beta_L^C\,R_c$, com β_L^C o usual parâmetro de deformação de carga [Ra87].

O comprimento de deformação isoescalar (massa) $\delta_{R,L}^N(U) = \delta_{I,L}^N(U) = \delta_L^N$, se relaciona com a probabilidade reduzida de transição isoescalar $B(ISL)$, considerando a definição pioneira normalizada em Z [Be69b], através da expressão:

$$B(ISL) \;=\; (\delta_L^N)^2 \left[\frac{3\,Z\,R_m^{L-1}}{4\pi}\right]^2 \tag{4.4}$$

onde $R_m = r_m\,A^{1/3}$, é o raio característico de massa.

A razão $B(EL)/B(ISL)$ é então expressa por:

$$\frac{B(EL)}{B(ISL)} = e^2 \left(\frac{\delta_L^C}{\delta_L^N}\right)^2 \left[\frac{R_c^{L-1}}{R_m^{L-1}}\right]^2 = e^2\,C_L^2 \left(\frac{r_c}{r_m}\right)^{2L-2} . \tag{4.5}$$

O parâmetro $C_L = \delta_L^C/\delta_L^N$ contém a informação relevante sobre a razão entre as contribuições de carga (prótons) e de massa (prótons+nêutrons) à excitação.

Partindo do estado fundamental de um núcleo ímpar-par, em uma etapa, um estado coletivo poderia ser alcançado por mais de um momento angular L transferido. Quando apenas um valor de L domina, na expressão da seção de choque fatora-se δ'^N_L, onde:

$$\delta'^N_L \;=\; \left[\frac{(2J_f+1)}{(2J_i+1)\,(2L+1)}\right]\,(\delta_L^N)\;, \tag{4.6}$$

que se reduz ao usual δ_L^N quando $J_i = 0$. As expressões de $B(EL)$ e $B(ISL)$ também são válidas com a substituição de δ_L^C por δ'^C_L e δ_L^N por δ'^N_L, respectivamente.

A comparação das distribuições angulares e/ou das funções de excitação experimentais, particularmente incluindo a região de máxima interferência coulombiana-nuclear, com previsões DWBA-DOMP, permite a extração dos parâmetros C_L e δ_L^N, por conveniência escolhidos para descrever a excitação. No parâmetro C_L, o fator de escala se cancela e esse também é o parâmetro que contém a informação do caráter de isospin da excitação com multipolaridade L, conforme apresentado na seqüência.

Se as relações:

$$B(ISL) = \left| \frac{Z}{A} (\mathbf{M_n} + \mathbf{M_p}) \right|^2 \tag{4.7}$$

e

$$B(EL) = e^2 |\mathbf{M_p}|^2 \tag{4.8}$$

são utilizadas, consistentemente com a definição de $B(ISL)$ suposta, a consideração de proporcionalidade entre as densidades de transição de nêutrons e prótons leva, para a razão entre os momentos multipolares das distribuições de nêutrons e prótons, às expressões:

$$\frac{M_n}{M_p} = \left| \frac{\mathbf{M_n}}{\mathbf{M_p}} \right| = \frac{A}{Z} \left(\frac{B(ISL)}{B(EL)/e^2} \right)^{1/2} - 1 = \frac{A}{Z} \left(\frac{r_m}{r_c} \right)^{L-1} C_L^{-1} - 1 \tag{4.9}$$

que evidenciam a relação de M_n/M_p com C_L. Note-se que $C_L \cong 1$ produz a normalmente denominada excitação coletiva homogênea, em que prótons e nêutrons contribuem na razão de seus números $(\frac{Z}{N})$.

Os cálculos DWBA-DOMP para a descrição dos espalhamento inelásticos foram realizados com o programa DWUCK4 [Ku74], utilizando os parâmetros ópticos globais de Perey e Perey [Pe76], Daehnick *et al.* [Da80] e Child *et al.* [Ch74] para dêuterons, e de England *et al.* [En82], para partículas alfa. Os parâmetros correlacionados C_L e δ_L^N são extraídos da comparação entre previsões e distribuições angulares ou funções de excitação experimentais. Como a previsão do modelo não é linear nos parâmetros, o procedimento minimiza, no ajuste, o χ^2, utilizando o método de Gauss-Marquardt. Os parâmetros

ajustados correspondem ao $\chi^2_{\min}$ e suas incertezas estatísticas são expressas na matriz de covariâncias.

A inspeção de previsões DWBA-DOMP utilizando os parâmetros do potencial óptico de Perey e Perey [Pe76], calculadas para três energias incidentes de dêuterons (10,0 MeV, 13,0 MeV e 16,0 MeV) e valores típicos de C_2 e δ_2^N, tomando a excitação ^{94}Mo($0_1^+ \rightarrow 2_1^+$) como exemplo, salientam as regiões de interesse para as medidas, ilustrando a potencialidade do método [Uk01]. Pode ser observado que um mínimo de interferência desenvolve-se para todas as energias incidentes e oscilações tipicamente "difrativas", devido à excitação nuclear, praticamente determinam a forma da distribuição angular em ângulos mais trazeiros. Portanto, dados detalhados ao redor do mínimo de interferência são essenciais para a extração de C_2 e a ângulos maiores fornecem a normalização global $(\delta_2^N)^2$.

4.2 Resultados

O exame dos espectros associados ao espalhamento ^{91}Zr(d,d') com dêuterons de 17 MeV, em sete ângulos de espalhamento entre 25° e 80° no laboratório, permitiu até 4,8 MeV de excitação, a detecção de 73 níveis, vários deles não identificados anteriormente [Ho86]. As energias de excitação obtidas estão em bom acordo com as de Blok *et al.* [Bl76] na análise de (p,p'), embora parece haver indicação de uma diferença sistemática crescente acima de 3,5 MeV. É interessante notar que um padrão simples de excitação foi salientado para esse núcleo ímpar-par, na medida que foi possível associar a $\sim$ 40 distribuições angulares, excitações puras de $L = 2$, 3 ou 5, embora misturas não fossem proibídas, concentradas em regiões de energia onde o caroço ^{90}Zr exibe estados 2^+, 3^- e 5^-. Os parâmetros parciais de deformação β'_L, obtidos na comparação com previsões DWBA-DOMP, calculadas tomando deformações $\beta_L^C = \beta_L^N$ iguais, já que na condição experimental de medida não havia possibilidade para o exame da interferência coulombiana-nuclear, mostram bom acordo com os extraídos no espalhamento (p,p') [Bl76] para $L = 2$, mas para $L = 3$ e $L = 5$ revelaram-se sistematicamente menores. Se comprimentos de deformação δ_L^C e δ_L^N fossem considerados iguais, essas discrepâncias seriam ainda maiores. Essas diferenças,

também observadas em outras regiões, podem estar refletindo inadequações do modelo de reação considerado. Os resultados salientaram ainda a alta probabilidade de excitação medida para o primeiro estado excitado do ^{91}Zr, associado à deformação $\beta_2^N = 0,18$, um fator ~ 2 acima dos valores de todos os núcleos com $A = 90 \pm 2$.

As distribuições angulares experimentais associadas ao espalhamento (α,α'), com alfas de 21,0 MeV, nos ^{90}Zr e ^{92}Zr, na excitação dos primeiros estados quadrupolares permitiram o exame do padrão de interferência coulombiana-nuclear. A comparação entre as distribuições angulares experimentais e as previsões DWBA-DOMP, revelaram, surpreendentemente na excitação dos estados 2^+, para o ^{90}Zr a razão usual β_L^N/β_L^C igual a 1, mas para no ^{92}Zr, o mínimo profundo da distribuição angular só foi reproduzido com uma razão β_L^N/β_L^C de ~ 2. As distribuições angulares experimentais de excitação dos estados 3_1^-, por outro lado, são semelhantes e bem reproduzidas pelas previsões com parâmetros de deformação nuclear e coulombiano iguais. Medidas de Rychel *et al.* [Ry87], com alfas de 35,4 MeV no ^{92}Zr, embora não sensíveis ao parâmetro de deformação coulombiano para a excitação de $L = 3$, também revelaram estrutura de interferência coulombiana-nuclear na distribuição de $L = 2$, que somente foi ajustada com um aumento semelhante do parâmetro de deformação nuclear. A análise em termos dos comprimentos de deformação reproduz os resultados comentados.

Referentes ao espalhamento de partículas alfa nos ^{100,102,104}Ru, a 172,8° no laboratório, as funções de excitação inelásticas na população dos estados 2_1^+, medidas em 8 passos regulares entre 9 MeV e 22 MeV [Go96], partindo da região bem abaixo da barreira coulombiana estenderam-se permitindo também boa caracterização da região de interferência. A distribuição angular inelástica, na excitação do primeiro estado quadrupolar no ^{100}Ru, com partículas alfa de 22 MeV, foi medida principalmente para confirmar a contribuição nuclear nessa excitação. Por outro lado, referentes ao espalhamentos elásticos, as funções de excitação nos ^{100,102,104}Ru e a distribuição angular no ^{100}Ru, experimentais, permitiram para a análise a escolha dos parâmetros ópticos globais de England *et al.* [En82], que são independentes da energia incidente, com uma melhor caracterização do valor da difusividade real. Os ajustes das funções de excitação inelásticas com as previsões DWBA-DOMP caracterizaram a razão δ_L^C/δ_L^N e o

comprimento de deformação δ_L^N, de forma discriminativa. As atribuições das incertezas foram, ainda nesse trabalho, feitas a partir de estimativas de $\pm 3\sigma$, variando δ_L^N com δ_L^C fixo ou δ_L^C com δ_L^N fixo, produzindo previsões que envolvem os pontos experimentais, nas regiões em que, respectivamente, predominam a excitação nuclear ou a excitação coulombiana. A sensibilidade dos dados é maior às variações de δ_L^C do que às de δ_L^N, com incertezas de $\sim 1{,}5\%$ e $\sim 3\%$, respectivamente. As funções de excitação nos três isótopos, quando observadas em conjunto, mostram uma inclinação decrescente e um maior valor das seções de choque para os três pontos experimentais de menor energia, na seqüência crescente das massas (^{100,102,104}Ru). Para cada isótopo, a variação de δ_L^C, na região de energias menores, de fato corresponde a apenas um diferente fator de escala na seção de choque da excitação coulombiana, entretanto não é possível selecionar um único valor de δ_L^N se somente os pontos de alta energia fossem medidos. Vale a pena salientar que há uma diferença fundamental na excitação de estados coletivos associados a multipolaridades $L > 2$, medida na situação de retroespalhamento explorada nesse trabalho [Go96]. Para multipolaridades maiores, os processos de excitação nuclear são claramente dominantes e somente δ_L^N pode ser extraído. Na excitação dos estados 3_1^- nos ^{100,102,104}Ru, de fato, há uma queda dramática da seção de choque para energias incidentes inferiores a 14 MeV e os valores de δ_L^N, extraídos na hipótese de deformações iguais para carga e massa, apontam um acordo básico com os valores da literatura [Re77, Vo76, Sp89]. A excitação hexadecapolar no ^{100}Ru, a 2,367 MeV, foi somente observada em 16,0 MeV e 17,0 MeV e o valor extraído de δ_L^N confirma sua extraordinária população no espalhamento inelástico, conforme relatado no espalhamento (p,p'), também medido em São Paulo [Si89].

Nos espalhamentos inelásticos ^{94,98}Mo(d,d'), as distribuições angulares experimentais na excitação dos primeiros estados quadrupolares, favoreceram, para a energia incidente de 13,2 MeV, a caracterização da interferência coulombiana-nuclear, enquanto que os dados a 16,0 MeV foram principalmente utilizadas na verificação da consistência dos resultados de δ_L^N [Uk01]. Tomando o espalhamento ^{94}Mo(d,d')^{94}Mo(2_1^+) com dêuterons de 13,2 MeV como exemplo, uma primeira etapa do exame das características de isospin nesse núcleo consistiu de uma análise crítica do procedimento para obter os parâmetros correlacionados C_2 e δ_2^N e suas incertezas [Du97]. As previsões DWBA-DOMP,

com parâmetros ópticos de Perey e Perey [Pe76], foram ajustadas aos dados e a comparação entre as curvas experimentais de nível de χ^2, no plano $C_2 \times \delta_L^N$, com elipses equivalentes, calculadas a partir dos parâmetros de Gauss-Marquardt, circunscrevendo espectativas estatísticas de 39,3%, 68,3% e 99,7%, revelou previsões praticamente coincidentes. O teste estatístico direto, com uma simulação de Monte Carlo, de "novos" dados Gaussianos, também produziu resultados equivalentes. A análise aplicada mostrou que, dentro do modelo adotado, os melhores ajustes produziram resultados para δ_2^N e C_2 com incertezas estatísticas de $\sim 1\%$ e $\sim 2\%$, respectivamente. Vale lembrar ainda que, nessa situação experimental, no valor de C_2 o erro de escala na seção de choque se cancela e alguns erros de modelo são diluídos. Como conseqüência da maior confiança adquirida, no exame dos espalhamentos ^{94,98}Mo(d,d') a duas energias incidentes, o ajuste das previsões DWBA-DOMP na primeira excitação quadrupolar sobre os dados, minimizando o χ^2, foi feito por um procedimento tipo Gauss-Marquardt, procurando simultaneamente os valores de três parâmetros: C_2, δ_2^N(13,2 MeV) e δ_2^N(16,0 MeV). A redução de um fator ~ 2 no mínimo de χ^2 no ajuste simultâneo das distribuições angulares, nas duas energias incidentes e para ambos os isótopos, obtido com o aumento de 2% dos raios reduzidos r_R e r_I, com relação aos valores originais de Perey e Perey [Pe76], na descrição do fator de forma, aponta para um significado físico associado. No espalhamento inelástico, esses núcleos parecem ser representados por um objeto um pouco maior do que no espalhamento elástico. As distribuições angulares para o ^{98}Mo, em ambas as energias, são mais estruturadas no primeiro máximo, quando comparadas com as do ^{94}Mo e podem estar revelando comportamentos não descritos no modelo de reação adotado. As incertezas estatísticas nos valores obtidos nos ajustes vinculados são de $\sim 2\%$ para C_2 e $\sim 1\%$ para δ_2^N(13,2 MeV) e δ_2^N(16,0 MeV), mas nos dois últimos parâmetros incide ainda a contribuição das incertezas nos fatores de escala das seções de choque absolutas. As transições associadas às excitações dos estados 3_1^-, em ambos os isótopos, são fortemente dominadas pela interação nuclear. A análise vinculada das distribuições angulares nos ^{94,98}Mo, correspondentes a dêuterons de 13,2 e 16,0 MeV, puderam também ser realizadas, fornecendo valores de C_3 com incertezas estatísticas bem maiores de $\sim$ 6-7%.

4.3 Discussão

4.3.1 O Caráter de Isospin das Excitações 2_1^+ e 3_1^-

Na interpretação dos resultados do espalhamento (d,d') no ^{91}Zr [Ho86], foi possível relacionar os β_L obtidos em transições experimentais, associados ao mesmo L e a J_f conhecidos, com os parâmetros de deformação de possíveis estados do caroço ^{90}Zr [Fi82]. Assim, dos cinco β_2 extraídos para os primeiros níveis a baixa energia de excitação, alcançados pela transferência de $L = 2$, quatro são compatíveis com o parâmetro de deformação do estado a 2,18 MeV no ^{90}Zr [To73]. A exceção é o estado a 1205 keV que revelou, surpreendentemente, grande valor de β_2, maior por um fator ~ 2. Todos os estados alcançados por $L = 2$, acima de 2,5 MeV de excitação, revelam, por outro lado, valores de β_2 compatíveis com os três estados 2^+ do ^{90}Zr nessa faixa de energia [To73]. Já para $L = 3$, dos 10 estados com J conhecido, detectados na faixa de $\pm$ 0,5 MeV ao redor de 2,75 MeV, energia de excitação do 3_1^- do ^{90}Zr, apenas cinco revelaram β_L compatível com o desse estado do caroço, enquanto os valores dos demais foram sensivelmente inferiores. O único β_4 extraído é também compatível com o parâmetro de deformação do estado a 3,08 MeV do ^{90}Zr [To73]. Os β_5 obtidos para os primeiros três estados na transferência de $L = 5$ concordam com o parâmetro de deformação do estado 5_1^- no ^{90}Zr [To73]. Os resultados informam que no núcleo ^{91}Zr, a mistura entre graus de liberdade de partícula e coletivos do caroço não é suficiente para destruir a relação com estados deste (caroço). O estado $\frac{1}{2}^+$ a 1205 keV de excitação, revela-se de especial interesse, fortemente excitado no espalhamento (d,d'), acessado por intermédio de reações de transferência de um nêutron também mostra forte parentesco com o estado fundamental do ^{90}Zr [Bl76]. Partindo do estado fundamental do ^{91}Zr, de caráter praticamente puro de partícula $2d_{5/2}$ [Go75], foram então feitas, considerando as informações espectroscópicas, estimativas da contribuição das transições de valência na excitação do estado $\frac{1}{2}^+$, que entretanto não conciliaram a excitação coletiva desse estado à do 2_1^+ do ^{90}Zr. Complementando a discussão, as informações de propriedades eletromagnéticas associadas ao estado $\frac{1}{2}^+$ a 1205 keV de excitação no ^{91}Zr [Ga69, Gi74, Me77], quando colocadas em comparação com os resultados do espalhamento (d,d') de São Paulo [Ho86] apontam deformação

de carga inferior à de massa.

O exame da interferência coulombiana-nuclear com partículas α em São Paulo [Ho89], na excitação do primeiro estado quadrupolar nos isótopos vizinhos do ^{91}Zr, revelou comportamento muito diferenciado. De fato, embora no ^{90}Zr a excitação coletiva homogênea usual tenha sido observada, o ^{92}Zr, com dois nêutrons fora da camada fechada, revelou um fator ~ 2 para a razão β_2^N/β_2^C, como também foi extraído para o estado $\frac{1}{2}^+$ a 1205 keV no ^{91}Zr. Rychel *et al.* [Ry87] observaram, com o mesmo projétil, basicamente os mesmos comportamentos utilizando partículas alfa com energia de 35,4 MeV. Essa concordância pode ser interpretada como indicativa de uma descrição adequada para o mecanismo de excitação.

No estudo da interferência coulombiana-nuclear com partículas α em funções de excitação nos ^{100,102,104}Ru [Go96], o acesso às contribuições nucleares e de carga na excitação dos estados 2_1^+ permitiu também, de forma clara, determinar a normalização relativa de δ^N e δ^C. Um comportamento crescente de δ^C, como função de A revela-se em acordo com os resultados obtidos em estudos de excitação coulombiana [Hi98, La80, Bo79]. Com respeito aos valores de δ^N, a previsão do modelo coletivo homogêneo é obtida para o ^{100}Ru, mas os valores embora monotonicamente crescentes como função de A, não seguem a mesma razão de crescimento de δ^C. Assim, no ^{104}Ru, δ^N é $\sim 18\%$ menor do que δ^C. O comportamento das razões M_n/M_p extraídas estabelece de forma inequívoca um decréscimo da importância dos nêutrons em relação aos prótons, na primeira excitação quadrupolar, quando um e dois pares de nêutrons são adicionados ao ^{100}Ru.

Na caracterização das primeiras excitações quadrupolares e octupolares através do espalhamento (d,d') nos núcleos ^{94,98}Mo [Uk01], os valores de $C_2 > 1$ e $C_3 \geq 1$ indicam contribuição maior dos prótons em ambas as excitações, nos dois isótopos. As incertezas maiores em C_3, em comparação a C_2, refletem a menor sensibilidade dos dados à razão dos comprimentos de deformação de carga e massa na excitação octupolar. Os valores de δ_2^N e δ_3^N são, por outro lado, determinados com a mesma precisão e produzem valores de β_L^N que concordam com os da literatura, extraídos em espalhamentos inelásticos de prótons [Lu71, Aw72] e dêuterons [Wa78]. Os valores de $M_n/M_p \sim 0,9$, obtidos nas excitações quadrupolares, em ambos os isótopos, são menores do que $\frac{N}{Z} =$

$1,2-1,3$ e são outra maneira de caracterizar o papel dos nêutrons relativamente aos prótons nessas excitações. Nesse cálculos, os valores $r_c = 1,22$ fm e $r_m = 1,16$ fm foram utilizados para os raios reduzidos de carga e de massa [Du97] das respectivas distribuições de corte abrupto. Salienta-se que as razões M_n/M_p obtidas são afetadas não apenas pelas incertezas experimentais, mas também pelas incertezas, difíceis de serem especificadas, associadas ao modelo de reação, mas pelo menos um algarismo significativo deve ser preservado. A evolução crescente, praticamente paralela, de $B(IS2)$ e $B(E2)$ do ^{94}Mo para o ^{98}Mo mostra novamente que as características de isospin não mudam drasticamente para os dois isótopos. A excitação octupolar no ^{98}Mo também é mais coletiva do que no ^{94}Mo.

Os valores de C_2, pouco maiores do que 1,1, são aproximadamente os mesmos nos ^{94}Mo e ^{98}Mo e, consequentemente, também as razões $B(E2)/B(IS2)$ [Uk01]. Por outro lado, conforme mostram os resultados de (α,α') nos ^{100,102,104}Ru [Go96], o comportamento de C_2, para esses isótopos, é crescente em função da massa, partindo do ^{100}Ru, isótono do ^{98}Mo, que se revela praticamente coletivo homogêneo. Para esses núcleos também uma pequena predominância dos prótons sobre os nêutrons, como para os ^{94}Mo e ^{98}Mo, é detectada na primeira excitação quadrupolar. Situação marcadamente oposta é a contribuição muito maior dos nêutrons relativa aos prótons na transição para o estado 2_1^+ no ^{92}Zr [Ho89], isótono do ^{94}Mo, enquanto que no ^{90}Zr [Ho89], contribuições usuais na razão $\frac{N}{Z}$ são apontadas.

Embora não se encontrem na literatura outros estudos de interferência coulombiana-nuclear na região, medidas de espalhamentos elásticos e inelásticos de partículas α de 35,4 MeV e ^{6}Li de 70 MeV nos ^{90,92,94,96}Zr foram analisadas em detalhes na busca de informações sobre o caráter de isospin das transições para os estados 2_1^+ e 3_1^- [Ho93, Lu95, Ho96]. Do ponto de vista teórico, foram realizados cálculos microscópicos para os potenciais de transição, obtidos compondo num *"folding"* a densidade de transição entre os estados envolvidos com a interação efetiva entre o projétil e cada nucleon do alvo. As análises nos trabalhos do grupo de Horen [Ho93, Lu95, Ho96] foram realizadas com densidades de transição obtidas em cálculos na aproximação de fase aleatória para quase-partículas (QRPA - quasi-particle random phase approximation), ou com densidades de transição do modelo coletivo padrão de Bohr-Mottelson. As in-

terações efetivas utilizadas foram da forma gaussiana para alfas e para o ^{6}Li, da forma simples de Yukawa. Há uma tendência geral das seções de choque previstas usando as densidades de transição QRPA serem pequenas quando comparadas com as experimentais, quer nos espalhamentos com partículas α, quer com ^{6}Li. Assim, embora um bom acordo tenha sido obtido para o 2_1^+ no ^{90}Zr, para os outros isótopos houve a necessidade de intensificar a contribuição dos nêutrons. Quanto à contribuição dos prótons, revelou-se demasiado forte no ^{96}Zr e satisfatória nos outros isótopos, conforme apontado pelos $B(E2)$ experimentais [Ra87]. As seções de choque teóricas para a excitação dos estados 3_1^- também ficaram de 20-50% abaixo das medidas. É bastante encorajador entretanto que os valores de M_n/M_p, conforme comentou Horen *et al.* [Ho96], com os ajustes mencionados para reproduzir os dados sejam próximos aos valores obtidos usando as densidades de transição do modelo padrão de Bohr-Mottelson [Lu95] e reproduzam o comportamento evolutivo da razão extraída utilizando o potencial óptico deformado para o potencial de transição, particularmente para o primeira excitação quadrupolar. De fato, é bem conhecido que as seções de choque para os espalhamentos inelásticos em questão são determinadas principalmente pela intensidade do potencial de transição na região do raio de forte absorção, onde a reação acontece, e onde a descrição DOMP e *"folding"* com a densidade de transição do modelo padrão não diferem substancialmente.

4.3.2 Excitações Duotriacontapolares

Os estudos de espalhamentos inelásticos com dêuterons e partículas α em isótopos de Zr, Mo e Ru, realizados em São Paulo, revelaram nesses núcleos excitação de $L = 5$, que motivou um levantamento na literatura dessa excitação na região de $A \sim 100$ [Ho99]. A investigação, compreendendo núcleos par-par de número atômico entre $Z = 40 - 50$ mostrou, em cada cadeia de isótopos, primeiros estados excitados 5^- com comportamento peculiar. Esses estados aparecem nos núcleos par-par a energia de excitação aproximadamente constante de $(2,4 \pm 0,2)$ MeV e são associados, onde estudados por espalhamentos inelásticos, a excitações coletivas em uma etapa. Esse comportamento também sobrevive em núcleos ímpares vizinhos, com estados membros de um multipleto de níveis, com características de acoplamento fraco, como já foi comentado no

trabalho referente ao ^{91}Zr [Ho86]. A soma das energias dos estados 2_1^+ e 3_1^-, que no modelo harmônico vibracional deveria ser a do centróide para o estado correspondente de dois fónons, é sempre maior do que a dos 5_1^- citados. As informações experimentais acessíveis para os níveis 5_1^-, tomadas de forma global, parecem excluir sua interpretação via o acoplamento das primeiras excitações quadrupolar e octupolar. Por outro lado, excluem também a interpretação proposta, em particular próximo de camadas fechadas, simplesmente envolvendo prótons nos orbitais $\pi 1g_{9/2}$ e $\pi 2p_{1/2}$ [Ca69, Ba59], embora essa componente esteja presente na função de onda desses estados. Nos núcleos ^{94,98}Mo, os níveis de energia dos estados 5_1^-, bem como os parâmetros de deformação extraídos 0,048 e 0,040, respectivamente, na análise de sua excitação coletiva em uma etapa por (d,d'), se ajustam às propriedades gerais diagnosticadas e apontam para um caráter duotriacontapolar dessa excitação [Ho99].

4.4 Conclusões

Estudos de interferência coulombiana-nuclear em espalhamentos inelásticos, realizados em São Paulo, com dêuterons e partículas α nos núcleos ^{94,98}Mo [Uk01], ^{90,92}Zr [Ho89] e ^{100,102,104}Ru [Go96], permitiram o acompanhamento do caráter de isospin, principalmente da primeira excitação quadrupolar. Para os isótopos ^{94}Mo e ^{98}Mo [Uk01], os C_2 obtidos no espalhamento (d,d'), iguais dentro do desvio estatístico e ligeiramente maiores do que 1, caracterizaram na comparação dos valores de M_n/M_p associados, menores em $\sim$ 30% dos respectivos $\frac{N}{Z}$, aspectos não homogêneos. A análise de (α,α') nos ^{100,102,104}Ru [Go96], por outro lado, revelou comportamento monotonicamente crescente para C_2, de 1,04 para 1,22, como função da massa. Esses valores mostram para o ^{100}Ru, isótono do ^{98}Mo, apenas levíssima predominância dos prótons na excitação, mas que essa predominância se salienta na seqüência dos isótopos com um ou dois pares de nêutrons a mais, em que as razões M_n/M_p calculadas são, respectivamente, $\sim$ 22% e $\sim$ 30% menores do que $\frac{N}{Z}$. As informações extraídas para o ^{90}Zr [Ho89] mostram para esse núcleo comportamento coletivo homogêneo usual, mas para o ^{92}Zr [Ho89], isótono do ^{94}Mo e também em marcante contraste com este, apontam claramente predominância dos nêutrons sobre os prótons,

ultrapassando $\frac{N}{Z}$, na razão dos momentos quadrupolares de nêutron e próton, em mais do que $\sim 50\%$.

Do ponto de vista teórico, existem estudos microscópicos detalhados feitos por Horen *et al.* [Ho96] no exame das excitações 2_1^+ e 3_1^-, nos ^{90,92,94,96}Zr, com alfas e ^{6}Li. As razões M_n/M_p calculadas utilizando densidades transição QRPA precisam ser normalizadas para reproduzir as seções de choque experimentais. Por outro lado, os valores ajustados são próximos dos obtidos com as densidades de transição do modelo coletivo padrão de Bohr-Mottelson [Lu95] que acompanham, principalmente para a primeira excitação quadrupolar, a evolução revelada na análise, muito mais simples, com o potencial de transição DOMP.

O trabalho extenso do grupo nos isótopos de Zr, Mo e Ru diagnosticou, no bojo da investigação, um padrão peculiar da primeira excitação associada a $L = 5$ em espalhamentos inelásticos, que desvendou com primazia de São Paulo, entre $Z = 40$ e $Z = 50$ excitações coletivas duotriacontapolares [Ho99].

Capítulo 5

Comentários Finais e Perspectivas

A procura de indicadores simples de estrutura nuclear, particularmente no exame das motivantes regiões de transição, é certamente uma das preocupações da área, com interesse renovado nos últimos anos, tendo em vista o acesso a feixes nucleares radioativos. A caracterização de aspectos microscópicos e macroscópicos do comportamento nuclear, principalmente nessas regiões, ao longo de cadeias de isótopos ou isótonos, constitui-se em uma ferramenta poderosa de diagnóstico. Ainda em núcleos de massa intermediária, a região de $A \sim 70$ também faz parte da arena de interesse. De fato, os isótopos de Ge e Se apresentam uma série de feições que podem ser colocadas em analogia com características observadas em núcleos de Zr e Ru. Em particular, os estados 0_2^+, também excepcionalmente baixos em energia nos isótopos de Ge apresentam resposta à transferência de um par de nêutrons [Re80] e ao espalhamento de prótons[Ro86] semelhante ao verificado na região de Zr. No ^{72}Ge o estado 0_2^+ é o primeiro estado excitado, havendo indícios de transição de forma entre o ^{72}Ge e o ^{74}Ge [Se85]. O acompanhamento da evolução dos valores de $B(E2)$ nessa região [Ra89] também revela, como a região $A \sim 100$, comportamento que evidencia transição, mais abrupta nos isótopos de Se ($Z = 34$) e mais suave nos de Ge ($Z = 32$). Os valores de $B(E2)$ são máximos em ambas as cadeias para $N = 42$. Os isótopos de Zn, por outro lado, com $Z = 30$, mostram valores de $B(E2)$ praticamente constantes entre $N = 32$ e $N = 42$ [Ra89, Le98].

A região de $A \sim 100$, em particular os isótopos de Ru, foram alvos de extenso programa de investigação em São Paulo. Utilizando como projétil o dêuteron, estudos de reações de transferência de um nucleon apontaram, no

seguimento da sistemática dos níveis *"yrast"*, nos Ru ímpares, coexistência a baixa energia de excitação [Bo98, Ba98]. Os trabalhos em preparação trazem informações experimentais complementares e enfocam as características de buraco (partícula) do ^{98}Ru (^{100}Ru) partindo do ^{99}Ru, revelando conjuntos de estados alcançados por transferência de ℓ puro não previstas [Ro01a, Ro01b, Ho01]. O interesse se estende, considerando a importância da interação p-n entre parceiros spin-órbita [Fe77, Fe79] na região, à busca de informações referentes à ocupação $\nu 1g_{7/2}$, principalmente em isótopos de Pd, onde não existem relatos. Pela expectativa de existência de estados do ^{94}Mo parentes do ^{90}Zr + α [Ok95, Bu95], a investigação da reação ^{90}Zr(^{6}Li,d), salientando possíveis estruturas de aglomerado α é complementar para visualização do panorama global da região.

O acompanhamento da evolução da coletividade associada aos estados 2_1^+ e 3_1^- ao longo de cadeias de núcleos levou ao desenvolvimento de metodologia para análise de interferência coulombiana-nuclear (ICN) em espalhamentos inelásticos com projeteis de interação isoescalar. Essa metodologia permite caracterizar a probabilidade reduzida de transição isoescalar $B(IS2)$ e também da razão $B(E2)/B(IS2)$. A análise das excitações octupolares apresenta menor sensibilidade. É importante salientar que a coletividade é em geral acompanhada apenas através da probabilidade reduzida de transição elétrica $B(EL)$ não havendo informações sobre $B(ISL)$ agora acessíveis, de forma mais controlada, através de medidas de ICN em espalhamentos inelásticos. Na extração dos parâmetros que caracterizam na excitação a razão dos momentos multipolares de prótons e nêutrons, elementos sensíveis no teste de modelos, a vantagem dessa metodologia é o cancelamento de alguns erros quer de origem experimental, quer de origem teórica. Na região de $A \sim 100$, a metodologia foi aplicada utilizando dêuterons e partículas α em isótopos de Mo [Uk01] e Ru [Go96]. Com o pano de fundo que diagnostica dificuldades na descrição teórica dos isótopos ímpares de Ru, estão programadas medidas inéditas de ICN com dêuterons nos ^{99}Ru e ^{101}Ru, os únicos isótopos ímpares estáveis. Ainda na região de $A \sim 100$, esse método está sendo aplicado em ^{104,106,108,110}Pd acompanhando a transição nesses isótopos [Ra89].

Na região de $A \sim 70$, informações sobre características de isospin nas excitações 2^+ e 3^- não são encontradas na literatura. O projétil isoescalar ^{6}Li viabiliza o uso da técnica de ICN em espalhamentos inelásticos nessa região,

pois dificuldades experimentais impedem a utilização de dêuterons e partículas alfa. De fato, o acesso à máxima interferência coulombiana-nuclear exige com dêuterons diminuir a tensão do terminal do Pelletron atingindo $\sim$ 4 MV, inviabilizando o controle da máquina e por outro lado, feixe de partículas alfa não está disponível . Testes realizados de validação do método e investimentos para propiciar melhor controle do feixe de ^{6}Li a partir da fonte de *"sputtering"* [Ba01], salientaram a possibilidade de utilização dessa técnica com ^{6}Li na região de $A \sim 70$. Na validação, dados utilizando como alvo o ^{100}Ru e três projéteis isoescalares: dêuteron [Go93], partícula alfa [Go96] e ^{6}Li [Si00], mostraram a consistência da análise. Assim, os esforços envidados abriram novo horizonte experimental e as primeiras medidas referentes a distribuições angulares detalhadas da primeira excitação quadrupolar na região de ICN com ^{6}Li de 28 MeV nos isótopos ^{70,72,74}Ge [Ba01] apontaram comportamentos contrastantes: enquanto nos ^{70,72}Ge contribuições praticamente homogêneas de nêutrons e prótons foram detectadas, os dados do ^{74}Ge requereram claramente uma cotribuição mais intensa dos nêutrons. Outro ponto que merece investimento refere-se à possível utilização de feixes isoescalares de ^{10}B e ^{12}C potencializando comparações frutíferas.

Bibliografia

[Ar87] J. M. Arias, C. E. Alonso, and M. Lozano, Nucl. Phys. **A466**, 295 (1987).

[Aw72] Y. Awaya, K. Matsuda, T. Wada, N. Nakanishi, S. Takeda, and S. Yamaji, J. Phys. Soc. Jpn **33**, 881 (1972).

[Ba59] B. F. Bayman, A. S. Reiner, and R. K. Sheline, Phys. Rev. **115**, 1627 (1959).

[Ba66] R. H. Bassel, Phys. Rev. **149**, 791 (1966).

[Ba73] W. H. Barkas, *Nuclear Research Emulsions* (Academic Press, New York). Vol. **1** (1963) and vol. **2** (1973).

[Ba92] C. M. Baglin, Nuclear Data Sheets **66**, 347 (1992).

[Ba97] M. D. L. Barbosa, J. L. M. Duarte, T. Borello-Lewin, L. B. Horodynski-Matsushigue, G. M. Ukita, and L. C. Gomes, *"Generalized Loss of Particle and Hole Neutron Spectroscopic Intensity in ^{103}Ru: a Sign of Significant Differences between the Odd Nucleus and the G.S. of both Even Neighbors"*, in Proceedings of the XX Brazilian Workshop on Nuclear Physics (World Scientific, Guaratinguetá, São Paulo, Brazil, 1997) 99-101.

[Ba98] M. D. L. Barbosa, T. Borello-Lewin, L. B. Horodynski-Matsushigue, J. L. M. Duarte, G. M. Ukita, and L. C. Gomes, Phys. Rev. C **58**, 2689 (1998) [Anexo 1.4].

[Ba01] M. D. L. Barbosa, *"Interferência Nuclear-Coulombiana nos Isótopos de Germânio"*, Tese a ser apresentada ao Instituto de Física da Universidade de São Paulo para obtenção do título de Doutor (2001).

[Be69a] F. G. Becchetti and G. Greenlees, Phys. Rev. **182**, 1190 (1969).

[Be69b] A. M. Bernstein, Adv. Nucl. Phys. **3**, 325 (1969).

[Be77] A. M. Bernstein, V. R. Brown, and V. A. Madsen, Phys. Lett. **71B**, 48 (1977).

[Be81a] A. M. Bernstein, V. R. Brown, and V. A. Madsen, Phys. Lett. **103B**, 255 (1981).

[Be81b] A. M. Bernstein, V. R. Brown, and V. A. Madsen, Phys. Lett. **106B**, 259 (1981).

[Be82] G. P. A. Berg, M. Demarteau, A. Hardt, W. Hürlimann, S. A. Martin, J. Meissburger, W. Oelert, H. Seyfarth, B. Styczen, M. Köhler, I. Oelrich, and J. Scheerer, Nucl. Phys. **A379**, 93 (1982).

[Be83] A. M. Bernstein, V. R. Brown, and V. A. Madsen, Comments Nucl. Part. Phys., 203 (1983).

[Bh78] S. Bhattacharaya and S. K. Basu, Phys. Rev. C **18**, 2765 (1978).

[Bl76] H. P. Block, L. Hulstman, E. J. Kapstein, and J. Blok, Nucl. Phys. **A273**, 142 (1976).

[Bl91] J. Blachot, Nuclear Data Sheets **63**, 305 (1991).

[Bo75] A. Bohr and B. R. Mottelson, *Nuclear Structure* (Benjamin, New York, 1975).

[Bo79] A. Bockish, M. Miller, A. M. Kleinfeld, A. Gelberg, and U. Kaup, Z. Phys. A **292**, 265 (1979).

[Bo94] T. Borello-Lewin, L. B. Horodynski-Matsushigue, J. L. M. Duarte, L. C. Gomes, and G. M. Ukita, *"New Experimental Systematics in the $A \sim 100$ Region"*, in Perspectives for the Interacting Boson Model on the Occasion of Its 20th Anniversary (World Scientific, Padova, 1994) 449-452.

[Bo97a] T. Borello-Lewin, J. L. M. Duarte, L. B. Horodynski-Matsushigue, and M. D. L. Barbosa, *"Evidence for Poor Overlap between the Ground States of Odd Ru Isotopes and their Even Neighbours"*, in Proceedings of the 8th International Conference on Nuclear Reaction Mechanisms (Varenna). Ricerca Scietifica ed Educazione Permanente, Supp. **111**, 86 (Universitá degli studi di Milano, Italy, 1997).

[Bo97b] T. Borello-Lewin, L. B. Horodynski-Matsushigue, G. M. Ukita, L. C. Gomes, and J. L. M. Duarte, *"Comparative Studies of $B(IS2)$ and $B(E2)$ in the Region of $A \sim 100$"*, in Proceedings of the 8th International Conference on Nuclear Reaction Mechanisms (Varenna). Ricerca Scietifica ed Educazione Permanente, Supp. **111**, 587 (Universitá degli studi di Milano, Italy, 1997).

[Bo98] T. Borello-Lewin, J. L. M. Duarte, L. B. Horodynski-Matsushigue, and

M. D. L. Barbosa, Phys. Rev. C **57**, 967 (1998) [Anexo 1.3].

[Bu87] D. G. Burke *et al.*, Mc Master Acc. Lab. Annual Report, p. 48 (1987).

[Bu90] D. G. Burke and G. Kajrys, Nucl. Phys. **A517**, 1 (1990).

[Bu95] B. Buck., A. C. Merchant, and S. M. Perez, Phys. Rev. C **51**, 559 (1995).

[Ca69] M. R. Cates, J. B. Ball, and E. Newman, Phys. Rev. **187**, 1682 (1969).

[Ch74] J. D. Childs, W. W. Daehnick, and M. J. Spisak, Phys. Rev. C **10**, 217 (1974).

[Ch83] A. Chalupka *et al.*, Nucl. Inst. and Meth. **217**, 113 (1983).

[Ch92] M. S. Chowdhury, M. A. Zaman, and H. N. Sen Gupta, Phys. Rev. C **46**, 2273 (1992).

[Cl80] T. P. Cleary, W. D. Collender, and R. K. Sheline, Phys. Rev. C **21**, 2244 (1980).

[Cr78] E. R. da Cruz, *"Estudo das Características de um Espectrógrafo Magnético"*, Dissertação de Mestrado, IFUSP (1978).

[Cu85] R. A. Cunningham *et al.*, Nucl. Inst. and Meth. **A234**, 67 (1985).

[Da80] W. W. Daehnick, J. D. Childs, and Z. Vrcelj, Phys. Rev. C **21**, 2253 (1980).

[Di70] R. C. Diehl, B. L. Cohen, R. A. Moyer, and L. H. Goldman, Phys. Rev. C **1**, 2085 (1970).

[Di86] S. A. Dickey, J. J. Kraushaar, and M. A. Rumore, J. Phys. G **12**, 745 (1986).

[Du88] J. L. M. Duarte, L. B. Horodynski-Matsushigue, T. Borello-Lewin, and O. Dietzsch, Phys. Rev. C **38**, 664 (1988) [Anexo 1.1].

[Du94] J. L. M. Duarte, L. B. Horodynski-Matsushigue, and T. Borello-Lewin, Phys. Rev. C **50**, 666 (1994) [Anexo 1.2].

[Du97] J. L. M. Duarte, G. M. Ukita, T. Borello-Lewin, L. B. Horodynski-Matsushigue, and L. C. Gomes, Phys. Rev. C **56**, 1855 (1997) [Anexo 2.4].

[Eb88] J. Eberth, R. Meyer, and K. Sistemich (Editors), *Nuclear Structure of the Zirconium Region* (Springer-Verlag, Berlim, 1988).

[Ed57] A. R. Edmonds, *Angular Momentum in Quantum Mechanics* (Princeton, Princeton University, 1957).

[En82] J. B. England *et al.*, Nucl. Phys. **A388**, 573 (1982).

[Er79] J. R. Erskine, Nucl. Inst. and Meth. **162**, 371 (1979).

[Fa85] L. B. C. W. Faro, H. Takai, K. Koide, A. Bairrio Nuevo Jr., e O. Dietzsch, Relatório do Departamento de Física Experimental, p. 84, IFUSP (1985).

[Fe77] P. Federman and S. Pittel, Phys. Lett. B **69**, 385 (1977).

[Fe79] P. Federman and S. Pittel, Phys. Rev. C **20**, 820 (1979).

[Fi82] C. A. Fields, R. A. Ristinen, L. E. Samuelson, and P. A. Smith, Nucl. Phys. **A385**, 449 (1982).

[Fo71] H. T. Fortune, G. C. Morrison, J. A. Nolen Jr., and P. Kienle, Phys. Rev. C **3**, 337 (1971).

[Ga69] L. N. Gal'perin, A. Z. Il'yasov, I. Kh. Lemberg, and G. A. Firsonov, Yad. Fiz. **9**, 225 (1969) [Sov. J. Nucl. Phys. **9**, 133 (1969)].

[Ga82] M. M. Gazzaly, N. M. Hintz, G. S. Kyle, R. K. Owen, G. W. Hoffmann, M. Barlett, and G. Blanpied, Phys. Rev. C **25**, 408 (1982).

[Ga92] P. E. Garret and D. G. Burke, Nucl. Phys. **A550**, 1 (1992).

[Gi74] G. A. Gill, R. D. Gill, and G. A. Jones, Nucl. Phys. **A224**, 152 (1974).

[Go75] L. C. Gomes, M. Sc. thesis, Instituto de Física da Universidade de São Paulo (1975).

[Go93] L. C. Gomes, *"Estudo dos Primeiros Estados Coletivos de Isótopos de Rutênio"*, Tese de Doutoramento, Instituto de Física da Universidade de São Paulo (1993).

[Go96] L. C. Gomes, L. B. Horodynski-Matsushigue, T. Borello-Lewin, J. L. M. Duarte, J. Hirata, S. Salém Vasconcelos, and O. Dietzsch, Phys. Rev. C **54**, 2296 (1996) [Anexo 2.3].

[He87] R. Hertenberger *et al.*, Nucl. Inst. and Meth. **A258**, 201 (1987); H. Wessner *et al.*, Nucl. Inst. and Meth. **A286**, 175 (1990).

[Hi98] J. H. Hirata, S. Salém-Vasconcelos, M. J. Bechara, L. C. Gomes, and O. Dietzsch, Phys. Rev. C **57**, 76 (1998).

[Ho77] C. L. Hollas, K. A. Aniol, D. W. Gebbie, M. Borsaru, J. Nurzynski, and L. O. Barbopoulos, Nucl. Phys. **A276**, 1 (1977).

[Ho86] L. B. Horodynski-Matsushigue, T. Borello-Lewin, and O. Dietzsch, Phys. Rev. C **33** 1594 (1986) [Anexo 2.1].

[Ho87] L. B. Horodynski-Matsushigue e J. L. M. Duarte, Relatório do Departamento de Física Experimental, p. 187, IFUSP (1987).

[Ho89] L. B. Horodynski-Matsushigue, T. Borello-Lewin, and J. L. M. Duarte, *"Coulomb-Nuclear Interference in Inelastic Scattering of 21 MeV Alpha-*

Particles on $^{90,92}Zr$", in Proceedings of the International Nuclear Physics Conference - IUPAP (São Paulo, Brazil). Contributed Papers, Vol. 1, 307 (1989) [Anexo 2.2].

[Ho93] D. J. Horen, R. L. Auble, J. Gomez del Campo, G. R. Satchler, R. L. Varner, J. R. Beene, B. J. Lund, V. R. Brown, P. L. Anthony and V. A. Madsen, Phys. Rev. C **47**, 629 (1993).

[Ho96] D. J. Horen, G. R. Satchler, S. A. Fayans, and E. L. Trykov, Nucl. Phys. **A600**, 193 (1996).

[Ho99] L. B. Horodynski-Matsushigue, G. M. Ukita, T. Borello-Lewin, and J. L. M. Duarte, Phys. Rev. C **60**, 047301-1 (1999) [Anexo 2.5].

[Ho01] L. B. Horodynski-Matsushigue, C. L. Rodrigues, F. C. Sampaio, and T. Borello-Lewin, *"Is the* ^{100}Ru *vibrational?"*, em preparação.

[Im73] N. Imanishi, I. Fujiwara, and T. Nishi, Nucl. Phys. **A205**, 531 (1973).

[Is80] P. Van Isacker and G. Puddu, Nucl. Phys. **A348**, 125 (1980).

[Ka86] G. Kajrys, J. Dulong, P. Larivière, S. Pilotte, W. Del Bianco, and S. Monaro, Phys. Rev. C **34**, 1629 (1986).

[Kl75] W. Klamra and J. Rekstad, Nucl. Phys. **A243**, 395 (1975).

[Ko83] K. Koide, A. Bairrio Nuevo, H. Takai, B. Marechal, and O. Dietzsch, Nucl. Inst. and Meth. **215**, 177 (1983).

[Ku74] P. D. Kunz, programa DWUCK4, Colorado University (1974).

[La80] S. Landsberger, R. Lecomte, P. Paradis, and S. Monaro, Phys. Rev. C **21**, 588 (1980).

[Le98] S. Leenhart *et al.*, Il Nuovo Cimento **111**, 733 (1998).

[Lo74] J. M. Lohr and W. Haeberli, Nucl. Phys. **A232**, 381 (1974).

[Lu71] H. F. Lutz, D. W. Heikkinen, and W. Bartolini, Phys. Rev. C **4**, 934 (1971).

[Lu95] B. J. Lund, N. P. T. Bateman, S. Utku, D. J. Horen and G. R. Satchler, Phys. Rev. C **51**, 635 (1995).

[Ma75a] V. A. Madsen, V. R. Brown, and J. D. Anderson, Phys. Rev. C **12**, 1205 (1975).

[Ma75b] R. G. Markham and R. G. H. Robertson, Nucl. Inst. and Meth. **129**, 131 (1975).

[Ma91] A. Maino, A. Ventura, A. M. Bizzeti-Sona, and P. Blasi, Z. Phys. **A340**, 241 (1991).

[Me77] F. R. Metzger, Phys. Rev. C **16**, 597 (1977).

[Mu88] S. M. Mullins, D. L. Watson, and H. T. Fortune, Phys. Rev. C **37**, 587 (1988).

[Mu90] H. W. Müller, Nuclear Data Sheets **60**, 835 (1990).

[Ni79] H. Niizeki, S. Kageyama, T. Tamura, and Z. Matumoto, J. Phys. Soc. Japan **47**, 26 (1979).

[Ok95] S. Okubo, Phys. Rev. Lett. **74**, 2176 (1995).

[Op78] T. R. Ophel and A. Johnston, Nucl. Inst. and Meth. **157**, 461 (1978).

[Pa71] J. Y. Park and G. R. Satchler, Part. Nucl. **1**, 233 (1971).

[Pe74] C. M. Perey and F. G. Perey, Atomic Data and Nuclear Data Tables **17**, 1 (1974).

[Pe76] C. M. Perey and F. G. Perey, At. Data Nucl. Data Tables **17**, 1 (1976).

[Pu91] D. Pulino, G. M. Sipahi, G. M. Ukita, T. Borello-Lewin, L. B. Horodynski-Matsushigue, J. L. M. Duarte, W. G. P. Engel, and J. C. de Abreu, Revista Brasileira de Aplicações de Vácuo **10**, 87 (1991).

[Ra87] S. Raman, C. H. Malarkey, W. T. Milner, C. W. Nestor, and P. H. Stelson, At. Data Nucl. Data Tables **36**, 1 (1987).

[Ra89] S. Raman *et al.*, At. Data Nucl. Data Tables **42**, 1 (1989).

[Re75] Y. Rekstad, Nucl. Phys. **A247**, 7 (1975).

[Re77] J. Rekstad and P. O. Tjöm, J. Phys. G **3**, 411 (1977).

[Re80] A. C. Restler, J. B. Ball, and R. L. Auble, Nucl. Phys. **A346**, 371 (1980).

[Ro84] C. D. Van Rooden, D. Spaargaren, H. P. Blok, and J. Blok, Nucl. Phys. **A430**, 125 (1984).

[Ro86] L. H. Rosier, J. Jabbour, B. Ramstein, P. Avignon, and R. Tamisier, Nucl. Phys. **A453**, 389 (1986).

[Ro92] J. N. Roy, A. P. Majumder, and H. N. Sen Gupta, Phys. Rev. C **46**, 144 (1992).

[Ro01a] M. R. D. Rodrigues, T. Borello-Lewin, L. B. Horodynski-Matsushigue, J. L. M. Duarte, C. L. Rodrigues, M. D. L. Barbosa, G. M. Ukita, and G. B. da Silva, *"Neutron spectroscopic strength in ^{99}Ru(d,t) reaction"*, em preparção.

[Ro01b] C. L. Rodrigues, L. B. Horodynski-Matsushigue, J. L. M. Duarte, T. Borello-Lewin, M. R. D. Rodrigues, M. D. L. Barbosa, G. M. Ukita, and G. B. da Silva, *"Single particle strength in ^{100}Ru with the ^{99}Ru(d,p)*

reaction", em preparção.

[Ry87] D. Rychel, R. Gyufko, B. van Krüchten, M. Lahanas, P. Singh and C. A. Wiedner, Z. Phys. A **326**, 455 (1987).

[Sa83] G. R. Satchler, *Direct Nuclear Reactions* (Clarendon Press, Oxford, 1983).

[Se85] S. Sen, S. E. Darden, R. C. Luhn *et al.*, Phys. Rev. C **31**, 787 (1985).

[Si89] S. Sirota, J. L. M. Duarte, L. B. Horodynski-Matsushigue, and T. Borello-Lewin, *"Hexadepolar excitation in ^{100}Ru"*, Phys. Rev. C **40**, 1527 (1989).

[Si90] B. Singh and J. A. Sznes, Nuclear Data Sheets **60**, 1 (1990).

[Si00] G. B. da Silva, *"Espalhamento Inelástico de ^{6}Li por ^{100}Ru na Região ICN"*, Dissertação de Mestrado, Instituto de Física da Universidade de São Paulo (2000).

[Sp67] J. E. Spencer and H. A. Enge, Nucl. Inst. and Meth. **49**, 181 (1967).

[Sp89] R. H. Spear, Atomic Data and Nuclear Data Tables **42**, 55 (1989).

[St75] E. W. Stoub, R. A. Ristinen, and R. R. Sercely, Nucl. Inst. and Meth. **127**, 329 (1975).

[Ta93] I. Talmi, *Simple Models of Complex Nuclei* (Harwood, Switzerland, 1993).

[To73] F. Todd-Baker, T. H. Kruse, J. L. Mattews, and M. E. Williams, Part. Nucl. **5**, 29 (1973).

[Uk97] G. M. Ukita, T. Borello-Lewin, L. B. Horodynski-Matsushigue, J. L. M. Duarte, L. C. Gomes, and M. D. L. Barbosa, *"First Excited 2^+ and 3^- States in $^{94,98}Mo$: Predominance of the Proton Contribution"*, in Proceedings of the XX Brazilian Workshop on Nuclear Physics (World Scientific, Guaratinguetá, São Paulo, Brazil, 1997) 105-107.

[Uk01] G. M. Ukita, T. Borello-Lewin, L. B. Horodynski-Matsushigue, J. L. M. Duarte, and L. C. Gomes, Phys. Rev. C **64**, 014316-1 (2001) [Anexo 2.6].

[Va85] V. R. Vanin, A. Pássaro, and A. M. Pássaro, Phys. Rev. C **32**, 1349 (1985).

[Vo76] M. J. A. de Voigt, J. F. W. Jansen, F. Bruining, and Z. Sujkowski, Nucl. Phys. **A270**, 141 (1976).

[Wa78] T. Wada, Nucl. Phys. **A307**, 425 (1978).

[Wa92] D. L. Watson, S. M. Mullins, and H. T. Fortune, Phys. Rev. C **45**, 592 (1992).

[Wh86] C. S. Whisnant, K. D. Carnes, R. H. Castain, F. A. Rickey, G. S. Samudra, and P. C. Simms, Phys. Rev. C **34**, 443 (1986).

[Zh95] Y. M. Zhao and Y. Chen, Phys. Rev. C **52**, 1453 (1995).

Anexo 1.1

PHYSICAL REVIEW C VOLUME 38, NUMBER 2 AUGUST 1988

Level structure of ^{101}Ru from the ^{100}Ru(d,p) reaction

J. L. M. Duarte, L. B. Horodynski-Matsushigue, T. Borello-Lewin, and O. Dietzsch
Instituto de Física da Universidade de São Paulo, São Paulo, Brasil
(Received 2 October 1987)

Energy levels of ^{101}Ru have been studied by the ^{100}Ru$(d,p)^{101}$Ru reaction at an incident deuteron energy of 12 MeV. Outgoing particles were momentum analyzed by a magnetic spectrograph and detected in nuclear emulsion plates, with an energy resolution of 7.5 keV. A total of 68 levels up to 3.2 MeV excitation energy was identified, about two-thirds of them reported for the first time. Experimental angular distributions were compared to distorted-wave Born approximation predictions and reduced spectroscopic factors obtained. The total $l=2$ and 75% of $l=0$, 4, and 5 spectroscopic strengths were located. Attention is drawn to transitions to low-lying states in ^{101}Ru (below $E_{exc}=0.75$ MeV) with $l=3$ and $l=1$ character.

I. INTRODUCTION

The region of nuclei around $A=100$, in particular, the ruthenium isotopes, continues to attract attention, from both theoretical and experimental points of view, due to conflicting aspects revealed by the data when confronted with the simpler models. In fact, level energy systematics and decay properties of the lighter even ruthenium isotopes tend to follow a vibrational description, as revealed also by interacting boson approximation (IBA) calculations.[1,2] However difficulties have been found in describing the neighboring odd-A isotopes on the same footing. In particular, it was, until recently, not possible to account for the spreading in energy of levels which, according to the vibrational model, should belong to the same multiplet.[3,4]

Recently, predictions of a symmetric prolate rotor (with a variable moment of inertia) plus particle model, including Coriolis coupling, allowed the identification in ^{99}Ru of several particle-core multiplets,[5] with the correct γ-decay properties, due to the dominance of a particular value of core angular momentum R and quasiparticle parentage. In agreement with experiment, a lowering of the low spin members of the multiplets, especially those based on high-j-particle states, is predicted.

Very recently, Arias *et al.*[6] performed, for the Tc, Ru, Rh, and Pd isotopes, extensive calculations within the proton-neutron interacting boson-fermion approximation (IBFA-2) and, where comparison was made, not only level energy systematics, but also one-particle transfer spectroscopic strengths and electromagnetic properties could be satisfactorily reproduced.

From an experimental point of view, one-particle stripping reactions could help to put into evidence mainly those low spin members of the multiplets, not easily populated by (HI, $xn\gamma$) or even $(\alpha,xn\gamma)$ and (^{3}He,$xn\gamma$) reactions, through admixtures of the even-core ground-state components into the wave functions of these excited states of the odd nucleus. The nucleus ^{101}Ru has been the subject of γ-ray studies with $(\alpha,3n)$ (Refs. 7 and 8), (^{3}He,$2n$) (Ref. 8), and (α,n) (Ref. 9) reactions, and from the decay of ^{101}Rh^{m,g}.[4] On the other hand, a previous (d,p) work[10] covered an excitation energy range of only 1.9 MeV with an energy resolution of 25 keV. In the present experiment the ^{100}Ru$(d,p)^{101}$Ru reaction has been studied with better resolution to provide a detailed determination of the level spectrum and spectroscopic strengths in ^{101}Ru. A wider range of excitation energies than in the previous (d,p) study[10] has been covered, several new energy levels have been detected, and definite values of l have been assigned to a larger number of transitions.

II. EXPERIMENTAL PROCEDURE

Angular distributions and absolute cross sections for the (d,p) reaction on targets enriched to 97.2% in ^{100}Ru were measured with 12-MeV deuterons from the tandem Pelletron accelerator of the University of São Paulo. The scattered protons were detected with nuclear emulsion plates (Kodak type NTB 50 μm thick) placed in the focal surface of an Enge split-pole magnetic spectrograph. Aluminum foils, thick enough to absorb heavier reaction products, covered the emulsion. The total number of incident deuterons was determined by a current integrator, which measured the charge collected in a Faraday cup with electron suppression. Elastically scattered deuterons detected at 41.5° by a surface barrier position sensitive detector placed in the focal surface of the spectrograph provided the absolute normalization, obtained from the deuteron elastic cross section given by an optical model prediction using the potential parameters shown in Table I. The uncertainty in the absolute cross section scale is estimated to be ±15%, taking into account an uncertainty of ±10%, due to different optical model predictions for the elastic cross section and an uncertainty of ±10%, from the nonuniformity of the targets.

Targets were made by evaporation[11] of metallic ruthenium powder onto thin carbon backings. The thicknesses of the three different uniform ruthenium films used

TABLE I. Bound-state and optical model parameters used in DWBA calculations.

	Deuteron[a]	Bound neutron	Proton[b]
V (MeV)	97.32	[c]	$60.87-0.32E_p$
r_0 (fm)	1.15	1.17	1.17
a_0 (fm)	0.81	0.75	0.75
$V_{s.o.}$ (MeV)	7.0	$\lambda_{s.o.}=25$	6.2
$r_{s.o.}$ (fm)	0.75		1.01
$a_{s.o.}$ (fm)	0.50		0.75
W (MeV)	0		$0.22E_p-2.7$
r_W (fm)	0		1.32
a_W (fm)	0		0.60
W_D (MeV)	17.28		$13.34-0.25E_p$
r_D (fm)	1.34		1.32
a_D (fm)	0.68		0.60
r_C (fm)	1.30		1.25

[a]From Refs. 15 and 16.
[b]From Ref. 17.
[c]Adjusted to reproduce the neutron binding energy.

during this experiment were around 20 μg/cm^2.

The protons produced in the reaction were observed at seven angles, from 10° to 68°, and the exposed plates were scanned in steps of 0.2 mm along the plate. An energy resolution [full width at half maximum (FWHM)] of 7.5 keV was achieved. The spectrum obtained at a laboratory scattering angle of 52° is shown in Fig. 1 and can be regarded as typical of the spectra measured at other angles. Peaks corresponding to transitions to levels of ^{101}Ru are numbered, the ground-state group being labeled by zero. The inset in Fig. 1 shows the region of levels 2 and 3 scanned with higher magnification and in smaller steps. The identification of peaks corresponding to states in ^{101}Ru was made following the procedures described in detail elsewhere.[12]

III. RESULTS

The excitation energies shown in Table II are the average of the energies obtained from the spectra, making use of the calibration of the spectrograph.[13] Deviations of individual energy determinations and the mean were in most cases lower than 3 keV. Reported in Table II are the levels clearly detected at at least four different angles. Also shown in Table II are the results of Hollas *et al.*[10] from a study of the same reaction at 11.5 MeV with a resolution of 25 keV. The adopted levels of ^{101}Ru in the compilation of Blachot[14] are also reproduced in Table II. A comparison of the level energies obtained in the present work with the energies reported by Blachot[14] shows a good agreement. Differences with the measurements of γ-decay work[14] are typically less than 2 keV.

The experimental angular distributions, for those transitions for which at least five points were measured, are shown in Figs. 2 and 3. The error bars include contributions of statistical deviations and uncertainties due to plate scanning, background subtraction, and relative normalization.

The angular distributions were compared with predictions of distorted-wave Born approximation (DWBA) calculations, with corrections to include finite range and

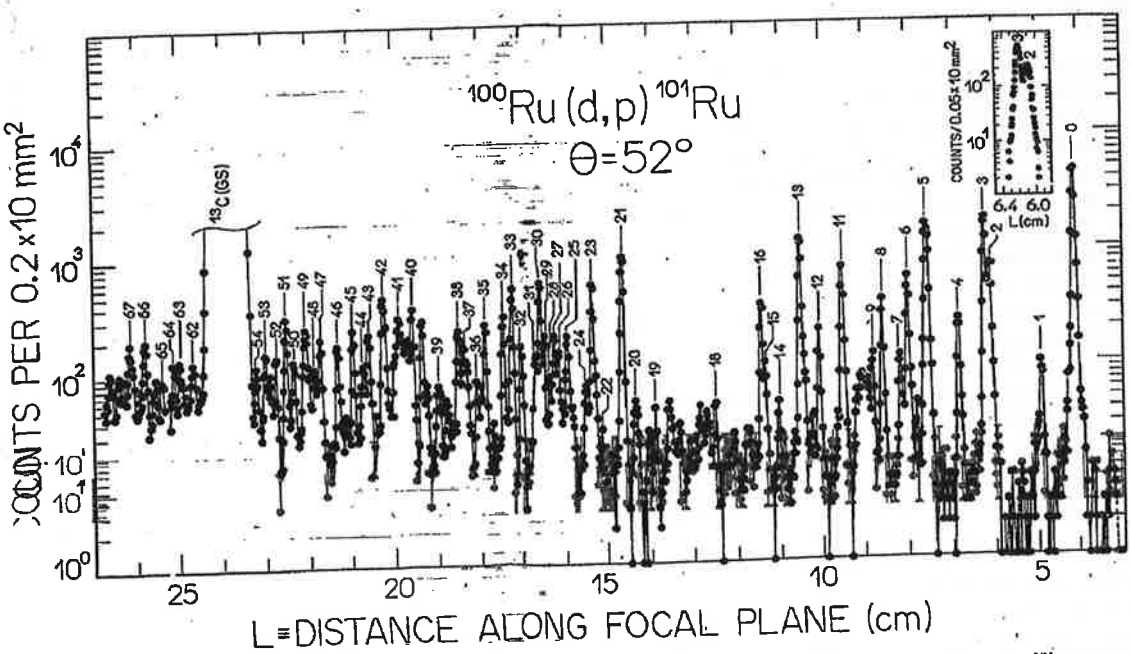

FIG. 1. Proton spectrum from the ^{100}Ru$(d,p)^{101}$Ru reaction at $\theta_{lab}=52°$. Peaks corresponding to transitions to ^{101}Ru levels are labeled with the numbers used in Table II. The inset shows the region of levels 2 and 3 scanned with higher magnification and smaller steps.

TABLE II. Summary of the results for ^{101}Ru from the ^{100}Ru(d,p) reaction and comparison with previous experiments. Assignments given in parentheses are tentative.

	Present work					Hollas *et al.*[a]				Nuclear data[b]	
Level number	E_{exc} (MeV)	$[\sigma_{exp}(\theta)]^{c}_{max}$ (mb/sr)	l	j	S'_{lj}	E_{exc} (MeV)	l	j	S'_{lj}	E_{exc} (MeV)	J^{π}
0	0.000	2.7±0.2	2	$\frac{5}{2}$	2.10	0.000	2	$\frac{5}{2}$	2.09	0.000	$\frac{5}{2}^+$
1	0.127	0.071±0.006	2	$\frac{3}{2}$	0.067	0.127	2	$\frac{1}{2}$	0.08	0.12723	$\frac{3}{2}^+$
2	0.307	0.49±0.14	4	$\frac{7}{2}$	5.3					0.30685	$\frac{7}{2}^+$
										0.31134	$\frac{5}{2}^+, \frac{3}{2}^+$
3	0.326	4.2±0.3	0	$\frac{1}{2}$	0.96	0.325	0	$\frac{1}{2}$	1.30	0.32515	$\frac{1}{2}^+$
										0.3441	
4	0.421	0.19±0.05	2	$\frac{3}{2}$	0.15	0.408	2	$\frac{3}{2}$	0.20	0.4221	$\frac{3}{2}^+$
										0.4623	
			5	$\frac{11}{2}$	5.8					0.5275	$\frac{11}{2}^-$
5	0.533	1.08±0.06[d]	2	$\frac{5}{2}, \frac{3}{2}$	0.72, 0.75	0.535	2	$\frac{5}{2}, \frac{3}{2}$	0.85, 1.03	0.535	$(\frac{5}{2}^+, \frac{3}{2}^+)$
										0.54508	$\frac{7}{2}^+$
6	0.597	0.59±0.05	3	$\frac{7}{2}, \frac{5}{2}$	0.60, 0.74	0.599	4	$\frac{7}{2}$	3.62	0.5983	
										0.6163	$(\frac{7}{2}^+)$
										0.6234	$(\frac{7}{2}^+)$
7	0.622	0.26±0.02	0	$\frac{1}{2}$	0.063	0.625	0	$\frac{1}{2}$	0.09	0.6235	$\frac{1}{2}^+$
										0.6438	
8	0.685	0.25±0.02	2	$\frac{5}{2}, \frac{3}{2}$	0.17, 0.18	0.684	0+2	$\frac{1}{2}, \frac{3}{2}$	0.03, 0.15	0.684	
9	0.718	0.065±0.010	1	$\frac{3}{2}, \frac{1}{2}$	0.017, 0.018	0.714					
										0.7200	$\frac{9}{2}^+$
10	0.742	0.055±0.010									
11	0.823	0.53±0.03	2	$\frac{5}{2}, \frac{3}{2}$	0.40, 0.43	0.827	2	$\frac{5}{2}, \frac{3}{2}$	0.39, 0.46	0.827	
										0.84278	$(\frac{7}{2}^+)$
12	0.908	0.26±0.02	1	$\frac{3}{2}, \frac{1}{2}$	0.057, 0.060	0.910					
										0.92872	$(\frac{7}{2}^+, \frac{9}{2}^+$
										0.93847	$(\frac{7}{2}^+)$
										0.9586	$(\frac{15}{2}^-)$
13	0.972	0.88±0.06	2	$\frac{5}{2}, \frac{3}{2}$	0.63, 0.70	0.976	2	$\frac{5}{2}, \frac{3}{2}$	0.59, 0.71	0.9734	$(\frac{5}{2}^+, \frac{3}{2}^+)$
										1.0012	$\frac{11}{2}^+$
14	1.051	0.026±0.005	4	$\frac{7}{2}$	0.28						
15	1.098	0.23±0.04	0	$\frac{1}{2}$	0.028						
16	1.112	0.81±0.05	0	$\frac{1}{2}$	0.17	1.110	0	$\frac{1}{2}$	0.19	1.110	$\frac{1}{2}^+$
										1.2068	
										1.2190	
17	1.227	0.14±0.04	0	$\frac{1}{2}$	0.016						
18	1.268	0.031±0.008	2	$\frac{5}{2}, \frac{3}{2}$	0.019, 0.022						
										1.3215	$(\frac{11}{2}^+)$
19	1.501	0.56±0.010								1.3899	
										1.4993	
20	1.544	0.074±0.026								1.5010	$\frac{13}{2}^+$
21	1.584	0.75±0.04	2	$\frac{5}{2}, \frac{3}{2}$	0.45, 0.50	1.588	2	$\frac{5}{2}, \frac{3}{2}$	0.38, 0.46	1.5873	$(\frac{5}{2}^+)$
										1.6223	$(\frac{19}{2}^-)$
22	1.659	0.022±0.005									
23	1.689	0.26±0.03	5	$\frac{11}{2}$	3.7	1.695	5	$\frac{11}{2}$	2.14	1.695	$(\frac{11}{2}^-, \frac{9}{2}^-)$
24	1.714	0.057±0.008	0	$\frac{1}{2}$	0.012						
										1.7618	
										1.7743	$(\frac{13}{2}$ to $\frac{19}{2})$
25	1.779	0.130±0.014	1	$\frac{3}{2}, \frac{1}{2}$	0.027, 0.028						
26	1.813	0.10±0.02	2	$\frac{5}{2}, \frac{3}{2}$	0.064, 0.068						
27	1.825	0.13±0.02	2	$\frac{5}{2}, \frac{3}{2}$	0.075, 0.081	1.825	2	$\frac{5}{2}, \frac{3}{2}$	0.13, 0.16	1.825	$(\frac{5}{2}^+, \frac{3}{2}^+)$
28	1.842	0.08±0.02	2	$\frac{5}{2}, \frac{3}{2}$	0.041, 0.043					1.8434	
29	1.861	0.29±0.03	0	$\frac{1}{2}$	0.062						

TABLE II. (*Continued.*)

Level number	Present work E_{exc} (MeV)	$[\sigma_{exp}(\theta)]^c_{max}$ (mb/sr)	l	j	S'_{lj}	Hollas *et al.*[a] E_{exc} (MeV)	l	j	S'_{lj}	Nuclear data[b] E_{exc} (MeV)	J^π
										1.8622	$\frac{15}{2}^+$
30	1.878	0.44±0.03	2	$\frac{5}{2}$, $\frac{3}{2}$	0.25, 0.27	1.875	2	$\frac{5}{2}$, $\frac{3}{2}$	0.38, 0.46	1.875	$(\frac{3}{2}^+, \frac{5}{2}^+)$
31	1.893	0.12±0.03									
32	1.936	0.26±0.02	0	$\frac{1}{2}$	0.061						
										1.9615	
33	1.969	0.35±0.02	2	$\frac{5}{2}$, $\frac{3}{2}$	0.20, 0.21						
34	1.997	0.21±0.02	2	$\frac{5}{2}$, $\frac{3}{2}$	0.12, 0.13						
										2.0175	$(\frac{13}{2}$ to $\frac{19}{2})$
35	2.057	0.33±0.03	0	$\frac{1}{2}$	0.076						
										2.0634	
36	2.087	0.05±0.01									
37	2.133	0.14±0.02	1	$\frac{3}{2}$, $\frac{1}{2}$	0.037, 0.039						
38	2.147	0.22±0.02	(1)	$(\frac{3}{2})$, $(\frac{1}{2})$	(0.043), (0.046)						
										2.1740	$\frac{17}{2}^+$
39	2.218[e]	0.075±0.009								2.2229	$(\frac{11}{2}$ to $\frac{19}{2})$
40	2.299	0.16±0.06	2	$\frac{5}{2}$, $\frac{3}{2}$	0.098, 0.105						
41	2.348	0.10±0.01	(1)	$(\frac{3}{2})$, $(\frac{1}{2})$	(0.020), (0.021)					2.3459	
										2.3772	
42	2.404[f]	0.44±0.04	2	$\frac{5}{2}$, $\frac{3}{2}$	0.20, 0.23						
43	2.443	0.22±0.02	2	$\frac{5}{2}$, $\frac{3}{2}$	0.09, 0.10						
44	2.459	0.05±0.01	(3)	$(\frac{7}{2})$, $(\frac{5}{2})$	(0.042), (0.056)						
										2.4732	$(\frac{32}{2}^-)$
45	2.493	0.14±0.03	2	$\frac{5}{2}$, $\frac{3}{2}$	0.063, 0.072						
46	2.544	0.12±0.03									
47	2.600	0.14±0.02	3	$\frac{7}{2}$, $\frac{5}{2}$	0.12, 0.14						
48	2.624	0.12±0.02									
49	2.654[e]	0.22±0.02									
50	2.694	0.08±0.01	2	$\frac{5}{2}$, $\frac{3}{2}$	0.038, 0.042						
										2.7979	$(\frac{21}{2}^+)$
51	2.718	0.22±0.02	1	$\frac{3}{2}$, $\frac{1}{2}$	0.046, 0.049						
52	2.752	0.09±0.01									
53	2.784	0.15±0.03	3	$\frac{3}{2}$, $\frac{1}{2}$	0.026, 0.027						
54	2.815	0.08±0.02									
55	2.844	0.14±0.02	(3)	$(\frac{7}{2})$, $(\frac{5}{2})$	(0.10), (0.11)						
										2.8236	$\frac{19}{2}^+$
56	2.867	0.13±0.04[h]									
57	2.881									2.8853	
58	2.901	0.06±0.01									
59	2.918	0.15±0.04									
60	2.931	0.14±0.02									
61	2.977	0.08±0.02								2.9842	
62	3.019	0.15±0.02								3.0520	$(\frac{15}{2}$ to $\frac{23}{2})$
63	3.065	0.16±0.02									
64	3.083	0.18±0.06									
65	3.120	0.06±0.02									
66	3.173	0.13±0.02									
67	3.228	0.24±0.02	0	$\frac{1}{2}$	0.031						

[a]Reference 9.
[b]Reference 13.
[c]Maximum cross section measured.
[d]Integrated cross section ($l=5+l=2$).
[e]Possible doublet.
[f]Doublet.
[h]Integrated cross section (levels 56 and 57).

nonlocality effects, performed by means of the code DWUCK4.[15] The correction parameters employed were $R_{FR}=0.62$ fm, $\beta_d=0.54$ fm, $\beta_p=0.85$ fm. The optical model parameters for the entrance and exit channels were taken from the analysis of Perey and Perey[16] for deuteron scattering, with the addition of a spin-orbit term suggested by Lohr and Haeberli[17] and from the analysis of Becchetti and Greenlees[18] for proton scattering. The captured neutron was assumed to be bound by a real potential well of Woods-Saxon shape plus a spin-orbit term. The calculations were performed supposing, as usual, that the bound neutron occupies an orbital near the Fermi surface. In the case of $l=1$ and $l=3$ transfers, orbitals $3p$ and $2f$, of the next major shell, were assumed. The parameters used are presented in Table I.

Fits to the angular distributions are shown in Figs. 2 and 3 in comparison with the data, whenever an assignment of transferred angular momentum l was attempted. The reduced spectroscopic factors S'_{lj} were extracted in the fitting procedures according to the relationship

$$\sigma_{\text{exp}}(\theta)=1.53S'_{lj}\frac{\sigma^{\text{DW}}_{lj}(\theta)}{2j+1} .$$

The values of S'_{lj} are related to the spectroscopic factor by

$$S'_{lj}=\frac{2J_f+1}{2J_i+1}S_{lj}=(2j+1)S_{lj} ,$$

where J_i $(=0)$ and J_f $(=j)$ are, respectively, the spins of the target and final nuclei.

The values obtained for l and S'_{lj} are shown in Table II.

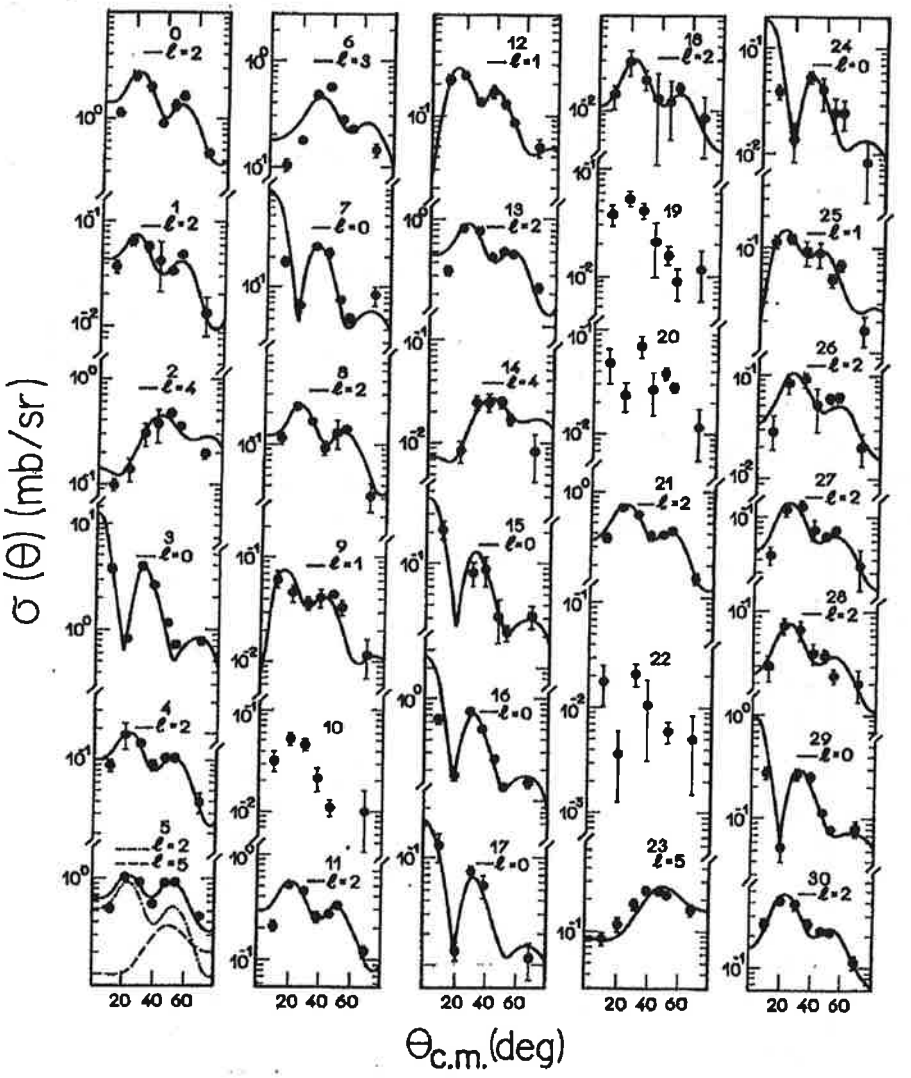

FIG. 2. Angular distributions of transitions in the ^{100}Ru$(d,p)^{101}$Ru reaction. The experimental points are given with error bars corresponding to statistics and uncertainties in plate scanning, background subtraction, and relative normalization. The solid lines are DWBA curves fitted to the experimental data.

If different global prescriptions, for the optical model parameters, are used in entrance[16,17,19] and exit[18,20] channels, a maximum variation of ±15% in the reduced spectroscopic factors occurs.

Transferred l values were extracted without ambiguities for levels below 2.0 MeV, except for levels numbered 6, 10, 19, 20, 22, and 31. The experimental angular distributions related to levels 10, 19, and 31 are similar, but their shape is not reproduced by one-step DWBA predictions, while those associated to levels 20 and 22 present no discernible structure. An $l=4$ attribution was attempted for the transition to the state at 0.597 MeV (No. 6), following Hollas *et al.*,[10] but the quality of the fit was poor when compared with other $l=4$ fits. On the other hand, this angular distribution is better reproduced by an $l=3$ transfer, especially if, as usual, emphasis is put on fitting the experimental points around the first forward-angle maximum of the cross section and its ensuing decrease. The criterium also took into account that, for the $l=2$ transfers in this excitation energy region, the data corresponding to the smallest angles lie systematically below the DWBA prediction. Figure 4 compares the quality of the $l=3$ and $l=4$ fits to both ^{100}Ru$(d,p)^{101}$Ru and ^{102}Ru$(d,t)^{101}$Ru reaction populating the state at 0.597 MeV. The pickup results, reproduced from Ref. 21, clearly characterize the transition as $l=3$. The fact that the authors of a recent (p,d) work[22] do not report a level at approximately 0.60 MeV is probably due to the poor resolution (24 keV) of these data. In their published spectrum the peak corresponding to the 0.623-MeV state presents, at the right position, a shoulder of appropriate magnitude, if compared to the (d,t) results.[21]

The transition to the state detected at 0.533 MeV (No. 5) reveals a predominant $l=2$ component, but there is a

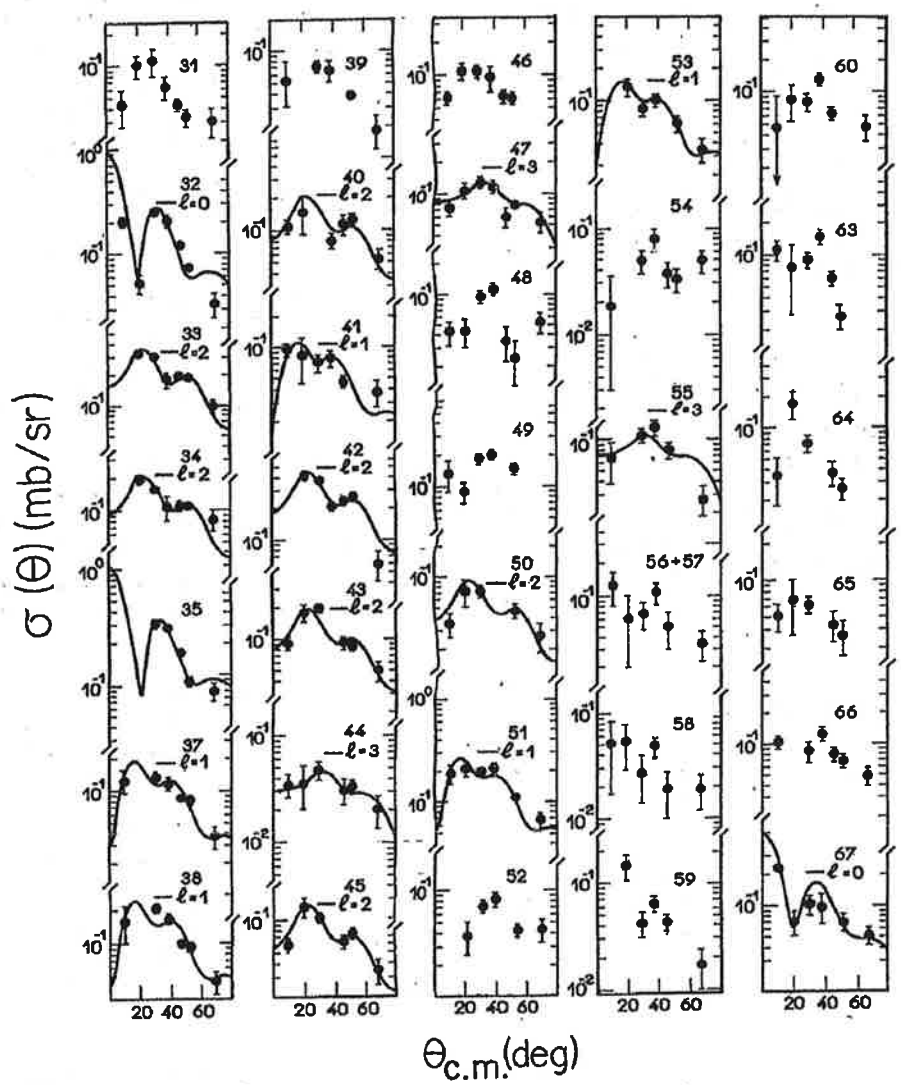

FIG. 3. ^{100}Ru$(d,p)^{101}$Ru angular distributions (see caption of Fig. 2).

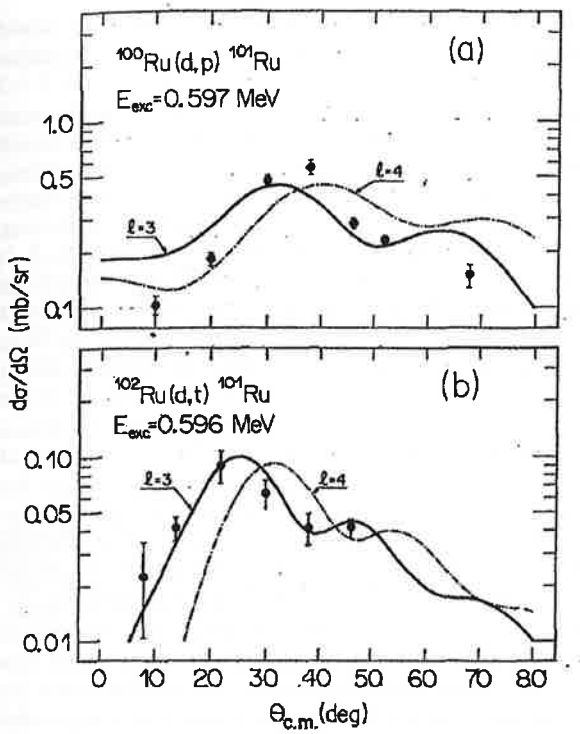

FIG. 4. (a) ^{100}Ru$(d,p)^{101}$Ru at 12 MeV, and (b) ^{102}Ru$(d,t)^{101}$Ru at 16 MeV, angular distributions corresponding both to the same 0.597-MeV final state. The curves are DWBA predictions for $l=3$ and $l=4$ transfers. (b) is reproduced from Ref. 21.

clear necessity to consider an $l=5$ contribution corresponding to the known $\frac{11}{2}^-$ level at 0.5275 MeV. The spectroscopic factors of the states involved were extracted by a least-squares fitting procedure.[23] The cross section at $\theta=10°$ for state No. 8 excludes contributions from an $l=0$ component, in disagreement with Hollas *et al.*[10]

Above 1.9 MeV most of the levels reported here have been seen for the first time. For levels 35 to 39 the carbon contamination of the spectrum at 20°, where a minimum of the cross section for an $l=0$ transfer is expected, is an impairment to the distinction between $l=0$ and $l=1$ transfers. Due to the overall fit for levels 35 and 37, $l=0$ and $l=1$ attributions, respectively, were preferred. For level 38 the $l=1$ value is tentative.

The values of the reduced spectroscopic factors are in good agreement with those published by Hollas *et al.*,[10] whenever a comparison can be made. An exception is the $l=5$ level at $E_{exc}=1.689$ MeV, where the discrepancy amounts to a factor 1.7. Due to the low excitation probability of states reached by $l=5$ transfer, this discrepancy is not incompatible with the experimental errors in the data and the uncertainties in the DWBA predictions for different optical potentials.

IV. DISCUSSION AND CONCLUSIONS

The distribution of the reduced spectroscopic factor S'_{lj} associated to a given l value is presented in Fig. 5 as a function of excitation energy. Only levels with a reliable l value attribution were included. For the detected $l=2$ spectroscopic strength there is a concentration of intensity corresponding to the known $\frac{5}{2}^+$ ground state (g.s.) and a spreading among many levels. The intensity of this strongest transition is consistent with the presence of two $2d_{5/2}$ neutron holes in the g.s. of ^{100}Ru. For the other $l=2$ transitions a $d_{3/2}$ character was arbitrarily assumed. The spectroscopic strength thus associated to the $d_{3/2}$ orbital is heavily fragmented with components extending up to 2.7 MeV of excitation. In the case of $l=0$ transitions, there is also an experimental fragmentation, but one level alone is responsible for 66% of the detected spectroscopic strength. Most of the $l=0$ and $l=2$ strengths were already located by Hollas *et al.*[10] The detected strength for $l=4$ transitions is almost totally (95%) concentrated in the state at 0.307 MeV, which was not detected by Hollas *et al.*,[10] probably due to lack of resolution in presence of the intense $l=0$ state at 0.325 MeV. Only two levels reached by $l=5$ transfers were seen. A small fragmentation for the $l=5$ strength is thus observed, since the limit of detection corresponds, in this case, approximately to $S'=0.6$.

The present experiment locates the total $l=2$ and 72% of the $l=0$ strengths, relative to the sum-rule limits. In the case of $l=4$ and $l=5$, respectively, 70% and 79% of the total spectroscopic strengths were detected, if restricted to the shell 50–82. Transitions with $l=1$ and

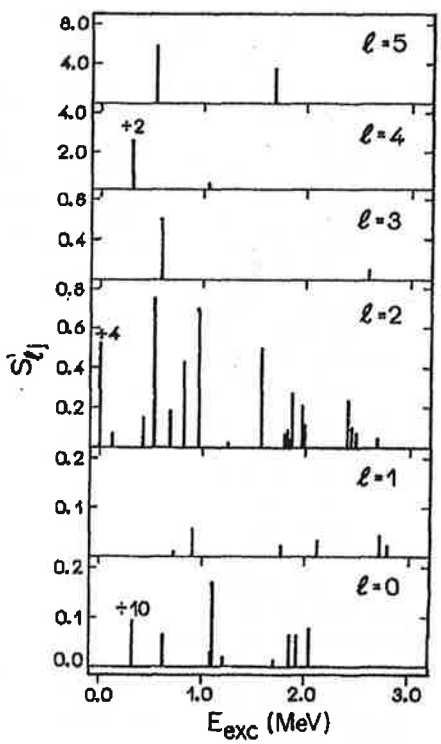

FIG. 5. Reduced spectroscopic factors obtained for all states reached by the same l transfer, as a function of excitation energy.

$l=3$ character were observed, and only lower limits of $\sum S'$ were obtained. Weak $l=1$ transitions were located below 2.8 MeV and are spread in a 2-MeV interval. For the $l=3$ transfer, on the other hand, 83% of the detected strength is carried by one state at 0.597 MeV.

Arias *et al.*[6] present a comparison of spectroscopic strengths below 1.0 MeV for $3s_{1/2}$, $1g_{7/2}$, $2d_{5/2}$, and $2d_{3/2}$ transfers in ^{100}Ru$(d,p)^{101}$Ru, as predicted by their IBFA-2 calculations, in comparison with the results of Hollas *et al.*[10] The very satisfactory agreement with experiment would perhaps be even better if the present results were taken, since the low-lying $l=4$ strength is now clearly located 0.30 MeV below the former attribution.

It is believed that the distribution of the neutron single-particle strengths among levels in ^{101}Ru, up to approximately 3.2 MeV of excitation, is now quite well established. The same experimental detail is not available for the other odd ruthenium isotopes. However, general features emerge from previous (d,p) reaction studies on ^{96}Ru (Refs. 10 and 24), ^{102}Ru (Refs. 25 and 26), and ^{104}Ru (Refs. 25 and 27). In each isotope, the strongest $l=2$ transition populates the lowest $\frac{5}{2}^+$ state and a heavy fragmentation of the remaining $l=2$ strength is observed. All the referred isotopes are found to have a strong low-lying $\frac{1}{2}^+$ state with much weaker $l=0$ strength distributed among higher excited states. A very light fragmentation is observed for the $l=4$ and $l=5$ strengths. Transitions of $l=1$ character were, up to now, reported only in the present reaction and in ^{104}Ru$(d,p)^{105}$Ru (Refs. 25 and 27), while low-lying $l=3$ strengths have been observed in ^{101}Ru and ^{103}Ru (Refs. 25 and 26), concentrated in single transitions, and in ^{105}Ru (Ref. 27), possibly split.

Negative parity states, based on the single particle orbital $h_{11/2}$, are expected in the mass region of the Ru isotopes. The simpler models, however, are not able to reproduce important experimental results. For instance, it is not evident how to bring $l=3$ and $l=1$ single-particle strengths, from the next shell down to within hundreds of keV from the ground states. Recently, Whisnant *et al.*[5] coupling the quasiparticle to a symmetric, slightly deformed prolate rotor were able to reproduce some vibrational-like features for ^{99}Ru. In particular, the calculations[5] characterized a multiplet associated to the dominant $R=2$ core excitation and $1h_{11/2}$ quasiparticle and predicted it to be spread through an 1.2-MeV interval, in good accordance with experiment. The lowest-lying member is the $\frac{7}{2}^-$ state at 1.105 MeV, in correspondence with the experimental level at 1.290 78 MeV. However, previous calculations[28,29] for the heavier ^{101,103}Ru isotopes, based on the same model, did not put a multiplet structure into evidence and present considerable differences in the predictions for ^{103}Ru. These differences may possibly be due to the consideration of an oblate core deformation for negative parity states and the neglect of part of the recoil term[29] in the calculations by Imanishi *et al.*[28] For ^{101}Ru only the results of Imanishi *et al.*[28] are available and no theoretical negative parity state, besides the $\frac{11}{2}^-$ at 0.529 MeV, is presented below 1.0 MeV.

As already pointed out, through admixtures of $R=0$ components into predominantly $R>0$ states, these could be accessible to one-particle transfer reactions. In particular, the low-lying $\frac{7}{2}^-$ levels would be seen as $l=3$ transfers in (d,p). In fact, in ^{103}Ru the experimental counterpart of the theoretical state[29] at 0.191 MeV could be the level at 0.297 MeV populated by an $(l=3)$ transition,[25,26] with a spectroscopic strength which is in agreement with the prediction.[29] Considering the lowest-lying levels populated by $l=3$, for the various isotopes, it is verified that, in going from ^{105}Ru to ^{101}Ru, their energy follows closely the increase in energy of the $\frac{11}{2}^-$ states with the strongest $l=5$ spectroscopic strengths. In ^{99}Ru, this trend would point to the level at 1.290 78 MeV, identified by Whisnant *et al.*[5] as the $\frac{7}{2}^-$ member of the $R\simeq 2$ multiplet. For ^{101}Ru the suggested accordance with the model would thus locate the $\frac{7}{2}^-$ member at 0.597 MeV. Similar considerations[30] could account for the presence of low-lying $l=1$ strength, through the contribution of $R=4$ dominant core components, resulting in the presence of $J^\pi=\frac{1}{2}^-$ states. In fact, in the recent calculation of Arias *et al.*,[6] besides the low-lying $\frac{7}{2}^-$ states, which deserved special remarks, $\frac{3}{2}^-$ states were predicted, at about 1 MeV in each isotope above the lowest $\frac{11}{2}^-$ level. In this paper[6] IBFA-2 calculations for $A\simeq 100$ nuclei were performed in a systematic way, considering the transition from SU(5) to O(6) symmetries. Arias *et al.*[6] found it necessary to include contributions of the $2f_{7/2}$ and $1h_{9/2}$ orbitals into their fermion space to match the properties of the negative parity states for which, unfortunately, no theoretical one-particle transfer strengths were published. Both approaches,[5,6] though starting from different theoretical ingredients, are thus equally able to predict important experimental evidences in the Ru isotopes. In particular, negative parity states lying relatively close in energy to the lowest $\frac{11}{2}^-$ levels seem now clearly interpreted as $\frac{7}{2}^-$, resulting essentially from the coupling of the 2_1^+ core state (which may have different descriptions) to an $1h_{11/2}$ quasiparticle.

Though the picture presented seems tempting, there are other experimental results,[9,31,32] some of them also recent, which are in possible contradiction to the mentioned $\frac{7}{2}^-$ attributions in ^{101,103,105}Ru. Kajrys and coworkers,[9,31] in $(\alpha,n\gamma)$ experiments populate the levels here interpreted as $\frac{7}{2}^-$, at 0.598 MeV in ^{101}Ru and at 0.297 MeV in ^{103}Ru, and assign to both spin and parity $\frac{3}{2}^+$. The corresponding level in ^{101}Ru was not reported by Klamra *et al.*[8] in their $(\alpha,3n\gamma)$ and $(^3\text{He},2n\gamma)$ studies. In the case of ^{103}Ru, on the other hand, the result of Kajrys *et al.*[31] would supersede the $\frac{7}{2}^-$ attribution to the 0.297-MeV level made by Klamra and Rekstad,[33] based on experimental information extracted from the same reaction with more complete excitation function measurements. It is felt that, taking into account the usual difficulties[33] in spin and parity attribution through that kind of analysis, the measurements of Kajrys and coworkers[9,31] certainly do not exclude a $\frac{5}{2}^-$ attribution, although a $\frac{7}{2}^-$ may be more difficult to sustain. It is to be remembered that the $l=3$ transfer characterized by the present experiment would not be in disagreement with

$J^{\pi}=\frac{5}{2}^-$ for the 0.598-MeV state. Also, for ^{105}Ru, the analysis of all the available information led de Frenne *et al.*[32] to make a $(\frac{5}{2}^-,\frac{3}{2})$ assignment for the lowest-lying level reached by $l=(3)$ in the (d,p) reaction.[27] A $\frac{7}{2}^-$ attribution is, in this case, improbable if a misassignment or a doublet structure are excluded, in face of the γ feeding pattern exhibited.

A theoretical counterpart for such low-energy $\frac{5}{2}^-$ levels would be difficult to find within the framework of the models discussed.[5,6] The connection between the odd and even Ru nuclei may, however, be considerably more complicated than supposed by these models.[5,6] In fact, in exploring the properties of the $\frac{5}{2}^+$ g.s. of ^{101}Ru through one neutron pickup reactions,[34,23] this state was found to be strongly related, through $l=2$ transfers, to levels of the even core at excitation energies above 2.2 MeV, not usually considered important core states in the calculations.[5,6]

ACKNOWLEDGMENTS

We are grateful to D. R. Bès and C. L. Lima for stimulating and helpful discussions. This work was partially supported by Fundação de Amparo à Pesquisa do Estado de São Paulo (FAPESP), Conselho Nacional de Desenvolvimento Científico e Tecnológico (CNPq), and Financiadora de Estudos e Projetos S. A. (FINEP).

[1]J. Stachel, P. Van Isacker, and K. Heyde, Phys. Rev. C **25**, 650 (1982).
[2]P. Van Isacker and G. Puddu, Nucl. Phys. **A348**, 125 (1980).
[3]S. Bhattacharaya and S. K. Basu, Phys. Rev. C **18**, 2765 (1978).
[4]V. R. Vanin, A. Pássaro, and A. M. Pássaro, Phys. Rev. C **32**, 1349 (1985).
[5]C. S. Whisnant, K. D. Carnes, R. H. Castain, F. A. Rickey, G. S. Samudra, and P. C. Simms, Phys. Rev. C **34**, 443 (1986).
[6]J. M. Arias, C. E. Alonso, and M. Lozano, Nucl. Phys. **A466**, 295 (1987).
[7]C. M. Lederer, J. M. Jaklevic, and J. M. Hollander, Nucl. Phys. **A169**, 489 (1971).
[8]W. Klamra, K. Fransson, B. Sundström, M. Brenner, S. Engman, and R. Kvarnstrom, Nucl. Phys. **A376**, 463 (1982).
[9]G. Kajrys, R. Lecomte, S. Landsberger, and S. Monaro, Phys. Rev. C **28**, 1504 (1983).
[10]C. L. Hollas, K. A. Aniol, D. W. Gebbie, M. Borsaru, J. Nurzynski, and L. O. Barbopoulos, Nucl. Phys. **A276**, 1 (1977).
[11]K. Koide, F. C. Sampaio, E. M. Takagui, J. H. Hirata, and O. Dietzsch, Nucl. Instrum. **215**, 61 (1983).
[12]T. Borello-Lewin, C. Q. Orsini, O. Dietzsch, and E. W. Hamburger, Nucl. Phys. **A249**, 284 (1975).
[13]E. R. Cruz, M. Sc. thesis, Instituto de Física da USP, São Paulo, Brasil, 1978; this calibration was supplemented by data on ^{90}Zr(α,α') up to 5.9 MeV of excitation energy.
[14]J. Blachot, Nucl. Data Sheets **45**, 701 (1985).
[15]P. D. Kunz (unpublished).
[16]C. M. Perey and F. G. Perey, Phys. Rev. **132**, 755 (1963).
[17]J. M. Lohr and W. Haeberli, Nucl. Phys. **A232**, 381 (1974).
[18]F. D. Becchetti Jr. and G. W. Greenlees, Phys. Rev. **182**, 1190 (1969).
[19]W. W. Daehnick, J. D. Childs, and Z. Vrcelj, Phys. Rev. C **21**, 2253 (1980).
[20]F. G. Perey, Phys. Rev. **131**, 745 (1963).
[21]F. C. Sampaio, J. L. M. Duarte, L. B. Horodynski-Matsushigue, T. Borello-Lewin, and O. Dietzsch, Proceedings of the International Conference on Nuclear Structure, Amsterdam, 1982. Vol. 1, p. 54; (to be published).
[22]S. A. Dickey, J. J. Krausbaar, and M. A. Rumore, J. Phys. G **12**, 745 (1986).
[23]F. C. Sampaio, M. Sc. thesis, Instituto de Física da USP, São Paulo, Brasil, 1981.
[24]L. R. Medsker, L. H. Fry Jr., and J. L. Yntema, Phys. Rev. C **15**, 649 (1977).
[25]H. T. Fortune, G. C. Morrison, J. A. Nolen, Jr., and P. Kienle, Phys. Rev. C **3**, 337 (1971).
[26]G. P. A. Berg, M. Demarteau, A. Hardt, W. Hürlimann, S. A. Martin, J. Meissburger, W. Oelert, H. Seyfarth, B. Styczen, M. Köhler, I. Oelrich, and J. Scheerer, Nucl. Phys. **A379**, 93 (1982).
[27]P. Maier-Komor, P. Glässel, E. Huenges, H. Rösler, H. J. Scheerer, H. K. Vonach, and H. Baier, Z. Phys. **A278**, 327 (1976).
[28]N. Imanishi, I. Fujiwara, and T. Nishi, Nucl. Phys. **A205**, 531 (1973).
[29]J. Rekstad, Nucl. Phys. **A247**, 7 (1975).
[30]F. S. Stephens, Rev. Mod. Phys. **47**, 43 (1975).
[31]G. Kajrys, J. Dubuc, P. Larivière, S. Pilotte, W. del Bianco, and S. Monaro, Phys. Rev. C **34**, 1629 (1986).
[32]D. de Frenne, E. Jacobs, M. Verboven, and P. de Gelder, Nucl. Data Sheets **47**, 261 (1986).
[33]W. Klamra and J. Rekstad, Nucl. Phys. **A243**, 395 (1975).
[34]R. J. Peterson, R. A. Emigh, and R. E. Anderson, Nucl. Phys. **A348**, 8 (1980).

Anexo 1.2

PHYSICAL REVIEW C VOLUME 50, NUMBER 2 AUGUST 1994

Neutron-spectroscopic strength in Ru isotopes

J. L. M. Duarte, T. Borello-Lewin, and L. B. Horodynski-Matsushigue
Instituto de Física da Universidade de São Paulo, São Paulo, Brasil
(Received 22 February 1994)

A systematic, high resolution (6–8 keV) study of (d,t) reactions on ^{100,102,104}Ru is reported. Spectroscopic factors were extracted by comparison of experimental angular distributions with distorted wave Born approximation predictions. All of the information for ^{99}Ru and, for excitation energies above 0.9 MeV, for ^{103}Ru is new. Most of the strength expected for the 50–82 neutron shell was found. The strength distributions are discussed, also in comparison with the corresponding stripping reactions. Special attention is focused on extremely low and relatively intense $l = 3$ excitations and on the $l = 4$ transfer pattern observed.

PACS number(s): 25.45.Hi, 27.60.+j, 21.10.Jx

I. INTRODUCTION

The precise location of single particle and hole spectroscopic strengths is a powerful tool in pinning down nuclear structure properties, since the spreading pattern thus determined is a sensitive test on detailed model predictions [1,2]. In the spherical independent particle shell model the one particle or hole configuration is concentrated at a unique excitation energy. Any collective correlations tend to wash this feature out, in a way which is characteristic of the interactions considered [2,3]. Thus any sudden structure transition should, in particular, also be evidenced through an abrupt change in the particle and hole strength distributions. A survey of the literature reveals, however, that in the challenging region around the $A = 100$ nuclides [4] the information on these strengths is far from complete [5–7]. The interest in a precise and comparative study of, in particular, the Ru isotopes through transfer reactions was furthermore fostered by the discovery of an intense $l = 3$ transition at low excitation energy in the ^{100}Ru$(d,p)^{101}$Ru reaction measured by the USP Nuclear Emulsion Group [8]. The present paper refers to results obtained at the São Paulo spectrograph facility for the ^{100,102,104}Ru$(d,t)^{99,101,103}$Ru reactions, which located most of the hole spectroscopic strength in the odd isotopes.

II. EXPERIMENTAL PROCEDURE

The deuteron beam of the São Paulo Pelletron accelerator, with an incident energy of, respectively, 15.5 and 16.0 MeV, was focused on ^{100}Ru and ^{102,104}Ru enriched targets, after passing defining slits of 1.0×3.0 mm^2. Table I presents the isotopic compositions of the Ru metal used, in powder form, for target preparation in a well controlled electron bombardment evaporation technique [9,10]. The ejectiles of the reactions were momentum analyzed by the Enge split-pole spectrograph and detected in nuclear emulsion (Kodak NTB or NTA 50 μm thick). The careful determination of the focal plane of the respective reaction, the use of nuclear emulsions, uniform targets, adequate spectrograph objects, and also good accelerator characteristics, resulted in energy resolutions from 6 to 8 keV, almost determined by the intrinsic resolution of the spectrograph. The emulsion plates were scanned, after processing, in strips of 200 μm across the plates. Typical spectra for the three reactions are presented in Fig. 1.

Relative normalization of the spectra obtained at each angle was achieved by measuring the beam current in an aligned Faraday cup, with electron suppression, connected to a current integrator, while continuously monitoring the direction of the beam. Absolute normalization of the cross sections was referred to optical-model predictions for the elastic scattering of deuterons on the same target, measured under similar conditions. Three well-established families from the systematics of Perey and Perey (PP) [11], Lohr and Haeberli (LH) [12], and Daehnick *et al.* (DCV) [13] (see Table II) were employed and produced cross sections which differed in at most ±11%. Due, furthermore, to target nonuniformity, plate scanning, and statistics in the elastic scattering data, a maximum uncertainty of 15% is estimated for the absolute cross section scale.

The parameters identified as PP (with the spin orbit term taken from LH) were finally chosen for the absolute normalization of the cross sections and also to generate the distorted incident waves. The distorted wave Born approximation (DWBA) calculations were performed with the code DWUCK4 (Ref. [14]), with usual corrections to account for finite range and nonlocality effects. The outgoing triton channel was described by the optical-model parameters of the systematics by Becchetti

TABLE I. Isotopic composition of the targets.

	Composition specified by fabricant (ORNL)						
Target	^{96}Ru	^{98}Ru	^{99}Ru	^{100}Ru	^{101}Ru	^{102}Ru	^{104}Ru
^{100}Ru	0.05	0.05	0.54	97.24	1.20	0.83	0.19
^{102}Ru	0.02	0.01	0.07	0.09	0.24	99.35	0.22
^{104}Ru	0.02	0.02	0.08	0.13	0.27	3.14	96.39

0556-2813/94/50(2)/666(16)/$06.00

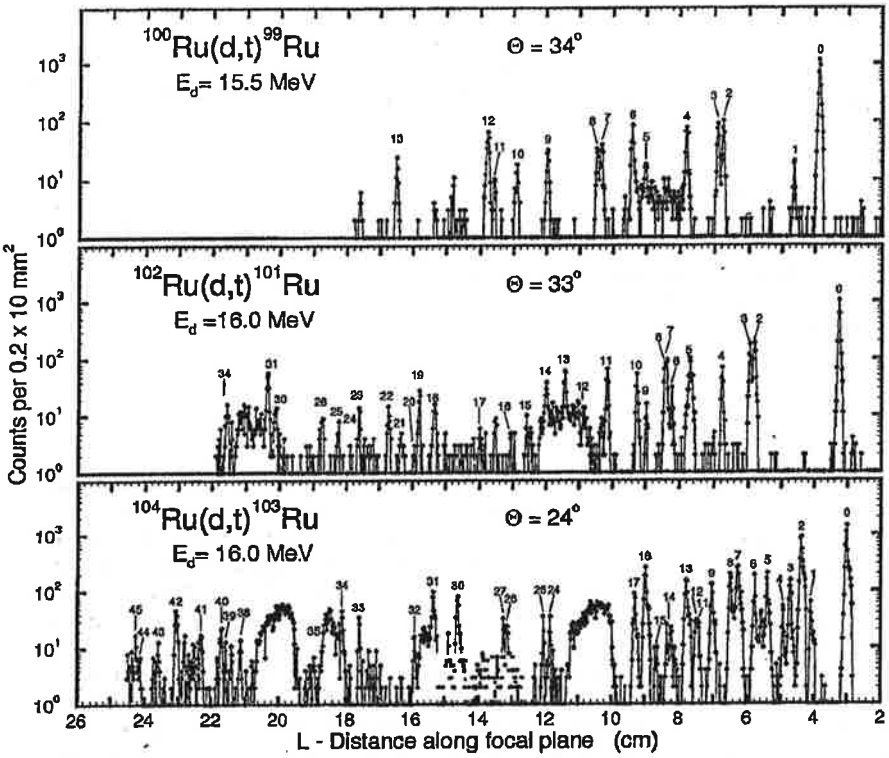

FIG. 1. Spectra of tritons emerging from ^{100,102,104}Ru(d,t) reactions at the angles indicated.

TABLE II. Optical parameters employed in the DWBA calculations.

Colliding nuclei	Parameter set[a]	V_R (MeV)	r_R (fm)	a_R (fm)	V_{SO} (MeV)	r_{SO} (fm)	a_{SO} (fm)	W (MeV)	r_W (fm)	a_W (fm)	W_D (MeV)	r_D (fm)	a_D (fm)
^{100}Ru+d	PP	96.55	1.15	0.81							18.12	1.34	0.68
	LH	111.98	1.05	0.86	7.00	0.75	0.50				10.12	1.43	0.78
	DCV	92.81	1.17	0.74	6.88	1.07	0.66	1.81	1.33	0.86	10.79	1.33	0.86
^{102}Ru+d	PP	96.31	1.15	0.81							18.24	1.34	0.68
	LH	111.85	1.05	0.86	7.00	0.75	0.50				9.99	1.43	0.78
	DCV	92.63	1.17	0.74	6.87	1.07	0.66	1.87	1.33	0.86	10.75	1.33	0.86
^{104}Ru+d	PP	96.19	1.15	0.81							18.24	1.34	0.68
	LH	111.71	1.05	0.86	7.00	0.75	0.50				9.86	1.43	0.79
	DCV	92.57	1.17	0.74	6.87	1.07	0.66	1.87	1.33	0.86	10.75	1.33	0.86
^{A}Ru+n	BG	[b]	1.17	0.75	$\lambda_{SO} = 25$[c]								
^{99}Ru+t	BG	164.29 $-0.17\,E_t$	1.20	0.72	2.50	1.20	0.72	33.78 $-0.33\,E_t$	1.40	0.88			
^{101}Ru+t	BG	164.18 $-0.17\,E_t$	1.20	0.72	2.50	1.20	0.72	31.84 $-0.33\,E_t$	1.40	0.88			
^{103}Ru+t	BG	164.07 $-0.17\,E_t$	1.20	0.72	2.50	1.20	0.72	29.98 $-0.33\,E_t$	1.40	0.88			

[a]PP: Reference [11].
LH: Reference [12].
DCV: Reference [13].
BG: Reference [15].
[b]Adjusted by well-matching procedure.
[c]Thomas factor.

and Greenlees [15], presented in Table II, where the geometrical parameters of the bound neutron potential are also shown. Except for the $1g_{9/2}$, $3p$, and $2f$ orbits, the neutron single particle orbitals taken were those of the 50–82 shell.

The spectroscopic intensities C^2S_{lj} were extracted by comparing measured and calculated angular cross section distributions through the expression

$$C^2S_{lj} = \frac{1}{3.33}(2j+1)\frac{\sigma_{\rm exp}(\theta)}{\sigma_{\rm DW}(\theta)},$$

where $\sigma_{\rm DW}(\theta)$ are the cross sections predicted by the DWBA analysis for the transfer of a neutron with orbital angular momentum l and total spin j from the even Ru to the incident deuteron. The factor $(3.33)^{-1}$ is due to the overlap of the triton and deuteron wave functions, taken, respectively, in the Irving-Gunn and Hulthén descriptions [16].

The differences in $\sigma_{\rm DW}(\theta)$ produced by the three deuteron optical-model sets in use are at most ±15%, while the shapes of the curves are practically not changed.

The excitation energy scale was set by internal calibration through strong transitions clearly identified with levels reported in γ-ray studies and indicated by asterisks in Tables III, IV, and V. The resulting calibration of the spectrograph focal plane was compatible with the calibration in common use, taken over a greater interval of bending radii, through the analysis of the ^{90}Zr (α,α') reaction up to 5.9 MeV of excitation. The excitation energies presented in Tables III, IV, and V for the states populated by one neutron transfer were obtained as mean values of the energies calculated at each angle with the aid of a relativistic kinematics code. The tables present excitation energy values whenever a level was clearly isolated at least at three angles, but to be included in Figs. 2–4 an angular distribution had to consist of a minimum of five experimental points.

III. RESULTS

A. The ^{100}Ru$(d,t)^{99}$Ru reaction

No previous stripping or pick-up work leading to ^{99}Ru is reported in the literature. Table III and Fig. 2 present the findings of the present work, for which the excitation energy region accessible to clean study is limited to 1.4 MeV by the appearance, on the focal plane, of the elastic peak and its associated tail. The detection limit below 1.4 MeV is $\sim$ 9 μb/sr and above this excitation energy it is $\sim$ 150 μb/sr. The level energies shown in Table III are characterized by standard deviations which are typically 1 keV and are never more than 2 keV. Of the 14 levels clearly identified, nine could be associated to

TABLE III. Experimental results for ^{99}Ru from the ^{100}Ru(d,t) reaction in comparison with the levels adopted by Nuclear Data Sheets. The asterisk denotes levels used in energy calibration.

Present Work						Nuclear data[a]	
Level number	$E_{\rm exc}$ (MeV)	$[\sigma_{\rm exp}(\theta)]_{\rm max}$ (mb/sr)	l	j	C^2S_{lj}	$E_{\rm exc}$ (MeV)	J^π
0	0.000*	4.2±0.3	2	5/2	1.8	0.00000	$5/2^+$
1	0.090	0.077±0.013	(2)	(3/2)	(0.037)	0.08968	$3/2^+$
2	0.322*	0.32±0.03	2	5/2; 3/2	0.20; 0.25	0.32237	$(3/2)^+$
3	0.340	0.19±0.02	4	7/2	1.8	0.34074	$7/2^+$
4	0.442*	0.84±0.10	0	1/2	0.13	0.44271	$(1/2)^+$
5	0.576	0.028±0.009				0.57589	$(5/2)^+$
						0.61791	$7/2^+$
6	0.618*	0.76±0.10	0	1/2	0.16	0.61803	$(1/2)^+$
7	0.719*	0.083±0.008	4	9/2	0.55	0.71987	$9/2^+$
8	0.734	0.12±0.02				0.73413	$(5/2^+)$
9	0.897*	0.115±0.010	2	5/2; 3/2	0.057; 0.069	0.89692	$(1/2^+;3/2;5/2^+)$
10	1.000	0.050±0.017				0.99874	$(1/2^+;3/2;5/2^+)$
						1.04863	$(11/2)^+$
11	1.072	0.034±0.010	(5)	(11/2)	(0.55)	1.06994	$11/2^-$
12	1.093[b]	0.26±0.03	2	5/2; 3/2	0.24; 0.30		
						1.1184	$(7/2^+)$
						1.2007	
						1.26124	$7/2^+$
						1.27759	$(7/2^+;9/2^+)$
						1.29078[c]	$7/2^-$
						1.3061	$(7/2^+)$
						1.3199	$(11/2^+)$
13	1.385	0.13±0.05				1.38316	$(1/2^+;3/2)$

[a]Reference [5].
[b]Possible doublet.
[c]Levels observed in Ref. [17].

TABLE IV. Experimental results for ^{101}Ru from the ^{102}Ru(d,t) reaction in comparison with previous transfer studies and the levels adopted by Nuclear Data Sheets. The asterisk denotes levels used in energy calibration.

	Present work					(p,d)[a]			(d,p)[b]			Nuclear data[c]	
Level number	E_{exc} (MeV)	$[\sigma_{exp}(\theta)]_{max}$ (mb/sr)	l	j	C^2S_{lj}	E_{exc} (MeV)	l	C^2S_{lj}	E_{exc} (MeV)	l	C^2S_{lj}	E_{exc} (MeV)	J^π
0	0.000*	5.62±0.23	2	5/2	1.8	0.000	2	2.25	0.000	2	2.1	0.00000	$5/2^+$
1	0.127	0.015±0.004	(2)	(3/2)	(0.006)	0.127	2	0.013	0.127	2	0.067	0.12723	$3/2^+$
2	0.307		4	7/2	2.3		4	2.86	0.307	4	5.3	0.30685	$7/2^+$
2′	0.311	0.56±0.04[d]	2	5/2; 3/2	0.19; 0.23		2	0.29				0.31133	$5/2^+;3/2^+$
3	0.324*	2.43±0.12	0	1/2	0.32	0.325[e]	0	0.16	0.326	0	0.96	0.3248	$1/2^+$
												0.3440	
4	0.421*	0.38±0.06	2	3/2	0.22	0.422	2	0.20	0.421	2	0.15	0.4223	$3/2^+$
			5	11/2	1.2		5	0.99		5	5.8	0.5275	$11/2^-$
5	0.534[f]	0.57±0.04[g]	2	5/2; 3/2	0.26; 0.33	0.540[e]	2	0.27; 0.34	0.533[e]	2	0.72; 0.75	0.535	$5/2^+;3/2^+$
												0.54508	$7/2^+$
6	0.597	0.15±0.02	3	7/2; 5/2	0.09; 0.13				0.597	3	0.60; 0.74	0.5983	$7/2^-;5/2^-$
7	0.615	0.61±0.06	2	5/2; 3/2	0.23; 0.30		2	0.31; 0.40				0.6163	$(5/2;3/2)^+$
												0.623[h]	$5/2^+;3/2^+$
8	0.622*	1.07±0.10	0	1/2	0.12	0.623[e]	0	0.063	0.622	0	0.063	0.6235	$1/2^+$
9	0.684	0.062±0.007	(1)	(3/2; 1/2)	(0.007; 0.009)	0.687	2	0.024; 0.031	0.685	2	0.17; 0.18	0.684	$5/2^+;3/2^+$
									0.718	1	0.017; 0.018	0.718	$3/2^-;1/2^-$
10	0.719	0.135±0.015	4	9/2	0.50	0.720	4	0.29				0.7200	$9/2^+$
									0.742				
11	0.824	0.32±0.03	2	5/2; 3/2	0.18; 0.22	0.822	2	0.13; 0.17	0.823	2	0.40; 0.43	0.823	$5/2^+;3/2^+$
												0.84278	$(7/2)^+$
12	0.907	0.09±0.02	1	3/2; 1/2	0.011; 0.012	0.927	2	0.048; 0.062	0.908	1	0.057; 0.060	0.908	$3/2^-;1/2^-$
												0.927	$5/2^+;3/2^+$
												0.92872	$9/2^+$
												0.93847	$(7/2)^+$
												0.9582	$15/2^-$
13	0.974	0.25±0.02	2	5/2; 3/2	0.14; 0.18	0.975	2	0.14; 0.17	0.972	2	0.63; 0.70	0.9734	$5/2^+;3/2^+$
												1.0012	$11/2^+$
14	1.038	0.15±0.02	2	5/2; 3/2	0.08; 0.10	1.041	2	0.094; 0.12				1.041	$5/2^+;3/2^+$
									1.051	4	0.28	1.051	$9/2^+;7/2^+$
									1.098	0	0.028	1.098	$1/2^+$
15	1.111	0.13±0.02	0	1/2	0.022	1.112	0	0.012	1.112	0	0.17	1.110	$1/2^+$
16	1.164	0.054±0.008				1.169	2	0.036; 0.045				1.169	$5/2^+;3/2^+$
												1.2068	
												1.2190	
						1.225	4	0.19; 0.33				1.225	$9/2^+;7/2^+$
									1.227	0	0.016	1.227	$1/2^+$
17	1.266	0.026±0.010							1.268	2	0.019; 0.022	1.268	$5/2^+;3/2^+$
						1.276	0	0.011				1.276	$1/2^+$
												1.3215	$(11/2^+)$
												1.3899	
18	1.425	0.047±0.009				1.440							

TABLE IV. (*Continued*).

Present work						(p,d)[a]			(d,p)[b]			Nuclear data[c]	
Level number	E_{exc} (MeV)	$[\sigma_{exp}(\theta)]_{max}$ (mb/sr)	l	j	C^2S_{lj}	E_{exc} (MeV)	l	C^2S_{lj}	E_{exc} (MeV)	l	C^2S_{lj}	E_{exc} (MeV)	J^π
19	1.477	0.19±0.02	2	5/2; 3/2	0.11; 0.13	1.510	2	0.16; 0.20					
20	1.498	0.014±0.006							1.501			1.4993	
												1.5010	$13/2^+$
21	1.542	0.04±0.02				1.555	2	0.055; 0.065	1.544			1.510[i]	$5/2^+;3/2^+$
22	1.585	0.082±0.009	2	5/2; 3/2	0.063; 0.079	1.597	2	0.085; 0.100	1.584	2	0.45; 0.50	1.555	$5/2^+;3/2^+$
												1.5873	$5/2^+$
23	1.688	0.07±0.02							1.659			1.6223	$19/2^-$
									1.689	5	3.7	1.689	$11/2^-;9/2^-$
24	1.714	0.10±0.01	0	1/2	0.016	1.701	(2)	(0.078; 0.093)				1.701	$(5/2^+;3/2^+)$
25	1.758	0.10±0.01	0	1/2	0.016	1.731	0	0.026	1.714	0	0.012	1.714	$1/2^+$
						1.777	0	0.021					
												1.7618	
												1.7743	$11/2^-$
												1.777[j]	$1/2^+$
26	1.812	0.055±0.006	2	5/2; 3/2	0.042; 0.052	1.833	2	0.081; 0.095	1.779	1	0.027; 0.028	1.779	$3/2^-;1/2^-$
27	1.822	0.020±0.003							1.813	2	0.064; 0.068		
28	1.839	0.013±0.002							1.825	2	0.075; 0.081	1.825	$5/2^+;3/2^+$
29	1.858	0.013±0.002							1.842	2	0.041; 0.043	1.8434	$5/2^+;3/2^+$
									1.861	0	0.062	1.861	$1/2^+$
												1.8622	$15/2^+$
									1.878	2	0.25; 0.27	1.8801	$5/2^+;3/2^+$
						1.884							
									1.893				
									1.936	0	0.061	1.936	$1/2^+$
												1.9615	
30	1.969	0.067±0.010	2	5/2; 3/2	0.049; 0.061	1.984	2	0.061; 0.071	1.969	2	0.20; 0.21	1.9710	$5/2^+;3/2^+$
												1.984[k]	$5/2^+;3/2^+$
31	1.996	0.35±0.02	1	3/2; 1/2	0.09; 0.10				1.997	2	0.12; 0.13	1.9970	$5/2^+;3/2^+$
												2.0170	
												2.0175	
									2.057	0	0.076	2.057	$1/2^+$
32	2.068	0.021±0.002				2.076						2.0634	
33	2.083	0.02±0.01				2.100			2.087			2.0867	
34	2.131	0.18±0.02				2.156			2.133	1	0.037; 0.039	2.133	$3/2^-;1/2^-$

[a]Reference [18].
[b]Reference [8].
[c]Reference [6].
[d]Integrated cross section (Levels 2 and 2′).
[e]Levels experimentally unresolved. Least squares fit in angular distribution.
[f]Energy attributed to the $l = 2$ component of unresolved doublet.
[g]Integrated cross section ($l = 2$ and $l = 5$).
[h]Level proposed to correspond to level 7.
[i]Level proposed to correspond to level 19.
[j]Level proposed to correspond to level 25.
[k]Level proposed to correspond to level 30.

TABLE V. Experimental results for ^{103}Ru from the ^{104}Ru(d,t) reaction in comparison with previous transfer studies and the levels adopted by Nuclear Data Sheets. The asterisk denotes levels used in energy calibration.

Present work						(d,t)[a]			(p,d)[b]			Nuclear data[c]	
Level number	E_{exc} (MeV)	$[\sigma_{exp}(\theta)]_{max}$ (mb/sr)	l	j	C^2S_{lj}	E_{exc} (MeV)	l	C^2S_{lj}	E_{exc} (MeV)	l	C^2S_{lj}	E_{exc} (MeV)	J^π
												0.00000	$3/2^+$
0	0.002	3.80±0.02	2	5/2	1.11	0.000	2	1.97	0.0054	2	1.29	0.00281	$5/2^+$
1	0.136*	0.24±0.01	2	5/2	0.072	0.133	(2)	(0.11; 0.14)	0.1356	2	0.13	0.136079	$5/2^+$
2	0.174*	2.42±0.02	0	1/2	0.29	0.171	0	0.43	0.1742	0	0.28	0.17426	$1/2^+$
3	0.213*	0.31±0.03	4	7/2	2.07	0.210	4	2.36	0.2128	4	0.96	0.21356	$7/2^+$
4	0.239	0.20±0.02	5	11/2	1.47	0.235	5	1.92	0.2397	5	1.55	0.2382	$11/2^-$
5	0.297*	0.38±0.03	3	7/2; 5/2	0.16; 0.22	0.294	(0)	(0.08)	0.2971	3	0.17	0.2971	$(7/2^-)$
												0.29748	$(3/2^+)$
6	0.346	0.30±0.02	2	5/2; 3/2	0.10; 0.13	0.343	2	0.16	0.3464	2	0.14	0.34638	$3/2^+$
												0.40415	$7/2^+$
7	0.406	1.00±0.06	2	5/2; 3/2	0.35; 0.44	0.402	2	0.62	0.4056	2	0.31; 0.34	0.40608	$5/2^+;3/2^+$
8	0.432*	0.60±0.03	0	1/2	0.070	0.428	0	0.12	0.4329	0	0.09	0.43206	$1/2^+$
9	0.501	0.46±0.03	2	5/2; 3/2	0.17; 0.20	0.497	2	0.26	0.5011	2	0.22	0.50115	$(5/2)^+$
												0.5354	$(5/2^+;3/2^+)$
10	0.540											0.54821	$1/2^+$
11	0.548	0.145±0.013[d]				0.545	1	0.068					
										2	0.10		
									0.5511*	0	0.02	0.55458	$(1/2^+)$
12	0.556											0.5577	(9/2)
												0.56287	$(5/2^+;3/2^+)$
												0.56817	$(1/2^+)$
									0.5930	2	0.21	0.59197	$(5/2)^+$
13	0.592	0.54±0.03	2	5/2; 3/2	0.21; 0.25	0.587	2	0.38	0.6281	(2)	(0.05)	0.6220	$(5/2^+)$
												0.6537	$15/2^-$
						0.658	(2)	(0.03; 0.04)	0.6630	2	0.05	0.66155	$(3/2)^+$
14	0.662	0.040±0.009				0.693	4	0.47	0.7012	4	0.34	0.6972	$9/2^+;7/2^+$
15	0.697	0.04±0.01										0.7352	$(5/2^+)$
												0.73689	$1/2^+$
16	0.737	0.71±0.05	0	1/2	0.086	0.731	0	0.15	0.7388	0	0.09	0.7488	$(5/2^+)$
												0.7741	$(11/2^+)$
									0.7770	2	0.17	0.77477	$(5/2^+;3/2)$
17	0.775	0.28±0.10	2	5/2; 3/2	0.11; 0.13								
18	0.855	0.025±0.004										0.87371	$(5/2^+;3/2^+)$
												0.90305	$(<5/2^+)$
19	0.908	0.108±0.008	(2)	(5/2; 3/2)	(0.050; 0.061)	0.902	2	0.07	0.9039	2	(0.08; 0.09)	0.90536	$5/2^+;3/2^+$
												0.90764	$(<5/2^+)$
												0.9116	$(7/2^+)$
20	0.928	0.04±0.01										0.92724	$(3/2^+;1/2^+)$
												0.9313	(5/2; 3/2)
21	0.942	0.040±0.005										0.94050	
												0.9544	(3/2)
												0.9916	

TABLE V. (*Continued*).

Present work						(d,t)[a]			(p,d)[b]			Nuclear data[c]	
Level number	E_{exc} (MeV)	$[\sigma_{exp}(\theta)]_{max}$ (mb/sr)	l	j	C^2S_{lj}	E_{exc} (MeV)	l	C^2S_{lj}	E_{exc} (MeV)	l	C^2S_{lj}	E_{exc} (MeV)	J^π
22	1.005	0.034±0.005										1.005	$5/2^+;3/2^+$
												1.0181	(7/2; 5/2)
												1.0204	$(13/2^-)$
23	1.067	0.026±0.004										1.06514	$7/2^+;5/2^+;3/2^+$
24	1.080	0.08±0.01	(4)	(9/2; 7/2)	(0.40; 0.68)							1.0796	
												1.1067	$1/2^+$
25	1.109	0.050±0.005	(2)	(5/2; 3/2)	(0.024; 0.031)							1.1101	$(5/2^+;3/2;1/2)$
												1.1106	$(11/2^+)$
												1.1337	
												1.1406	(5/2; 3/2)
												1.1713	(3/2; 1/2)
												1.17408	(3/2)
26	1.238	0.100±0.009	2	5/2; 3/2	0.050; 0.062							1.1999	$13/2^+$
27	1.251	0.077±0.008	2	5/2; 3/2	0.036; 0.043								
												1.245	$5/2^+;3/2^+$
												1.2698	
												1.2882	
												1.3015	$(19/2^-)$
28	1.325	0.18±0.03										1.3136	$11/2^+$
29	1.338	0.16±0.02										1.3244	
												1.34712	
30	1.403	0.26±0.08										1.3784	
												1.40098	
												1.43112	
												1.4437	$(15/2^+)$
31	1.491	0.27±0.02										1.4738	
32	1.559	0.051±0.006	2	5/2; 3/2	0.026; 0.029								
												1.550	$(5/2^+;3/2^+)$
												1.60447	
												1.7171	
33	1.756	0.23±0.02	1	3/2; 1/2	0.05; 0.06							1.7304	
34	1.817	0.11±0.01										1.80508	$(1/2^+)$
												1.83588	
35	1.892	0.029±0.006										1.88054	
												1.90614	
36	1.916	0.035±0.005											

TABLE V. (*Continued*).

Level number	Present work E_{exc} (MeV)	$[\sigma_{exp}(\theta)]_{max}$ (mb/sr)	l	j	C^2S_{lj}	(d,t)[a] E_{exc} (MeV)	l	C^2S_{lj}	(p,d)[b] E_{exc} (MeV)	l	C^2S_{lj}	Nuclear data[c] E_{exc} (MeV)	J^π
												1.96192	$(5/2^+;3/2^+)$
												2.0037	
37	2.022	0.114±0.013											
												2.1319	$19/2^+$
												2.132	$(23/2^-)$
38	2.167	0.23±0.07	4	9/2; 7/2	1.6; 2.7								
												2.20611	
39	2.217	0.039±0.005											
												2.2236	
40	2.232	0.145±0.015											
41	2.299	0.24±0.02	1	3/2; 1/2	0.04; 0.05								
42	2.384	0.37±0.02	1	3/2; 1/2	0.07; 0.08								
43	2.444	0.13±0.03											
44	2.507	0.076±0.008	1	3/2; 1/2	0.013; 0.018								
45	2.520	0.155±0.015											

[a] Reference [19].
[b] Reference [20].
[c] Reference [7].
[d] Integrated cross section for levels 10, 11, and 12.
[e] Levels experimentally unresolved. Least squares fit in angular distribution.

FIG. 2. Angular distributions for the ^{100}Ru$(d,t)^{99}$Ru reaction in comparison with DWBA predictions. Error bars represent uncertainties due to statistics, plate scanning, and background (and/or contaminant) subtraction and do not include any error in the absolute cross section scale (see text).

definite l transfers, and the corresponding C^2S_{lj} values are also presented in Table III. This table also shows, for comparison, the levels adopted by the nuclear data compilation [5]. Additional levels, at 1.1184 and 1.29078 MeV reported by Whisnant *et al.* [17], are also presented in columns 7 and 8. Although no clear discrimination between $l=4$ and $l=5$ is allowed by the data, the level excited at 1.072 MeV is supposed to be the known $11/2^-$ state. An $l=3$ transition was searched for, in particular at 1.291 MeV, where a (^{3}He,$2n\gamma$) work [17] located a $(7/2^-)$ level, but was not observed above the detection limit.

B. The ^{102}Ru$(d,t)^{101}$Ru reaction

In this experiment a detection limit of only 3 μb/sr could be achieved in the excitation energy region below 2.2 MeV, due to a relatively clean target. Table IV shows the present results in comparison with a (p,d) study by Dickey *et al.* [18], which has a poorer energy resolution

of only 24 keV. Also the results of the (d,p) work of this group [8] and the adopted levels [6] are tabulated. In Fig. 3 the experimental angular distributions are displayed together with DWBA predictions.

The level energies in Table IV were determined with standard deviations of less than 2 keV for all levels below 1.9 MeV and no more than 3 keV above this energy. The difference between the attributed excitation energies and the adopted ones is always smaller than 2 keV, where identification with levels based on γ-ray results is unambiguous. Also, agreement between the excitation energies obtained in the present (d,t) and the former (d,p) work [8] is excellent. On the other hand, the results of the previous (p,d) study [18] are clearly affected by a systematic discrepancy with respect to both, the (d,t) and γ-ray information. The excitation energy difference is of the order of +(10–20) keV, starting at about 1 MeV, as is evidenced especially through the comparative analysis of the stronger transitions detected in both pick-up studies. The worst case is the level 19 where +33 keV of energy shift is verified. Thus, several levels presented in the recent nuclear data compilation [6], which are based exclusively on information by Dickey *et al.* [18], should have their excitation energies revised.

General agreement between neutron hole spectroscopic strength extracted in the present (d,t) and in the former (p,d) [18] works is observed. Specific comments on the experimental results are made in the following.

Level 1 lies below the detection limit, except at the 3 angles around the maximum for $l = 2$ transfer, thus the value of $C^2S_{d_{3/2}}$ between parenthesis is an estimate. Peaks numbered 17, 27, 28, 29, 32, and 33 were also only observed at $\theta_{\rm lab} = 10°, 22°$, and 28° and, since they do not correspond to levels with known spins and parities, only excitation energies are reported. Peaks 2 and 2′ could not be adequately separated by the peak fitting routine and the $l = 4$ and $l = 2$ contributions were extracted through a least-squares fit on the integrated angular distribution, as shown in Fig. 3. Peak 5 is dominated by the strong $l = 2$ transition at 0.535 MeV and the $l = 5$ contribution was also obtained by the same fitting procedure, the extracted $C^2S_{h_{11/2}}$ being uncertain

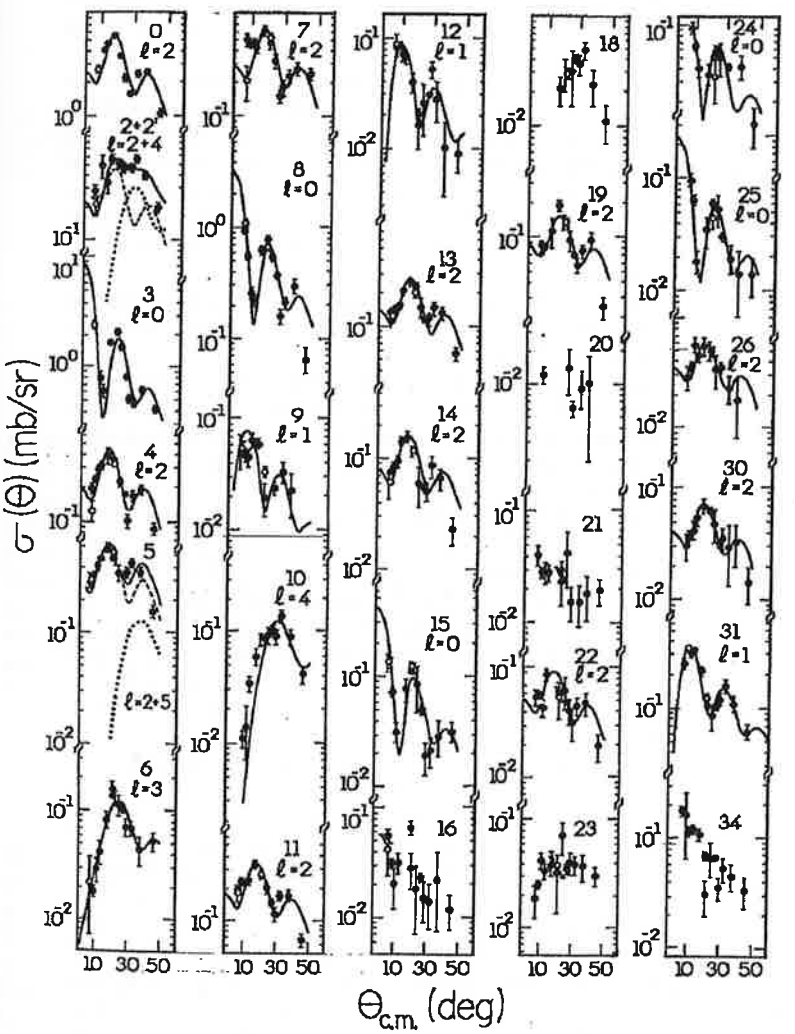

FIG. 3. Angular distributions for the ^{102}Ru$(d,t)^{101}$Ru reaction in comparison with DWBA predictions. See caption of Fig. 2.

to 25%.

Level 6 corresponds in energy to the $l = 3$ transition seen in (d,p) [8] and is very well characterized by the same orbital angular momentum transfer. Dickey *et al.* [18] could not resolve this state, present as a shoulder in the published spectrum, from the neighboring $l = 2+l = 0$ transitions at 0.615 and 0.622 MeV, which they also could not separate. So, the level at 0.623 MeV with $J^\pi = 5/2^+, 3/2^+$, indicated in the nuclear data tabulation [6] as measured by Dickey *et al.* [18], is already represented by the adopted level at 0.6163 MeV, $J^\pi = (5/2^+, 3/2^+)$ and should be excluded.

Level 9 is, in (d,t), better described as $l = 1$ transfer (see Fig. 3) than as the $l = 2$ previously attributed in (p,d) [18] and (d,p) [8]. The attributions may thus be open to questioning. At 0.719 MeV, level 10 corresponds predominantly to $l = 4$ in the present work and (p,d) [18]. A closer inspection shows, however, that the agreement with the DWBA prediction at forward angles is subtly worse than for other typical $l = 4$ transfers. In the angular distribution obtained in (p,d), this effect is substantially enhanced and could signify an additional $l = 1$ transfer being detected. In fact, the (d,p) reaction located at 0.718 MeV an $l = 1$ transfer, which only through severe contamination at the forward angles, could be associated to an $l = 4$ transfer. It seems thus that two levels with different characteristics are being preferentially populated in the pick-up and stripping reactions. Dickey *et al.* [18] did, in fact, not attribute any $l = 1$ transfer in their work. The inspection of the angular distribution associated to the state at 0.927 MeV, which Dickey *et al.* [18] report as populated by $l = 2$, also shows a behavior that is not in disagreement with an $l = 1$ transfer. Thus, this state is tentatively identified with the level at 0.907 MeV seen in the present study and already adopted as $3/2^-$, $1/2^-$ by Nuclear Data Sheets [6]. No transition to the level at 1.225 MeV, reported in the (p,d) work [18], was observed above the detection limit. Level 17 was seen at only three angles, but the data available, although compatible with an $l = 2$ transfer, exclude an $l = 0$ character. This level should thus correspond to the 1.268 MeV reported by the (d,p) work, but not to the 1.276 MeV level by Dickey *et al.* [18]. A clear $l = 1$ transition was detected to the level 31, in apparent disagreement with the experimental findings of the (d,p) study [8], which reports an $l = 2$ transfer. The (d,p) angular distribution is, however, compatible with an $l = 1$ transfer due to the absence of data at scattering angles smaller than 20°. In this case, the extracted reduced spectroscopic factor, $C^2S^i_{lj}$, should be 0.04 and spin and parity of the correspondent level should be revised.

C. The ^{104}Ru$(d,t)^{103}$Ru reaction

This experiment extended the excitation energy interval analyzed by pick-up reactions up to 2.6 MeV. The detection limit was 10 μb/sr, due to a relatively thin target, somewhat more contaminated during evaporation. Previous pick-up studies [19,20], including a (d,t) work [19], did not exceed 0.9 MeV of excitation energy. Their results are presented in Table V in comparison with the present ones and with the adopted levels [7]. The work of Berg *et al.* [20] was performed at a high dispersion spectrograph with 5–8 keV of resolution and studied both the (p,d) and (d,p) reactions leading to ^{103}Ru, unfortunately with very poor statistics. They ascertained that the stripping reaction populates preferentially the ground state, while pick-up selects the known state [7] at 2.81 keV, associated by them to their level at 5.4 keV. In the present work the excitation energy of level 0, as obtained from the internal calibration with the levels marked with an asterisk, is 2 ± 1 keV and thus confirms the predominant excitation of the first excited level in pick-up. Inspection of Table V reveals excellent agreement between the level energies here obtained and all those of both previous pick-up studies.

The comparison of the extracted spectroscopic strengths with those reported for the same reaction at 17 MeV by Diehl *et al.* [19] shows general agreement for the relative values, although the absolute values of the older work are systematically higher. The lack of finite range and nonlocality corrections in the older DWBA calculation can be responsible for part of the discrepancy. Diehl *et al.* [19] also did not publish the geometry of the potential that binds the transferred neutron, another known source of differences in absolute values. The results of the (p,d) work of Berg *et al.* [20] are, on the other hand, in good agreement with the present ones, exception made to the first $l = 2$ and the lowest $l = 4$ excitations, where the discrepancies of up to a factor of two are directly related to the reported cross sections and cannot be attributed to analysis.

Figure 4 displays the angular distributions obtained in this work and, in the following, comments on some specific attributions are made.

Level 5, at 0.297 MeV, is a clear $l = 3$ transition. The misattribution in the (d,t) work of Diehl *et al.* [19] may have been caused by the lack of data at forward angles, crucial to distinguish the correct value from $l = 0$. Berg *et al.* [20] also attribute $l = 3$ to this transition. A triplet of levels (10, 11, and 12) could be clearly resolved where Diehl *et al.* [19] located an $l = 1$ transition, but separated angular distributions were not obtained. Berg *et al.* [20] who also analyzed integrated cross sections, decided for a superposition of $l = 2$ and $l = 0$ transfer in this energy region, on a rather structureless experimental angular distribution. The present data are not sufficient for deciding on the divergence exposed, because of contamination at $\theta = 8°$. The cross section associated to level 15 was at crucial forward angles near the detection limit, but if an $l = 4$ transfer is supposed the C^2S_{lj} value would be compatible with other studies.

Above level 20 all information is new and the identification with levels adopted by the nuclear data compilation [7] is tentative. Attention is drawn especially to the observation of an intense $l = 4$ excitation at 2.167 MeV and of three clean $l = 1$ transfers around 2.4 MeV, besides the lower $l = 1$ at 1.756 MeV. Another ($l = 4$) and several $l = 2$ transitions are also reported for the first time. Relatively strong excitations (peaks 30 and 31) at

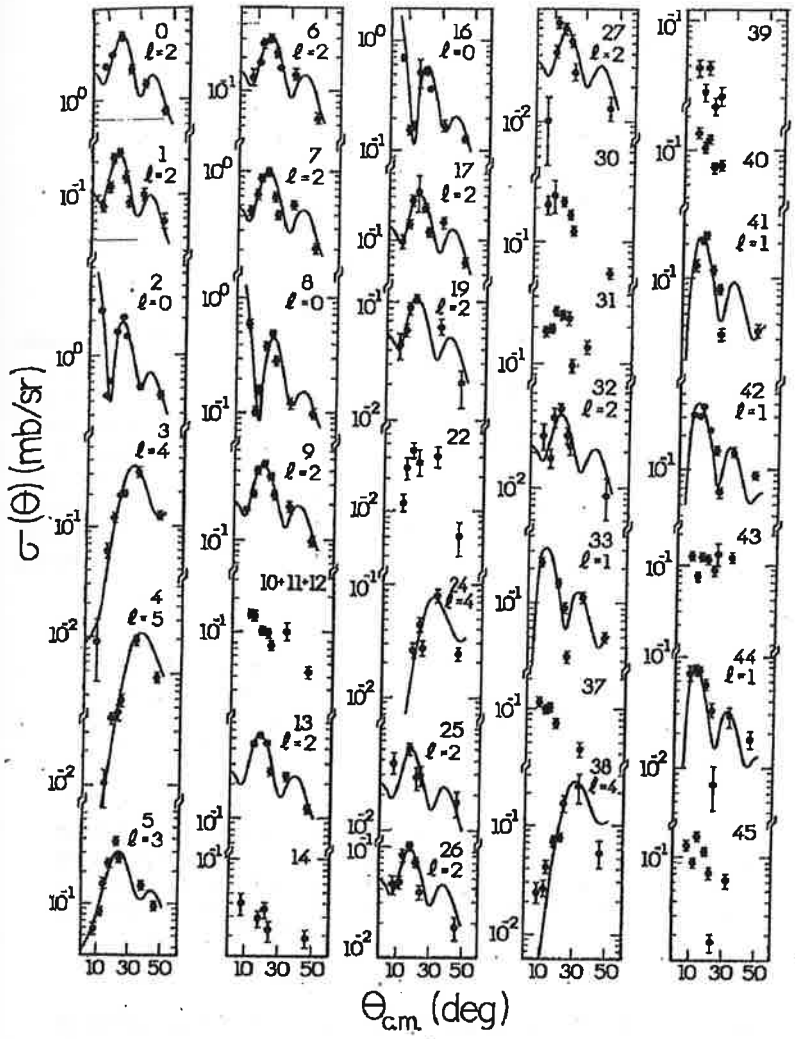

FIG. 4. Angular distributions for the ^{104}Ru$(d,t)^{103}$Ru reaction in comparison with DWBA predictions. See caption of Fig. 2.

1.403 and 1.491 MeV correspond to forward peaked angular distributions, but cannot be clearly identified. If associated to $l = 2$ transfer, their summed spectroscopic strength would amount to $C^2S_{d_{5/2}} \sim 0.3$. Peaks 28 and 29 are also relatively intense and their angular distributions, not shown in Fig. 4 since represented by less than five data points, show maxima at respectively $\theta = 18°$ and 12° and, if corresponding to $l = 2$ and $l = 1$, respectively, would mean additional C^2S_{lj} of ~ 0.04 and ~ 0.04.

IV. DISCUSSION

For comparative appreciation, Fig. 5 displays, as bars, the observed spectroscopic strengths as a function of excitation energy for the three Ru isotopes under investigation and for the several l transferred (taken where the level spin is not known, as associated to $j = l+1/2$). An arrow indicates, for each nuclide, the maximum excitation energy scanned. An overall similarity may be noted, but for all l transfers the strengths tend to be located at progressively lower excitation energies as the neutron number is increased.

Most of the detected strength is, as expected, associated to even l values. The principal $l = 0$ excitations are found below 0.8 MeV and correspond to at most three levels. It can be stated that, since the detection limit for $l = 0$ is low, no important fragmentation occurs. For all studied isotopes the by far strongest $l = 2$ component is located at the first $5/2^+$ level (note the scale factor of 1/4 for these bars). The remaining detected $l = 2$ strength is for ^{101,103}Ru spread among several levels in a wide energy range. In ^{99}Ru, on the other hand, at most five states with $l = 2$ characteristics were observed. Very similar and intense $l = 4$ transfers are associated to the first known $7/2^+$ levels below 0.4 MeV in all three isotopes, while the first known $9/2^+$ states appear with one fourth of that strength at ~ 0.7 MeV in ^{99,101}Ru. Several levels which could, in principle, be excited by $l = 4$ transfer are known, from other reactions or decay, in all three isotopes (see Tables III, IV, and V), but are populated below the detection limit (in the worst case $C^2S_{g_{7/2}} = 0.4$). Attention is to be called to the first observation in ^{103}Ru of a

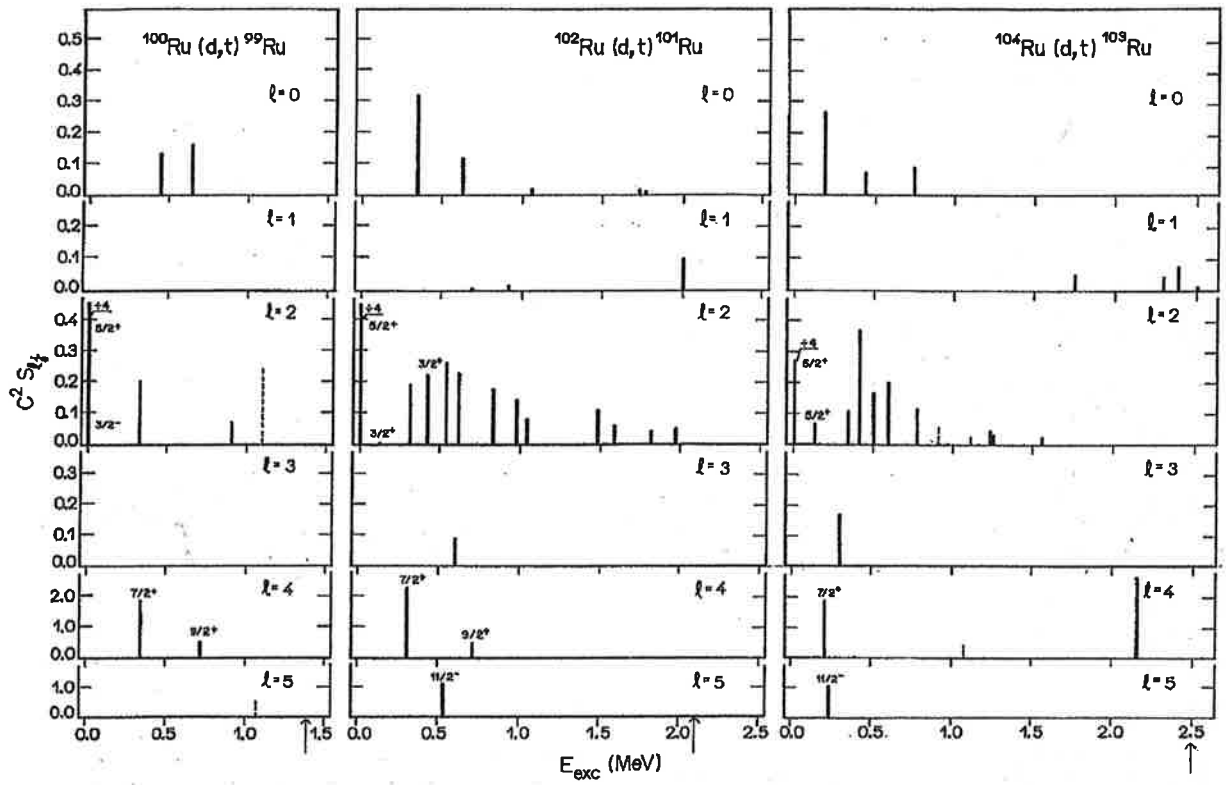

FIG. 5. Spectroscopic strength distributions, organized as functions of l transfer and excitation energy, obtained from the one neutron pick-up reactions indicated. Note the reduction factors for the strongest $l = 2$ transitions. Tentative attributions are shown as broken bars and known spins (Refs. [5–7]) are marked. Where spins are not known, bars represent the spectroscopic strength associated to $j = l + 1/2$, exception made to the level at 2.2 MeV in ^{103}Ru, excited through $l = 4$, which was taken as $7/2^+$.

state with clear and strong $l = 4$ characteristics at 2.167 MeV. In fact, this $l = 4$ excitation would correspond to $C^2S_{g_{7/2}} = 2.7$, even higher than the intensity to the first $7/2^+$ state, if this spin value should prevail.

With respect to the levels excited by an odd l transfer, no $l = 1$ was seen in ^{99}Ru below 1.5 MeV and all the important strengths seen in ^{101,103}Ru lie above 1.7 MeV. Also no $l = 3$ strength was located in ^{99}Ru above the detection limit of $C^2S_{f_{7/2}} = 0.04$, while the $l = 3$ excitation seen at 0.597 MeV in ^{100}Ru$(d,p)^{101}$Ru was confirmed and also $l = 3$ was definitely associated to the level at 0.297 MeV in ^{103}Ru. It is extremely interesting to note that no other, besides these very low-lying, $l = 3$ excitations were detected up to, respectively, 2.2 and 2.5 MeV in ^{101,103}Ru, which clearly demonstrates the singular character of these levels. The $l = 3$ strength was, thus, located with higher intensity at progressively lower energy with increasing neutron number, if the $7/2^-$ level at 1.291 MeV in ^{99}Ru (Ref. [17]) is supposed undetected by experimental limitations. The $l = 5$ strength, also located in a single level, decreases in energy in a similar way. For $l = 5$ excitations the detection limit corresponds in the worst case, to $C^2S_{h_{11/2}} = 0.5$.

It has long been established that one nucleon transfer reactions, especially if well-known light projectiles are employed, result in clean spectroscopic informations of two kinds. On one side, a global view of the spectroscopic strengths is associated to occupation and vacancy of shell-model orbitals in the ground state of the target nucleus. Such information is systematized in Table VI for the occupancy data extracted in this work and will be further discussed below. On the other side, specific states in the residual nucleus may have their quasiparticle character defined, especially if results of the complementary stripping or pick-up reactions are also available. Figure 6, later presented, will be used to point these aspects out.

In Table VI the summed spectroscopic strength of excitations which could be associated without doubt to each l transfer is shown for the three target nuclei investigated. The column labelled $1g$ presents only the strength which can with certainty be attributed to the $1g_{7/2}$ orbital. Thus the population of $9/2^+$ levels, hole states in the $N = 50$ core in ^{99,101}Ru, and of a state of unknown spin at 1.08 MeV in ^{103}Ru, all with $C^2S_{g_{9/2}} \sim 0.5$, was not considered in this table. The total detected $l = 1$ and $l = 3$ strengths are shown, respectively, in columns 3 and 5, under the hypothesis that states associated to the next major shell are excited. This assumption will be fundamented, with basis on (d,p) results, in the further

TABLE VI. Sums of the one neutron pick-up spectroscopic strength associated to each l value for ^{100,102,104}Ru. The last column indicates the total spectroscopic strength associated with certainty to the 50–82 neutron shell (see text).

Target nucleus	$\sum C^2S$ 3s	3p	2d	2f	1g	1h	Total spectroscopic strength
^{100}Ru	0.29	0.00	2.30	0.00	1.8	0.6	5.0
^{102}Ru	0.49	0.10	3.36	0.09	2.3	1.2	7.4
^{104}Ru	0.45	0.17	2.23	0.16	2.1 (4.8)	1.5	6.3 (9.0)

discussion. For the $l = 2$ transfers, when the final j is not known, the strength for $j = l + 1/2$ was arbitrarily taken. If this choice should prove incorrect for all those levels, the summed spectroscopic strength would increase by at most 5%, 10%, and 10% for ^{100,102,104}Ru, respectively. For the ^{104}Ru nucleus, if the $l = 4$ excitation at 2.167 MeV could be characterized as an $1g_{7/2}$ contribution, the values indicated in parenthesis result. The last column of Table VI presents thus the total summed spectroscopic strength which is with certainty associated to the 50–82 shell, the $3p$ and $2f$ transfers being excluded.

The present results make it clear that in the reactions studied most of the strength was found. In fact, if the $N = 50$ core could be considered closed, ^{100,102,104}Ru should correspond, respectively, to 6, 8, and 10 valence neutrons. For ^{104}Ru the total spectroscopic strength detected would percentually be similar to those of the other two isotopes studied, if the value in parenthesis is con-

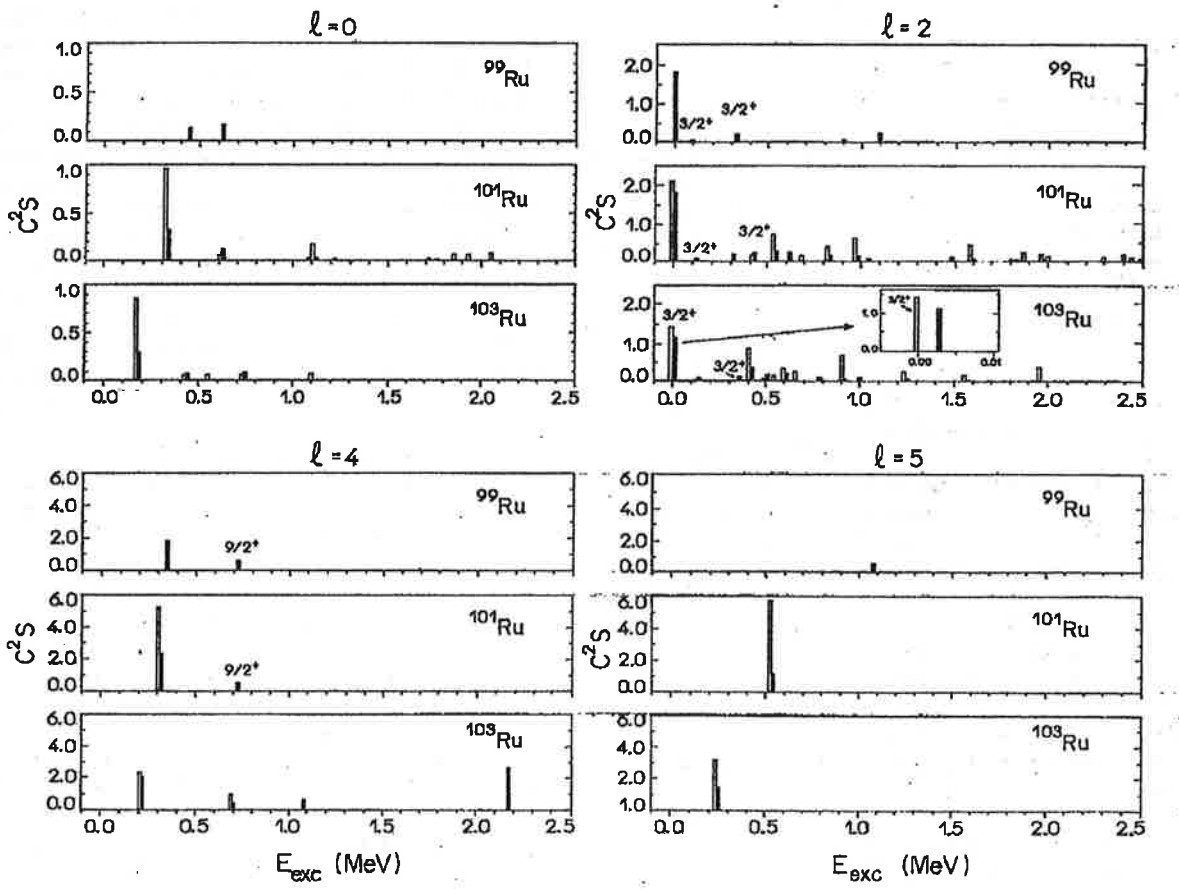

FIG. 6. Hole (represented as solid bars) and particle (represented as open bars) strengths as a function of excitation energy and l transfer in ^{99,101,103}Ru. The particle strength was taken from Duarte *et al.* (Ref. [8]) for ^{101}Ru and Fortune *et al.* (Ref. [21]) for ^{103}Ru, up to 2.0 MeV, and for ^{99}Ru there is no experimental information. Hole strength is represented to the right of the excitation energy of the respective level while the particle strength is represented to the left. Note the inset for the two first levels excited by $l = 2$ in ^{103}Ru.

sidered. A global view of Table VI demonstrates that the neutron hole strength is widely spread among all the spherical shell-model valence orbitals. If exception is possibly made to the $1g_{7/2}$ orbital in ^{104}Ru, none other is seen to concentrate more than about one-third of the respective sum rule limit and no filling pattern with increasing N emerges. The missing strength of only about $\sum C^2S = 1.0$ in each isotope (if the value in parenthesis is taken) is not expected to disrupt this picture.

Figure 6 displays, in addition to the present results, also the spectroscopic strengths [taken as $C^2S'_{lj} = C^2(2j+1)S_{lj}$] for the ^{100,102}Ru$(d,p)$ reactions [8,21]. For better comparative visualization, the same scales are employed for each l transfer for the three isotopes. It is to be noted that absolute values are presented for $C^2S'_{lj}(d,p)$ and $C^2S_{lj}(d,t)$ and that the maximum values on scale are about $(2j+1)/2$. Levels with known J^π of $3/2^+$ and $9/2^+$ are marked. Inspection of Fig. 6 demonstrates that, as expected on simple lines, most of the levels strongly excited in the pick-up reactions are also in the corresponding stripping reactions. An exception is the known $9/2^+$ level at 0.7 MeV in ^{101}Ru, which was not detected in ^{100}Ru(d,p). This is not surprising for $1g_{9/2}$ states, since they should correspond to a totally occupied orbital in the $N = 50$ core. The nonobservation in ^{102}Ru(d,p) of the level excited at 1.1 MeV in ^{104}Ru(d,t) with a strength similar to that of the above mentioned one in ^{102}Ru(d,t), makes it a candidate for also being a $9/2^+$ state. Even if no (d,p) information is available for ^{99}Ru, by comparison with the other two isotopes, a similar pattern seems to emerge. In particular, there also exists a $9/2^+$ level at 0.7 MeV in ^{99}Ru and the most important $l = 4$, $l = 2$, and $l = 0$ excitations have their counterparts in ^{101}Ru. The overall similarity prevails also with ^{103}Ru. Two important exceptions should, however, be focused: As already pointed out, the ground state of ^{103}Ru, preferentially excited in (d,p), is not so in (d,t), where, in turn, a predominant population of the $5/2^+_1$ level at 3 keV is observed (note the amplified energy scale in the inset of Fig. 6) and no excitation similar to the $(7/2,9/2)^+$ state at 2.2 MeV seems to exist at least in ^{101}Ru. It is to be regretted that the ^{102}Ru(d,p) reaction by Fortune *et al.* [21], which could help to define the spin of this state, did not cover excitation energies above 2.0 MeV.

Concerning odd l transfers, not much experimental information is available. The strong $l = 5$ excitations detected are associated to known $11/2^-$ levels and show, as expected, increasing hole character as N is augmented. No fragmentation was observed, although it should be remembered that the detection limit for $l = 5$ is relatively high. The $l = 1$ strength seen in the present (d,t) work for ^{101,103}Ru, being perhaps undetected in ^{99}Ru by experimental limitations, lies mostly in the higher excitation energy region. Although $l = 1$ excitations are also seen in ^{100}Ru(d,p) (Ref. [8]), no clearcut relation with the (d,t) results is established and the most intense $l = 1$ transfers observed in ^{104}Ru(d,t) lie outside the energy interval analyzed in the corresponding (d,p) reaction. As for the challenging low-lying $l = 3$ levels, they are stronger excited in (d,p) than in (d,t), especially in the case of the 0.6 MeV state in ^{101}Ru, where the factor between $C^2S'_{lj}$ and C^2S_{lj} (see columns 12 and 6 of Table IV) is about seven. This information was taken as indicative that these states are not core excitations of the $1f$ orbital.

Figure 7 displays the excitation energy of the levels populated through $l = 3$, taken as $7/2^-$, and of possibly related levels in ^{99}Ru (Ref. [17]) and ^{105}Ru (Ref. [22]) as a function of mass number, together with that of the known $11/2^-$ states. A relationship of the $l = 3$ and $l = 5$ excitations seems clear and may be of the same origin as that exposed for ^{99}Ru by the particle plus rotor Coriolis coupled calculations of Whisnant *et al.* [17], although conflicting data in the literature open room for controversies [8]. Figure 7 also illustrates the relative constancy of the excitation energy of the first $7/2^+$ levels, which also appear to have a quite peculiar character, not being influenced by the progressive addition of neutrons to the $N = 50$ core. Also shown in the figure are the excitation energies of the first 2^+ and 3^- states in the even ruthenium isotopes. It is to be noted that the 3^-_1 levels, normally referred to as octupolar vibrations associated to a coherent superposition of particle-hole pairs in adjacent shells and therefore less affected by neutron filling, go down in energy by 0.5 MeV from ^{98}Ru to ^{104}Ru, even more than the 2^+_1 states, formerly supposed as characterizing increasing quadrupolar deformation.

It is, on the other hand, also amazing to recall that, although the spectroscopic strength seen in the transfer reactions on the even target isotopes is widely spread among the several orbital angular momenta associated to the 50 to 82 shell, for each l value, as may be appreciated in Fig. 6, the pick-up reactions under study clearly select, for very preferential population, one, or at most a few, state(s) of the final nuclei with neat quasiparticle character. This excitation pattern is not expected if the Ru isotopes were simple rigid rotors with deformations cor-

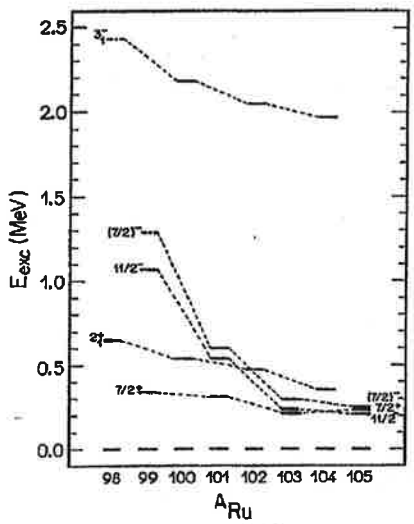

FIG. 7. Excitation energies of the $7/2^+_1$, $11/2^-_1$, and $(7/2)^-_1$ states for the odd isotopes and of the 2^+_1 and 3^-_1 levels for the even isotopes of Ru, as a function of mass number.

responding to the experimentally determined [23,24] β_2, which range between 0.21 and 0.27 for ^{100}Ru to ^{104}Ru. In fact, if the expansion coefficients of states in a statically deformed well onto a spherical basis, as calculated by Chi [25], are analyzed for each transferred l and j, it is verified that an important splitting should occur, especially between the several deformed states which originate from the same spherical orbital [26]. For this range of β_2, Coriolis coupling is not supposed to completely alter the picture [27]. A simple statically deformed core with a deformation parameter of about 0.2 being experimentally discarded, the necessity to resort to variable moment of inertia (VMI) procedures in the rotor analysis by Whisnant *et al.* [17] may reflect the need of relaxing this condition. It is also worthwhile to note that all model calculations [17,28] for the odd ruthenium isotopes with rotor ingredients had, in order to obtain accord, to adhere to β_2 values smaller, by about a factor of two, than those experimentally determined for the even cores. An additional complicator may arise if the recently disclosed hexadecapolar degree of freedom [29] is to be considered.

Perhaps interacting boson-fermion model (IBFM) calculations, which are able to intrinsically absorb a certain softness and, if needed, also collectivity associated with multipolarities of higher order, could provide systematically more consistent results. However, the two existing IBFM studies do not publish spectroscopic factors for the complete chain of Ru isotopes, presenting pick-up results only on ^{104}Ru (Ref. [30]) and ^{102}Ru (Ref. [31]), both below 1.1 MeV. Furthermore, these two calculations only present spectroscopic factors associated to valence orbitals for ^{103}Ru, being the information further restricted to positive parity ones in ^{101}Ru. Thus, the challenging low-lying $l = 3$ and $l = 1$ states cannot have their properties confronted with theory. As far as their predictions go, Arias *et al.* [30] and Maino *et al.* [31] were able to appoint the general trends for the strength distributions, respectively, for the hole states in ^{103}Ru and ^{101}Ru, but could not reproduce the spreading, especially of the $l = 2$ strength. Both works concentrate important $l = 4$ strength in the first $7/2^+$ levels, in accordance with experiment. Besides this, in ^{103}Ru, Arias *et al.* [30] only foresee a second $7/2^+$ state at 1.1 MeV to be populated by pick-up with a relatively small spectroscopic factor, but this state seems to correspond to a level seen in (d,t) and (d,p) at 0.7 MeV and certainly not to the strong $l = 4$ excitation, observed at 2.2 MeV. As previously argued, it is felt that the interpretation of this excitation pattern and of the low-lying odd parity states, in addition to the rest of the systematic experimental information put into evidence by the present work, could represent a quite stringent test on the premises of this or other nuclear models.

ACKNOWLEDGMENTS

This work was partially supported by CNPq (Conselho Nacional do Desenvolvimento Científico e Tecnológico–Brasil), FINEP (Financiadora de Estudos e Projetos), and FAPESP (Fundação de Amparo à Pesquisa do Estado de São Paulo) and this is gratefully acknowledged.

[1] G. R. Satchler, *Direct Nuclear Reactions* (Clarendon, Oxford, 1983).
[2] A. Bohr and B. R. Mottelson, *Nuclear Structure* (Benjamin, New York, 1969, 1975), Vols. 1 and 2.
[3] J. M. Eisenberg and W. Greiner, *Microscopic Theory of the Nucleus* (North Holland, Amsterdam, 1972).
[4] *Nuclear Structure of the Zirconium Region*: Proceedings of International Workshop, Bad Honnef, edited by J. Ebert, R. A. Meyer, and K. Sistemich (Springer, Berlin, 1989).
[5] H. W. Müller and Chmielewska, Nucl. Data Sheets **48**, 663 (1986).
[6] J. Blachot, Nucl. Data Sheets **45**, 701 (1985); **63**, 305 (1991).
[7] D. de Frenne, E. Jacobs, and M. Verboven, Nucl. Data Sheets **45**, 363 (1985); J. Blachot, *ibid.* **68**, 311 (1993).
[8] J. L. M. Duarte, L. B. Horodynski-Matsushigue, T. Borello-Lewin, and O. Dietzsch, Phys. Rev. C **38**, 664 (1988).
[9] K. Koide, F. C. Sampaio, E. M. Takagui, J. H. Hirata, and O. Dietzsch, Nucl. Instrum. Methods **215**, 61 (1983).
[10] D. Pulino, G. M. Sipahi, G. M. Ukita, T. Borello-Lewin, L. B. Horodynski-Matsushigue, J. L. M. Duarte, W. G. P. Engel, and J. C. de Abreu, Rev. Bras. Apl. Vácuo, **10**, 87 (1991).
[11] C. M. Perey and F. G. Perey, Phys. Rev. **132**, 755 (1963).
[12] J. M. Lohr and W. Haeberli, Nucl. Phys. **A232**, 381 (1974).
[13] W. W. Daehnick, J. D. Childs, and Z. Vrcelj, Phys. Rev. C **21**, 2235 (1980).
[14] P. D. Kunz, DWUCK4 code, University of Colorado, 1974 (unpublished).
[15] F. G. Becchetti and G. Greenlees, Phys. Rev. **182**, 1190 (1969).
[16] R. H. Bassel, Phys. Rev. **149**, 791 (1966).
[17] C. S. Whisnant, K. D. Carnes, R. H. Castain, F. A. Rickey, G. S. Samudra, and P. C. Simms, Phys. Rev. C **34**, 443 (1986).
[18] S. A. Dickey, J. J. Kraushaar, and M. A. Rumore, J. Phys. G **12**, 745 (1986).
[19] R. C. Diehl, B. L. Cohen, R. A. Moyer, and L. H. Goldman, Phys. Rev. C **1**, 2085 (1970).
[20] G. P. A. Berg, M. Demarteau, A. Hardt, H. Hürlimann, S. A. Martin, J. Meissburger, W. Oerlert, H. Seyfarth, B. Styczen, M. Kohler, I. Oelrich, and J. Scheerer, Nucl. Phys. **A379**, 93 (1982).
[21] H. T. Fortune, G. C. Morrison, J. A. Nolen Jr., and P. Kienle, Phys. Rev. C **3**, 337 (1971).
[22] P. Maier-Komor, P. Glässel, E. Huenges, H. Rösler, H. J. Scheerer, H. K. Vonach, and H. Baier, Z. Phys. **A278**, 327 (1976).
[23] S. Landsberger, R. Lecomte, P. Paradis, and S. Monaro, Phys. Rev. C **21**, 588 (1980).
[24] J. H. Hirata, Doctoral thesis, Instituto de Física da USP, São Paulo, Brasil, 1984.
[25] B. E. Chi, Nucl. Phys. **83**, 97 (1966).

[26] B. Elbek and P. O. Tjom, Adv. Nucl. Phys. **3**, 259 (1969).
[27] F. S. Stephens, Rev. Mod. Phys. **47**, 43 (1975).
[28] J. Rekstad, Nucl. Phys. **A247**, 7 (1975).
[29] S. Sirota, J. L. M. Duarte, L. B. Horodynski-Matsushigue, and T. Borello-Lewin, Phys. Rev. C **40**, 1527 (1989).
[30] J. M. Arias, C. E. Alonso, and M. Lozano, Nucl. Phys. **A466**, 295 (1987).
[31] G. Maino, A. Ventura, A. M. Bizzeti-Sona, and P. Blasi, Z. Phys. A **340**, 241 (1991).

Anexo 1.3

BRIEF REPORTS

Brief Reports are short papers which report on completed research or are addenda to papers previously published in the **Physical Review.** *A Brief Report may be no longer than four printed pages and must be accompanied by an abstract.*

Systematics of yrast levels in odd Ru isotopes: Do they point to coexistence at low excitation?

T. Borello-Lewin, J. L. M. Duarte, L. B. Horodynski-Matsushigue, and M. D. L. Barbosa
Instituto de Física, Universidade de São Paulo, C.P. 66318, 05315-970, São Paulo, SP, Brazil
(Received 3 October 1997)

New spectroscopic strength information extracted through ^{102}Ru$(d,p)^{103}$Ru shows the $3/2^+$ ground state in ^{103}Ru to be poorly populated in both one-neutron transfer reactions, in contrast with former claims. In comparison with ^{101}Ru, particle and hole strengths are significantly reduced in ^{103}Ru and these facts are interpreted as signs of a poor overlap of the odd isotope with its even neighbors plus or minus one neutron. Very-low-lying $3/2^+$ levels, associated with small one-particle spectroscopic factors, are shown to exist in most odd-neutron nuclei in the region and may represent the lowest state of a coexisting configuration. [S0556-2813(98)06202-5]

PACS number(s): 21.10.Jx, 25.45.Hi, 27.60.+j

Within our systematic experimental research program of the $A\sim100$ nuclei [1,2] we came recently across some peculiar characteristics linking the ground states of even Ru isotopes with states of their odd neighbors. This prompted us to follow those characteristics along the region and this is the theme of the present Brief Report. The São Paulo Nuclear Spectroscopy Group has for more than one decade been involved with experimental nuclear structure research in which light ions (in particular deuterons, protons, and alphas for which the interaction parameters are well established) are employed as spectroscopic tools. Because of the good beam characteristics of the Pelletron accelerator and of the use of nuclear emulsions as detectors at the focal plane of an Enge spectrograph, in addition to the especially prepared thin and uniform targets, high quality data are usually obtained. In fact, the recent ^{102}Ru$(d,p)^{103}$Ru results of the São Paulo Group [1] extended the spectroscopic information up to 3.8 MeV of excitation and revealed 39 levels observed for the first time in this reaction. Figure 1 shows part of the proton spectrum obtained at $\theta_{lab}=8°$, one of the ten angles at which the reaction was observed [1]. Above $E_{exc}=0.9$ MeV much was gained in spectroscopic detail. In all, 79 states were detected, their excitation energies being in excellent agreement with the pertinent adopted values of the Nuclear Data compilation [3]. In particular, γ-ray results, for the 20 levels up to 2.00 MeV of excitation, for which a clear correspondence with states reached by one-neutron transfer may be established, agree with the (d,p) energies mostly within 1 keV, as may be appreciated comparing the energies presented in Fig. 1 with the adopted ones [3]. In this context, the value of $E_{exc}=(3.3\pm0.7)$ keV determined for the lowest energy transition [1] means that in the (d,p) reaction, as well as in the formerly measured (d,t) one [2], the known $5/2^+$ first excited state is populated in a preferential manner. This finding supersedes the indetermination of previous studies [4] which could not decide if the ground state or the first excited state was reached in (d,p). In the emulsion detection technique no possibility of such a difference being due to an

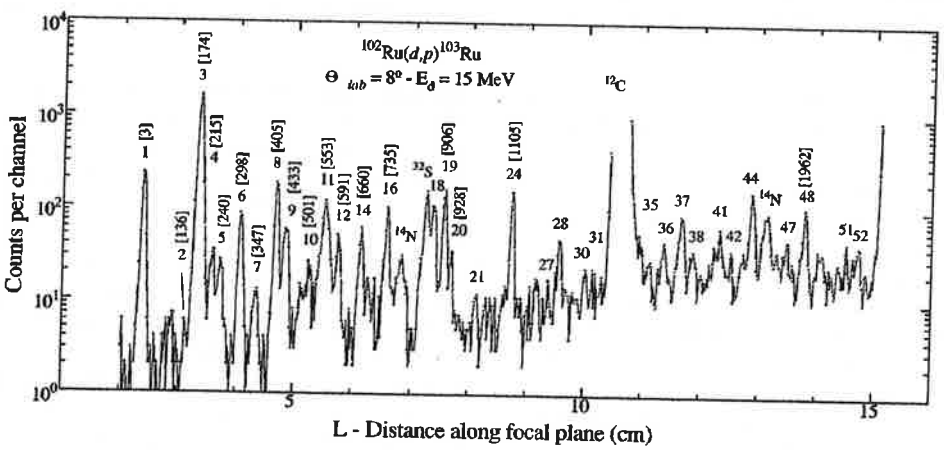

FIG. 1. Partial spectrum (up to ~ 2.1 MeV) of protons emerging from the ^{102}Ru(d,p) reaction at $\theta_{lab}=8°$. The ^{103}Ru levels which were identified in the reaction are sequentially numbered. The energies (in keV) of those levels which have been associated with γ-ray results are presented above, within square brackets.

0556-2813/98/57(2)/967(4)/$15.00

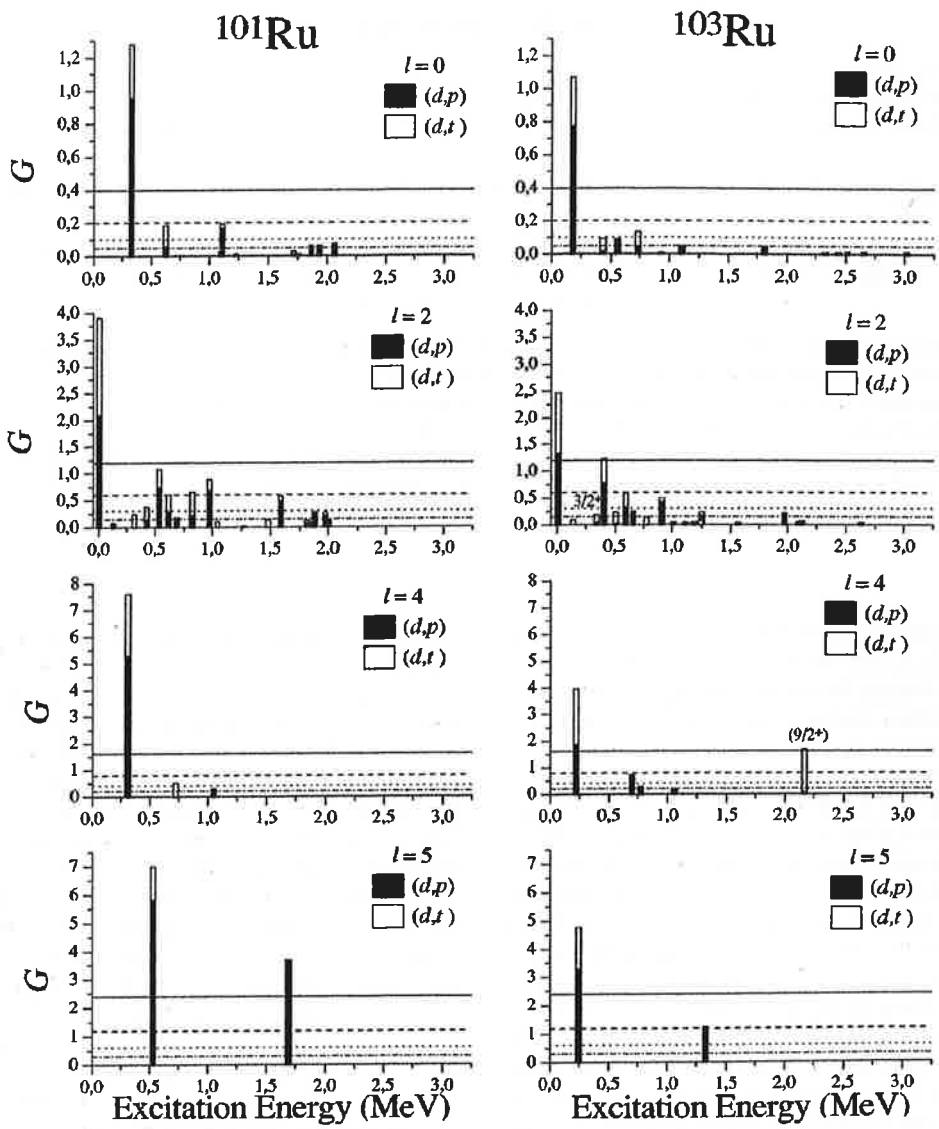

FIG. 2. Spectroscopic strengths, classified according to transferred l, in ^{101,103}Ru [1,2,5]. The symbol $G=G_{\text{pick}}+G_{\text{strip}}$ stands for the summed spectroscopic strengths, with $G_{\text{pick}}=C^2S(d,t)$ and $G_{\text{strip}}=C^2S'(d,p)$. Horizontal lines correspond to cuts at the 2.5%, 5%, 10% and 20% values of the total expected strength, for each l.

experimental zero or scale calibration error exists. In the chain of odd Ru isotopes, $A=101$ [2,5] and $A=103$ [1,2] are now known with similar spectroscopic detail. Figure 2 shows, in an additive and comparative manner, the spectroscopic strengths gathered through the ^{100,102}Ru(d,p) and ^{102,104}Ru(d,t) reactions studied by the São Paulo Group, as superposed solid and open bars, respectively. The information is classified according to transferred orbital angular momentum l, and horizontal lines serve to indicate where cuts, at predetermined fractions of the respective $(2j+1)$ limit of the valence shell, would lie. In the case of $l=2$, the cuts correspond, arbitrarily, to $j=5/2$, as do the strengths, if the level spin is not known. For the other l values, for unknown level spin, the spin of the valence shell model orbital was taken. This procedure may superestimate the valence strengths for $l=2$, 4, and 5. It is to be stressed that, as Fig. 2 shows, the detection limits of the experiments are, except for $l=5$, extremely low and mostly below 1%. An interesting feature put into evidence through Fig. 2 is that in both ^{101,103}Ru, for each l transferred, the levels situated lowest in excitation energy are the most intensely populated. For these states the summed strengths (hole plus particle) always exceed 60% of the limit of the corresponding spherical shell model orbital in ^{101}Ru, while in ^{103}Ru, although the yrast levels still preserve their predominantly quasiparticle character, the strengths are appreciably reduced. A global overview of the information shows that, for each l, in ^{101}Ru the total expected strength was almost all found, but in ^{103}Ru up to $\sim$ 3 MeV of excitation strength is certainly lacking. This loss of strength necessarily indicates that it is difficult to form the ^{103}Ru nucleus starting from either the ^{102}Ru or ^{104}Ru ground states. Other peculiarities are observed for ^{103}Ru. First, it is to be remembered that the first excited state and not the ground state is preferentially populated through $l=2$ transfer, starting both from ^{102}Ru and from ^{104}Ru, defining the lowest ^{103}Ru configuration to be of small similar-

TABLE I. Excitation energy and spectroscopic small intensity of the $3/2^+$ yrast state in ^{A}Ru isotopes.

A	E_{exc} (MeV)	$C^2S'(d,p)$	$C^2S(d,t)$
97	0.18922 [7]	low [8]	—
99	0.08968 [9]	—	0.037 [2]
101	0.12723 [10]	0.067 [5]	0.006 [2]
103	0 [3]	low [1]	low [2]
105	0 [11]	0.009 [6]	

ity with the ground states of the neighboring even isotopes. Second, the state at 2.2 MeV of excitation reached by $l=4$ is, through its excitation characteristics, most probably associated with the $1g_{9/2}$ orbital and, thus, an excitation of the $N=50$ core [1]. Both the high strength and the relatively low excitation energy of this state are rather unexpected.

The uncommon situation of a ground state being poorly populated in one-particle transfer reactions, as was evidenced for ^{103}Ru, merits a closer investigation, both from experimental and theoretical points of view. In fact, the next odd isotope of the ruthenium chain, ^{105}Ru, also displays the same behavior in ^{104}Ru(d,p) [6] and otherwise also very similar spectroscopic characteristics [7]. A survey of the experimental information, for the odd ruthenium isotopes and for the isotones of ^{101,103}Ru (always taken from the most recent Nuclear Data Sheets compilations), can be appreciated for the known yrast states with $J^\pi=1/2^+$ to $9/2^+$ and $J^\pi=7/2^-$ and $11/2^-$ in Figs. 3 and 4. It is seen that a yrast $3/2^+$ is known in most nuclei, appearing for the majority of them at excitation energies lower than 0.3 MeV, this value being exceeded only for ^{97}Zr and ^{109}Sn with known semimagic properties. Table I shows this yrast level to be consistently weakly populated in one-neutron transfer for all cited Ru isotopes, being thus similar to the ^{103,105}Ru ground states. Not many other odd nuclei were studied with similar spectroscopic detail in this mass region; in particular little transfer information is available for the isotones, lying 3–11 neutrons above the magic $N=50$ shell. The $3/2^+$ yrast is, however, known to have small spectroscopic factors also in ^{105}Pd [11] and ^{101}Mo [9]. Other regularities in the here high-

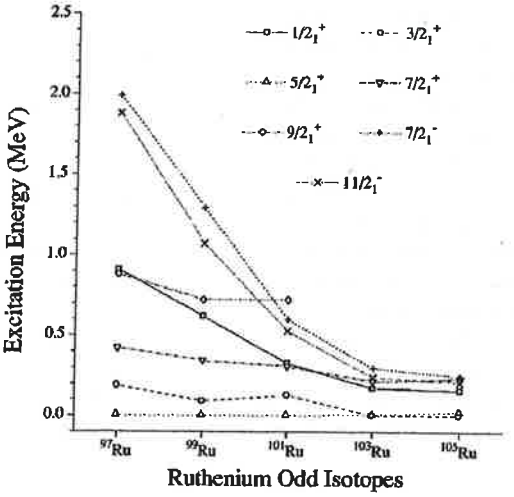

FIG. 3. Yrast states for Ru isotopes.

lighted isotopes and isotones are disclosed through Figs. 3 and 4: the yrast $7/2^+$ and $9/2^+$ levels, where known, and with the exception of ^{97}Zr and ^{107}Sn lie almost constant, respectively, 0.2–0.4 MeV and 0.7–0.9 MeV above the ground state, while the energy of the $11/2^-$ level, followed, where already detected, by a "companion" $7/2^-$ yrast, varies by a factor of 9, being lowest for ^{103,105}Ru. Transfer reactions show all these levels, as well as the $5/2_1^+$, to have an important quasiparticle character in Ru, in contrast to the lowest $3/2^+$ levels. However, it is to be stressed again that the yrast $5/2^+$, $7/2^+$, and $11/2^-$ have their strengths about halved, when going from $A=101$ to $A=103$. The yrast $1/2^+$ level lowers its energy in the Ru isotopes, between $N=53$ and $N=61$, by a factor of about 5, but never becomes a ground state, as it is for the lighter isotones (Sr, Zr, Mo) with $N=57$ and $N=59$. As far as studied, the yrast $1/2^+$ exhausts a rather constant fraction of about half of the expected $3s_{1/2}$ quasiparticle strength throughout the region.

It seems clear that in the $A\sim100$ region, in most odd neutron nuclei, a low-lying $3/2^+$ level exists which has, where measured, a small overlap with the neighboring 0^+

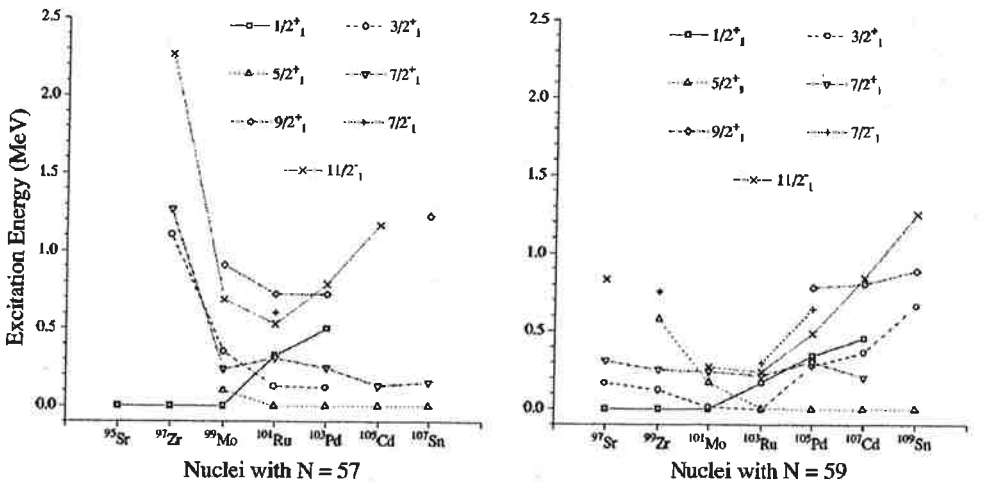

FIG. 4. Yrast states for ^{101,103}Ru isotones.

ground states plus one quasiparticle. Gamma-ray decay properties show it to be linked to other $(3/2^+, 5/2^+)$ levels which are poorly populated in transfer and also to the $1/2_1^+$ one, which in turn has, as already mentioned, an appreciable single-quasiparticle character. This singular $3/2^+$ state may represent the survival of $(2d_{5/2})^3$ characteristics, as interpreted in $^{93}Zr_{53}$ and $^{95}Mo_{53}$ by Talmi [12], as far from the $N=50$ shell as $^{105}Pd_{59}$, a fact which would be certainly surprising. Instead, it could indicate the presence in the odd neutron nuclei in this mass region of still more complex configurations at very low excitation. Both situations may be taken as characterizing a coexistence phenomenon in these nuclei, put also into evidence through a very consistent γ decay pattern, which always favors the feeding of either, one or the other, the yrast $5/2^+$ or the yrast $3/2^+$ states. A "parent" configuration for these coexisting states in the odd Ru isotopes is not easily traced in the even neighbors. The broken pair $(2d_{5/2})^2$ would be obviously absent in the even ground state, but it is also not evident in the rest of the spectra if available experimental information is taken into account; nor is there any other configuration which could provide the basis for a direct interpretation of the $3/2_1^+$ state in the odd neutron nuclei.

This work was partially supported by Conselho Nacional de Desenvolvimento Científico e Tecnológico (CNPq), Coordenação do Aperfeiçoamento de Pessoal de Nível Superior (CAPES), Financiadora de Estudos e Projetos (FINEP), and Fundação de Amparo à Pesquisa do Estado de São Paulo (FAPESP).

[1] M. D. L. Barbosa, Master thesis, Instituto de Física da Universidade de São Paulo, São Paulo, Brazil, 1997; M. D. L. Barbosa, T. Borello-Lewin, J. L. M. Duarte, and L. B. Horodynski-Matsushigue (unpublished).
[2] J. L. M. Duarte, T. Borello-Lewin, and L. B. Horodynski-Matsushigue, Phys. Rev. C **50**, 666 (1994).
[3] J. Blachot, Nucl. Data Sheets **68**, 311 (1993).
[4] G. P. A. Berg, M. Demarteau, A. Hardt, W. Hürlimann, S. A. Martin, and J. Mei, Nucl. Phys. **A379**, 93 (1982).
[5] J. L. M. Duarte, L. B. Horodynski-Matsushigue, T. Borello-Lewin, and O. Dietzsch, Phys. Rev. C **38**, 664 (1988).
[6] P. Maier-Komor, P. Glässel, E. Huenges, H. Rösler, H. J. Scheerer, H. K. Vonach, and H. Baier, Z. Phys. A **278**, 327 (1976).
[7] A. Artna-Cohen, Nucl. Data Sheets **70**, 85 (1993).
[8] L. R. Medsker, L. H. Fry, Jr., and J. L. Yntema, Phys. Rev. C **15**, 649 (1977).
[9] L. K. Peker, Nucl. Data Sheets **73**, 1 (1994).
[10] J. Blachot, Nucl. Data Sheets **63**, 305 (1991).
[11] D. de Frenne and E. Jacobs, Nucl. Data Sheets **68**, 935 (1993).
[12] I. Talmi, *Simple Models of Complex Nuclei* (Harwood, Chur, Switzerland, 1993).

Anexo 1.4

Single particle strengths in ^{103}Ru with the ^{102}Ru(d,p) reaction

M. D. L. Barbosa, T. Borello-Lewin, L. B. Horodynski-Matsushigue, J. L. M. Duarte, G. M. Ukita, and L. C. Gomes
Instituto de Física, Universidade de São Paulo, Caixa Postal 66318, CEP 05389-970, São Paulo, SP, Brazil
(Received 10 June 1998)

The ^{102}Ru$(d,p)^{103}$Ru reaction was studied at the Pelletron-Enge-spectrograph facility up to 3.5 MeV with the nuclear emulsion technique. In all 73 levels were populated and for 64 of them angular distributions are presented. Through the usual distorted wave Born approximation analysis, transferred l values and the corresponding spectroscopic factors could be attributed with certainty to 31 and doubtfully to ~20 more excitations, several of them new. Most of the one-particle strength is concentrated in the yrast levels, below 0.3 MeV. Only the $l=2$ strength is appreciably fragmented. Even within the extended excitation energy range and with the low detection limit of the present experiment, about half of the expected (d,p) strength remains undetected in ^{103}Ru, in contrast to ^{101}Ru. [S0556-2813(98)00711-0]

PACS number(s): 21.10.Jx, 25.45.Hi, 27.60.+j

I. INTRODUCTION

Although having been intensely investigated for at least two decades, the chain of ruthenium isotopes, as well as several other nuclei in the $A\sim100$ mass region, still presents challenges for both theoretical and experimental research. The São Paulo Nuclear Spectroscopy Group has been involved in experiments through which detailed information on the single particle and single hole neutron strength distributions for several Ru isotopes was obtained with the use of (d,p) [1,2] and (d,t) [3] reactions, taking advantage of the good energy resolution and low background allowed for by the experimental setup. The results thus obtained, which owe their quality mostly to the nuclear emulsion technique [3] and to the good characteristics of the beam, could definitely assign values of transferred orbital momentum l to several transitions in the isotopes studied and showed, in particular, a rather intense population of low-lying $7/2^-$ levels in ^{101,103}Ru [1,3]. Other features which pointed to singular nuclear structure properties of the $^{99-103}$Ru isotopes also appeared in systematic one-neutron pickup studies [3]: the lowest-lying level, detected for each characteristic l of the valence shell, always concentrates the highest spectroscopic intensity, is populated with an appreciable fraction of the total expected strength, and lies, for the heavier isotopes, mostly below 0.5 MeV. All spherical valence orbitals are thus filling, irrespective of neutron number. No filling systematic is apparent [2,3] and, for each orbital, not much fractionating is observed.

Furthermore, in the ^{104}Ru$(d,t)^{103}$Ru reaction [3] an intense $l=4$ transition, formerly unknown, was observed at 2.2 MeV of excitation, which was tentatively assigned as transferring $j=7/2$ [3]. Although previous ^{102}Ru(d,p) data existed [4,5], none of those studies covered the region above 2 MeV. Also, former work [4,5] did not exhaust the expected ^{102}Ru(d,p) strength, in contrast to what the Nuclear Spectroscopy Group found for ^{100}Ru (d,p) [1] and this could in part be due to lack of detail and/or restricted excitation energy range in the previous studies. The present work was begun mostly to confirm the characteristics of the level at 2.2 MeV, but brought, besides a much greater detail for the already investigated [4,5] range of excitation energy, several important new pieces of spectroscopic information [2], which challenge a theoretical interpretation.

II. EXPERIMENTAL PROCEDURE

The 15.0 MeV deuteron beam of the São Paulo Pelletron accelerator was focused on a uniform target of ^{102}Ru (enriched to 99.35%), after passing defining slits of 1.0 $\times$3.0 mm^2. The target was prepared by electron bombardment evaporation of metallic ruthenium powder onto a thin carbon backing [6]. The thickness of the ruthenium film was about 15 μg/cm^2. The protons produced in the reaction were momentum analyzed by an Enge split-pole spectrograph and detected in nuclear emulsion. Aluminum foils, thick enough to absorb heavier reaction products, covered the emulsion. The protons were observed at ten angles, from $\Theta_{lab}=8°$ to $\Theta_{lab}=55°$, and the exposed plates were scanned, after processing, in strips of 200 μm across the plates. An energy resolution of 11 keV was achieved. The spectrum corresponding to $\Theta_{lab}=45°$ is shown in Fig. 1 and can be regarded as typical of the spectra measured at other angles.

Relative normalization of the spectra was obtained by measuring with a current integrator the total charge collected in an aligned Faraday cup with electron suppression, while continuously monitoring the direction of the beam. Absolute normalization of the cross sections was referred to optical model predictions for elastic scattering of deuterons on the same target, measured under similar conditions. Elastic spec-

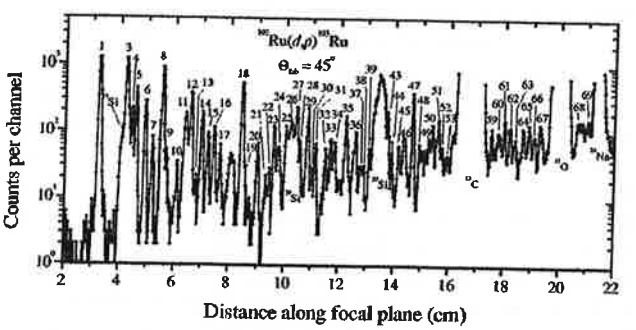

FIG. 1. Spectrum of protons at $\Theta_{lab}=45°$.

TABLE I. Optical potential for the exit and entrance channels and potential which binds the transferred neutron.

Particle	Potential	V_0 (MeV)	r_0 (fm)	a_0 (fm)	W (MeV)	r_w (fm)	a_w (fm)	W_D (MeV)	r_D (fm)	a_D (fm)	V_{s0} (MeV)	r_{s0} (fm)	a_{s0} (fm)	r_c (fm)
Proton	BG [a]	55.17	1.17	0.75	1.48	1.32	0.61	35.19	1.32	0.61	24.80	1.01	0.75	1.25
	PP [b]	50.54	1.25	0.65				54.00	1.25	0.47	30.00	1.25	0.47	1.25
Deuteron	LH [c]	111.85	1.05	0.86				39.96	1.43	0.78	14.00	0.75	0.50	1.15
	PP [b]	96.54	1.15	0.81				72.00	1.34	0.68	14.00	0.75	0.50	1.15
	DA [d]	92.89	1.17	0.74	0.29	1.33	0.86	49.20	1.33	0.86	13.80	1.07	0.66	1.15
Bound neutron	BG [a]	fitted	1.17	0.75							$\lambda=25$			

[a]Reference [16].
[b]Reference [7].
[c]Reference [8].
[d]Reference [9].

tra were obtained at six laboratory scattering angles, from 30° to 80°. Three families of optical potentials, from the systematics of Perey and Perey (PP) [7], Lohr and Haeberli (LH) [8], and Daehnick *et al.* (DCV) [9] (see Table I), produced cross sections which differed, in the mentioned range of angles, by at most 6%. Considering furthermore the contributions of the target nonuniformity, plate scanning, and statistics in the elastic scattering data, a maximum scale uncertainty of 8% is estimated for the absolute cross section.

III. RESULTS

The excitation energies shown in Table II are the averages of the energies which resulted for each level in the several spectra, employing the calibration of the spectrograph in common use, which was obtained through the analysis [10] of the ^{90}Zr(α,α') reaction up to 5.9 MeV of excitation, covering thus a great interval of bending radii. No transitions were considered unless a peak could be discerned at the appropriate location in at least three of the spectra. For the most intense transitions, in particular those associated with levels below $E_{exc}=1.0$ MeV, the totality of the ten spectra determined the excitation energy values of Table II. The dispersion of the individual values around their mean, as measured through their standard deviations, is typically 2 keV, resulting in statistical uncertainties in the excitation energies of ≤ 1 keV. In addition to these uncertainties a scale uncertainty, to be discussed below, should be considered.

The previous stripping studies [4,5] were limited to a couple of MeV of excitation energy. Their results are shown in Table II in comparison with the present ones and also with the results of the (d,t) work of the São Paulo Group [3] and the adopted levels [11]. The present experiment extended the excitation energy interval analyzed by stripping reactions up to 3.5 MeV. The detection limit below ~ 1.5 MeV is less than 10 μb/sr and somewhat higher above this energy. Fortune *et al.* [4], in their (d,p) study with deuterons of 14 MeV and an energy resolution of 12 keV, declare in most cases total uncertainties of 5 keV in their excitation energies, which are thus in very good agreement with the present results. The work of Berg *et al.* [5] was performed at a high-dispersion spectrograph with deuterons of 45 MeV, a resolution between 8 and 12 keV, and has stated uncertainties of 2–3 keV in the excitation energies, but did not exceed 0.9 MeV of excitation. Berg *et al.* [5] studied both the (p,d) and (d,p) reactions leading to ^{103}Ru, unfortunately with very poor statistics. They argued that the lowest-lying $l=2$ transfer selects in the pickup reaction the known $5/2^+$ first excited state [11], in agreement with the findings of the (d,t) studies of Duarte *et al.* [3]. On the contrary, the stripping data were taken by Berg *et al.* [5] as indicating a preferential population of the $3/2^+$ ground state. If, however, the level labeled 1 in present study was forced to correspond to the excitation energy zero, an average discrepancy of (-3.3 ± 0.2) keV with respect to the excitation energies of the Nuclear Data Sheets (NDS) compilation [11] resulted, for the about 20 strong transitions (up to 2 MeV) for which a clear correspondence with levels reported in γ ray studies [12–14] could be established. This result points to an also preferential population of the first excited state at 2.81 keV [11] in the stripping, as well as in the pickup reactions, in disagreement with the indication of Berg *et al.* [5], which was adopted by the compilation [11]. Niizeki *et al.* [14] in their analysis of ^{103}Ru, following the study of the β^- decay of ^{103}Tc, had already argued in favor of this attribution.

Taking into account, furthermore, the experimental definition of the centroids of the peaks associated with level 1, in the present study an energy value of (3.3 ± 0.7) keV is finally attributed to this level. Inspection of Table II reveals excellent agreement between the level energies here obtained and those measured by γ decay [11]. It may thus be presumed that the excitation energy scale uncertainty associated with the spectrograph calibration in use is rather small. We estimate that below 2.0 MeV the scale uncertainty is ≤ 2 keV and it should not exceed 5 keV below 5.0 MeV of excitation energy.

It is to be noted that with respect to the recent Nuclear Data Sheets compilation [11], in the present study many levels were seen which had not been formerly reported, in particular above 2.2 MeV of excitation. In fact, the present study detected 73 levels, which are to be compared to the 24 ones (up to 2.0 MeV) and 18 ones (up to 0.77 MeV) previously known through the deuteron stripping reactions performed, respectively, by Fortune *et al.* [4] and Berg *et al.* [5].

Figures 2–5 display the experimental angular distributions, for those transitions for which the cross section was

TABLE II. Results of the present work in comparison with former one neutron transfer results and the adopted levels.

	Present work E_d=15 MeV				(d,p)[a] E_d=45 MeV				(d,p)[b] E_d=14 MeV			(d,t)[c] E_d=16 MeV				NDS[d]	
Peak	E_{exc} (MeV)	l	j	C^2S'	E_{exc} (MeV)	l	j	C^2S'	E_{exc} (MeV)	l	C^2S'	E_{exc} (MeV)	l	j	C^2S	E_{exc} (MeV)	J^π
																0.000	$3/2^+$
1	0.003	2	5/2	1.35	0.001	2	(3/2)	1.44	0.000	2	1.40	0.002	2	5/2	1.11	0.00281	$5/2^+$
2	0.136	2	5/2	0.012					0.139	(2)	(≤0.01)	0.136	2	5/2	0.072	0.136079	$5/2^+$
3	0.174	0	1/2	0.75	0.176	0	1/2	1.05	0.170	0	0.85	0.174	0	1/2	0.29	0.17426	$1/2^+$
4	0.215	4	7/2	1.80	0.215	4	7/2	1.57	0.213	4	2.35	0.213	4	7/2	2.07	0.21356	$7/2^+$
5	0.240	5	11/2	3.2	0.242	5	11/2	2.35	0.237	5	3.25	0.239	5	11/2	1.47	0.2382	$11/2^-$
6	0.298	3	7/2	0.40	0.299	3	(7/2)	0.26	0.295	(1;3)	(0.17;1.5)	0.297	3	7/2;5/2	0.16;0.22	0.2971	$(7/2^-)$
																0.29748	$(3/2^+)$
7	0.347	2	3/2	0.060	0.350	2	(5/2)	0.05	0.339	(2)	(≤0.06)	0.346	2	5/2;3/2	0.10;0.13	0.34638	$3/2^+$
																0.40415	$7/2^+$
8	0.405	2	5/2;3/2	0.82;0.92	0.405	2	5/2;3/2	0.94;1.1	0.401	2	0.85	0.406	2	5/2;3/2	0.35;0.44	0.40608	$5/2^+;3/2^+$
9	0.433	0	1/2	0.027	0.435	0	1/2	0.08	0.429	0	0.06	0.432	0	1/2	0.070	0.43206	$1/2^+$
10	0.501	2	(5/2)	0.032	0.504	2	(5/2)	0.02	0.499	(2)	(≤0.05)	0.501	2	5/2;3/2	0.17;0.20	0.50115	$(5/2)^+$
					0.535	(2)	(5/2)	0.03	0.541	2	0.14	0.540				0.5354	$(5/2^+;3/2^+)$
		(1)	(3/2)	(0.018)								0.548				0.54821	$(1/2^+)$
11	0.553	0	1/2	0.046					0.551	0	0.06					0.55458	$(1/2^+)$
		2	(5/2)	0.074													
												0.556				0.5577	(9/2)
					0.562	(2)	(3/2)	0.13								0.56287	$(5/2^+;3/2^+)$
																0.56817	$(1/2^+)$
12	0.591	2	(5/2)	0.35	0.593	2	5/2	0.22	0.589	2	0.33	0.592	2	5/2;3/2	0.21;0.25	0.59197	$(5/2)^+$
13	0.624	(2)	(5/2)	(0.009)	0.626	(2)	(5/2)	0.04								0.6220	$(5/2^+)$
																0.6537	$15/2^-$
14	0.660	2	(3/2)	0.251	0.661	2	3/2	0.18	0.658	2	0.24	0.662				0.66155	$(3/2)^+$
15	0.697	4	7/2	0.71	0.697	4	(7/2)	0.37	0.696	4	1.00	0.697				0.6972	$7/2^+;9/2^+$
																0.7352	$(5/2^+)$
16	0.735	0	1/2	0.053	0.736	0	1/2	0.17	0.735	0	0.06	0.737	0	1/2	0.086	0.73689	$1/2^+$
																0.7488	$(5/2^+)$
17	0.771	4	(7/2)	0.30	0.774	(0;2)		(0.1;0.03)									
																0.7741	$(11/2^+)$
												0.775	2	5/2;3/2	0.11;0.13	0.77477	$(5/2^+;3/2)$
												0.855					
																0.87371	$(5/2^+;3/2^+)$
																0.90305	$(\leq 5/2^+)$

TABLE II. (*Continued.*)

	Present work E_d=15 MeV				(d,p)[a] E_d=45 MeV				(d,p)[b] E_d=14 MeV			(d,t)[c] E_d=16 MeV				NDS[d]	
Peak	E_{exc} (MeV)	l	j	C^2S'	E_{exc} (MeV)	l	j	C^2S'	E_{exc} (MeV)	l	C^2S'	E_{exc} (MeV)	l	j	C^2S	E_{exc} (MeV)	J^π
18	0.906	2	5/2;3/2	0.47;0.51	0.906	2	3/2	0.52	0.906	2	0.67	0.908	(2)	(5/2;3/2)	(0.050;0.061)	0.90536	$5/2^+;3/2^+$
																0.90764	$(\leq 5/2^+)$
																0.9116	$(7/2^+)$
19	0.928	0	1/2	0.008								0.928				0.92724	$(1/2^+;3/2^+)$
																0.9313	(5/2;3/2)
												0.942				0.94050	
																0.9544	(3/2)
																0.9916	
20	1.003	2	5/2;3/2	0.049;0.053					1.005	2	0.09	1.005				1.005	$5/2^+;3/2^+$
																1.0181	(5/2;7/2)
																1.0204	$(13/2^-)$
21	1.057	(4)	(7/2)	(0.17)													
												1.067				1.06514	$3/2^+;5/2^+;7/2^+$
22	1.078	(4)	(9/2;7/2)	(0.09;0.13)								1.080	(4)	(9/2;7/2)	(0.40;0.68)	1.0796	
23	1.105	0	1/2	0.066					1.105	0	0.08					1.1067	$1/2^+$
												1.109	(2)	(5/2;3/2)	(0.024;0.031)	1.1101	$(5/2^+;3/2;1/2)$
																1.1106	$(11/2^+)$
																1.1337	
24	1.138															1.1406	(5/2;3/2)
																1.1713	(1/2;3/2)
																1.17408	(3/2)
25	1.182	2	5/2;3/2	0.039;0.045													
																1.1999	$13/2^+$
26	1.215	2	5/2;3/2	0.031;0.035													
												1.238	2	5/2;3/2	0.050;0.062		
27	1.248	2	5/2;3/2	0.165;0.186					1.245	2	0.26	1.251	2	5/2;3/2	0.036;0.043	1.245	$5/2^+;3/2^+$
28	1.269	(1;2)		(0.010;0.026)												1.2698	
																1.2882	
																1.3015	$(19/2^-)$
																1.3136	$11/2^+$
29	1.322	5	11/2	1.37					1.320	(3;5)	(0.4;1.0)	1.325				1.3244	
												1.338					
30	1.346	(≤ 3)														1.34712	
31	1.370	(4;5)		(0.29;0.41)													
																1.3784	
												1.403				1.40098	

TABLE II. (*Continued.*)

	Present work E_d=15 MeV			(d,p)[a] E_d=45 MeV				(d,p)[b] E_d=14 MeV			(d,t)[c] E_d=16 MeV				NDS[d]	
Peak	E_{exc} (MeV)	l	j	C^2S'	E_{exc} (MeV)	l	j	C^2S'	E_{exc} (MeV)	l	C^2S'	E_{exc} (MeV)	l	j	C^2S	E_{exc} (MeV)	J^π
32	1.430	(2;3)		(0.039;0.047)												1.43112	
33	1.461	(2;3)		(0.052;0.058)												1.4437	$(15/2^+)$
34	1.486															1.4738	
35	1.554	(2)	(5/2;3/2)	(0.134;0.153)					1.55	(2)	(0.15)	1.491 1.559	2	5/2;3/2	0.026;0.029	1.550	$(5/2^+;3/2^+)$
36	1.604															1.60447	
37	1.642																
38	1.662	(2)	(5/2;3/2)	(0.019;0.021)													
39	1.699																
40	1.717	($\leq$2)														1.7171	
41	1.751	(1;2)		(0.011;0.030)												1.7304	
42	1.780	(2;3)		(0.031;0.043)								1.756	1	3/2;1/2	0.05;0.06		
43	1.809	0	1/2	0.081					1.805	(0)	(0.07)					1.8050	$(1/2^+)$
44	1.834											1.817					
45	1.876	(2;3)		(0.045;0.063)												1.83588	
																1.88054	
46	1.910	(1)	(3/2;1/2)	(0.019;0.020)								1.892				1.90614	
47	1.962	2	5/2;3/2	0.253;0.284					1.96	(2)	(0.35)	1.916					
48	2.004	(1;2)		(0.018;0.040)												1.96192 2.0037	$(5/2^+;3/2^+)$
49	2.058	(2)	(5/2;3/2)	(0.022;0.026)								2.022					
50	2.082	2	5/2;3/2	0.054;0.062													
51	2.118	(2)	(5/2;3/2)	(0.075;0.084)													
																2.1319	$19/2^+$
52	2.137	(2)	(5/2;3/2)	(0.016;0.018)												2.132	$(23/2^-)$
53	2.167	4	9/2	0.08								2.167	4	9/2;7/2	1.6;2.7		
54	2.207															2.20611	
												2.217					

TABLE II. (*Continued.*)

	Present work E_d=15 MeV			$(d,p)^a$ E_d=45 MeV				$(d,p)^b$ E_d=14 MeV			$(d,t)^c$ E_d=16 MeV				NDS[d]	
Peak	E_{exc} (MeV)	l	j	C^2S'	E_{exc} (MeV)	l	j	C^2S'	E_{exc} (MeV)	l	C^2S'	E_{exc} (MeV)	l	j	C^2S	E_{exc} (MeV)	J^π
55	2.224															2.2236	
												2.232					
56	2.248																
57	2.280																
												2.299	1	3/2;1/2	0.04;0.05		
												2.384	1	3/2;1/2	0.07;0.08		
58	2.405																
59	2.436																
60	2.489	(≤2)															
												2.507	1	3/2;1/2	0.013;0.018		
61	2.515	0	1/2	0.033								2.520					
62	2.548	1	3/2;1/2	0.033;0.034													
63	2.578															2.57620	
64	2.627	2	5/2;3/2	0.044;0.050													
65	2.657																
																2.680	$(23/2^+)$
66	2.694																
67	2.723																
68	2.960																
69	3.015	(0;1)		(0.037;0.025)													
70	3.062																
																3.080	$(27/2^-)$
71	3.204																
72	3.325																
73	3.512																

[a]Reference [5].
[b]Reference [4].
[c]Reference [3].
[d]Reference [11].

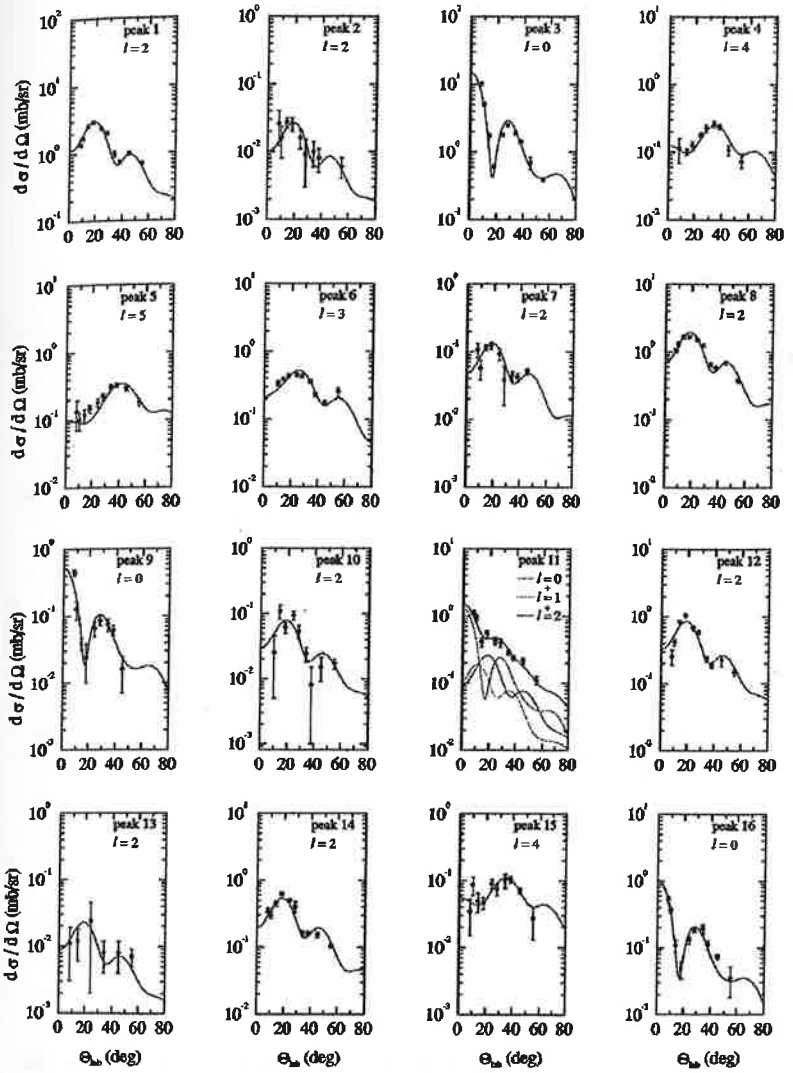

FIG. 2. Angular distributions for ^{102}Ru$(d,p)^{103}$Ru in comparison with DWBA predictions. The uncertainty bars represent contributions of statistics, plate scanning, and background (and/or contaminant) subtraction and do not include any error in the absolute cross section scale. The levels are sequentially labeled and the corresponding energies are shown in Table II.

measured at, at least, five angles. The uncertainty bars include contributions of statistical deviations and uncertainties due to plate scanning, background subtraction, and relative normalization.

The angular distributions were compared with predictions of distorted wave Born approximation (DWBA) calculations, with corrections to include finite range and nonlocality effects, performed by means of the code DWUCK4 [15]. The correction parameters for finite range and nonlocality employed were $R_{\rm FR}=0.62$ fm, $\beta_d=0.54$ fm, $\beta_p=0.85$ fm. The optical model parameters for the entrance and exit channels were taken from the analysis of Perey and Perey [7] for deuteron scattering, with the addition of a spin-orbit term suggested by Lohr and Haeberli [8], and from the analysis of Becchetti and Greenlees [16] for proton scattering. The captured neutron was assumed to be bound by a real potential well of Woods-Saxon shape plus a spin-orbit term of the usual Thomas form. The parameters used are presented in Table I, under the labels PP and BG. Except for the $1g_{9/2}$, $3p$, and $2f$ orbits, the neutron single particle orbitals taken were those of the 50–82 shell.

Least squares fits of the DWBA results to the experimental angular distributions are shown in Figs. 2–5, whenever an assignment of transferred angular momentum l was attempted. The reduced spectroscopic intensities $C^2S'_{lj}$ were extracted through the relationship

$$\sigma_{\rm expt}(\theta)=1.55\ \ C^2S'_{lj}\frac{\sigma^{\rm DW}_{lj}(\theta)}{2j+1}.$$

The values obtained for l and $C^2S'_{lj}$ are also shown in Table II. If different global prescriptions for the optical model parameters are used in the entrance [7–9] and exit [7,16] channels, a maximum variation of $\pm 15\%$ in the reduced spectroscopic factors occurs, while the shapes of the angular distributions are practically not changed.

Where comparison is possible, general agreement is found between the results of the present and former (d,p) works [4,5]. Specific comments on the experimental results are made in the following.

The region around 0.55 MeV of excitation in ^{103}Ru is recognized [11] as spectroscopically complex. In fact, the Nuclear Data compilation [11] presents six levels between 535.4 and 568.17 keV, at least two of which have inconsistent spin attributions in the different experiments. The peaks

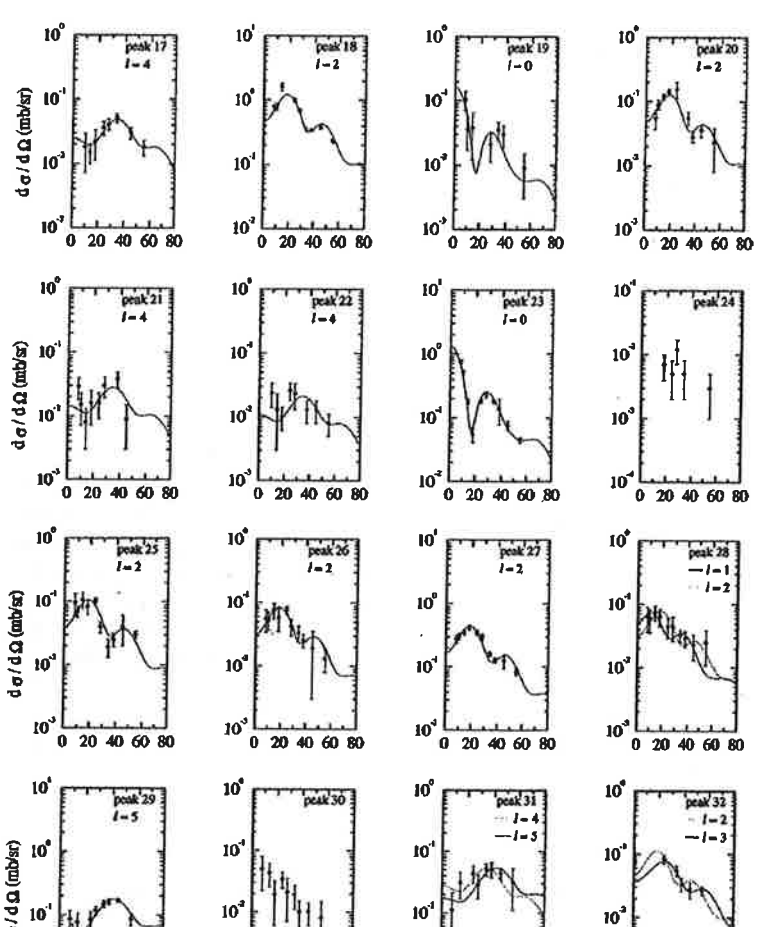

FIG. 3. Angular distributions for ^{102}Ru$(d,p)^{103}$Ru (see Fig. 2).

associated in the present experiment with level 11, in the several spectra, are at least doublets and most probably triplets. A tail is clearly seen in the higher-energy region, but the peaks are, in most spectra, also broader in the lower-energy portion. The integrated angular distribution, which is shown in Fig. 2, reveals, at the two most forward angles, a predominant $l=0$ contribution, at 552 keV of excitation energy. The spectrum at the minimum for $l=0$ ($\Theta_{\rm lab}=18°$), however, showed that admixtures of higher l are also present, but no unambiguous excitation energy attribution could be made. A good fit to the integrated angular distribution, consistent with the information contained in the spectra, was achieved through a superposition of $l=1$, $l=0$, and $l=2$ transfers (see Fig. 2). It is even possible that a fourth level contributes somewhat to the integrated cross section. In the former (d,t) work [3] three peaks were seen, the lower one at 540 keV being much weaker than the other two. Reanalysis of the published integrated angular distribution (see Fig. 6) showed these higher-lying two peaks to possibly correspond to $l=1$ and $l=4$ components, predominating in that reaction, with a smaller contribution of $l=0$ or perhaps $l=2$. The $l=0$ would correspond to the 554.58 keV ($1/2^+$) level, integrated into these other two. If $l=2$ should be considered instead, its contribution exceeds what could correspond to the intensity at 540 keV. The information available in the literature for this region is conflicting. To begin with, the weakly excited level at 535 keV was reported only by the (d,p) study of Berg *et al.* [5], was not identified in their published spectra, and is incompatible with the present findings. The 541 keV level was separated by Fortune *et al.* [4] from their predominant $l=0$ excitation at 551 keV through a peak-shape fitting procedure. The present study rules an $l=2$ excitation with the spectroscopic intensity proposed by Fortune *et al.* [4] at as low an energy as 541 keV completely out. Of the three levels identified in this region as ($1/2^+$) by the compilation [11], the lowest one, at 548.21 keV, has had formerly an attributed spin and parity of $(5/2)^-$ in the (n,γ) study [17] and in the older $(\alpha,n\gamma)$ one [13]. The (n,γ) work [17] based its attribution on the $E2+M1$ character determined for the γ transition to the 297.3 keV state, which in turn, as stated by the authors, decays by an $(E1+M2)$ transition to the $5/2_1^+$ level. The $J^\pi=(5/2)^-$ value would be consistent with the $7/2^-$ character for the intermediate state, but $J^\pi=3/2^-$ could possibly also accomodate the experimental information, and would then correspond to the $l=1$ excitation seen in (d,p) and (d,t). The 548.21 keV level is not seen in β^- decay. On the other hand, the adopted level at 554.58 keV, seen in β^- decay [14] and (n,γ) [17] which has by both attributed ($1/2^+$), is most probably to be associated

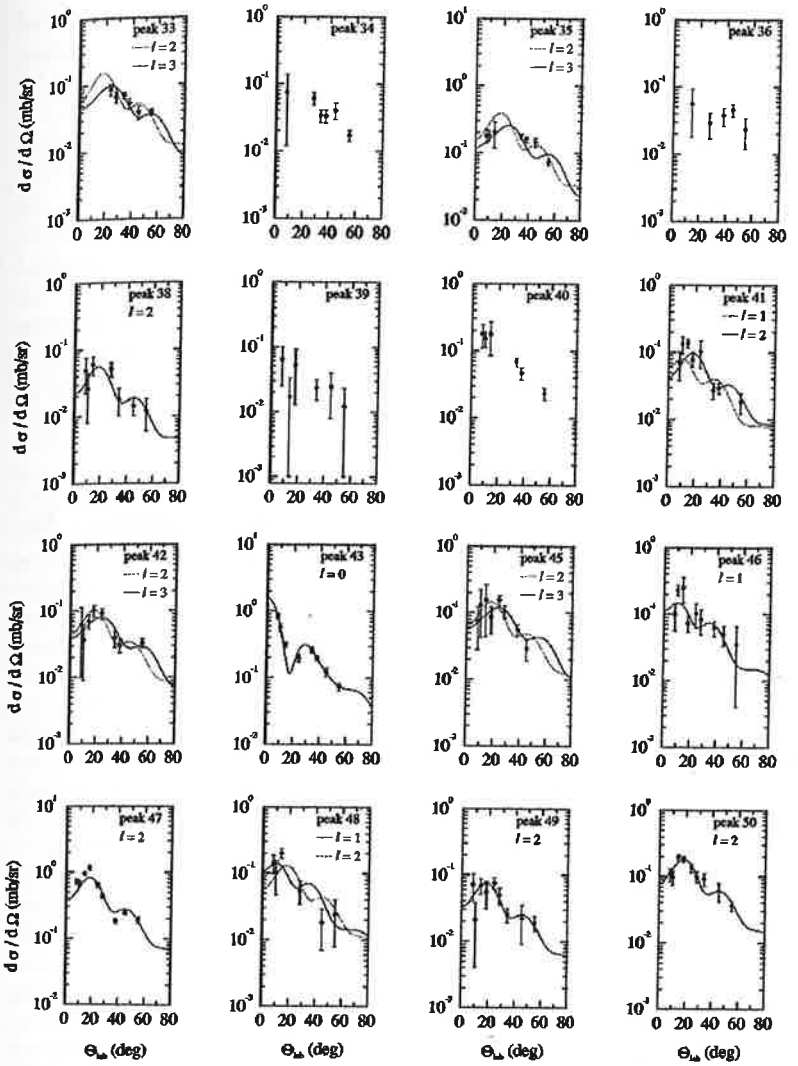

FIG. 4. Angular distributions for ^{102}Ru$(d,p)^{103}$Ru (see Fig. 2).

with the predominant $l=0$ component located by the present work at 552 keV and at 551 keV by Fortune *et al.* [4]. The $(\alpha,n\gamma)$ works [13,18] defined a (9/2) level at 557.7 keV, not seen in the other γ ray studies, and this probably corresponds to the $l=4$ component seen in (d,t). Finally, all γ works locate a level at ~563 keV with possibly $(3/2^+,5/2^+)$ characteristics, but present differing decay modes for it. This level, if excited, should appear as integrated into the peak labeled 11, being seen as a tail. This tail could also contain a contribution to the 568.17 keV level seen in (n,γ) and $(\alpha,n\gamma)$. This last level is now assumed to have $J^\pi=(1/2^+)$ [11], but had, in the older γ works, $(3/2,5/2,7/2)^-$ attributed to it [13]. The $l=(2)$ level located by Berg *et al.* [5] at 562 keV, and for which no angular distribution was shown, cannot correspond to the present result, in view of its high spectroscopic strength.

Peak 17 was detected at eight angles, the corresponding excitation energy of 770.9 keV presents a standard deviation of only 1.6 keV, and the angular distribution displays a clear $l=4$ transfer pattern. On the other hand, the ^{104}Ru(d,t) reaction had previously populated [3] an $l=2$ excitation at 775 keV, which was associated with the adopted [11] 774.77 keV $(5/2^+,3/2)$ excitation formerly seen in the (n,γ) [17]. Considering also the energy difference of 4 keV, the complementary transfer reactions are almost certainly exciting different states in this energy region. The angular distribution at 774 keV associated by Berg *et al.* [5] with a superposition of $l=0+2$ could, in fact, be interpreted as due to $l=4$.

Peaks 21, 25, and 26 are new results of this work and lie below the detection limit stated by Fortune *et al.* [4]. Peak 35, contaminated at intermediate angles, shows an angular distribution which is consistent with the former $l=2$ attributions [3,4] and will be considered as sure in the computation of the total strength. It is worth noting that the corresponding level energy of 1550(10) keV, adopted by Ref. [11], is based only on the former (d,p) work by Fortune *et al.* [4], being thus in accordance with the other transfer results. New $l=2$ and $l=0$ excitations were also seen above 2.0 MeV (levels 50, 64, and 61).

Table II shows that the values of the reduced spectroscopic factors are in good agreement with those published by Fortune *et al.* [4], in general even better than if those were affected by the estimated uncertainty of 50%, declared by the authors. An exception is the level number 6, where the discrepancy, considering their tentative $l=3$ attribution, amounts to a factor of 4. However, even in this case, the spectroscopic strengths extracted in both studies turned out compatible in reanalyzing the data of Fortune *et al.* [4] under

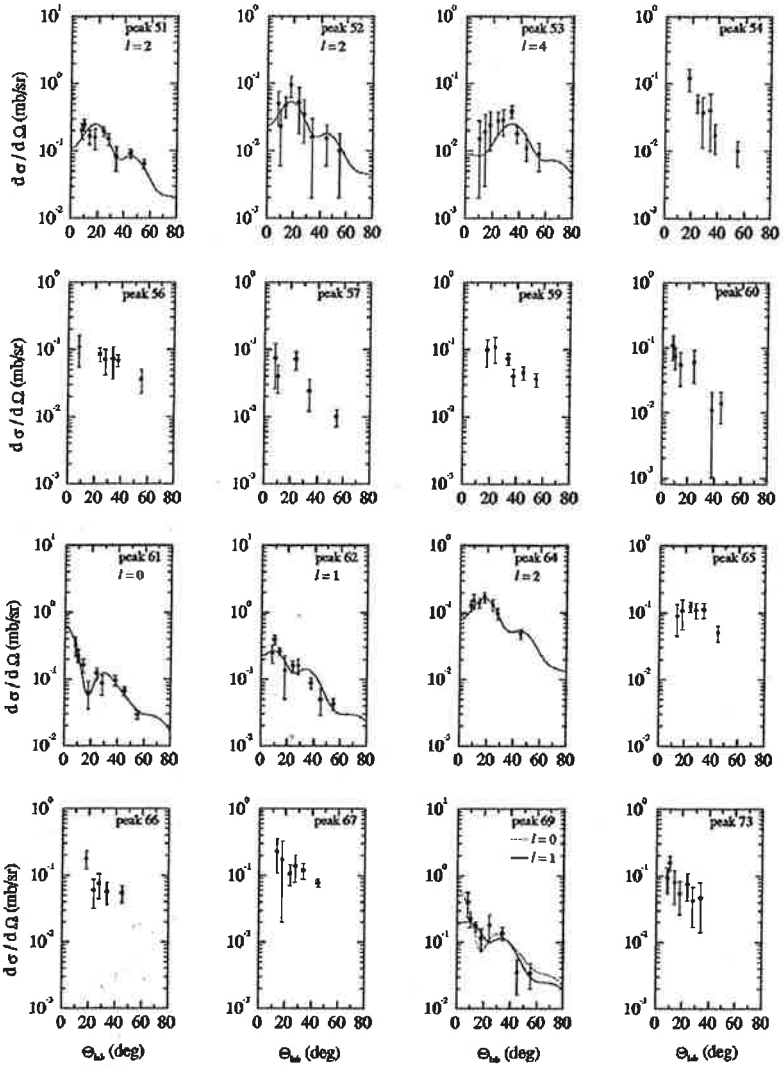

FIG. 5. Angular distribution for ^{102}Ru$(d,p)^{103}$Ru (see Fig. 2).

the assumption, which is here preferred, which considers this transition associated with the $2f_{7/2}$ orbital, of the next shell and not with the $1f_{7/2}$ one. The spectroscopic factors of Berg *et al.* [5] are, considering their declared uncertainty of 30%, in agreement with the present ones, with an exception made to the $l=0$ excitations, mainly those at 435 and 736 keV. The inspection of the corresponding experimental angular distributions reveals a poor fit by the DWBA predictions, particularly in the region of the first valley, indicating possible problems of background or contaminant subtractions in their analysis.

IV. DISCUSSION

A. Comparison with results from gamma ray studies

Besides having been extensively studied by one-neutron transfer reactions, ^{103}Ru has formerly been observed in a series of other reactions through the detection of γ rays. These results form the basis for most of the adopted levels [11] shown in Table II; therefore, the information is briefly discussed.

Of the 19 levels seen, below 1.1 MeV, in the β^- decay of the $5/2^+$ ground state of ^{103}Tc [14] to ^{103}Ru, only the 404.4

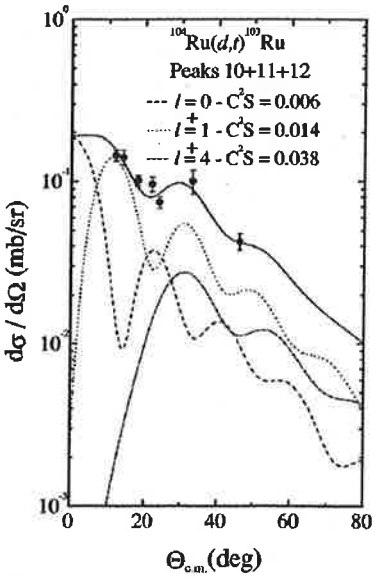

FIG. 6. Integrated angular distribution corresponding to peaks 10+11+12 of Ref. [3], detected in ^{104}Ru(d,t), respectively, at 540, 548, and 556 keV. The extracted spectroscopic intensity for each component is presented.

keV level and the 562.9 keV one, besides the ground state, could not be discerned in the present study or in the previous (d,t) one [3]. The neutron capture reaction on ^{102}Ru [17] reports 47 levels below 2.6 MeV in ^{103}Ru. With exceptions made to the ground state, the difficult region around 0.55 MeV and the triplet of levels at ~0.91 MeV (seen as one in the present work), only three further levels [at 991.6, 1174.08, and 1730.4 keV, all adopted [11] exclusively with basis on the ^{102}Ru (n,γ) results] were not detected in transfer. The γ decay following the neutron capture populates preferentially the $3/2^+$ ^{103}Ru ground state.

In contrast to the former γ ray studies, and in part due to the possibility of a higher angular momentum transfer in this reaction, ^{100}Mo$(\alpha,n\gamma)$ [13,18] populates several levels in ^{103}Ru, below its detection limit at 2.1 MeV, which are not observed in one-neutron transfer. Thus, of the 45 levels attributed to this reaction by the Nuclear Data compilation in their summary [11], even excluding the complex region around 0.55 MeV, 22 levels are not populated in any of the transfer reactions. Several of these have tentative spin attributions which make them, in principle, accessible to one-neutron transfer. In particular, in the excitation energy region above 0.91 MeV there are about ten levels, which have only been seen in the most recent [18] of the two ^{100}Mo$(\alpha,n\gamma)$ studies. Some of them, as the 911.6 and 931.3 keV levels, could be smaller components integrated into neighboring excitations, but several of them would be isolated states and are, if existent, weakly excited in transfer.

Therefore, in contrast to what was determined under similar experimental conditions for ^{99,101}Ru [3], several adopted levels [11] in the low-excitation-energy region were not seen either in (d,p) or (d,t). The most intriguing situation refers to levels which might be associated with $(3/2^+,5/2^+)$: altogether 24 such levels are reported below 1.11 MeV by Ref. [11], but only about half are observed in transfer, in spite of the low detection limit of the present study. The situation is different for the two lighter Ru isotopes investigated. All eight states which in this energy region have attributed spin parity $(3/2^+,5/2^+)$ in ^{99}Ru were detected in (d,t) [3], and of the 11 levels of this type existent in ^{101}Ru below 1.11 MeV, only one was not seen in transfer [3]. These findings can mean either that ^{103}Ru really presents a considerably more complex structure than ^{99,101}Ru or that the γ ray studies were able to reveal more detail for this nucleus.

B. One-neutron particle strength distributions

To complement the information already presented in a previous Brief Report [2], Fig. 7 displays additional results obtained in ^{102}Ru(d,p), for $l=1$ and $l=3$ transfers, which lie outside the $N=50$–82 valence space and were not formerly shown. Logarithmic scales are employed for the spectroscopic strengths, $G_{\rm strip}=C^2S'$, and the $l=0$, $l=2$, $l=4$, and $l=5$ data are again displayed, this time showing only those states where the l attribution is certain.

When the level spin J is not known, the valence orbital j was taken in computing the strength. For $l=2$, if the level had not been attributed $3/2^+$, $j=5/2$ was arbitrarily assumed, giving for those levels, where this assumption should prove incorrect, a somewhat subestimated strength. For $l=1$ and $l=3$ transfers, in computing $G_{\rm strip}$, respectively, the $3p_{3/2}$ and the $2f_{7/2}$ orbitals were supposed.

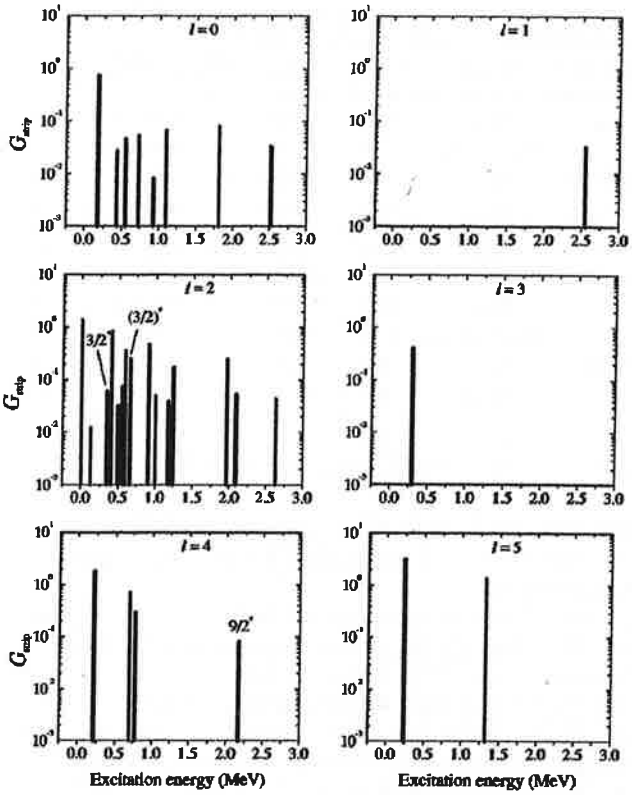

FIG. 7. One-neutron particle strength distributions for ^{103}Ru.

Most of the levels strongly excited in stripping are also excited in pickup [3], as may be seen with the help of Table II. In particular, both reactions populate, contrary to previous assumptions [5], preferentially the first excited $5/2^+$ state in ^{103}Ru and not the ground state. The state at 2.167 MeV, reached by an $l=4$ transfer, which in part motivated the present study, was, on the other hand, shown to be very little excited through (d,p), displaying therefore a strong hole characteristic and pointing on simple lines to a parentage to the $1g_{9/2}$ orbital. The high value of $C^2S=1.6$ thus determined for this state through the ^{104}Ru(d,t) results is remarkable, since this orbital belongs to the "closed" $N=50$ core. In comparing ^{103}Ru with ^{101}Ru, no such state is seen in the lighter isotope.

In contrast to what is verified for the majority of the other levels, most of the states associated with $l=1$ transitions, being thus states outside the valence shell, which were detected in ^{104}Ru(d,t) were not seen in the present study (see Table II). These weakly populated states are spread over a wide excitation energy range and the associated hole strength, given by the (d,t) results [3], is larger than the particle one, seen in this work, considering only the sure attributions. This fact is taken as indicative that most of the $l=1$ hole spectroscopic strengths formerly detected may be possibly associated with core excitations of the $2p$ orbitals and should perhaps have their strengths revised, while the states reached by $l=1$ in the present work could be the particle ones, pertaining to the $3p$ orbitals of the next shell. Only the lower-lying state of the two reached by $l=5$ in the (d,p) reaction was also characterized in (d,t), as seen

TABLE III. Strength distribution for ^{100,102}Ru.

Isotope	Orbital	ΣG_{strip}	ΣG_{pick}	$\Sigma G_{strip}+\Sigma G_{pick}$	$2j+1$
^{100}Ru	$3s_{1/2}$	1.48	0.29	1.77	2
	$2d_{5/2}+2d_{3/2}$	5.95	2.30	8.25	10
	$1g_{7/2}$	5.6	1.8	7.4	8
	$1h_{11/2}$	9.5	0.6	10.1	12
	Total	22.5	5.0	27.5	32
^{102}Ru	$3s_{1/2}$	1.06	0.49	1.55	2
	$2d_{5/2}+2d_{3/2}$	4.19	3.36	7.55	10
	$1g_{7/2}$	2.8	2.3	5.1	8
	$1h_{11/2}$	4.6	1.2	5.8	12
	Total	12.6	7.4	20.0	32

through Table II, but it has to be remembered that the detection limit for $l=5$ is higher than for the lower l values, in both reactions.

Figure 7 demonstrates that, for both $l=0$ and $l=2$ transfers, the values for the spectroscopic factors determined in the present experiment vary over two orders of magnitude. Only the $l=2$ strength is appreciably fractionated. If uncertain $l=(2)$ attributions were considered, somewhat more strength could be added. However, besides the levels at 1554 keV, already commented on, and the one at 2118 keV, each of the other ones would correspond to values of $C^2S' \leq 0.05$. Several levels were excited through $l=0$, but with about an order of magnitude smaller spectroscopic factors than the yrast one. The doubtful $l=(0)$ strength is very small. In addition to the very-low-lying $l=3$ excitation, there could be some more $l=(3)$ strength in the energy range around 1.5 MeV, but corresponding each to an order of magnitude smaller value of C^2S' than that relatively strong transition. Three certain $l=4$ excitations, which are probably associated with the $1g_{7/2}$ orbital, are seen below 1 MeV of excitation. Only three other of the states detected could be $l=(4)$, all weaker than the certain ones. The detection limit for $l=4$ transfer in the present study is estimated to lie below $C^2S'=0.1$ and to be about $C^2S'=0.2$, for $l=5$. Only one more state, at 1370 keV, could doubtfully be $l=(5)$, it then being weaker by almost an order of magnitude than the strongest excitation.

C. Total spectroscopic strengths

Another way of employing the data for spectroscopic purposes is to extract information on shell model vacancy in the ground state of the even Ru nucleus from which the reaction starts. Table III shows the summed spectroscopic strengths which could be associated, without doubt, with each l transferred in reactions which start from the ground states of the nuclei ^{100,102}Ru. As discussed in Sec. IV B, adding the strength corresponding to transitions with doubtful l attribution would not alter significantly the picture. Occupancy data ($\Sigma G_{pick}=\Sigma C^2S$) extracted from the analysis of ^{100,102}Ru$(d,t)^{99,101}$Ru reactions by Duarte *et al.* [3] and vacancy information ($\Sigma G_{strip}=\Sigma C^2S'$) from ^{100}Ru$(d,p)^{101}$Ru [1] are employed to complement the results of the present work. According to the previous discussion, the contribution of the $l=4$ transition to the state at 2.167 MeV for ^{102}Ru(d,p) was not considered in the vacancy value computed for $1g_{7/2}$ and, similarly in the occupancy, the strength to the known ^{101}Ru $9/2^+$ level at 0.719 MeV [3] was not included. Vacancy plus occupancy for each orbital is shown in column 4, and should be compared with the limit $(2j+1)$ or, for $l=2$, to the sum of the limits for $2d_{5/2}$ and $2d_{3/2}$. Therefore, in ^{102}Ru, experimentaly only 78%, 76%, 64%, and 48% of the expected total strength associated with the 50–82 shell was detected, respectively, for $l=0$, $l=2$, $l=4$, and $l=5$. Lines 6 and 12 of Table III inform the summed strength detected in (d,p) and (d,t) and the total experimental strength associated with the shell model orbitals of the $N=50$–82 shell. For this shell an upper limit of 32 for the total strength is expected, while ΣG_{pick} should, for ^{100,102}Ru, correspond, respectively, to 6.0 and 8.0 at maximum, under the assumption of a $N=50$ closed core. It may be appreciated that both (d,t) reactions located at least 83% of the expected neutron particles in the ^{100,102}Ru ground states, although spread among all available orbitals and with no apparent systematics in the filling pattern. Since the ^{100}Ru$(d,t)^{99}$Ru reaction was only able to study the region below $E_{exc}=1.2$ MeV, due to its relatively low Q value and the consequent contamination with inelastic scattering [3], a loss of ~17% in strength is of no concern. In contrast, even with this possible loss, in ^{100}Ru, the total sum $\Sigma(G_{pick}+G_{strip})_{valence}$ exhausts 86% of the expectation, while, in ^{102}Ru, only 62% of the total expected strength was seen. This is due to the very low value of ΣG_{strip} for ^{102}Ru, corresponding to a little more than half of the expectation. The already commented characteristics of our experimental method rule out the possibility of an appreciable part of (d,p) strengths being simply lost below 3.5 MeV. It is to be stressed that the ^{104}Ru(d,t) reaction [3] which also leads to ^{103}Ru, previously studied, leaves 37% of the valence strength outside the first 2.5 MeV of excitation (considering the $l=4$ excitation at 2.2 MeV associated with the $1g_{9/2}$ orbital, as seems now probable). This lack of intensity is taken as evidence that it is difficult to form the odd neutron ^{103}Ru nucleus starting from the ground states of the neighboring even-even isotopes.

D. Systematics of the spectroscopic information

As already put forward in previous publications of the Nuclear Spectroscopy Group [2,3], one-neutron transfer reactions which lead to the odd Ru isotopes show several peculiar characteristics: the strength is, for each of the valence shell orbitals, heavily concentrated in the lowest state, exception being made to the $2d_{3/2}$; the strength is widely spread among all valence orbitals; and for ^{103,105}Ru the $3/2^+$ ground states have small overlap with the ground states of their neighboring even-even isotopes [2]. Besides, similar $3/2^+$ levels exist in other Ru nuclei and in their isotones [2]. In spite of several available theoretical interpretations which at first sight seem conclusive, the chain of Ru isotopes has for a long time defied a consistent description. In fact, on closer inspection, it is verified that Whisnant *et al.* [19] had to take the collectivity of the even ^{98}Ru core as almost half of what is experimentally verified, besides employing the variable moment of inertia (VMI) approach in their apparently very

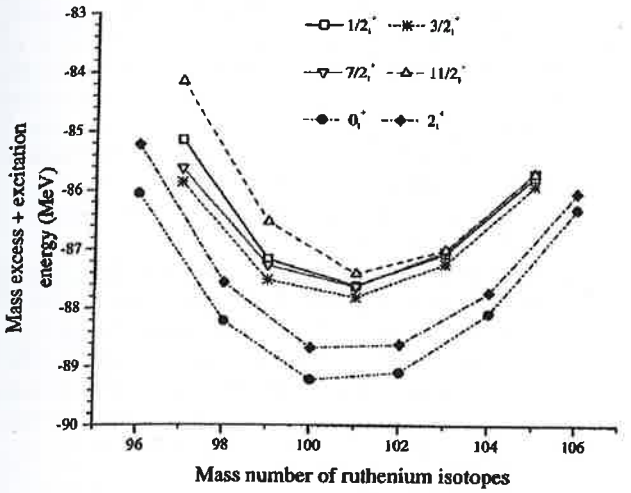

FIG. 8. Yrast levels of Ru isotopes on an absolute scale. The information was always taken from the most recent Nuclear Data Sheets compilation, except for the $1/2_1^+$ level of ^{99}Ru where the (d,t) result [3] was preferred.

complete interpretation of ^{99}Ru within a particle-symmetric-rotor model with Coriolis coupling. Within a similar model, Imanishi *et al.* [20] for ^{101,103}Ru and Rekstad [21] for ^{103}Ru had also to resort to such decreased collectivity of the cores, producing furthermore for the isotope here studied considerably discrepant results. A further difficulty verified in the cited model predictions is that they are unable to put negative and positive parity states on the same absolute energy scale. Interacting boson-fermion model (IBMF) calculations that consider neutron and proton degrees separately seem to do better [22,23], but a definite evaluation of their success must wait for more systematic interpretations.

From an experimental point of view, it is interesting to compare levels with similar characteristics in this mass region. Such systematics has been presented in a previous Brief Report [2]. Here, Fig. 8 completes the analysis showing some of the there highlighted levels of the odd Ru isotopes on the same absolute energy scale as the ground states and the lowest quadrupolar excitations of their even-even cores, taking into account the experimental mass excesses.

The mass "parabola" shows ^{101}Ru to be the tightest bound odd isotope and, in general, displays the regularity of the evolution. In particular, the $11/2_1^-$ level (and the $7/2_1^-$ accompanying [2] one) grossly follows the average values of the neighboring cores, but clearly comes down in energy, even on an absolute scale. In contrast, the $3/2^+$ and $7/2^+$ yrast levels follow in detail the behavior of the mean energies of the ground states of the neighboring even isotopes. On this absolute energy scale the yrast $5/2^+$ levels lie very close to the $3/2^+$ ones: at most 0.19 MeV below (^{97}Ru) and at most 0.03 MeV above (^{105}Ru).

The $3/2_1^+$ state merited special attention in the previous publication [2]. It has a small overlap with the ground states of its even-even neighbors and is either the proper ground state or lies very low in energy in the odd neutron nuclei in this mass region [2]. The addition of neutron pairs little affects the $3/2_1^+$ state, as Fig. 8 indicates. The same is true for proton pairs [2] unless very close to the ^{96}Zr or Sn cores, which have been since long detached for their semimagic character. On the other hand, the evolutionary behaviors of the excitation energies of the $1/2_1^+$ and $11/2_1^-$ levels in the isotones [2] clearly demonstrate that structure changes occur as protons are added beyond $Z=38$, even if the neutron number is maintained the same.

A survey of the Nuclear Data compilations shows that for odd neutron nuclei in the $A\sim80$ region a low-lying $7/2^+$ level (which is the ground state of some nuclei, in particular ^{81}Kr, ^{79}Se, and possibly ^{83}Sr) is observed, it also being weakly populated in one-neutron transfer reactions. This state, sometimes called an anomalous coupling state, was by some authors taken as resulting from a $(1g_{9/2})^3$ configuration. In analogy, a $(2d_{5/2})^3$ coupling to $3/2^+$ could be invoked for the yrast state of this spin and parity in the $A\sim100$ mass region and explain its small population in one-neutron transfer. The puzzling ingredient in such assumptions is that most $(j)^n$ states may not be quantitatively explained by the usually taken pairing interaction energy. An important long-range interaction must be added to an empirical effective interaction [24] and, in fact for $j\geq5/2$, the state with a resulting spin of $J=j-1$ is sufficiently lowered. As stated by Bohr and Mottelson [25], an alternative interpretation could be given in terms of a coupling to quadrupole deformations, either dynamical or statical. For this interpretation drawbacks also exist, as far as the $3/2_1^+$ levels follow the trend of the 0_1^+ states and not of the 2_1^+ ones and the γ decay pattern in the odd nuclei is not typical of collective excitations. The $3/2_1^+$ level is, in particular in ^{103}Ru, linked mostly to other $(3/2^+,5/2^+)$ states which are also weakly excited in transfer, such as the $5/2_2^+$ level at 136.079 keV, the $3/2_2^+$ one at 346.38 keV, and the 562.87 keV $(5/2^+,3/2^+)$ one [11]. Those levels are, incidentally, the most populated ones, besides the ground state, in the β^- decay to ^{103}Ru [14], starting from the $5/2^+$ ground state of ^{103}Tc (which, for $Z=43$, is not a valence shell single proton state). In general, two sets of levels, intraconnected by preferential γ decay, may be discerned in ^{103}Ru, the first one being related to the $3/2_1^+$ and the $5/2_2^+$ levels, while the second one connects with the $5/2^+$ first excited state. Most levels also strongly populated in the one-neutron transfer reactions, as the $7/2_1^+$ at 213.56 keV, the $(7/2_1^-)$ at 297.1 keV, and the 406.08 keV $(5/2^+,3/2^+)$ belong to the second set, while the $1/2_1^+$ state at 174.26 keV, although strongly excited in (d,p), is clearly more akin to the first set, whose levels are, in general, weakly seen in the transfer studies. It is significant that the $5/2_2^+$ and $3/2_2^+$ states which pertain to the here so-called first set of levels could not be explained by the particle-rotor interpretation of ^{103}Ru [21].

V. CONCLUSIONS

This section summarizes the principal conclusions which were drawn in this study and also refers to several results from previous works of the Nuclear Spectroscopy Group on $^{99-103}$Ru. It was shown that in ^{102}Ru(d,p), the ^{103}Ru ground state is weakly or not populated and, therefore, has a small similarity with ^{102}Ru in its ground state coupled to a single neutron. The complementary ^{104}Ru(d,t) reaction had already shown that, in an analogous manner, little overlap exists between the ground state of this odd isotope and that of

^{104}Ru and a neutron hole. If data collected through gamma ray studies are also taken into account, it seems that in ^{103}Ru two sets of levels may be distinguished: one with states akin to the $3/2^+$ ground state and populated in β^- decay from the $5/2^+$ ground state of ^{103}Tc; and the other akin to the first excited $5/2^+$ level and populated in one-neutron transfer. The $1/2_1^+$ level is an exception to this statement. In all, 73 levels were populated below 3.5 MeV in ^{102}Ru(d,p) and for 64 of them an angular distribution was presented. For 31 states a transferred l value could be attributed with certainty and, for some 20 others, either a doubtful value or limits were imposed. Several l identifications are new in the literature, it being remarkable that at least five of them are sure attributions above 2 MeV. The $l=4$ excitation at 2167 keV was associated with the $1g_{9/2}$ orbital. It was shown that most of the strength is concentrated in few states, only the $l=2$ strength being appreciably fragmented. At this level of experimental detail, it is possible to argue that, up to the experimental limit in excitation energy, a considerable fraction of spectroscopic strength is lacking, in a similar but even more impressive way than was determined for ^{104}Ru(d,t). All these observations may point to coexistence phenomena at low excitation in ^{103}Ru, so that one set of levels is not built on the ground states of the even neighbors. On the other hand, for each transferred l value, it is always the state detected at lowest energy which concentrates the largest fraction of the spectroscopic strength, in a manner which also characterizes the lighter odd Ru isotopes. The behavior of these yrast levels can be followed along the isotopic chain and presents several systematic features. The now well-documented strong and low-lying $l=3$ excitation fits into the overall picture established through the study of the other odd Ru nuclei. Finally, it may be said that ^{101,103}Ru are now experimentally well known.

From a theoretical point of view, on the other hand, there seem to be still some ingredients lacking in the available theoretical interpretations of the $A\sim100$ region. In particular, it is clear that only a part of the spectrum of the odd nuclei will be explained, if calculations which start from the neighboring even nuclei adding one single quasiparticle are performed. The greatest difficulties are probably to be expected for ^{103,105}Ru.

ACKNOWLEDGMENTS

This work was partially supported by Conselho Nacional de Desenvolvimento Científico e Tecnológico (CNPq), Coordenação do Aperfeiçoamento de Pessoal de Nível Superior (CAPES), Financiadora de Estudos e Projetos (FINEP), and Fundação de Amparo à Pesquisa do Estado de São Paulo (FAPESP).

[1] J. L. M. Duarte, L. B. Horodynski-Matsushigue, T. Borello-Lewin, and O. Dietzsch, Phys. Rev. C **38**, 664 (1988).
[2] T. Borello-Lewin, J. L. M. Duarte, L. B. Horodynski-Matsushigue, and M. D. L. Barbosa, Phys. Rev. C **57**, 967 (1998).
[3] J. L. M. Duarte, T. Borello-Lewin, and L. B. Horodynski-Matsushigue, Phys. Rev. C **50**, 666 (1994).
[4] H. T. Fortune, G. C. Morrison, J. A. Nolen, Jr., and P. Kienle, Phys. Rev. C **3**, 337 (1971).
[5] G. P. A. Berg, M. Demarteau, A. Hardt, W. Hürlimann, S. A. Martin, J. Meissburger, W. Oelert, H. Seyfarth, B. Styczen, M. Köhler, I. Oelrich, and J. Scheerer, Nucl. Phys. **A379**, 93 (1982).
[6] D. Pulino, G. M. Sipahi, G. M. Ukita, T. Borello-Lewin, L. B. Horodynski-Matsushigue, J. L. M. Duarte, W. G. P. Engel, and J. C. Abreu, Rev. Bras. Aplic. Vácuo **10**, 87 (1991).
[7] C. M. Perey and F. G. Perey, At. Data Nucl. Data Tables **17**, 1 (1974).
[8] J. M. Lohr and W. Haeberli, Nucl. Phys. **A232**, 381 (1974).
[9] W. W. Daehnick, J. D. Childs, and Z. Vrcelj, Phys. Rev. C **21**, 2235 (1980).
[10] L. B. Horodynski-Matsushigue and J. L. M. Duarte, *Relatório de Atividades do Departamento de Física Experimental* (Instituto de Física da Universidade de São Paulo, São Paulo, 1987), p. 108.
[11] J. Blachot, Nucl. Data Sheets **68**, 311 (1993).
[12] H. Bartsch, K. Huber, U. Kneissl, and H. Krieger, Nucl. Phys. **A252**, 1 (1975).
[13] W. Klamra and J. Rekstad, Nucl. Phys. **A243**, 395 (1975).
[14] H. Niizeki, S. Kageyama, T. Tamura, and Z. Matumoto, J. Phys. Soc. Jpn. **47**, 26 (1979).
[15] P. D. Kunz, computer code DWUCK4, University of Colorado, 1974.
[16] F. G. Becchetti and G. Greenlees, Phys. Rev. **182**, 1190 (1969).
[17] H. Seyfarth, H. H. Guven, and B. Viardon (private communication).
[18] G. Kajrys, J. Dulong, P. Lariviere, S. Pilotte, W. Del Bianco, and S. Monaro, Phys. Rev. C **34**, 1629 (1986).
[19] C. S. Whisnant, K. D. Carnes, R. H. Castain, F. A. Rickey, G. S. Samudra, and P. C. Simms, Phys. Rev. C **34**, 443 (1986).
[20] N. Imanishi, I. Fujiwara, and T. Nishi, Nucl. Phys. **A205**, 531 (1973).
[21] J. Rekstad, Nucl. Phys. **A247**, 7 (1975).
[22] A. Maino, A. Ventura, A. M. Bizzeti-Sona, and P. Blasi, Z. Phys. A **340**, 241 (1991).
[23] J. M. Arias, C. E. Alonso, and M. Lozano, Nucl. Phys. **A466**, 295 (1987).
[24] I. Talmi, *Simple Models of Complex Nuclei* (Harwood Academic, Chur, Switzerland, 1993).
[25] A. Bohr and B. R. Mottelson, *Nuclear Structure* (Benjamim, Reading, MA, 1975), Vol. 2.

Anexo 2.1

PHYSICAL REVIEW C VOLUME 33, NUMBER 5 MAY 1986

Collective aspects of ^{91}Zr by (d,d') scattering at 17 MeV

L. B. Horodynski-Matsushigue, T. Borello-Lewin, and O. Dietzsch
Instituto de Física da Universidade de São Paulo, São Paulo, Brasil
(Received 31 December 1985)

The ^{91}Zr(d,d')^{91}Zr* reaction has been investigated at 17 MeV incident energy. Up to 4.8 MeV excitation, 73 levels, some of them new, were identified. Angular distributions associated to ~40 levels were attributed to pure $L=2$, 3, or 5 excitations, concentrated in energy regions where the ^{90}Zr core exhibits 2^+, 3^-, and 5^- states. The partial deformation parameters β'_L obtained show agreement with those from low energy proton scattering for $L=2$, but there is a systematic difference for $L=3$ and $L=5$, which is discussed. Attention is drawn to the high excitation probability of the first excited state of ^{91}Zr, as measured by the $\beta_2 \simeq 0.18$ value obtained, a factor of ~2 above all other values for nuclei with $A=90\pm2$.

I. INTRODUCTION

The nuclei with mass number around $A=90$ have been subject to considerable interest, both from theoretical[1–7] and experimental[8–26] points of view, since the neutron shell closure at $N=50$ seems to be accompanied by semiclosures at $Z=38$ and $Z=40$, as is evidenced by the high-lying first excited states in ^{88}Sr and ^{90}Zr. Such features should make it possible to understand those nuclei and their neighbors on relatively simple terms.

Inelastic scattering studies have in the past been used to put into evidence collective aspects of even-even nuclei, but experiments on odd-A nuclei have been relatively less frequent. The number of basis states necessary for a good description of an odd nucleus in terms of its even neighbors is a measure of the interweaving of particle and collective degrees of freedom. Microscopic calculations for inelastic scattering[17,27,28] indicate that valence transitions contribute relatively little to the measured cross section, especially for low multipole excitations, particularly in the $A=90$ region. Inelastic scattering could then be used to also put into evidence collective aspects of the wave functions for odd-A nuclei. As long as simple patterns emerge, this type of experiment could then help to unravel the structure of odd-A nuclei. Following this line of ideas, the nucleus ^{91}Zr, which is just one neutron above a closed shell, was chosen as an interesting study case, the more so since other inelastic scattering data,[29–35] in particular from a precise (p,p') study,[8] exist for this target.

II. EXPERIMENTAL PROCEDURE

A self-supporting target of 540 μg/cm^2 enriched to 89% in ^{91}Zr was bombarded by 17 MeV deuterons from the three-stage Van de Graaff accelerator of the University of Pittsburgh. The scattered deuterons were detected at seven angles from $\theta_{lab}=25°$ to 80° with nuclear emulsion plates (Kodak-type NTB, 50 μm thick) placed in the focal surface of an Enge split-pole magnetic spectrograph. During the experiment elastically scattered deuterons were continuously monitored by two NaI scintillators fixed symmetrically at $\theta_{lab}=38.7°$ relative to the incident beam. The emulsion plates were scanned at the University of São Paulo in steps of 0.2 mm along the plate. An energy resolution (FWHM) of ~15 keV was obtained for all spectra.

A typical spectrum, obtained at a laboratory scattering angle of 35°, is shown in Fig. 1. Deuteron groups corresponding to transitions to ^{91}Zr levels are indicated by the calculated excitation energies of ^{91}Zr states expressed in keV and, when corresponding to transitions to levels of contaminant isotopes, by the name of the isotope. Peaks of larger widths labeled by t are associated to triton groups from the (d,t) reaction on ^{91}Zr and correspond to levels above 5 MeV excitation energy in ^{90}Zr. The peak labeled p at the left-hand side of Fig. 1 corresponds to the proton group from the ^{91}Zr(d,p)^{92}Zr(g.s.) reaction. A description of the procedures used for the identification of peaks corresponding to states in ^{91}Zr has been given in detail elsewhere.[36,37]

The excitation energies presented in Table I represent the average of the excitation energies calculated at each angle, making use of the calibration of the spectograph and taking the energy of the state at (1204.8±0.4) keV, as measured by gamma decay,[38] as a reference. The rms deviation of the energy measurements at six angles was in most cases less than 2 keV. Indicated in Table I by parentheses are those levels, with only tentative assignments, that presented a rms deviation of the energy measurements of more than 3 keV, but always smaller than 6 keV. The absolute excitation energy scale is estimated to be uncertain by ±0.15%, corresponding to an absolute uncertainty of less than ±7 keV in the tabulated excitation energies.

Relative normalization of the (d,d') cross sections was obtained from the number of elastically scattered deuterons detected by the monitors during each exposure. The absolute normalization was obtained from the deuteron elastic cross section given by the optical model prediction using the potential parameters given in Table II. The use of five different sets of optical model parameters (see the next section) resulted in differences $\lesssim 8\%$ in the absolute normalization. The absolute cross section is estimated to be uncertain by at most 25%, due essentially to uncertainties in beam alignment and definition of the solid angles

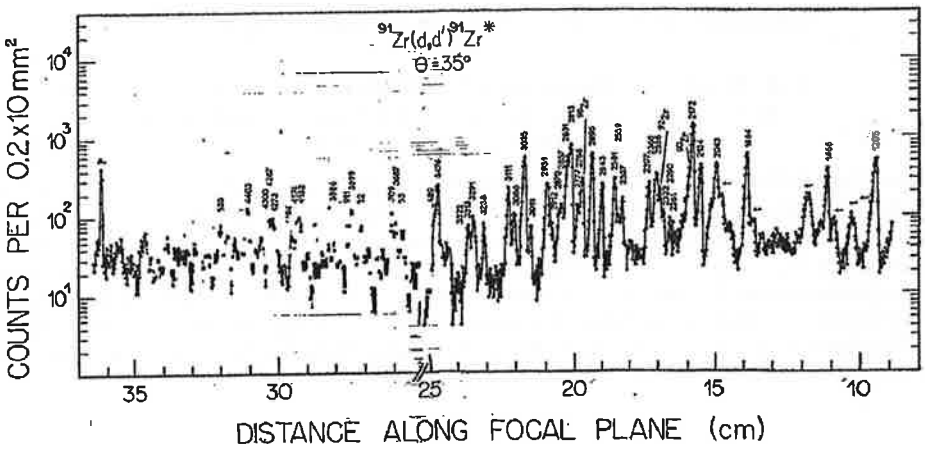

FIG. 1. Deuteron spectrum from the ^{91}Zr(d,d')^{91}Zr* reaction at $\theta=35°$. Peaks corresponding to transitions to ^{91}Zr states are labeled by the excitation energies of the states expressed in keV. The peaks due to the presence of contaminant zirconium isotopes in the target are identified by the name of the isotope. The peaks labeled by t or by p are associated to triton or proton groups from the reactions (d,t) or (d,p) on the ^{91}Zr target.

of the monitors.

The experimental angular distributions of 42 levels are shown in Figs. 2 and 3. The error bars show the combined effect of statistical deviations and uncertainties due to plate scanning, background subtraction, and relative normalization.

III. DWBA ANALYSIS

The angular distributions were compared with predictions of distorted-wave Born approximation (DWBA) calculations, performed by means of the code DWUCK,[39] with a macroscopic collective form factor using complex coupling. Coulomb excitation was considered in the usual way[39] and a nonlocality correction parameter $\beta=0.54$ fm was employed. The optical model parameters were taken from the systematics of Childs, Daehnick, and Spisak[40] for 17 MeV deuterons and are shown in Table II. For the optical parameters of the exit channel the same energy dependence suggested by Perey and Perey[41] was supposed. Calculations employing the optical parameters of Perey and Perey[41] predicted angular distributions practically coincident with the former in the angular range of interest to this experiment.

The fits to the angular distributions are shown in Figs. 2 and 3 in comparison with the data, whenever an assignment of L was attempted. In the fitting procedure the aim was to match the average behavior of the experimental angular distribution. Partial deformabilities β'_L were extracted in the fitting procedure. If only one L value is important in each transition, the relation between experimental and predicted cross sections is written as

$$\sigma^{\exp}(\theta)=\beta'^2_L\sigma^{\mathrm{DW}}_L(\theta)$$

with β'_L related to the usual deformation parameter β_L by

$$\beta'_L=\left[\frac{(2j_f+1)}{(2j_i+1)(2L+1)}\right]^{1/2}\beta_L\,,$$

where j_i and j_f are the spins of the initial and final states.

In the present analysis equal deformation parameters for the real and imaginary part of the potential were assumed. Calculations with equal deformation length $\delta_r=\delta_i$ ($\delta=\beta R$) were also done and would lead to values of the deformation parameters which are between 5% to 7% larger.

The values of L and the squares of the partial deformabilities β'_L are listed in Table I. The errors associated to the values of β'^2_L, also listed in Table I, do not include uncertainties in the absolute cross sections or DWBA formalism.

IV. RESULTS

In Table I, the present results are compared with those of other experiments performed with good energy resolution.[8,38] It is worth noting that, for most of the levels above ~3 MeV excitation energy, the information presented by the Nuclear Data compilation[38] is heavily based on the experiments performed by Blok *et al.*[8] Within the attributed errors, there is very good agreement between the reported values and the present results for level energies, although there seems to be an indication for an increasing systematic difference above 3.5 MeV of excitation.

The nucleus ^{91}Zr has been studied by inelastic scattering of various projectiles by several authors.[29–35] Only the detailed results of Blok *et al.*[8] for ^{91}Zr(p,p') are presented in Table I since poor resolution affected most other work. Where comparison is possible with those older measurements there is general agreement. A previous inelastic deuteron scattering experiment,[29] performed at 15 MeV incident energy, did only obtain data at two scattering angles, with an energy resolution of 40 keV. All levels above 4.5 MeV excitation have not been reported before in inelastic scattering studies. As may be appreciated, by inspection of Table I, only some weak transitions reported

TABLE I. Summary of the results for $^{91}Zr(d,d')^{91}Zr^*$ inelastic scattering and comparison with other experiments. Assignments given in parentheses are tentative.

	Present experiment $^{91}Zr(d,d')$					Blok *et al.*[a] $^{91}Zr(p,p')$			Nuclear data[b]	
E_{exc} (keV)	$\left[\frac{d\sigma}{d\Omega}\right]_{max}$[c] (mb/sr)	L	$\beta_L^2\times10^2$	β_L	$G(L)$ (W.u.)	E_{exc} (keV)	L	$\beta_L^2\times10^2$	E_{exc} (keV)	J^π
1205	0.35±0.11	2	0.21±0.03	0.18	22	1205	(2)		1204.8	$\frac{1}{2}^+$
1466	0.21±0.05	2	0.13±0.02	0.081	4.5	1468	2	0.09	1466.3	$\frac{5}{2}^+$
1884	0.53±0.07	2	0.27±0.02	0.101	7.0	1884	2	0.30	1882.1	$\frac{7}{2}^+$
2043	0.22±0.03	2	0.13±0.02	0.099	6.9	2041			2042.2	$\frac{3}{2}^+$
2134	0.45±0.06	2	0.23±0.01	0.083	4.8	2131	2	0.22	2131.3	$(\frac{9}{2})^+$
2172	0.63±0.08	3	0.75±0.06	0.162	24	2170	3	1.15	2170.0	$(\frac{11}{2})^-$
						2189	5	0.082	2189.9	
(2203)						2201			2200.7	$(\frac{7}{2})^+$
2261						2261	5	0.051	2259.7	$(\frac{13}{2})^-$
2290	0.016±0.004	5	0.050±0.014	0.045	5	2289	5	0.105	2287.6	$(\frac{13}{2})^-$
2322[d]	0.022±0.007	5	0.072±0.023	0.063	9	2322	5	0.165	2320.1	$(\frac{11}{2})^-$
2358	0.12±0.03	(3)	0.12±0.04	0.16[e]	23	2358	3	0.18	2355.8	$\frac{1}{2}^-,\frac{3}{2}^-$
2368	0.040±0.014	(4)	0.088±0.021			2369	(3+5)		2366.9	$(\frac{7}{2}^-)$
2397	0.074±0.010	(3)	0.11±0.02	0.068	4.3	2397	3	0.22	2394.9	$(\frac{9}{2})^-$
2537	0.060±0.011	(2)	0.043±0.008	0.046[e]	1.5	2534	(2)	0.045	2534	$(\frac{3}{2}^+,\frac{5}{2}^+)$
2559	0.023±0.006[f]					2557			2556.0	$\frac{1}{2}^+$
2581	0.098±0.010	3	0.137±0.014	0.098[e]	9.0	2578	3	0.20	2577.5	
2643	0.081±0.009	3	0.106±0.016	0.105	10.4	2641	3	0.15	2641.0	$(\frac{3}{2})^-$
2696	0.21±0.02	3	0.29±0.04	0.142[e]	19	2695	3	0.44	2694.0	$(\frac{3}{2}^-)$
2766	0.016±0.005	(5)	0.048±0.014	0.048[e]	5	2766	5	0.09	2764.8	
2777	0.038±0.006	(3)	0.045±0.013	0.069	4.3	2777	3	0.082	2775.0	$(\frac{3}{2})^-$
2813	0.29±0.04	3	0.37±0.03	0.139[e]	18	2813	3	0.55	2810.9	$\frac{5}{2}^-,\frac{7}{2}^-$
2831	0.17±0.03	3	0.23±0.03	(0.155)[g]	(22)	2832	3	0.32	2826.0	
2857	0.027±0.010	(4)	0.055±0.016	0.046	3	2859	4	0.077	2856.8	$(\frac{13}{2})^+$
2870	0.041±0.007	(2)	0.032±0.007	0.049[h]	1.7	2874			2874	$\frac{3}{2}^+,\frac{5}{2}^+$
						2905				
2912	0.012±0.007[f]					2915			2914.1	$(\frac{9}{2})^+$
2931	0.15±0.02	2	0.100±0.008			2931			2932	
3011	0.018±0.004	3	0.025±0.005	(0.036)[i]	(1.2)	3008	3	0.040	3009.1	$\frac{5}{2}^-,\frac{7}{2}^-$
3035	0.20±0.02	3	0.27±0.04	0.106[e]	11	3032	3	0.39	3033	
						3053			3053	
3086[d]	0.029±0.004	(3)	0.037±0.006			3082	4	0.072	3085.1	$\frac{3}{2}^+,\frac{5}{2}^+$
3111	0.16±0.02	2	0.100±0.008	0.055[e]	2.1	3108	2	0.11	3108.1	$\frac{7}{2}^+,\frac{9}{2}^+$
						3143			3146.6	$(\frac{17}{2}^+)$
						3170			3167.0	$(\frac{21}{2}^+)$
3238	0.047±0.008	(2)	0.034±0.005			3235	(2)	0.047		
						3262			3262	$\frac{3}{2}^+$
						3283			3283	
3291	0.041±0.012	(2)	0.031±0.006	0.048[h]	1.6	3290			3290	$\frac{3}{2}^+,\frac{5}{2}^+$
3313[d]	0.018±0.008	(2)	0.014±0.005			3309			3309	

TABLE I. (*Continued*).

	Present experiment ^{91}Zr(d,d')					Blok *et al.*[a] ^{91}Zr(p,p')			Nuclear data[b]	
E_{exc} (keV)	$\left[\frac{d\sigma}{d\Omega}\right]_{max}$[c] (mb/sr)	L	$\beta_L^2\times10^2$	β_L	$G(L)$ (W.u.)	E_{exc} (keV)	L	$\beta_L^2\times10^2$	E_{exc} (keV)	jf
3322	0.011±0.006[f]					3317			3317	
						3335			3334	$\frac{1}{2}^+$
						3356			3356	
						3375			3375	
						3410			3410	
						3452	3		3455	$\frac{9}{2}^-,\frac{11}{2}^-$
						3466			3468	$\frac{7}{2}^+,\frac{9}{2}^+$
3476[e]	0.15±0.03	(2)	0.13±0.03			3474			3476	
3489	0.035±0.024[f]					3489			3489	
						3553			3554	$(\frac{7}{2})^+$
						3570			3576	$(\frac{3}{2})^-$
						3597			3597	$\frac{5}{2}^-,\frac{7}{2}^-$
						3635			3635	$\frac{3}{2}^+,\frac{5}{2}^+$
3653	0.022±0.004	(5)	0.069±0.015			3648	(5)		3648	
						3660			3666	
3687	0.059±0.007	2	0.040±0.005	0.055[h]	2.1	3683			3681	$\frac{3}{2}^+,\frac{5}{2}^+$
3709	0.098±0.010	2	0.072±0.011	0.046[j]	1.5	3704	2		3704	$\frac{7}{2}^+,\frac{9}{2}^+$
						3725			3725	
3753	0.019±0.004	(2)	0.017±0.003	(0.036)[k]	(0.9)	3749			3748	$\frac{3}{2}^+,\frac{5}{2}^+$
3777	0.011±0.003	(2)	0.010±0.003			3775			3774	
3822	0.021±0.005	(2)	0.019±0.006	0.027[j]	0.5	3817			3818	$(\frac{7}{2}^+,\frac{9}{2}^+)$
						3829			3829	$(\frac{5}{2}^+)$
3852	0.042±0.009	(2)	0.036±0.008	0.042[h]	1.3	3847			3848	$\frac{3}{2}^+,\frac{5}{2}^+$
						3884			3883	$(\frac{1}{2}^-,\frac{3}{2}^-)$
3899	0.076±0.013	(2)	0.065±0.013	0.049[j]	1.7	3893			3897	$\frac{7}{2}^+,\frac{9}{2}^+$
3911	0.020±0.011[f]					3903			3905	$\frac{9}{2}^-,\frac{11}{2}^-$
						3922			3924	$\frac{3}{2}^+,\frac{5}{2}^+$
3952						3944			3944	
3965						3959			3958	$\frac{7}{2}^+,\frac{9}{2}^+$
3986	0.013±0.003[f]					3980			3982	$\frac{3}{2}^+,\frac{5}{2}^+$
4010	0.021±0.005[f]					4003			4004	$\frac{7}{2}^+,\frac{9}{2}^+$
						4027			4024	
4043						4035			4036	$(\frac{3}{2}^+,\frac{5}{2}^+)$
4075						4065			4067	$\frac{9}{2}^-,\frac{11}{2}^-$
4116						4111			4111	$\frac{7}{2}^+,\frac{9}{2}^+$
4151						4145			4145	$(\frac{3}{2}^+,\frac{5}{2}^+)$
(4162)						4161			4163	
(4174)										
4194						4187			4195	
						4230			4230	
						4245			4245	
4273						4265			4263	$(\frac{1}{2}^-,\frac{3}{2}^-)$

TABLE I. (*Continued*).

Present experiment ^{91}Zr(d,d')						Blok *et al.*[a] ^{91}Zr(p,p')			Nuclear data[b]	
E_{exc} (keV)	$\left[\frac{d\sigma}{d\Omega}\right]_{max}$[c] (mb/sr)	L	$\beta_L^2\times10^2$	β_L	$G(L)$ (W.u.)	E_{exc} (keV)	L	$\beta_L^2\times10^2$	E_{exc} (keV)	j^π
(4287)						4273			4272	$\frac{7}{2}^+,\frac{9}{2}^+$
(4300)						4291			4293	$\frac{1}{2}^-,\frac{3}{2}^-$
						4323			4322	$\frac{3}{2}^-$
4340						4335			4335	
						4357			4353	$\frac{3}{2}^+,\frac{5}{2}^+$
						4376			4379	$\frac{7}{2}^+,\frac{9}{2}^+$
4403	0.039±0.006	(3)	0.076±0.011			4395			4398	
(4413)									4415	$\frac{9}{2}^-,\frac{11}{2}^-$
4440						4433			4433?	
						4450			4450	
(4464)						4459			4459	
4501									4511	$(\frac{1}{2}^-,\frac{3}{2}^-)$
4535									4535	$\frac{3}{2}^+,\frac{5}{2}^+$
4549										
4593									4582	
(4651)									4656	$(\frac{1}{2}^-,\frac{3}{2}^-)$
4690									4679	$(\frac{3}{2}^-)$
(4715)									4709	
4790	0.016±0.003	(3)	0.036±0.006						4780	

[a]Reference 8.
[b]Reference 38.
[c]Maximum cross section measured.
[d] ^{90}Zr contaminant contribution subtracted.
[e]Possible doublet.
[f]Cross section at 25°.
[g]Values calculated supposing $j^\pi=\frac{3}{2}^-$.
[h]Reference 51.
[i]Values calculated supposing $j^\pi=\frac{7}{2}^-$.
[j]Choice based on shell model arguments.
[k]Values calculated supposing $j^\pi=\frac{3}{2}^+$.

by Blok *et al.*[8] were not observed in the present work.

There is overall agreement between the L values extracted in the present experiment and in the work of Blok *et al.*,[8] however, especially in the excitation region above 2.85 MeV, some more L attributions are presented. The level at 2043 keV, for which no L value is cited by Blok *et al.*,[8] is reached by an $L=2$ transition in agreement with other experiments,[32,33] although Awaya *et al.*[34] suggested $L=3$. It was not possible to obtain angular distributions associated to the two weak $L=5$ transitions located by the (p,p') work[8] at 2189 and 2261 keV. In fact, the known ^{90}Zr(2$^+$) contaminant transition explains all the cross sections observed in the present experiment at 2.19 MeV. The level at 2368 keV has a tentative attribution of $j^\pi=(\frac{7}{2}^-)$, based on a Hauser-Feshbach analysis of a $(\alpha,n\gamma)$ experiment by Glenn *et al.*[42] Blok *et al.*,[8] although not presenting the corresponding fit, cite $L=(3+5)$ for this transition. In the present work $L=(4)$ was preferred, since the $(\alpha,n\gamma)$ data seem in fact to permit the assignment of a different value of j^π. The $L=2$ attribution for the level at 2931 keV is in agreement with a tentative attribution of Du Bard and Sheline.[33] The angular distribution associated to the level at 3086 keV, after the subtraction of the contamination due to the 4$^+$ level of ^{90}Zr, seems to be better described by an $L=3$ than by the $L=4$ transition indicated by Blok *et al.*[8] The tentative $L=3$ at-

TABLE II. Optical model parameters for deuterons of 17 MeV on ^{91}Zr.

Optical model parameters[a]	
r_c (fm)	1.25
V (MeV)	101.6
r_0 (fm)	1.1
a_0 (fm)	0.82
W_D (MeV)	15.9
r_D (fm)	1.29
a_D (fm)	0.75
V_{SO} (MeV)	5.63
r_{SO} (fm)	0.98
a_{SO} (fm)	1.00

[a]Reference 40.

tribution is, however, in disagreement with the $\frac{3}{2}^+, \frac{5}{2}^+$ spin and parity values cited by the Nuclear Data compilation, based on the analysis of (d,p) data. The level at 3238 keV is excited by an $L=(2)$ transition in both the present (d,d') and in the (p,p') (Ref. 8) experiments, and was also seen by Metzger[25] in his (γ,γ') work. A level was presented by the former Nuclear Data compilation[43] at 3235 keV, with $j^\pi=\frac{1}{2}^-, \frac{3}{2}^-$ associated to it through a distinctive $l_n=1$ transition seen in (p,d) and (d,t) experiments. Curiously no state is shown by the more recent compilation[38] near this excitation energy.

A comparison of the $\beta_L'^2$ extracted in the present experiment, by (d,d'), and by Blok *et al.*,[8] by means of inelastic scattering of 20 MeV protons, reveals that, while there is agreement between the $\beta_2'^2$, the values of $\beta_3'^2$ and $\beta_5'^2$ present a systematic discrepancy. It is interesting to note

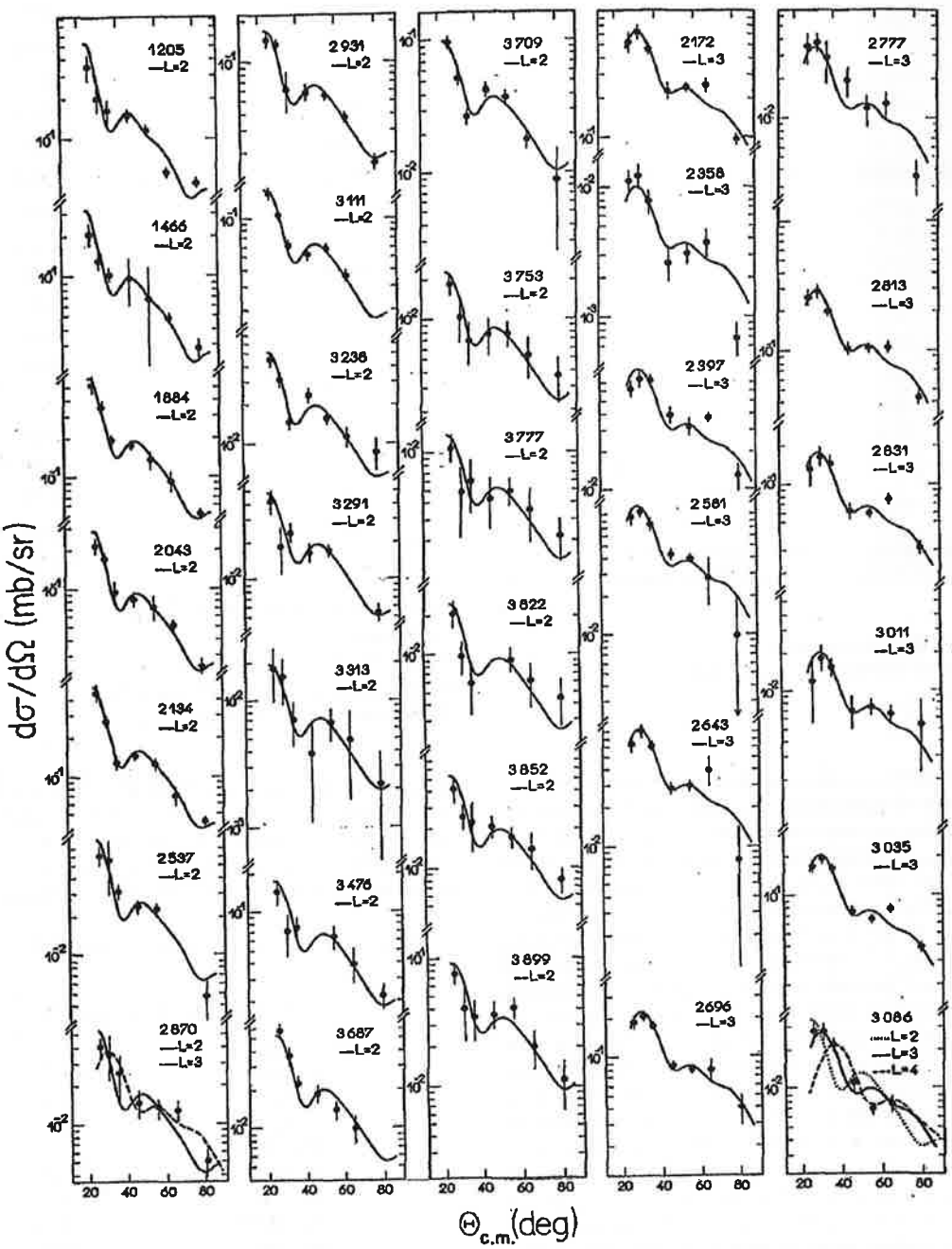

FIG. 2. Angular distributions of transitions in the ^{91}Zr(d,d')^{91}Zr* reaction. The experimental points are given with error bars corresponding to the combined effect of statistical deviations and uncertainties due to plate scanning, background subtraction, and relative normalization. The solid lines represent DWBA fits to the experimental angular distributions.

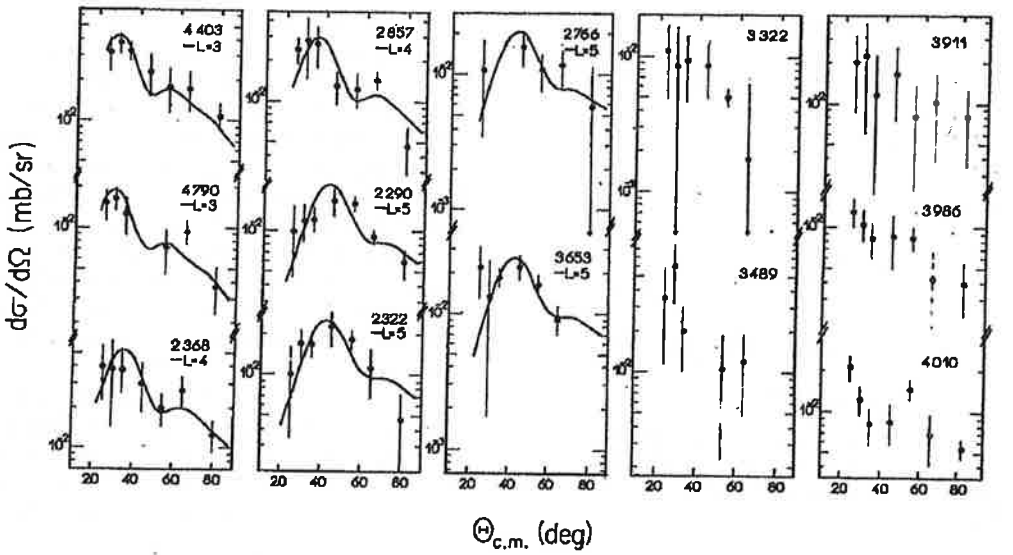

FIG. 3. See caption to Fig. 2.

that also the $\beta_2'^2$ value for the $\frac{1}{2}^+$ state at 1205 keV, is in agreement with the value which can be extracted from the analysis of the (p,p') cross sections measured by Blok *et al.*[8] using the recommended optical parameters, although not presented by the authors. The ratios $\beta_L'^2(\mathrm{p,p'})/\beta_L'^2(\mathrm{d,d'})$ associated to $L=3$ and $L=5$ are consistently larger than 1. The mean values obtained for these ratios for $L=3(5)$, considering the 6(3) strongest transitions, are, respectively, 1.46(2.1) with spreads of less than 10%. If a prescription of equal deformation lengths had been used in data analysis of both experiments the discrepancies would have been slightly larger. A similar effect is observed if δ_L obtained by $\lesssim$20 MeV proton inelastic scattering[15] are compared with 15 MeV deuteron[12] δ_L for the first 3^- and 5^- levels of ^{90}Zr.[44] It is felt that no reasonable change in optical model parameters could, within the reaction model adopted, reduce these discrepancies while simultaneously maintaining the accordance for $L=2$ results. In fact, less than 8% and 6% of variation was obtained for the ratios $\sigma_{3,\max}^{\mathrm{DW}}/\sigma_{2,\max}^{\mathrm{DW}}$ and $\sigma_{5,\max}^{\mathrm{DW}}/\sigma_{2,\max}^{\mathrm{DW}}$, in the analysis of 17 MeV deuteron scattering if different sets of optical model parameters were used. In the case of 20.4 MeV proton scattering, the variations of the ratios were, respectively, 11% and 7%, although the absolute values for each L transfer for protons and deuterons could be modified by up to 30%. These additional DWBA calculations were performed for deuteron scattering with three other global prescriptions[41,45,46] and with parameters[41] adjusted to reproduce elastic scattering at the same energy by odd nuclei of the same mass region and by ^{91}Zr at a lower energy.[10] One of the global potentials employed[45] for deuteron scattering used folding model ideas to confine the parameters within the range expected from nucleon scattering and allowed for a shell structure term near magic neutron numbers. For proton scattering, besides with the same parameter set used in data reduction by Blok *et al.*,[8] DWBA calculations were also done with the two global prescriptions[41] in common use in that energy region. An energy dependence of the β_L or δ_L values extracted in the usual way by low-energy inelastic proton scattering, pointed out by previous work in $A=40$,[28,47] $A=90$,[15,17,8] and $A=208$ (Ref. 48) regions, could be reflecting similar difficulties, probably due to inadequacies of the reaction model. In this sense it seems significant that Blok *et al.* normalized the sum of $\beta_L'^2$ values for every L value obtained at 14 MeV incident energy to the sum of those of their 20 MeV (p,p') experiment.[8] On the other hand there is no support in the literature to any hypothesis linking the differences to nuclear structure effects. Even in the case of excitation of 2_1^+ states in single-closed-shell nuclei, where the effects produced by the different response of protons and neutrons to the various projectiles should be enhanced,[49,50] it amounts to at maximum ~25% on the extracted δ_L values[49,51] and in the case of single-closed-neutron-shell nuclei would produce the smallest δ_2 values for low-energy proton scattering.

V. DISCUSSION

A. Distribution of $\beta_L'^2$ and comparison with β_L of possible core states

Figure 4 shows the values of $\beta_L'^2$ extracted for all the states reached by the same L transfer, as a function of excitation energy. The $L=2$ intensity is spread among several levels up to ~4 MeV of excitation. It is interesting, however, to note that most of the intensity is concentrated in five strongly excited levels between 1.2 and 2.1 MeV, which, incidentally, have attributed spin values in agreement with the values predicted by the coupling of a $d_{5/2}$ particle with a 2^+ state of the core. On the other hand, the $L=3$ intensity, although spread among several levels, is concentrated between 2.2 and 3.1 MeV of excitation, the highest intensity being associated to the known $\frac{11}{2}^-$ state at 2172 keV. Only two states, between 2.3 and

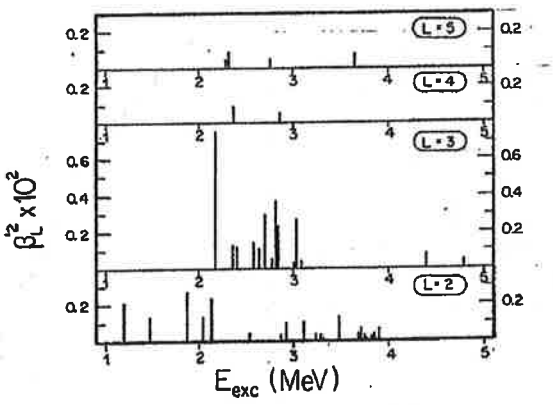

FIG. 4. Square of partial deformabilities β_L^2 obtained for all the states reached by the same L, as a function of excitation energy. The height of each line is proportional to the value of the corresponding β_L^2.

2.9 MeV, were tentatively associated to an $L=4$ transfer. The detected $L=5$ intensity is distributed among four states, three of them located in a range of ± 0.3 MeV around 2.5 MeV of excitation.

According to rules of angular momentum and parity conservation many known levels[38] of ^{91}Zr could in principle be reached by more than one L value. It is interesting, however, to note that the experimental angular distributions associated to almost all positive parity levels are similar, irrespective of their spin values, and that at least one of these levels, the $\frac{1}{2}^+$ state at 1205 keV, can be reached only by an $L=2$ transfer. On the other hand, the shapes of the angular distributions associated to some negative parity levels reveal different dominant L values. In particular, as can be seen in Figs. 2 and 3, the known $\frac{11}{2}^-$ levels at 2172 and 2322 keV are reached by, respectively, $L=3$ and $L=5$ transfer. In general, as may be appreciated in the mentioned figures, the essential features of most experimental angular distributions are reproduced by the DWBA predictions for single L transfer in one step excitation of collective states, indicating a selectivity of the transitions.

In the case of ^{91}Zr, particle-transfer experiments indicate that the ground state is predominantly formed by a $2d_{5/2}$ particle coupled to the ^{90}Zr core in its ground state.[38,11] As long as the contribution of the valence transition can be neglected, which seems to be the case for low-multipole excitations,[17,27,28] the β_L extracted should reflect the constitution in terms of the various core states involved. The extent to which polarization phenomena are important could be evaluated by the character of the ^{91}Zr ground state and by the excitation pattern of ^{92}Zr, which has two particles outside the ^{90}Zr core.[17]

The values of β_L as deduced from the experimental β_L^2 and j_f (Ref. 38) values are also presented in Table I. Where more than one j_f value is cited by the compilation, an option, based on arguments found in the literature, was made whenever possible. In particular, since the $(\vec{d},p)$ results by Rathmell *et al.*[52] were subjected to poor energy definition, due to their 160 keV resolution, it was assumed that the 2870 keV, 3291 keV, 3687 keV, and 3852 keV levels, also seen in the (d,p) experiment by Blok *et al.*[8] as rather strong $l_n=2$ excitations, are, respectively, the 2853 keV $(\frac{3}{2}^+)$, 3270 keV $(\frac{3}{2}^+)$, 3661 keV $(\frac{3}{2}^+)$, and 3824 keV $(\frac{5}{2}^+)$ levels reported by the polarization work. This correspondence would resolve the inconsistency noted[38] for the spin attribution of the adopted level at 2856.8 keV. In the same sense it is probable that the 3444 keV $(\frac{7}{2}^+)$ level of Rathmell *et al.*[52] is equivalent to the 3476 keV and not to the 3410 keV adopted level. On shell model arguments, the 3709 keV level observed in (p,d) experiments was supposed to have $j_f=(\frac{9}{2})^+$ and the 3822 keV and 3899 keV levels, observed in (d,p) experiments, were supposed to have $j_f=(\frac{7}{2})^+$. The 2696 keV level is cited by the Nuclear Data compilation as $(\frac{3}{2}^-)$, based on a two-point Hauser-Feshbach analysis of Glenn *et al.*[42] The same level has been observed as an $l_n=(3)$ transfer by Blok *et al.*[8] in their (d,p) work and as $L=3$ in inelastic scattering. Considering this evidence, the $(\frac{5}{2})^-$ attribution[8] was preferred.

Figure 5 is a comparison of the β_L obtained for all states to which a j_f value could be associated and which were excited by the same L transfer in the present experiment, with the deformation parameter of possible core states, as reported in the study of ^{90}Zr(d,d')^{90}Zr*, with deuterons of 15 MeV, by Todd-Baker *et al.*[12] The data are presented as a function of excitation energy and, to guide the eye, bands were drawn, each one centered at the β_L value and the experimental excitation energy of the possible parent state. These bands were extended arbitrarily by ± 0.5 MeV and their widths reflect an assumed uncertainty of $\pm 15\%$ in the deformation parameter. The β_2 extracted for the five levels at low excitation energy reached by $L=2$ transfer are compatible or larger than the deformation parameter of the state at 2.18 MeV in ^{90}Zr.[12] In particular, the β_2 associated to the $\frac{1}{2}^+$ state at 1205 keV is larger than the other by a factor of 2. All the $L=2$ states above 2.5 MeV of excitation are weakly populated when compared with the five states at low excitation energy and the extracted β_2 are compatible with those of the other three states associated to $L=2$ in ^{90}Zr in this

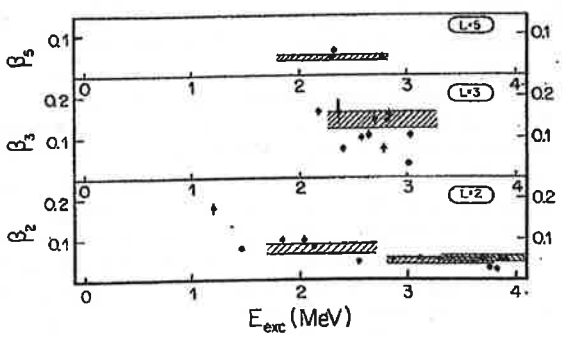

FIG. 5. Deformation parameters β_L obtained for all the states attributed to the same L transferred as a function of excitation energy and comparison with the deformation parameters of possible ^{90}Zr core states (Ref. 12). Each band is centered at the β_L value and excitation energy of the parent state.

energy range.[12] On the other hand, although ten states with known j_f were excited by $L=3$ in an energy range of about ± 0.5 MeV around 2.75 MeV, for only five of them the β_3 values extracted are compatible with the deformation parameter of the 3_1^- state of ^{90}Zr.[12] For the other states the extracted β_3 values are smaller than this value. Above the mentioned energy range, the next state, tentatively associated to $L=3$, was observed at an excitation energy ~ 0.7 MeV lower than the 3^- state detected at 5.12 MeV (Ref. 53) in ^{90}Zr. The only β_4 value extracted in the present work, associated to the state at 2857 keV, is also compatible with the deformation parameter of the state at 3.08 MeV of ^{90}Zr.[12] Note that the β_5 obtained for the first three states excited by $L=5$ transfer in ^{91}Zr agree with the deformation parameter of the 5_1^- state at 2.32 MeV of ^{90}Zr.[12] The next state reached by $L=5$ transfer, at 3653 keV, in the present experiment, which has no attributed spin value, was detected in the same energy region as the second 5^- state of ^{90}Zr.[12]

In situations where the coupling of an odd particle to an even core is considerable, the intermingling of particle and core degrees of freedom could result in extremely complex spectra.[54] Inspection of Fig. 5 reveals that in the case of ^{91}Zr this intermingling is not sufficient to completely destroy the relation to the core states.

B. Comparison with electromagnetic information

It has been usual in the literature to intercompare deformation parameters β_L (or deformation lengths, δ_L) extracted by different inelastic scattering experiments, also with information obtained from electromagnetic transition rates. Systematic discrepancies could, in principle, give information about differences in the neutron and proton components of nuclear states. In the usual homogeneous collective model it is assumed that neutrons and protons move in phase with the same amplitude, leading to $(\beta R)_{h,h'}=(\beta R)_{\rm em}$ (where h represents generically any hadron), as long as the reaction mechanisms are adequately described. On the other hand, in the extreme shell model, single-closed-shell nuclei would exhibit much reduced oscillations of that kind of nucleons which constitute the closed shell. Core polarization effects would act in a way tending to restore the homogeneous collective model result.[49]

Also listed in Table I are the reduced transition probabilities given in Weisskopf units, $G(L)$, which naively represent a measure of the number of particles involved in the transition, as deduced from the $\beta_L'^2$ and j_f values, by use of the relation:

$$G(L)=\frac{[(L+3)Z]^2}{4\pi}\left[\frac{r_{uL}}{r_{\rm em}}\right]^{2L}\frac{(2j_i+1)}{(2j_f+1)}\beta_L'^2 ,$$

where, following the recommendation of Owen and Satchler,[55] equivalent radii r_{uL} of 1.22, 1.27, 1.31, and 1.35 fm were used for $L=2$, 3, 4, and 5, respectively, and $r_{\rm em}$ was taken as 1.2 fm.

The comparison of the $G(L)$ obtained in this manner with the corresponding $G(EL)$ values extracted for the previously assumed core states by Singhal *et al.*,[16] in a study of ^{90}Zr(e,e'), shows the same general agreement already pointed out by Fig. 5. In fact, the values cited by the authors[16] are, respectively, (5.50 ± 0.48), (0.56 ± 0.15), and (1.68 ± 0.29) s.p.u. for the 2^+ levels at 2.18, 3.31, and 3.84 MeV, (25.2 ± 2.9) s.p.u. for the 3^- level at 2.75 MeV, (3.32 ± 0.90) s.p.u. for the 4^+ level at 3.08 MeV, and (8.37 ± 0.47) s.p.u. for the 2.32 MeV 5^- level in ^{90}Zr. Every $G(L)$ of the odd nucleus is smaller or of the order of the corresponding value in ^{90}Zr, except for the $G(2)=22$ W.u. for the transition to the $\frac{1}{2}^+$ level at 1205 keV in ^{91}Zr, which is about a factor of 4 larger than that of any $L=2$ transition in ^{90}Zr.

Direct comparison of the results obtained in the present experiment with information from electromagnetic probes is hampered by the scarcity of data for odd nuclei in general and for ^{91}Zr in particular. In fact, there are in the literature just one directly determined $B(EL)$ value[56] and two sets[57,58] of lifetime measurements, which unfortunately are not accompanied by detailed information on the multipolarities of the transitions. Table III lists, for further consideration, the referred measurements and other spectroscopic information available for those ^{91}Zr states below 3 MeV excitation energy which are appreciably populated in the present experiment and are, on the other hand, observed by one-neutron transfer reactions. Where the information can be confronted the two lifetime measurements are in general agreement and smaller or of the order of the value that would be obtained taking into account the $G(L)$ results of Table I, possibly indicating admixtures of lower multipolarity. The $B(E2)$ value for excitation of the $\frac{1}{2}^+$ level at 1205 keV corresponds to (11 ± 5) W.u. to be confronted with the $G(2)=(22\pm3)$ W.u. obtained in the present work. This transition admits no admixture of lower multipolarity and the $G(E2)=(54\pm19)$ W.u. which corresponds to the Doppler shift attenuation method (DSAM) lifetime of Gill, Gill, and Jones[57] is discrepant with both G values referred to above. However, a recent redetermination[59] of the lifetime of this level by DSAM leads to $\tau=(0.9\pm0.1)$ ps, which transforms to $G(E2)=(15\pm2)$ W.u. Although no clear-cut conclusion can be drawn from the presently available information, there is thus indication that the $G(E2)$ value is lower than the $G(2)$ value extracted by inelastic scattering for the transition to the 1205 keV level.

C. Comparison with other spectroscopic information

As can be seen in Table III, the states $\frac{1}{2}^+$ at 1205 keV, $\frac{3}{2}^+$ at 2043 keV, and $\frac{11}{2}^-$ at 2172 keV, although presenting high cross sections in (d,d'), leading to β_L values at least of the same order as those of the assumed core states, are associated to appreciable single particle behaviors. The values of $S_{\rm particle}$ and $S_{\rm hole}$ in Table III represent for each state the average of the results of three (d,p) and two (p,d) measurements,[8,52,60,61] respectively. The S values of all the other states which are strongly excited by inelastic scattering reveal small parentage with states of single particle or single hole character. On the other hand, several states with appreciable S values, such as the second $\frac{7}{2}^+$ and $\frac{1}{2}^+$ levels at 2201 keV and 2557 keV, respectively, are barely seen in any inelastic scattering experiments.

Estimates were made for the contribution which could

TABLE III. Spectroscopic factors, S_{particle} and S_{hole}, and deformation parameters β_L, for states of ^{91}Zr below 3 MeV excitation energy, detected in the present experiment and intensely populated by one-neutron transfer reactions. Also presented are the available $B(EL)$ and mean lifes τ.

E_{exc} (keV)	j^{π}[a]	S_{particle}[b]	S_{hole}[c]	β_L	$B(EL)$[d] $j_i \to j_f$ ($e^2\text{fm}^{2L}$)	τ[e] (ps)		τ[f] (ps)	
0	$\frac{5}{2}^+$	0.95	0.25						
1205	$\frac{1}{2}^+$	0.82	0.01	0.18	90±40	0.25	±0.09	3.2	±5.0
1466	$\frac{5}{2}^+$	0.03	0.002	0.081		0.28	±0.16	0.51	±0.16
1884	$\frac{7}{2}^+$	0.09		0.101				0.11	±0.02
2043	$\frac{3}{2}^+$	0.64	0.02	0.099		<0.030		0.016	±0.002
2134	$\frac{9}{2}^+$		0.07	0.083				0.17	±0.02
2172	$\frac{11}{2}^-$	0.33		0.162		>8			
2322	$\frac{11}{2}^-$	0.06		0.063					
2358	$(\frac{1}{2})^-$		0.09	0.16					
2813	$(\frac{7}{2})^-$	0.06		0.139				0.023	±0.004

[a]Reference 38.
[b]Mean values of S(d,p) from Refs. 8, 52, and 60.
[c]Mean values of $S(p,d)/(2j_f+1)$ from Refs. 8 and 61.
[d]Reference 56.
[e]Reference 57.
[f]Reference 58.

be expected from the valence transitions associated to these known single-particle components in the wave functions of the lowest lying positive parity levels, along the lines of Reehal and Sorensen.[62] As already mentioned, pickup data on ^{91}Zr reveal an almost pure $^{90}\text{Zr}(0_1^+)\otimes 2d_{5/2}$ character for the ground state.[11,38] Considering the available spectroscopic information, the first $\frac{1}{2}^+$ and $\frac{3}{2}^+$ states were supposed to consist of a superposition of only two components: a ^{90}Zr core excited to its 2_1^+ state weakly coupled to a $2d_{5/2}$ particle and a ^{90}Zr core in its ground state with the odd particle, respectively, in a $3s_{1/2}$ or $2d_{3/2}$ orbital. The amplitudes of these last components were taken as the square root of the S_{particle} presented in Table III and the single particle transition probabilities were estimated as, respectively,[62] 24 $e^2\text{fm}^4$ and 6.8 $e^2\text{fm}^4$. If the core excitation is given by the measured[16] $B(E2)_{0^+\to 2^+}=673$ $e^2\text{fm}^4$ for ^{90}Zr, a minimum polarization charge of $2.3e$ would be necessary to explain the $G(2)$ obtained for those transitions in this experiment. This value is well outside what is normally supposed to be reasonable for a neutron in this mass region, even with a restricted shell model basis.[1,3,4] If the $B(2)$ value obtained from inelastic deuteron scattering[12] on ^{90}Zr is to be used, the polarization charge would be still increased. It seems, therefore, that explicit consideration of the valence transition without *ad hoc* enhancement would not reduce the β_2 of the 1205 keV level to a value similar to that of the assumed core state.

Table IV lists for stable nuclei of $A=(90\pm2)$, the deformation parameters, β_2 and $\beta_{2\text{em}}$, associated to the 2_1^+ levels (or, for odd A nuclei, mean values, corresponding to the low-lying levels reached by $L=2$ transfer) as seen in inelastic scattering of hadrons and by electromagnetic excitation. The inspection of Table IV reveals that, for all the stable nuclei of the region, the β_2 and $\beta_{2\text{em}}$ values differ usually by less than 25% and are at least ~30% smaller than the $\beta_2\simeq 0.18$ obtained for the transition to the $\frac{1}{2}^+$ state at 1205 keV in ^{91}Zr. In particular, the β_2 associated to the 2_1^+ state of ^{92}Zr is 0.11, which seems to indicate that polarization phenomena are not sufficient to explain the value observed for ^{91}Zr. On the other hand, there exists the possibility of two-step transfer processes

TABLE IV. Deformation parameters β_2 and $\beta_{2\text{em}}$ for the stable nuclei in the interval of $A=(90\pm2)$, obtained, respectively, by inelastic scattering and Coulomb excitation experiments.

Nucleus	β_2[a]	$\beta_{2\text{em}}$[a,b]
^{88}Sr	0.12[c]	0.122[d]
^{89}Y	0.046[e]	0.068[e]
^{90}Zr	0.073[f]	0.094[f]
^{91}Zr	0.098[g]	
^{92}Zr	0.11[h]	0.105[h]
^{92}Mo	0.080[h]	0.114[h]

[a]For the odd A nuclei the average deformation parameter $(\Sigma\beta_2^2)^{1/2}$ for the low-lying states is presented.
[b]Obtained from published $B(E2)$ values.
[c]Reference 63.
[d]Reference 64.
[e]Reference 65, two states considered.
[f]Reference 44.
[g]Five states considered.
[h]Reference 66.

[e.g., ^{91}Zr(d-t-d')^{91}Zr* and ^{91}Zr(p-d-p')^{91}Zr* processes] that profit the high spectroscopic factors of the ground and $\frac{1}{2}^+$ states of ^{91}Zr, being responsible[67] for the apparent difficulties. Unfortunately the available CCBA codes[68] are not able, up to now, to handle the manifold possibilities opened up by the $\frac{5}{2}$ ground state spin.

VI. SUMMARY AND CONCLUSIONS

In the present study for the first time levels of ^{91}Zr have been identified, up to an excitation energy of 4.8 MeV, and L values attributed in inelastic scattering of deuterons. The only other inelastic scattering experiment of comparable quality was performed with 20 MeV protons and observed levels up to ~4.5 MeV. The overall agreement is excellent, both experiments fundamentally excite the same levels and lead to compatible values for β_2'. However, although there exists agreement of relative values, the β_3' and β_5' exhibit a systematic difference, when extracted by (d,d') and low energy (p,p'), which cannot be explained within the usual macroscopic DWBA analysis by uncertainties in the adopted optical model parameters. Similar effects were noted in other mass regions.

Inelastic scattering experiments on ^{91}Zr reveal a clear L selectivity of the transitions, which in conjunction with the extracted β_L values points to a direct relation of the states excited in the odd nucleus with the core states observed in the same excitation energy regions. If the intermingling of core and particle degrees of freedom had been severe no such selectivity would be expected. In this sense it is felt that inelastic scattering is putting into evidence collective aspects of the wave functions of the states excited. On the other hand, although a very simple configuration has been determined for the ground state, no such simplicity persists for the excited states and certainly there is no experimental basis for straight weak coupling arguments. In particular, some of the β_2 values associated to the first positive parity levels, which furthermore are populated with high spectroscopic factors in single particle transfer, are higher than that of the corresponding core state.

The information on electromagnetic excitation of the levels of ^{91}Zr is up to now scanty and accompanied by considerable uncertainties. The lifetime studies report no reliable multipolarity determination, so that a conclusive comparison with the results of the present work is not possible. There is indication, however, that the 1205 keV level is less strongly excited by electromagnetic means than by inelastic scattering of deuterons and protons. This could point to a real difference in the response of the neutron and proton components in the excitation of this state or to some inadequacies of the reaction mechanism assumed. The necessity to include in the analysis excitation of this level by two or more steps, via transfer reactions, making use of the high single particle amplitudes of the initial and final states, is suggested.

ACKNOWLEDGMENTS

The authors are indebted to G. R. Rao for exposing the plates at the University of Pittsburgh, and to B. L. Cohen and E. W. Hamburger for their support and interest in the present project. Helpful discussions with H. Miyake and O. Civitarese are appreciated. This work was partially supported by Fundação de Amparo à Pesquisa do Estado de São Paulo (FAPESP), Conselho Nacional de Desenvolvimento Científico e Tecnológico (CNPq), and Financiadora de Estudos e Projetos S/A (FINEP).

[1]D. H. Gloeckner, Nucl. Phys. A253, 301 (1975). D. H. Gloeckner and F. J. D. Serduke, *ibid.* A220, 477 (1974); S. Cohen, R. D. Lawson, and M. H. Macfarlane, Phys. Lett. 10, 195 (1964).
[2]K. Allaart and E. Boeker, Nucl. Phys. A198, 33 (1972).
[3]D. S. Chuu, M. M. King Yen, Y. Shan, and S. T. Hsieh, Nucl. Phys. A321, 415 (1979).
[4]J. Vervier, Nucl. Phys. 75, 17 (1966); N. Auerbach and I. Talmi, *ibid.* 64, 458 (1965).
[5]T. Paradellis, S. Hontzeas, and H. Blok, Nucl. Phys. A168, 539 (1971); S. K. Basu and S. Sen, *ibid.* A220, 580 (1974).
[6]I. Morrison, R. Smith, and K. Amos, J. Phys. G 3, 1689 (1977).
[7]G. Gneuss and W. Greiner, Nucl. Phys. A171, 449 (1971).
[8]H. P. Blok, L. Hulstman, E. J. Kaptein, and J. Blok, Nucl. Phys. A273, 142 (1976).
[9]T. Borello-Lewin, H. M. A. Castro, L. B. Horodynski-Matsushigue, and O. Dietzsch, Phys. Rev. C 20, 2101 (1979).
[10]S. S. Ipson, K. C. McLean, W. Both, J. G. B. High, and R. N. Glover, Nucl. Phys. A253, 189 (1975).
[11]L. C. Gomes, M. Sc. thesis, Instituto de Fisica da Universidade de São Paulo, 1975.
[12]F. Todd-Baker, T. H. Kruse, J. L. Mattews, and M. E. Williams, Part. Nucl. 5, 29 (1973).
[13]A. M. Van den Berg, N. Blasi, R. H. Siemssen, and W. A. Sterrenburg, Nucl. Phys. A403, 57 (1983).
[14]O. Schwentker *et al.*, Phys. Rev. Lett. 50, 15 (1983).
[15]L. T. Van der Bijl, H. P. Blok, J. F. A. van Hienen, and J. Blok, Nucl. Phys. A393, 173 (1983).
[16]R. P. Singhal *et al.*, J. Phys. G 1, 588 (1975).
[17]Y. Terrien, Nucl. Phys. A215, 29 (1973); R. A. Hinrichs, D. Larson, B. M. Preedom, W. G. Love, and F. Petrovich, Phys. Rev. C 7, 1981 (1973); A. Scott, F. Todd-Baker, W. G. Love, J. D. Wiggins, Jr., and M. L. Whiten, Nucl. Phys. A357, 9 (1981); M. L. Whiten, A. Scott, and G. R. Satchler, *ibid.* A181, 417 (1972); J. K. Dickens, E. Eichler, and G. R. Satchler, Phys. Rev. 168, 1355 (1968); F. Todd-Baker *et al.*, Nucl. Phys. A393, 283 (1983).
[18]H. W. Baer, R. L. Bunting, J. E. Glenn, and J. J. Kraushaar, Nucl. Phys. A218, 355 (1974).
[19]J. F. Morgan, R. G. Seyler, and J. J. Kent, Phys. Rev. C 8, 2397 (1973).
[20]S. P. Fivozinsky, S. Penner, J. W. Lightbody, Jr., and D. Blum, Phys. Rev. C 9, 1533 (1974).
[21]S. Cochavi *et al.*, Nucl. Phys. A233, 73 (1974).
[22]H. W. Fielding, R. E. Anderson, D. A. Lind, and C. D. Zafiratos, Nucl. Phys. A269, 125 (1976).
[23]E. R. Flynn, J. G. Beery, and A. G. Blair, Nucl. Phys. A218, 285 (1974).

[24]B. A. Brown, P. M. S. Lesser, and D. B. Fossan, Phys. Rev. C 13, 1900 (1976).
[25]F. R. Metzger, Phys. Rev. C 16, 597 (1977); 9, 1525 (1974).
[26]C. A. Fields, R. A. Ristinen, L. E. Samuelson, and P. A. Smith, Nucl. Phys. A385, 449 (1982).
[27]F. Todd-Baker, A. Scott, W. G. Love, J. A. Mowrey, W. P. Jones, and J. D. Wiggins, Nucl. Phys. A386, 45 (1982); W. T. Wagner, G. M. Crawley, and G. R. Hammerstein, Phys. Rev. C 11, 486 (1975).
[28]C. R. Gruhn, T. Y. T. Kuo, C. J. Maggiore, and B. M. Preedom, Phys. Rev. C 6, 944 (1972).
[29]R. K. Jolly, E. K. Lin, and B. L. Cohen, Phys. Rev. 128, 2292 (1962).
[30]C. R. Bingham, M. J. Halbert, and R. H. Bassel, Phys. Rev. 148, 1174 (1966).
[31]D. E. Rundqvist, M. K. Brussel, and A. I. Yavin, Phys. Rev. 168, 1287 (1968).
[32]H. P. Blok, G. D. Thijs, J. J. Kraushaar, and M. M. Stautberg, Nucl. Phys. A127, 188 (1969).
[33]J. L. Du Bard and R. K. Sheline, Phys. Rev. 182, 1320 (1969).
[34]Y. Awaya, K. Matsuda, N. Nakanishi, S. Takeda, and T. Wada, J. Phys. Soc. Jpn. 27, 1087 (1969).
[35]S. S. Glickstein and G. Tessler, Phys. Rev. C 10, 173 (1974).
[36]T. Borello, E. Frota Pessoa, C. Q. Orsini, O. Dietzsch, and E. W. Hamburger, Rev. Bras. Fis. 2, 157 (1972).
[37]T. Borello-Lewin, C. Q. Orsini, O. Dietzsch, and E. W. Hamburger, Nucl. Phys. A249, 284 (1975).
[38]H. W. Müller, Nucl. Data Sheets 31, 181 (1980).
[39]P. D. Kunz, University of Colorado (unpublished).
[40]J. D. Childs, W. W. Daehnick, and M. J. Spisak, Phys. Rev. C 10, 217 (1974).
[41]C. M. Perey and F. G. Perey, At. Data Nucl. Data Tables 17, 1 (1976).
[42]J. E. Glenn, H. W. Baer, and J. J. Kraushaar, Nucl. Phys. A165, 533 (1971).
[43]D. J. Horen, Nucl. Data Sheets 8, 1 (1972).
[44]D. C. Kocher, Nucl. Data Sheets 16, 55 (1975).
[45]W. W. Daehnick, J. D. Childs, and Z. Vrcelj, Phys. Rev. C 21, 2253 (1980).
[46]H. R. Bürgi *et al*, Nucl. Phys. A321, 445 (1979).
[47]C. R. Gruhn, T. Y. T. Kuo, C. J. Maggiore, H. McManus, F. Petrovich, and B. M. Preedom, Phys. Rev. C 6, 915 (1972).
[48]W. T. Wagner, G. M. Crawley, G. R. Hammerstein, and H. McManus, Phys. Rev. C 12, 757 (1975).
[49]A. M. Bernstein, V. R. Brown, and V. A. Madsen, Phys. Lett. 106B, 259 (1981).
[50]V. A. Madsen, V. R. Brown, and J. D. Anderson, Phys. Rev. C 12, 1205 (1975).
[51]A. M. Bernstein, V. R. Brown, and V. A. Madsen, Phys. Lett. 103B, 225 (1981).
[52]R. D. Rathmell, P. J. Bjorkholm, and W. Haeberli, Nucl. Phys. A206, 459 (1973).
[53]E. G. Martens and A. M. Bernstein, Nucl. Phys. A117, 241 (1968).
[54]B. R. Mottelson, J. Phys. Soc. Jpn. Suppl. 24, 96 (1968); D. Zawischa, Z. Phys. 266, 117 (1974); F. S. Dietrich, B. Herskind, R. A. Naumann, R. G. Stokstad, and G. E. Walker, Nucl. Phys. A155, 209 (1970).
[55]L. W. Owen and G. R. Satchler, Nucl. Phys. 51, 155 (1964).
[56]L. N. Gal'perin, A. Z. Il'yasov, I. Kh. Lemberg, and G. A. Firsonov, Yad. Fiz. 9, 225 (1969) [Sov. J. Nucl. Phys. 9, 133 (1969)].
[57]G. A. Gill, R. D. Gill, and G. A. Jones, Nucl. Phys. A224, 152 (1974).
[58]F. R. Metzger, Phys. Rev. C 16, 597 (1977).
[59]W. A. Seale, private communication.
[60]C. R. Bingham and M. L. Halbert, Phys. Rev. C 2, 2297 (1970).
[61]J. B. Ball and C. B. Fulmer, Phys. Rev. 172, 1199 (1968).
[62]B. S. Reehal and R. A. Sorensen, Phys. Rev. C 2, 819 (1970).
[63]R. L. Bunting and J. J. Kraushaar, Nucl. Data Sheets 18, 87 (1976).
[64]G. A. Peterson and Jonas Alster, Phys. Rev. 166, 1136 (1968).
[65]D. C. Kocher, Nucl. Data Sheets 16, 445 (1975).
[66]P. Luksch, Nucl. Data Sheets 30, 573 (1980).
[67]L. T. Van der Bijl, H. P. Blok, J. F. A. Van Hienen, and J. Blok, Nucl. Phys. A393, 173 (1983).
[68]P. D. Kunz, University of Colorado, code CHUCK (unpublished).

Anexo 2.2

PROCEEDINGS
VOLUME 1
CONTRIBUTED PAPERS

SPONSORED BY IUPAP
AND ORGANIZED BY THE
UNIVERSIDADE DE SÃO PAULO

P7-28

COULOMB-NUCLEAR INTERFERENCE IN INELASTIC SCATTERING OF 21 MeV ALPHA-PARTICLES ON ^{90,92}ZR

L.B. Horodynski-Matsushigue, T. Borello-Lewin, and J.L.M. Duarte
Instituto de Física, Universidade de São Paulo
C.P.20516, São Paulo, Brasil

Angular distributions for scattering of 21.0 MeV alphas by ^{90,92}Zr were measured at the S. Paulo split-pole spectrograph as part of a survey of collective properties in the Zr-Mo-Ru region. In order to optimize experimental conditions, retangular spot targets, essential for forward-angle measurements, and self-supporting thin evaporated targets[1], with improved Zr to C and O rates, important for intermediate angle spectra, were fabricated and employed. Detection in the focal surface proceeded either by nuclear emulsions or by position-sensitive gas detector[2]. Special attention was given to relative and absolute normalization of data. The angular distributions, corresponding to the excitation of the 3^-_1 states, are similar for both isotopes and well reproduced by collective model DWBA predictions[3] with equal nuclear and Coulomb parameters. However, the profound minimum observed for the excitation of the 2^+_1 state of ^{92}Zr, in contrast to what is observed for the corresponding state of ^{90}Zr, could only be reproduced if the nuclear deformation parameter is enhanced by a factor of 2 with respect to the Coulomb parameter. Measurements[4] at the incident energy of 35.4 MeV, although not sensitive to the Coulomb deformation parameters for L=3 excitations, also observed coulomb-nuclear interference structures in the L=2 angular distributions, which could only be fitted by a similar enhancement of nuclear deformation parameter. The fact that basically the same results are obtained at two different bombarding energies is indicative of an adequate description of the reaction mechanism, although it is difficult to understand, on nuclear structure arguments, how the addition of 2 neutrons to the closed shell ^{90}Zr nucleus may be responsible for the remarkable enhancement observed.

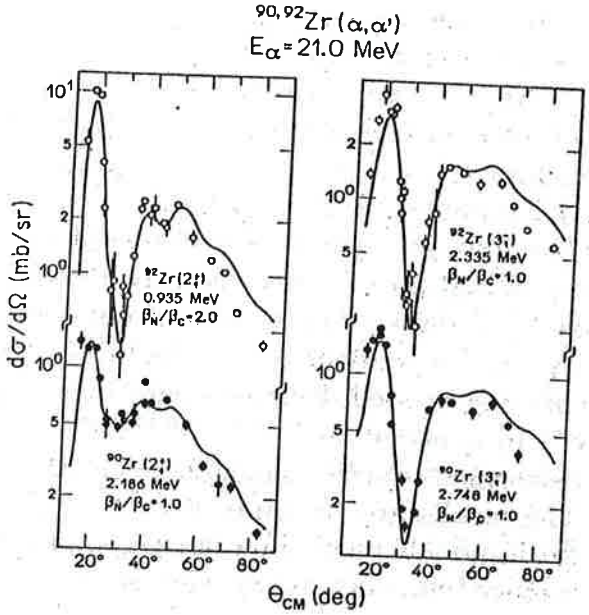

Experimental angular distributions and DWBA predictions. Optical model parameters are from Ref. 4.

(1) L.B. Horodynski-Matsushigue et al., Ci. Cult., 33 (1981) 311.
(2) K. Koide et al., Nucl. Instr. Meth., 215 (1983) 177.
(3) P.D. Kunz, code DWUCK4 (unpublished).
The optical model parameters are from Refs. 4 or 5.
(4) D. Rychel et al., Z. Phys. A326 (1987) 455.
(5) J.B.A. England et al., Nucl. Phys. A388 (1982) 573.

Partially supported by FINEP, CNPq and FAPESP.

Anexo 2.3

PHYSICAL REVIEW C VOLUME 54, NUMBER 5 NOVEMBER 1996

Coulomb-nuclear interference with α particles in the excitation of the 2_1^+ states in ^{100,102,104}Ru

L. C. Gomes, L. B. Horodynski-Matsushigue, T. Borello-Lewin, J. L. M. Duarte, J. H. Hirata, S. Salém-Vasconcelos, and O. Dietzsch

Instituto de Física, Universidade de São Paulo, Caixa Postal 66318, 05389-970 São Paulo, SP, Brazil

(Received 13 May 1996)

Coulomb-nuclear interference data for incident energies between 9 and 17 MeV were obtained in the form of elastic and inelastic (to the 2_1^+ states) excitation functions of backscattered ($\theta \simeq 172.8°$) alpha particles on ^{100,102,104}Ru. The analysis was done in a distorted-wave Born approximation within a deformed optical model approach. $B(E2)$ values, obtained from the charge deformation lengths δ^C extracted from the low energy data, are compatible for the three isotopes within $\sim 2\sigma$ with published values. The nuclear quadrupolar deformation lengths δ^N, obtained from the analysis of the interference region of the excitation functions, and also of one angular distribution at 22 MeV measured for ^{100}Ru are generally lower than the corresponding charge deformation lengths, the difference increasing with increasing A of the isotope, δ^N being 18% lower than δ^C for ^{104}Ru (2_1^+). Nuclear deformation lengths associated with the 3_1^- states of ^{100,102,104}Ru and with the 4_2^+ state of ^{100}Ru at 2.367 MeV were also obtained as a by-product of the present work. [S0556-2813(96)03111-1]

PACS number(s): 25.55.Ci, 21.10.Re, 21.10.Ky, 27.60.+j

I. INTRODUCTION

Characteristics associated with the first 2^+ state in even-even nuclei, such as excitation energies and $B(E2)$ values, have been extensively used as indicators of nuclear structure properties [1]. In more recent years, information concerning the relative contribution of neutrons and protons to the 2_1^+ excitations has also been considered as relevant tests of nuclear models. Although experimental and theoretical studies [2–4] point to the dominance of simple collective effects on most of these quadrupolar excitations, resulting in relative contributions of neutrons and protons of about N/Z, it is clear that a better pinning down of the uncertainties associated both with the experimental information and with the method of analysis can reveal explicit differences of theoretical interest.

The electromagnetic interaction is without doubt the best way to isolate the charge contribution to the excitation of nuclear states and, in fact, precise electromagnetic transition rates have been deduced from electron scattering, γ-decay, and Coulomb excitation studies. On the other hand, the understanding that inelastic hadron scattering in the regime of predominance of the nuclear interaction can be used to evidence also the neutron contribution, potentially different from the proton one, was basically started with the works of Bernstein and co-workers [5,3,6]. Aiming at the extraction of the relative contribution of neutrons and protons to the excitation of a particular collective configuration, attention must be paid to the interaction strength of the particular probe considered with each kind of nucleon [4,7]. Since the factor of 3 usually employed to characterize the relative interaction strength between unlike and like nucleon pairs is not precisely established, it is advantageous to utilize, for now, probes with isoscalar character. In addition, from an experimental point of view, if it is feasible to cover, with an isoscalar probe, both the region of pure Coulomb excitation and the region where the Coulomb-nuclear interference is maximum and, possibly, the region of predominance of the nuclear interaction, systematic errors that creep into the ratio of interest will be avoided. This line of research has nevertheless up to now not been sufficiently explored.

The chain of Ru isotopes, besides showing a slow and interesting transitional behavior, is extremely suited for a study of the type just brought forward, since the pertinent $B(E2)$ values have been precisely determined in at least a couple of works [8–10], allowing a nice consistency check of the results. The present analysis is concerned, in particular, with the excitation of the 2_1^+ states of ^{100,102,104}Ru through inelastic alpha scattering. The excitation of the same configurations using deuterons, also an isoscalar probe, as projectiles is the theme of a forthcoming paper [11].

II. EXPERIMENTAL PROCEDURE

Measurements of elastic and inelastic scattering of alpha particles, which were extracted from the São Paulo Pelletron accelerator, were performed on ^{100,102,104}Ru-enriched targets, at incident energies between 9 and 22 MeV. The targets, with thicknesses between $5\mu g/cm^2$ and $30\mu g/cm^2$, were prepared by electron bombardment evaporation of Ru metal, in powder form [12,13], on $\approx 20\ \mu g/cm^2$ carbon backings. The isotopic enrichments of the $A=100$, $A=102$, and $A=104$ targets are, respectively, $(97.2\pm0.1)\%$, $(99.35\pm0.03)\%$, and $(96.39\pm0.05)\%$. Surface barrier detectors with accurately known defining slits were used to observe the scattered alpha particles. The simultaneous monitoring of the elastic peaks with two detectors, mounted symmetrically at $\theta_{lab}=30°$, served normalization purposes. The backscattered alpha particles were measured at 172.8° laboratory scattering angle by an annular detector subtending a solid angle of 40.7 msr. The overall energy resolution was between 30 and 40 keV. A typical backscattering spectrum of 17 MeV alpha particles is shown in Fig. 1, for each isotope. Peaks associated with the elastic and the inelastic scattering to states with known spin and parity are indicated. The energies of the 2_1^+ levels (in MeV) under study are also given (within parentheses) in the figure. The good peak-to-valley ratio is due to special care with focusing and slit edge

0556-2813/96/54(5)/2296(8)/$10.00

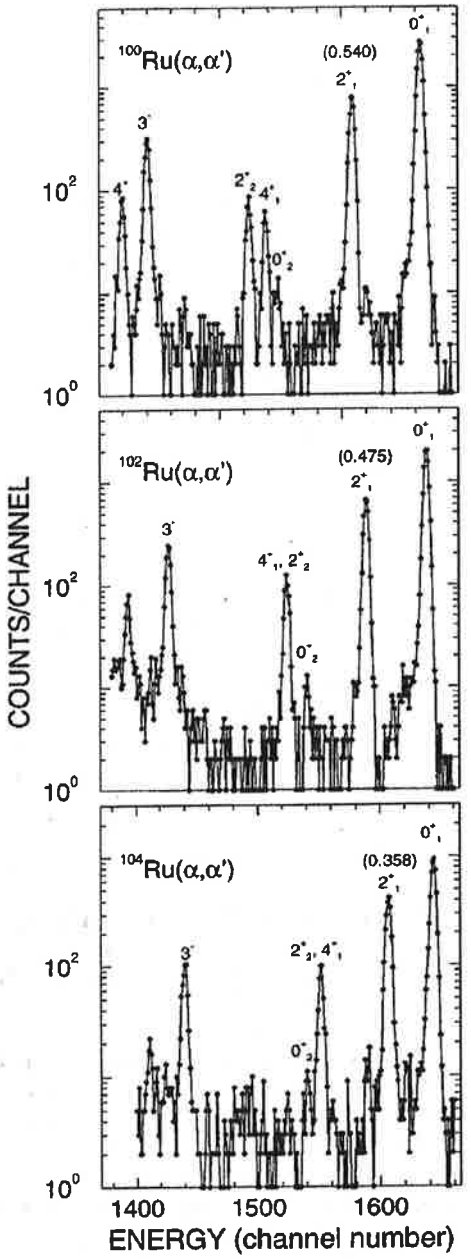

FIG. 1. Spectra of 17 MeV alpha particles backscattered by ^{100,102,104}Ru, measured at $\theta_{lab}=172.8°$. Indicated, for each isotope, are spin and parity of known levels and the excitation energies (in MeV) of the 2_1^+ states under study.

polishing. The experimental excitation functions, presented in Figs. 2 (elastic) and 3 (inelastic to the 2_1^+ states), are measured in regular steps from 9 MeV to 17 MeV, thus covering the interference region starting from well below the Coulomb barrier. Figures 4(a) and 4(b) show, respectively, the angular distributions taken at 22 MeV of the elastic and inelastic (to the 2_1^+ state) alpha scattering on ^{100}Ru. The curves presented in Figs. 2–4 are the adopted fits, as discussed in Sec. III. The error bars, where not explicitly shown, are smaller than, or of the order of, the size of the points in the figures and include the combined effect of statistical uncertainties, background subtraction, and relative normalization.

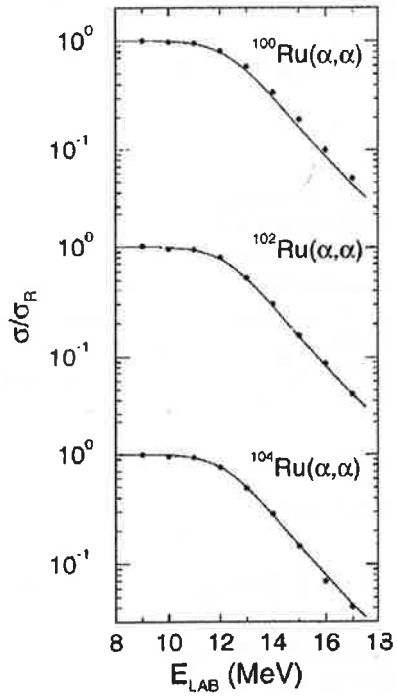

FIG. 2. Experimental elastic excitation functions at $\theta_{lab}=172.8°$, for ^{100,102,104}Ru and optical model predictions, with the parameters of Table I. Experimental uncertainties are smaller or of the order of the size of the points.

The absolute experimental cross sections were obtained referring the elastic peaks in the monitor measurements to optical model elastic cross section predictions, which can, at $\theta_{lab}=30°$ and for incident energies between 9 and 14 MeV, be considered equal to the Rutherford cross sections. In the region between 15 and 17 MeV the optical model predictions at this scattering angle are smaller than the Rutherford cross sections by at most 2.5%. At the incident energy where the angular distributions were measured (22 MeV), the difference with respect to the Rutherford cross section at $\theta_{lab}=30°$ is (10 ± 1)%, the uncertainty of 1% reflecting variance in predictions of different optical model parameter sets [14–16]. A maximum scale uncertainty of 4% is estimated for the absolute cross section, considering furthermore the careful assessment of the solid angles of the detectors and of the scattering angles, and would be reflected by a corresponding systematic error of about 2% in the experimental information of interest (deformation lengths), since the same experimental setup was used in the study of the three isotopes.

III. ANALYSIS

A. Quadrupolar excitations

The inelastic angular distributions and excitation functions were compared with predictions of distorted-wave Born approximation (DWBA) calculations, performed in the deformed optical-model potential (DOMP) description, em-

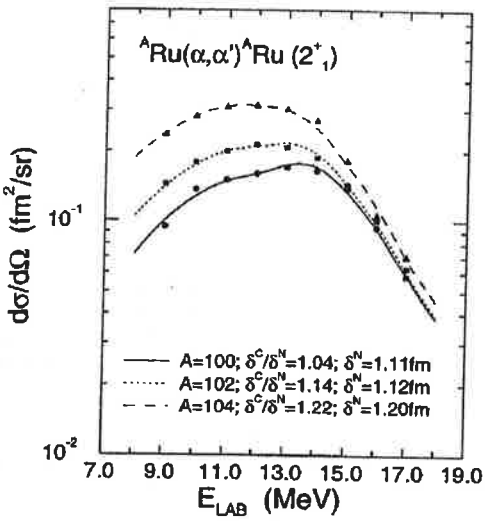

FIG. 3. DWBA-DOMP fits to experimental inelastic (2^+_1 state) excitation functions at $\theta_{lab}=172.8°$, for ^{100,102,104}Ru. Indicated are the corresponding δ^C/δ^N and δ^N parameters of the fits. Experimental uncertainties are smaller or of the order of the size of the points.

ploying a collective form factor with complex coupling, by means of the code DWUCK4 [17]. The form factors for Coulomb (F_2^C) and nuclear (F_2^N) excitation of the collective quadrupolar transitions by alpha particles are, thus, taken as

$$F_2^C(r)=\frac{8\pi e}{5}[B(E2)\uparrow]^{1/2}\frac{1}{r^3}=\delta^C R_{0C}\frac{6Ze^2}{5}\frac{1}{r^3}$$

for $r\geq R_{0C}=r_{0C}A^{1/3}$

and

$$F_2^N(r)=-\delta_R^N(U)\frac{dV(r)}{dr}-i\delta_I^N(U)\frac{dW(r)}{dr}$$

where Z, A are the atomic and mass numbers of the target, R_{0C} is the sharp cutoff charge radius, V and W are the real and imaginary depths of the optical potential U, and δ^C and $\delta^N=\delta_R^N=\delta_I^N$ are, respectively, the charge and potential deformation lengths, to be extracted through the analysis.

Coulomb excitation was, therefore, treated in the usual way [18] and the spherical Coulomb potential, relative to which the deformation is considered, was taken as that of an uniform charge distribution without diffuseness and radius R_{0C}. The Coulomb form factor was taken as zero inside the sharp cutoff charge radius and, since this one is well inside the strong absorption radius, the resulting approximation has no appreciable effect on the calculated cross sections. The potential deformation length δ^N was, as usually done in DOMP analyses, assumed equal to the nuclear or mass deformation length. In the fitting procedure the aim was to match the predictions of the DOMP calculations to the average behavior of the experimental angular distribution and excitation functions, extracting the reduced electric transition probabilities $B(E2)$ (for convenience parametrized through δ^C) and nuclear deformation lengths δ^N. If data of sufficiently low energies are available, $B(E2)$ values are extracted neatly, in a Coulomb excitation process. On the other hand, the value of δ^N always depends to some degree on the $B(E2)$ considered, due to the long-ranged character of the Coulomb interaction. In the present analysis a reduced charge radius of $r_{0C}=1.22$ fm was used for the sharp cutoff spherical charge distribution, in accordance with electron inelastic scattering and muonic atom data, as catalogued by Elton [19], Barrett and Jackson [20], and de Vries *et al.* [21], when reduced to sharp-edge distributions.

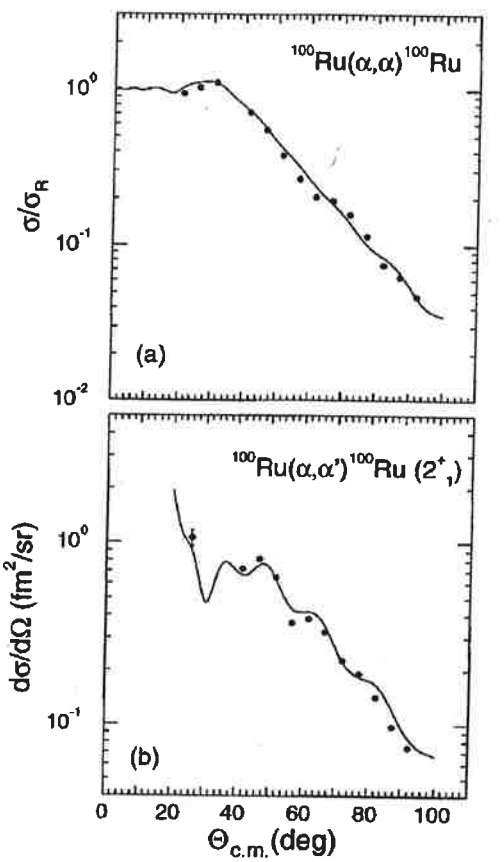

FIG. 4. Experimental, elastic and inelastic, scattering angular distributions taken at $E_{lab}=22$ MeV, in comparison with optical model and DWBA-DOMP predictions for ^{100}Ru. Error bars are shown whenever they exceed the size of the points.

The use of global potentials, prefixing the same family of parameters for the distorted waves, diminishes one of the sources of uncertainties in the method of analysis, in particular if chains of nuclei are considered. In the present work the optical model parameters (see Table I) were taken from the systematics of England *et al.* [14] and a nonlocality correction parameter $\beta=0.20$ fm was employed. For alpha particles, the systematics due to England *et al.* [14], obtained at 25 MeV, is the only global optical model parametrization, reported in the literature in the mass and energy regions of interest. Other sets of optical parameters available are specific to few nuclei and energies [15,16,22,23]. Optical model calculations have shown that almost all sets reproduce the trend of the data of the present study, in particular the elastic (see Fig. 5) and inelastic scattering of 22 MeV alphas on ^{100}Ru, although not always the details of the oscillations. An

TABLE I. Optical model parameters[a] for alpha particles on ^{100,102,104}Ru used in the present analysis. Here $r_W = 1.670$ fm, $a_W = 0.280$ fm, $r_{0C} = 1.22$ fm, and $a_0 = 0.515$ fm.

A	V (MeV)	r_0 (fm)	W (MeV)
100	93.5	1.554	12.3
102	91.3	1.555	11.7
104	89.1	1.557	11.0

[a]In accordance with the global optical parameters prescription of England *et al.* [14].

exception is the parametrization of Wit *et al.* [23], which uses geometrical parameters sensibly different from the other four sets and superestimates the data of the angular distribution in practically the whole angular range measured. It is to be noted that this general agreement is verified even being the five optical model sets under consideration obtained through the fitting of elastic alpha particle scattering data on ^{89}Y to ^{100}Mo, in the incident energy range 18–35 MeV. Global optical model parametrizations for protons and deuterons [24] have shown that the geometrical parameters, especially the ones associated with the real part, can be kept practically constant for moderate variations of the incident energy, the energy dependence appearing as rather small and systematic modifications of the intensities of the real and imaginary potentials. For alpha particles, this dependence corresponds, according to Fliesbach [25] in the range of energies of the present experiment, to an increase of depth for the real potential well of only +0.1% per MeV. In the present work, an option of not including any incident energy dependence of the parameters, in the global optical model systematic of England *et al.* [14], was made. It was furthermore verified that the value of the real diffusivity, $a_0 = 0.500$ fm, resulting from the global prescription, is not well established in the original work of England *et al.* [14]. Therefore, the value $a_0 = 0.515$ fm, which is a compromise

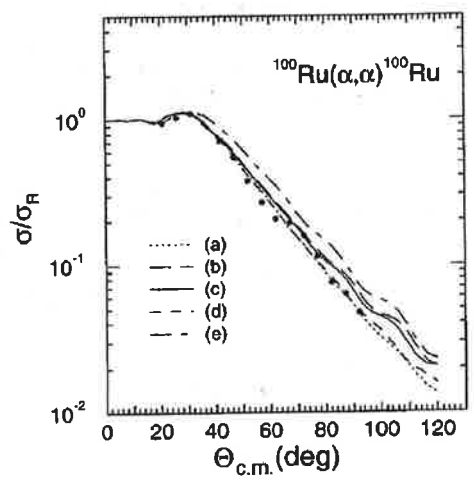

FIG. 5. Comparison of experimental elastic scattering angular distributions of 22 MeV alphas on ^{100}Ru, with five optical model predictions, where (a), (b), (c), (d), and (e) correspond to Refs. [15], [16], [14], [22], and [23], respectively.

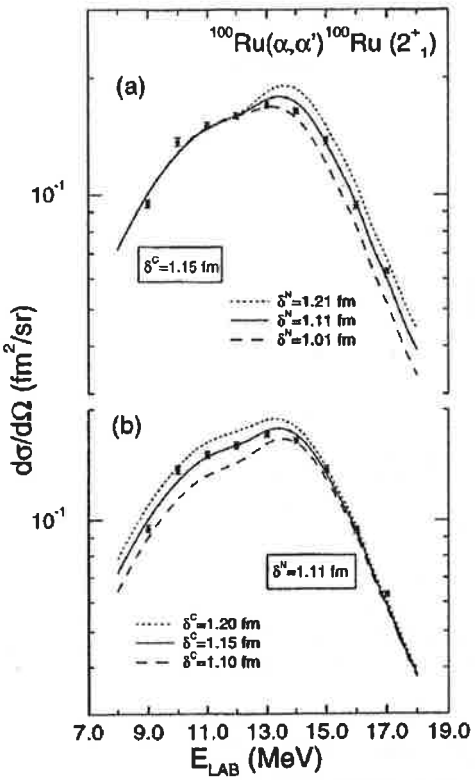

FIG. 6. Influence of $\pm 3\sigma$ variations on, respectively, δ^N with fixed δ^C [part (a)] and δ^C with fixed δ^N [part (b)] on DWBA-DOMP fits to the inelastic excitation function for ^{100}Ru. Error bars are shown whenever they exceed the size of the points.

among the values 0.510, 0.515, and 0.520 fm required for $A = 100$, 102, and 104 to best reproduce the experimental slopes, was adopted for the whole analysis. If the a_0 value had been taken differently for each isotope, the fits to the elastic excitation functions presented in Fig. 2 for ^{100,104}Ru would have been of the same quality as that for ^{102}Ru. However, as already stated, sticking, as far as possible, to prefixed and constant parameters in the comparative DOMP analyses assures a clearer understanding of the structure information to be extracted for the chain of isotopes under study.

The fits to the experimental inelastic excitation functions for backscattered alpha particles exciting the 2^+_1 state, in ^{100,102,104}Ru, are shown in Fig. 3 and the values of the corresponding correlated parameters of the fit, the ratio δ^C/δ^N and the potential deformation length δ^N, are also indicated. It is to be stressed that the simple homogeneous collective model predicts $\delta^C/\delta^N = 1.0$ [1]. Taking ^{100}Ru as an example, Fig. 6 demonstrates the sensitivity of the experimental information to parameter changes in the fit. For this purpose, each of the two quantities of physical interest, δ^N and δ^C, was allowed to vary by $\pm 3\sigma$(σ being the estimated standard deviation), while the other was maintained at its value of best fit. Part (a) of Fig. 6, thus, shows the effect of a $\pm 9\%$ variation in δ^N, with fixed δ^C. Part (b), on the other hand, illustrates how the $\pm 4.5\%$ change of δ^C, with fixed δ^N, affects the whole excitation function. In fact, the uncertainties were attributed to the deformation lengths, for each isotope, through comparisons similar to Fig. 6, by parameter varia-

TABLE II. Nuclear δ^N and charge δ^C quadrupolar deformation lengths obtained in the present work for ^{100,102,104}Ru. The deduced ratios M_n/M_p (quadrupolar neutron to proton moments) and values of N/Z are also shown.

A	δ^N (fm)	δ^C (fm)	$\frac{M_n}{M_p}$	$\frac{N}{Z}$
100 [a]	1.12(5)			
100 [b]	1.11(3)	1.154(17)	1.19	1.27
102 [b]	1.12(3)	1.277(17)	1.03	1.32
104 [b]	1.20(4)	1.464(23)	0.94	1.36

[a]Angular distribution result.
[b]Excitation function results.

tions sufficient to produce an envelope to the experimental points, then associated with a ~ 99.7% confidence interval. The results for δ^N and δ^C extracted and their estimated uncertainties are presented in columns 2 and 3 of Table II.

Figure 7 stresses the physical reasons for the greater sensitivity of the data to δ^C and for the impossibility of obtaining unique values of δ^N, if δ^C is unknown. Part (a) of this figure displays separately the contributions of Coulomb excitation and nuclear excitation and it is seen that, as is well known, in the incident energy range of only tens of MeV on medium-weight nuclei, the Coulomb contribution can never be ignored. Clearly, Coulomb excitation is largely predominant for the four lowest energy data. Figure 7(b) shows that, as a consequence, even wildly different predictions, if adjusted to those points, produce, as they should, an almost constant value of δ^C (to better than 1%). No unique δ^N may, on the other hand, be selected if only the higher energy points were available, as stressed by Fig. 7(c), where predictions, with the same δ^C/δ^N ratio as used in Fig. 7(b), can be adjusted to those points, however, resulting in different δ^N values. Thus, if data below 15 MeV were not available or if the $B(E2)$ value (proportional to the square of δ^C) was unknown, the impossibility of obtaining unique values of both parameters is pointed out by Fig. 7.

An inspection of Fig. 3, which displays on the same scale the experimental inelastic excitation functions for the three Ru isotopes studied, shows a decreasing slope and a higher value for the cross sections for the three lower energy points, in the sequence of increasing masses (^{100,102,104}Ru). The former aspect is predominantly a consequence of the determinant influence of the small decrease of the reaction $|Q|$ values on the Coulomb excitation. For each isotope the changing of δ^C, in the region of the lowest energies, would correspond only to a different scale factor for the Coulomb excitation cross section.

To confirm the nuclear contributions to the 2_1^+ excitation extracted from the analysis of the experimental excitation functions, an inelastic alpha particle angular distribution was measured at the higher incident energy of 22 MeV, exclusively for ^{100}Ru. These data are presented in Fig. 8 in comparison with the DOMP results corresponding to $\delta^C/\delta^N = 1.04$, as obtained from the excitation function analysis. Also shown are the predictions for δ^C/δ^N values of 0.63 and 1.41 and the corresponding δ^N. The experimental angular distribution is discriminative against low values of

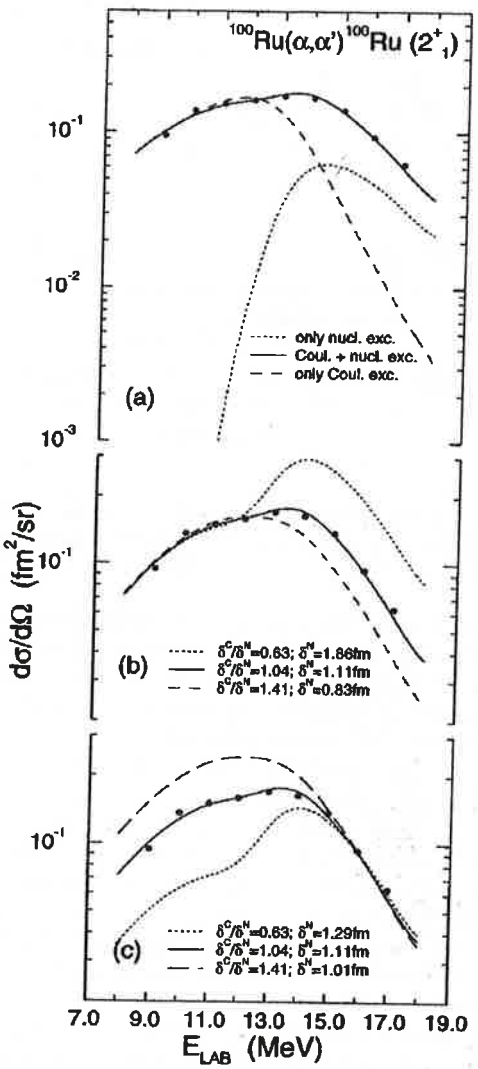

FIG. 7. DWBA-DOMP predicted excitation functions for ^{100}Ru. Part (a) displays separately the contributions of Coulomb and nuclear excitations to the best fit DOMP prediction. Parts (b) and (c) display three DOMP predictions with the same δ^C/δ^N ratios, as indicated, adjusted exclusively to the low (b) and high (c) energy data.

δ^C/δ^N even if data points around the interference minimum are lacking and, in fact, only the formerly established $\delta^C/\delta^N = 1.04$ also corresponds to a value of δ^N compatible with the excitation function information.

It is thus clear that the simultaneous extraction of δ^N and $B(E2)$ requires detailed inelastic scattering data which characterize not only strictly the nuclear-Coulomb interference region but also, especially, the region of almost pure Coulomb excitation.

B. Excitations of higher multipolarities

As may be noted in the 17.0 MeV spectrum presented in Fig. 1, besides the known 2_1^+ states, some other levels with known spins and parities were also excited in the present work in the three isotopes studied. There is, however, a fun-

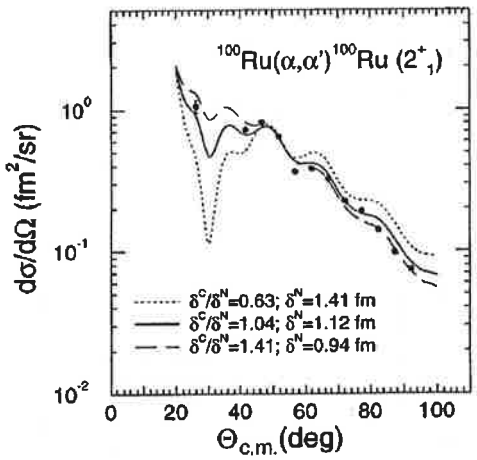

FIG. 8. Experimental inelastic angular distribution for the 2_1^+ state of ^{100}Ru in comparison with DWBA-DOMP predictions, corresponding to the δ^C/δ^N and δ^N parameters indicated.

damental difference with respect to the excitation mechanism when multipolarities of order $L>2$ are observed in the backscattering situation here employed: For the higher multipolarities the nuclear excitation processes are absolutely dominant, so that only δ^N may be extracted.

Figure 9 illustrates this fact for the 3_1^- states of ^{100,102,104}Ru and it may be observed that the dramatic drop of the cross sections which characterizes the offset of the nuclear interaction at incident energies below 14 MeV did not allow data acquisition at the lower end of the energy range examined, even for the intense octupolar excitations. Nevertheless, the mass deformation lengths extracted for the 3^- states, under the reasonable [18] assumption that protons and neutrons contribute equally, resulting in $\delta^C/\delta^N=1.00$, may be of spectroscopic interest and are given in Table III, in comparison with published values. It is to be noted that the presently obtained information is an absolute determination and part of a systematic study of the three isotopes. Other hadron inelastic scattering studies excited the 3_1^- levels with (d,d'), at 12 MeV in ^{102,104}Ru [26] and with (α,α') at 104 MeV in ^{100}Ru [27]. Although no uncertainties are quoted, the (d,d') work estimates $\pm 15\%$ on the absolute cross sections, while the value for ^{100}Ru results as a by-product of a $(\alpha,4n)$ study, from a fairly preliminary data set obtained with 100 keV resolution. Apparently no care was taken to account for Coulomb excitation in both works, which would modify the result at 12 MeV incident deuteron energy somewhat, but would hardly affect the 104 MeV alpha result. The experimental information of Refs. [26] and [27] is taken to also inform basically on δ^N and is thus presented in Table III. The other related physical quantities available in the literature are δ^C, the charge deformation lengths for the 3_1^- states, which may be deduced [28] from the published [8] $B(E3)$ values. It is seen that basic agreement exists, but that, possibly, the present results point to a revision of the adopted [29–31] spectroscopic information.

The hexadecapolar excitation in ^{100}Ru at 2.367 MeV was only observed at 16.0 MeV and 17.0 MeV and the $\delta^N=0.038(8)$ fm extracted confirms its extraordinary population in inelastic scattering [32].

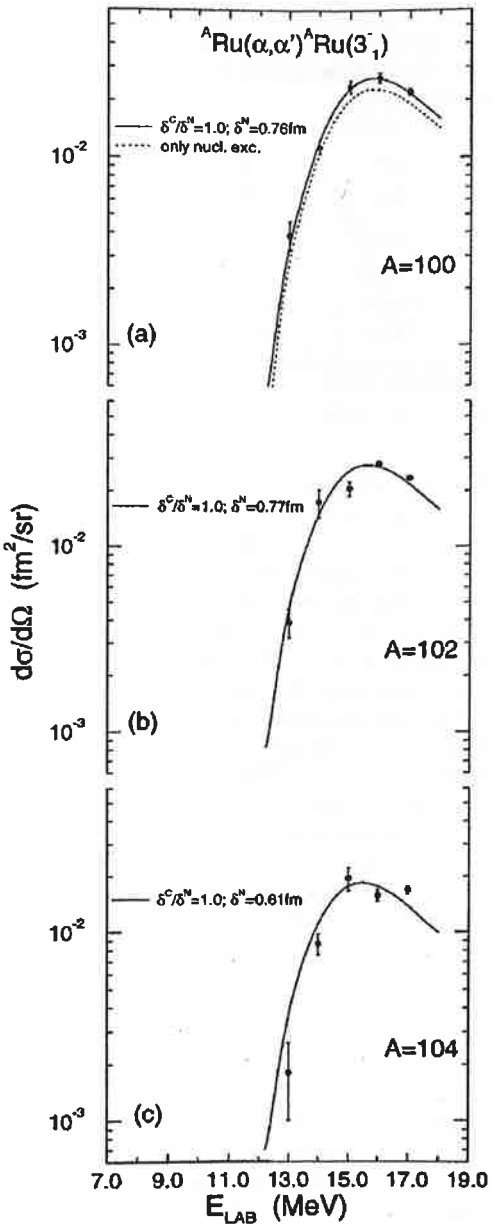

FIG. 9. DWBA-DOMP fits to experimental inelastic (3_1^- state) excitation functions at $\theta_{lab}=172.8°$, for ^{100,102,104}Ru. Indicated are the corresponding δ^N parameters of the fit. In part (a) the separated nuclear contribution to the excitation of the 3_1^- state in ^{100}Ru is shown as a dotted line.

IV. RESULTS AND DISCUSSION

Although some new information was also obtained for higher multipolarities (see Table III and Sec. II B), the principal aim of the present work was the assessment of nuclear and charge contributions to the excitation of the 2_1^+ states in ^{100,102,104}Ru, which shall merit a thorougher discussion in the sequence.

A critical inspection of Fig. 3 and Table II shows that, according to the arguments developed in the previous section, the comparison of the experimental cross sections with

TABLE III. Nuclear octupolar deformation lengths δ^N for ^{100,102,104}Ru, in comparison with charge deformation lengths δ^C, calculated [a] from $B(E3)\uparrow$ values.

A	δ^N (fm) Present work	δ^N (fm) [b]	δ^N (fm) [c]	δ^C (fm) [d]
100	0.76(2)	0.62		0.62(5); [0.82(8)]
102	0.77(4)		0.77	0.75(6); [0.81(12)]
104	0.61(7)		0.71	0.70(2); [0.83(5)]

[a] $\delta^C=(4\pi/3Ze)[B(E3)\uparrow]^{1/2}(1/r_{0C}^2A^{2/3})$, $r_{0C}=1.22$ fm.
[b] Reference [27].
[c] Reference [26].
[d] Reference [8]. The values in brackets are calculated considering the experimentally observed transitions and upper limits of all possible γ rays deexciting the 3^- levels, as cited by the authors.

DOMP predictions determines the quadrupolar deformation lengths δ^N and δ^C for ^{100,102,104}Ru with good precision. It is further to be stressed that through the interference region analyzed, a clear constraint is set between the relative normalization scales of δ^N and δ^C.

Table IV, besides the results of the present experiment for δ^C, also shows the δ^C values calculated in the usual way [33] from the $B(E2)$ measured in pure Coulomb excitation experiments by Hirata *et al.* [9], Landsberger *et al.* [8], and Bockish *et al.* [10], and their respective errors. An increasing trend of δ^C, as a function of mass number A, emerges in those Coulomb excitation studies [8,9], but there seems to be already among them some systematic differences. The δ^C values of the present work follow the same trend and, although still $\sim$2% lower than the results of Hirata *et al.* [9], differ from those by less than two standard deviations. The general agreement thus obtained can be understood as a consistency check on the adequacy of the analysis, allowing therefore a claim for good accuracy for the present results.

Table II, which is a summary of the results of this experiment, besides δ^C and δ^N, also presents in the last two columns the ratio of the quadrupolar neutron to proton moments (M_n/M_p), as obtained through the simple relation [34] $M_n/M_p=A\delta^N/Z\delta^C-1$, in comparison with the homogeneous collective model expectation N/Z. The homogeneous collective model expectation [1] is almost true for ^{100}Ru, but the experimental δ^N do not follow the same rate of increase as that of δ^C as a function of A, δ^N being smaller than δ^C by about 18% for ^{104}Ru, which is well outside experimental errors. Therefore, the ratios M_n/M_p, in which the relative differences of the deformation lengths are still heavily weighted by the A/Z factor, clearly show an increasing predominance of the protons in the 2_1^+ excitations for ^{102,104}Ru.

TABLE IV. Charge quadrupolar deformation length values δ^C extracted in the present work for ^{100,102,104}Ru, in comparison with values calculated [a] from the $B(E2)\uparrow$ results of pure Coulomb excitation measurements.

A	δ^C (fm) Present work	[b]	[c]	[d]
100	1.154(17)	1.180(4)	1.182(7)	
102	1.277(17)	1.309(4)	1.336(6)	1.312(5)
104	1.464(23)	1.492(6)	1.515(6)	

[a] $\delta^C=(4\pi/3Ze)[B(E2)\uparrow]^{1/2}(1/r_{0C}A^{1/3})$, $r_{0C}=1.22$ fm.
[b] Reference [9].
[c] Reference [8].
[d] Reference [10].

The δ^N values are to be compared to nuclear deformation lengths obtained from other hadron inelastic scattering studies which weigh neutrons and protons equally. The only two inelastic scattering results, with isoscalarly interacting probes, presented in the recent Nuclear Data Sheets compilations [29–31], correspond to the 12 MeV deuteron inelastic scattering experiment on ^{102,104}Ru by Rekstad and Tjöm [26] and to the measurements by de Voigt *et al.* [27] of 104 MeV inelastic alpha scattering to the 2_1^+ state of ^{100}Ru. Rekstad and Tjöm [26], using DWBA-DOMP calculations with locally adjusted optical model parameters to analyze experimental angular distributions, measured at angles greater than 40° and 45°, respectively, obtained the values of 1.23 fm and 1.34 fm for the δ^N associated to the 2_1^+ states of the 102 and 104 isotopes. These values can, however, not be put in direct comparison with the results of the present work since, although important at the deuteron energy employed in the study of Rekstad and Tjöm [26], no proper description of Coulomb excitation was by them included. The analysis of alpha scattering to the 2_1^+ state of ^{100}Ru by de Voigt *et al.* [27] was based on cross sections measured at only three scattering angles and resulted in an isoscalar inelastic transition strength $B(IS2)$, which, reduced to a mass deformation parameter, corresponds to $\delta^N=(1.13\pm0.12)$ fm. Although not referred by Nuclear Data Sheets, there exists also the study of Clement *et al.* [35] of 23 MeV inelastic deuteron scattering on ^{104}Ru. Those authors performed a coupled channel calculation and explicitly stress that, in their analysis, the transition to the 2_1^+ state is dominated by the one-step amplitude and that an equal mass and charge deformation constraint does not allow a proper adjustment to the data. The value $M_n/M_p=1.19(7)$ reported by Clement *et al.* [35], although smaller than N/Z, is, however, substantially higher than that obtained in the present study. Nevertheless, even if the absolute values of δ^N or, with a still smaller chance, M_n/M_p should be affected by some not foreseen systematic errors, the evolutionary behavior as a function of A of M_n/M_p disclosed in the present work (see Table II) should be preserved, since data taking and analysis were performed in a consistent way for the three isotopes. This behavior clearly establishes a decreasing relative influence of the neutrons on the first quadrupolar transition, as one and two pairs of neutrons are added to ^{100}Ru, a fact which is not easy to interpret in the light of current models.

ACKNOWLEDGMENTS

Financial support by CNPq (Conselho Nacional de Desenvolvimento Científico e Tecnológico), FINEP (Financiadora de Estudos e Projetos), and FAPESP (Fundação de Amparo à Pesquisa do Estado de S. Paulo) is gratefully acknowledged.

[1] A. Bohr and B.R. Mottelson, *Nuclear Structure* (Benjamin, New York, 1975).
[2] M.M. Gazzaly, N.M. Hintz, G.S. Kyle, R.K. Owen, G.W. Hoffmann, M. Barlett, and G. Blanpied, Phys. Rev. C **25**, 408 (1982).
[3] A.M. Bernstein, V.R. Brown, and V.A. Madsen, Phys. Lett. **71B**, 48 (1977).
[4] A.M. Bernstein, V.R. Brown, and V.A. Madsen, Phys. Lett. **103B**, 255 (1981).
[5] V.A. Madsen, V.R. Brown, and J.D. Anderson, Phys. Rev. C **12**, 1205 (1975).
[6] A.M. Bernstein, V.R. Brown, and V.A. Madsen, Comments Nucl. Part. Phys. 203 (1983).
[7] A.M. Bernstein, V.R. Brown, and V.A. Madsen, Phys. Lett. **106B**, 259 (1981).
[8] S. Landsberger, R. Lecomte, P. Paradis, and S. Monaro, Phys. Rev. C **21**, 588 (1980).
[9] J.H. Hirata *et al.* (unpublished).
[10] A. Bockish, M. Miller, A.M. Kleinfeld, A. Gelberg, and U. Kaup, Z. Phys. A **292**, 265 (1979).
[11] L.C. Gomes, L.B. Horodynski-Matsushigue, T. Borello-Lewin, J.L.M. Duarte, and G.M. Ukita (unpublished).
[12] K. Koide, F.C. Sampaio, E.M. Takagui, J.H. Hirata, and O. Dietzsch, Nucl. Instrum. Methods **215**, 61 (1983).
[13] D. Pulino, G.M. Sipahi, G.M. Ukita, T. Borello-Lewin, L.B. Horodynski-Matsushigue, J.L.M. Duarte, W.G.P. Engel, and J.C. de Abreu, Rev. Bras. Aplic. Vácuo **10**, 87 (1991).
[14] J.B. England *et al.*, Nucl. Phys. **A388**, 573 (1982).
[15] D. Rychel, R. Gyufko, B. Van Krüchten, M. Lahanas, P. Singh, and C.A. Wiedner, Z. Phys. A **326**, 455 (1987).
[16] J.Y. Park and G.R. Satchler, Part. Nucl. **1**, 233 (1971).
[17] P.D. Kunz, computer code DWUCK4, Colorado University, 1974.
[18] G.R. Satchler, *Direct Nuclear Reactions* (Clarendon Press, Oxford, 1983).
[19] L.R.B. Elton, *Nuclear Sizes* (Oxford University Press, New York, 1961).
[20] R. Barret and D.F. Jackson, *Nuclear Sizes and Structure* (Clarendon Press, Oxford, 1979).
[21] H. de Vries, C.W. de Jager, and C. de Vries, At. Data Nucl. Data Tables **36**, 495 (1987).
[22] E.J. Martens and A.M. Bernstein, Nucl. Phys. **A117**, 241 (1968).
[23] M. Wit, J. Schiele, K.A. Ederhard, and J.P. Schiffer, Phys. Rev. C **12**, 1447 (1975).
[24] C.M. Perey and F.G. Perey, At. Data Nucl. Data Tables **17**, 1 (1976).
[25] T. Fliessbach, Nucl. Phys. **A315**, 109 (1979).
[26] J. Rekstad and P.O. Tjöm, J. Phys. G **3**, 411 (1977).
[27] M.J.A. de Voigt, J.F.W. Jansen, F. Bruining, and Z. Sujkowski, Nucl. Phys. **A270**, 141 (1976).
[28] R.H. Spear, At. Data Nucl. Data Tables **42**, 55 (1989).
[29] B. Singh and J.A. Szues, Nucl. Data Sheets **60**, 86 (1990).
[30] D. de Frenne and E. Jacobs, Nucl. Data Sheets **63**, 406 (1991).
[31] J. Blachot, Nucl. Data Sheets **64**, 31 (1991).
[32] S. Sirota, J.L.M. Duarte, L.B. Horodynski-Matsushigue, and T. Borello-Lewin, Phys. Rev. C **40**, 1527 (1989).
[33] S. Raman, C.H. Malarkey, W.T. Milner, C.W. Nestor, and P.H. Stelson, At. Data Nucl. Data Tables **36**, 1 (1987).
[34] B.J. Lund, N.P.T. Bateman, S. Utku, D.J. Horen, and G.R. Satchler, Phys. Rev. C **51**, 635 (1995).
[35] H. Clement, G. Graw, H. Kader, F. Merz, H.J. Scheerer, P. Schiemenz, and N. Seichert, Nucl. Phys. **A451**, 219 (1986).

Anexo 2.4

Inelastic deuteron scattering in the Coulomb nuclear interference region: Procedures for estimating the precision of the extracted $B(E2)$ and $B(IS2)$ values

J. L. M. Duarte, G. M. Ukita, T. Borello-Lewin, L. B. Horodynski-Matsushigue, and L. C. Gomes
Instituto de Física, Universidade de São Paulo, Caixa Postal 66318, 05389-970, São Paulo, SP, Brazil
(Received 3 September 1996; revised manuscript received 28 February 1997)

Taking ^{94}Mo$(d,d')^{94}$Mo(2_1^+) at 13.2 MeV incident energy as an example, a discussion is made about the influence of known experimental uncertainties in the primary data on the precision of the $B(E2)$ and $B(IS2)$ values, extracted in Coulomb-nuclear interference (CNI) measurements in a correlated way. The reflexes of judicious variations of three optical model parameters (around the global prescription) on the extracted values are also examined. The good quality of the data obtained with the S. Paulo Pelletron-Enge-Spectrograph facility is shown to allow for a 2–3 % statistical uncertainty level for these quantities, within a distorted-wave Born approximation-deformed optical model approach. The accuracy of relative values of the ratio $B(E2)/B(IS2)$, which may be linked to the ratio of proton to neutron quadrupole moments, is argued to be of similar order. [S0556-2813(97)04810-3]

PACS number(s): 21.10.Re, 24.10.Ht, 25.45.De, 27.60.+j

I. INTRODUCTION

The literature shows scarce information on isoscalar reduced transition probabilities $B(ISL)$, in contrast to the corresponding quantities $B(EL)$ associated to the charge. Differences, in particular for 2_1^+ states of even nuclei, between $B(E2)$ and the $B(IS2)$ values would reflect unhomogeneous contributions of protons and neutrons to these excitations, which have been extensively used as indicators of nuclei structure properties [1]. Although experimental and theoretical studies [2,3] point to a dominance of simple homogeneous collective effects on most of these quadrupolar excitations, resulting in relative contributions of protons and neutrons of about Z/N, it is clear that a better pinning down of the uncertainties associated, both to the experimental information and to the method of analysis, can reveal explicit differences, of theoretical interest. In particular, it is expected that near single closed shells, protons and neutrons should contribute differently to the 2_1^+ excitation, in spite of core polarization effects [3].

Coulomb-nuclear interference (CNI) in inelastic scattering, with projectiles of isoscalar character, has long been known as an excellent instrument for the simultaneous measurement of $B(EL)$ and $B(ISL)$, since a relative normalization of the results is intrinsically given. Medium energy deuterons are convenient projectiles for the investigation of the 2_1^+ states through CNI studies. In fact, global optical potentials, important ingredients for the macroscopic analysis of inelastic scattering, besides well tested on elastic scattering, were, for deuterons, also extensively applied to several kinds of distorted-wave Born approximation (DWBA) analyses, thereby allowing regions of validity to be established, thus reducing the number of free parameters. In general, the intense collective first quadrupolar excitations are well described by the simple deformed optical model (DOMP) interpretation [4]. This method, if applied in the CNI region, allows the simultaneous extraction of the potential deformation length $\delta^{\rm pot}$, and the charge deformation length δ^C. As usual in DOMP analyses, $\delta^{\rm pot}$ is assumed equal to the nuclear or mass deformation length, which, in turn, specializing for quadrupolar excitations, with isoscalarly interacting projectiles is related to the isoscalar reduced transition probability $B(IS2)$ by

$$B(IS2)=(\delta^{IS})^2\left[\frac{3ZR_m}{4\pi}\right]^2,$$

with $\delta^{IS}\equiv\delta^{\rm pot}$, as supposed.

An analogous relation [5] transforms δ^C:

$$B(E2)\uparrow=(\delta^C)^2\left[\frac{3ZeR_c}{4\pi}\right]^2,$$

where $R_m=r_mA^{1/3}$ and $R_c=r_cA^{1/3}$ are, respectively, the characteristic radii of the mass and the charge distributions of the nucleus. Taking into account this direct quadratic relationship between the reduced transition probabilities and the deformation lengths, which are extracted in the DOMP analyses, the latter ones may be used equivalently in the physical discussion, as will be done in the present paper.

Our group which investigates nuclear structure properties with light ions at the University of São Paulo Pelletron Laboratory was, to our knowledge, the first to use CNI measurements with deuterons. The mass region between $A=90$ and $A=104$ has received our particular attention and disclosed interesting effects [6–8]. In general, differences between mass and charge deformations amount to about 10 to 20%, indicating the necessity of a rather detailed knowledge of the uncertainties which affect these physical informations. There are at least two sources of uncertainties in the extraction of the deformation lengths, if the macroscopic DWBA analysis is taken as sufficiently well founded. One is directly associated to the experimental errors, characteristic of the data taking procedure. The other reflects the uncertainties in the several parameters needed for the theoretical description of the process. Detailed data of the ^{94}Mo$(d,d')^{94}$Mo(2_1^+) reaction

recently obtained [8] at 13.2 MeV incident energy are here taken as example in discussing the methods applied in the effort of obtaining reliable uncertainties for the deformation lengths. On this issue, the present work focuses attention on the reflexes of the experimental statistical errors on the δ^{IS} and δ^{C} values, which are extracted in the CNI studies in a correlated way. These are investigated comparing the outcome of a Monte Carlo simulation around the data points of the experimental angular distribution, in accordance with their standard deviations, with the application of statistical recipes [9], up to now not in common use in nuclear physics analyses. It is to be stressed that in the effort of quantifying uncertainties for the results of experimental nuclear structure studies, it is mandatory, in first place, to be able to represent correctly the influence of the inherent statistical uncertainties, which are always present in the data, since these are, in principle, unambiguously attributed (obtaining thus uncertainties of type A). The recipes should be applicable also to other experimental situations in nuclear physics where two or more correlated parameters are of importance.

A second step towards a complete quantifications of the uncertainties of the $B(E2)$ and $B(IS2)$ would be to obtain trustworthy values for the uncertainties of type B, in particular for the several systematic errors due to the incomplete description of the intervening reaction mechanism. This is outside the scope of the present work. Only the effects of small variations of three optical model parameters, taken as the most relevant for the analysis of medium energy deuteron inelastic scattering, on the DWBA-DOMP outcomes were also taken under consideration. The objective is, up to now, to inspect especially chains of isotopes and isotones near closed shells and in known transitional regions of nuclear structure in a comparative way. In particular, ^{94}Mo is to be compared to ^{98}Mo and both to ^{92}Zr and ^{96}Zr, respectively, in a research program which is still in progress.

II. EXPERIMENTAL PROCEDURE

The experimental setup and precautions in the data-taking process will be presented here in some detail for the example chosen, ^{94}Mo$(d,d')^{94}$Mo(2_1^+), since they are typical for the procedures developed for the CNI studies with deuterons.

The deuteron beam of the São Paulo Pelletron accelerator, with an incident energy of 13.2 MeV, was focused on a ^{94}Mo enriched target, after passing defining slits of 1.0 $\times$2.0 mm^2, which guarantee an adequate object for the Enge split-pole spectrograph. Through patient focusing, ratios between current on the object defining slits and beam on target of about 1:30 could be achieved and maintained. On a circular slit of $\sim$6 mm diameter, situated about half a meter before the defining slits, a ratio of about 1:100 with respect to the beam was pursued, in further guarantee of an adequate profile of the beam. The very uniform target, enriched to (93.9$\pm$0.1)% and with a thickness of 32 μg/cm^2, was prepared [10] by electron bombardment evaporation of Mo metal, in powder form, on $\sim$10 μg/cm^2 carbon backings.

The ejectiles of the reaction were momentum analyzed by the spectrograph and detected at the focal plane in nuclear emulsion (Ilford G.5, 50 μm thick). The use of nuclear emulsion reduces dramatically the background associated with deuteron beams, since these detectors do not respond to the abundant γ and x rays provenient mostly from (n,γ) reactions in the spectrograph iron core, after deuteron breakup. The emulsion plates were scanned, after processing, in strips of 200 μm across the plates.

Figure 1 displays the relevant portion of three spectra (θ_{lab}= 14°, 18°, and 58°), showing the peak associated with the 2_1^+ excitation of ^{94}Mo, at 871.1 keV [11]. Two of the spectra are typical for data taken at forward scattering angles, the good energy resolution of $\sim$8 keV full width at half maximum (FWHM), being essential for evidencing the peak with respect to the background, which is due basically to the elastic tail. This background drops rapidly with increasing angle and, at θ_{lab}= 58°, the small peak associated to the ^{95}Mo$(d,d')^{95}$Mo$(\frac{9}{2}^+)$ excitation is clearly observed at the correct energy [12], in the proportion expected from the presence of ^{95}Mo in the target material. The horizontal opening angle of the spectrograph was maintained fixed, corresponding to $\Delta\theta_{lab}=\pm 1.9°$.

Relative normalization of the spectra was achieved by measuring the beam current in an aligned Faraday cup, with electron suppression, connected to a calibrated current integrator, while continuously monitoring the direction of the beam. Absolute normalization of the cross section was referred to optical-model predictions for the elastic scattering of deuterons on the same target, measured under similar conditions. Figure 2 shows the elastic scattering data in comparison with optical model calculations performed with the parameters of the global prescription of Perey and Perey [13] presented in Table I and also with the prescribed parameters but with the radii r_R and r_I increased by 2% (see further discussion). An error of $\pm$5% is estimated on the absolute cross section determinations.

The experimental angular distribution of the inelastic scattering to the 2_1^+ state is presented in Fig. 3, in comparison with DWBA-DOMP predictions (averaged over spectrograph opening angle). The error bars, where not explicitly shown, are smaller than, or of the order of, the size of the points in the figure and include the combined effect of statistics, plate scanning, and background (and/or contaminant) subtraction, but do not include any error in the absolute cross section scale. Scanning of the emulsion plates under an optical microscope by several calibrated "readers" demonstrated a very good reproductibility ($\pm$2%) for the number of tracks in each peak. Each spectrum was "read" by at least two persons, resulting in low scanning uncertainties.

In perspective, to obtain data with the quality necessary for the proposed CNI studies, for medium mass nuclei, where the interference minimum for deuterons of about 10 MeV appears at relatively forward angles, it is important to apply detection techniques with nuclear emulsions, in association with the excellent beam profile and energy characteristics provided by a Tandem-spectrograph facility.

III. ANALYSIS

The DWBA-DOMP angular distributions shown in Fig. 3 were calculated by means of the code DWUCK4 [14] with the macroscopic collective form factors [4], responsible, respectively, for the Coulomb and nuclear quadrupolar excitation processes:

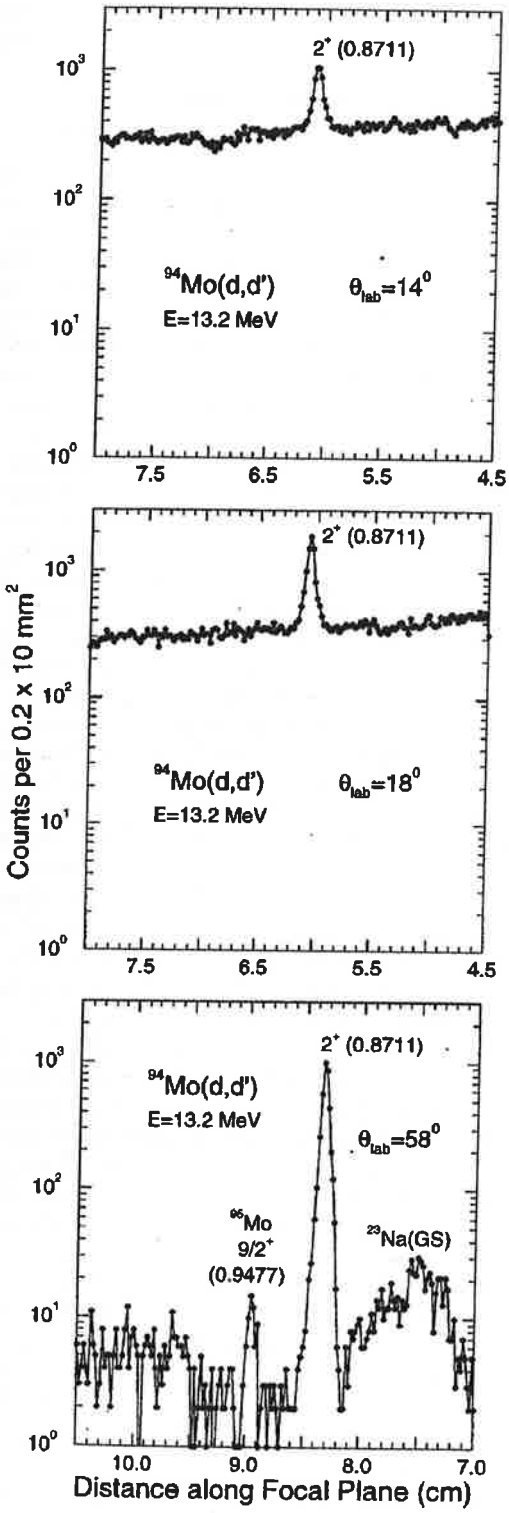

FIG. 1. Portions of the spectra of ^{94}Mo(d,d'), taken at θ_{lab} = 14°, 18°, and 58°. Indicated in parenthesis are the energies (in MeV) of the 2_1^+ state in ^{94}Mo [11] and of the contaminant $\frac{9}{2}^+$ state in ^{95}Mo [12]. Observe the very compressed log scale for the y coordinate.

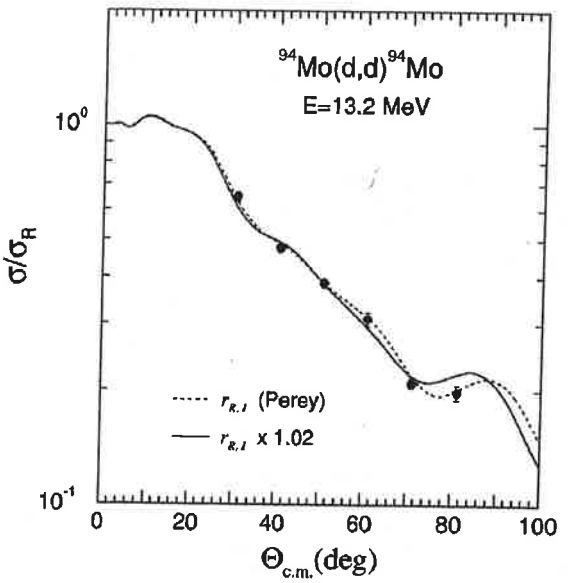

FIG. 2. Elastic angular distribution in comparison with optical model calculations, with parameters of Table I (dashed) and also increasing (see text) both real and imaginary, radii parameters by 2.0% (solid). Experimental uncertainties (error bars) represent the contributions of statistics, plate scanning, and background subtraction.

$$F_2^C(r)=\frac{4\pi e}{5}[B(E2)\uparrow]^{1/2}\frac{1}{r^3} \quad \text{for } r\geq R_c=r_cA^{1/3}$$

and

$$F_2^{\text{nuc}}(r)=-\delta_R^{\text{pot}}(U)\frac{dV(r)}{dr}-i\delta_I^{\text{pot}}(U)\frac{dW_D(r)}{dr},$$

where V and W_D are the real and surface imaginary depths of the optical potential U, taken with the usual Woods-Saxon and derivative Woods-Saxon forms, with given geometrical parameters (r_R, a_R and r_I, a_I). The parameters δ^C, related to $B(E2)\uparrow$, and $\delta^{IS}=\delta_R^{\text{pot}}(U)=\delta_I^{\text{pot}}(U)$, related to $B(IS2)$, are, respectively, the charge and isoscalar deformation lengths, to be extracted in the analysis.

Also shown in Fig. 3 are the separated contributions of Coulomb [due to $F_2^C(r)$] and nuclear [due to $F_2^{\text{nuc}}(r)$] excitations to the $0_1^+\rightarrow 2_1^+$ transition in ^{94}Mo. Coulomb excitation was treated in the usual way [4] and the spherical Coulomb potential, relative to which the deformation is considered, was taken as that of an uniform charge distribution without diffuseness and radius R_c. The Coulomb form factor was taken as zero inside the sharp cutoff charge radius

TABLE I. Global optical model parameters for elastic deuteron scattering prescribed by Perey and Perey [13]. In the analysis a Coulomb reduced radius of r_c = 1.22 fm was utilized and r_R and r_I were increased by 2.0%, with respect to the prescription.

V (MeV)	r_R (fm)	a_R (fm)	W_D (MeV)	r_I (fm)	a_I (fm)
96.6	1.15	0.81	17.6	1.34	0.68

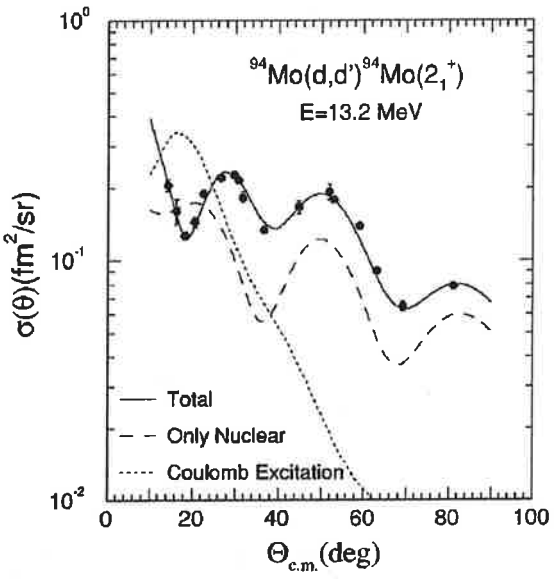

FIG. 3. Experimental inelastic scattering angular distribution used to exemplify the CNI method with deuterons. The solid curve is the best fit of the DWBA-DOMP predictions to the data, while the dotted and dashed ones show the contribution of, respectively, Coulomb and nuclear excitation separately. The parameters of the fit are the potential deformation length δ^{IS}, and the ratio $C = \delta^C/\delta^{IS}$, where δ^C is the charge deformation length. Error bars represent uncertainties due to statistics, plate scanning, and background subtraction and do not include the error in the absolute cross section scale.

and, since this one is well inside the strong absorption radius, the resulting approximation has no appreciable effect on the calculated cross sections. The global parameters which define the optical potential were taken from the well-known systematics of Perey and Perey [13], with a slight modification in the reduced radii to be discussed below.

It is seen that, in particular, the clearly defined interference minimum at $\theta_{lab} \sim 18°$ scales the relative contribution of the two excitation processes and that the absolute cross section values at $\theta_{lab} \geq 45°$ are mainly determined by the nuclear excitation. The correlated parameters directly extracted, in a χ^2-minimum fit of the prediction to the data, are δ^{IS} and the ratio $C = \delta^C/\delta^{IS}$, being predominantly influenced, respectively, by the larger angle results and by the pattern of the interference region.

Deuterons are loosely bound projectiles and, as such, subject to absorptive reactions at the very tail of the nuclear potential. This effect is represented in the optical model interpretation through the important role that the imaginary term of the potential plays in determining the pattern of the predicted angular distribution. There are, furthermore, theoretical expectations for possibly different W_D values, even for neighboring nuclei, due to different open reaction channels. The imaginary potential is, therefore, an expected source of uncertainty on the predictions of the model. The reflexes on the extracted deformation lengths of judicious variations of the depth and of the range of the imaginary potential around the globally predicted values [13], besides also of small modifications of the real radius parameter, will be investigated. The main piece of research to be presented in this section is, however, the effect of the known statistical uncertainties of the data on the quantities of physical interest.

A. Reliability of the extracted deformation lengths as a function of some relevant model parameters

In the macroscopic analysis of collective excitations through inelastic scattering, the optical model parameters have a twofold influence on the results: they determine the distorted waves in the entrance and exit channels of the reaction and also the interaction potential in the form factor. To allow for significant comparisons of the spectroscopic information to be extracted through the DWBA-DOMP analysis, in particular if chains of nuclei are to be compared, it seems best to stick, as far as possible, to well-known and approximately constant optical parameter values. This section is devoted to search for the necessity of relaxing this condition, especially for the imaginary term, as dictated by the experimental results. We, therefore, decided to investigate first the reflexes of small modifications of the W_D and r_I, and also of the r_R, parameters (with respect to the global prescription of Perey and Perey [13]) on the theoretical predictions and, in consequence, on the deformation lengths. For now, no other theoretical limitations are considered, so the ensuing discussion is not meant to quantify, in the present stage of the investigation, systematic errors due to a possibly faulty interpretation of the reaction mechanism.

Figure 4 shows, in a comparative way, the effect of modifications in each of the three optical model parameters, which were considered as most relevant, on the quality of the DWBA-DOMP fits to the data of Fig. 3. The vertical axes display χ^2_{min}, the smallest values of χ^2 obtained in adjusting, each time—that is, for each of the several changing values of W_D, r_I, or r_R—the values of δ^{IS} and of the ratio C for best fit. The range of variations of W_D, r_I, and r_R was chosen such as to provide an increase of a factor ~ 4 in χ^2_{min}. The plots in the left column of the figure display χ^2_{min} as a function of, respectively, the depth of the imaginary surface potential W_D [Fig. 4(a)], the reduced radius r_I of the imaginary potential [Fig. 4(b)], and the reduced radius of the real potential r_R [Fig. 4(c)], maintaining in each case all other optical model parameters fixed at their values of the global Perey and Perey [13] prescription. Arrows indicate the global prescription values of W_D, r_I, and r_R in the figures. The plots in the right column [Fig. 4(d), 4(e), and 4(f)] represent the corresponding results of χ^2_{min} (attention is called to the expanded vertical scale) for the situation where all parameters, except r_I and r_R, are taken (and fixed if not under study) at their prescribed values, the radii parameters being increased by 2.0%, due to considerations to be presented in what follows. So, Fig. 4(a) displays the values of χ^2_{min}, in a range of up to three times the value of $\chi^2_{min} = 117$ obtained at $W_D = 17.2$ MeV. It is seen that $W_D = 17.6$ MeV (see arrow) of the Perey and Perey prescription [13] is included in the "bottom" of the curve. Figures 4(b) and 4(c) indicate, on the other hand, that the respective minima of χ^2_{min} occur, for both radii, at values which are about 2% higher than the prescription [13]. Figure 4(c) furthermore tells us that an important reduction is achieved in χ^2_{min}, especially through the modification of the real reduced radius r_R. It may, thus, be noted that, contrary to expectations, the imaginary term

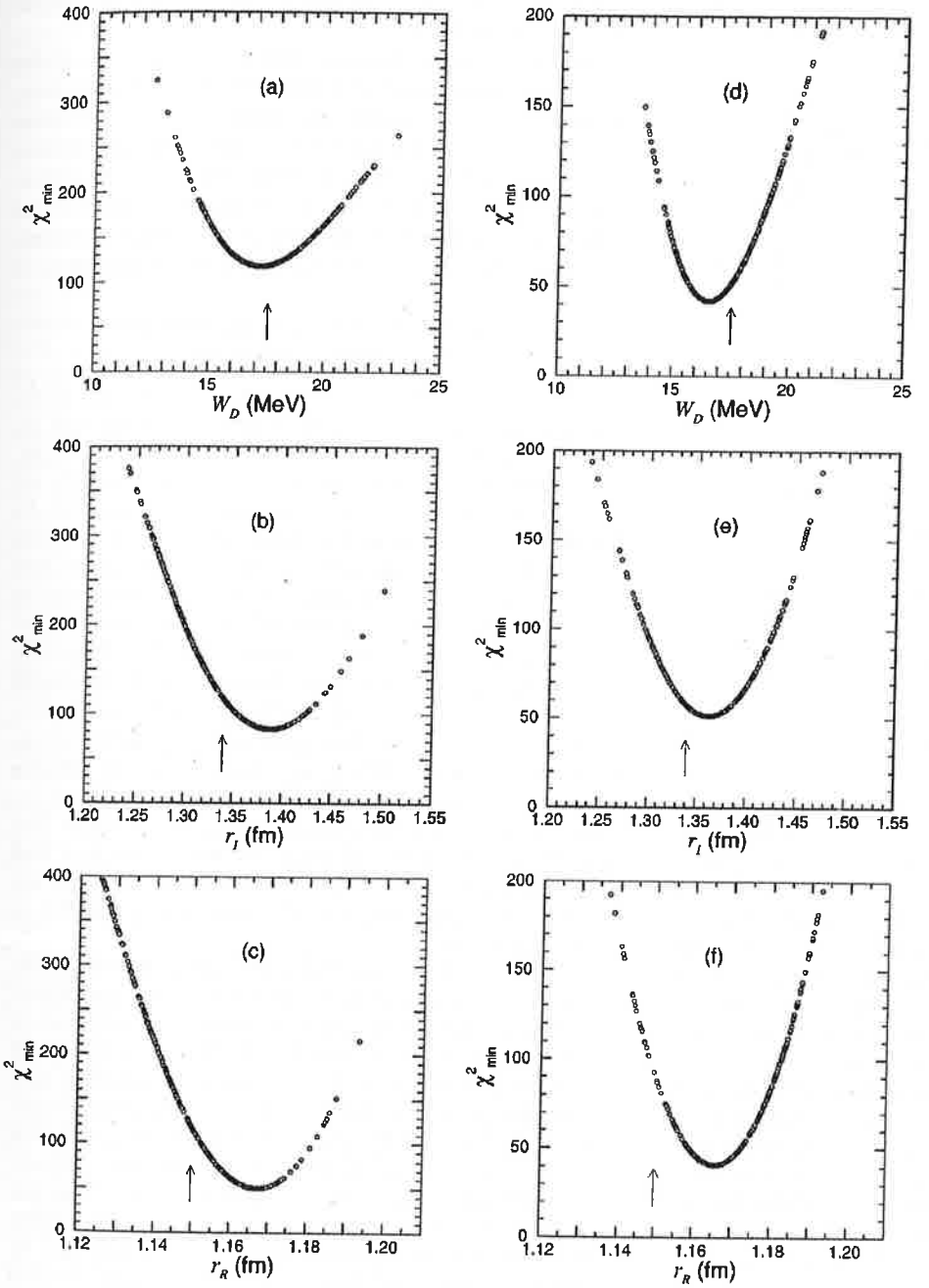

FIG. 4. Variation of the quality of the fit to the data of Fig. 3, as three optical parameters (W_D, r_I, and r_R), each at a time, are removed from their globally prescribed [13] values, indicated by arrows (see text). In (a) to (c), the parameters which were not under study were maintained fixed at their globally [13] prescribed values; in (d) to (f), the same procedure was adopted, but the r_R and r_I parameters, when fixed, were increased by 2.0% with respect to the prescription.

W_D of the global parameters of Perey and Perey [13] reproduces the data rather well. On the contrary, the 2% increase in r_R is essential to adjust the relative phase of the prediction to the data, since the real radius has, as is well known, a predominant influence on the width of the diffractive oscillations of the angular distribution. This effect is responsible for the reduction of a factor ~ 2 in χ^2_{min} shown in Fig. 4(c). In fact, direct inspection of the experimental results under consideration and also of those for the same reaction at 16.0 MeV deuteron energy and for the other isotope ^{98}Mo (at both energies) [15] had already shown the inelastic diffractive oscillations to correspond to an apparently larger object than appropriate for the representation of the elastic results. This may denote some particularity of the reaction mechanism for the weakly bound deuteron (since it was not observed with α's) which is beyond the DWBA-DOMP representation, but is stable with respect to deuteron energy and nuclear mass in the investigated region. Therefore, in the analysis of these CNI studies with deuterons on Mo, an option was made to modify both, the real and imaginary radii, by an increase of 2.0% with respect to the global prescription [13], in view also of maintaining their relative value. All other optical parameters, also W_D, were kept as globally prescribed, in accordance with the philosophy of aiming at an as uniform description of the intervening reaction mechanism for the whole mass region, as the data will allow for.

Figure 5 resumes, on one plot, the physical information associated to the right column of Figs. 4(d)–4(f). The three trajectories there displayed correspond, each, to the sequence of pairs (δ^{IS},C), determined by the best-fitting procedure

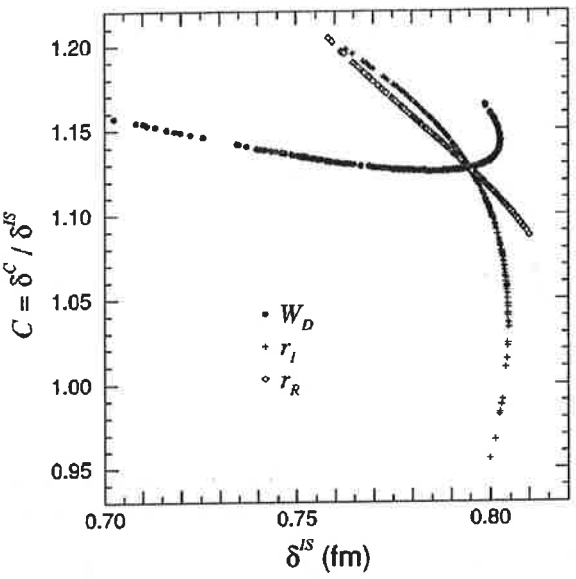

FIG. 5. Sequences of (δ^{IS},C) pairs obtained in the minimizing procedures represented in Figs. 4(d), (e), and (f), for each of the three selected optical model parameters (W_D, r_I, and r_R). The point of intercept correspond to the values of δ^{IS} and C taken to be the results of the present analysis (see text).

already described, with the several values of, respectively, W_D, r_I, and r_R. The particular points plotted in this figure are the result, as they are in Fig. 4, of Monte Carlo chosen values of the optical parameters around their globally prescribed [13] values. An inspection of Fig. 5 tells immediately the regions of variability of δ^{IS} and $C=\delta^C/\delta^{IS}$ associated with indeterminations in the here highlighted optical model parameters. It is seen that the radii and W_D have orthogonal effects on the physical results: the last one corresponds to a rather sharp value of C and a relatively large interval for δ^{IS}, while the contrary is verified for variation in the radii. The point of intercept in the figure is the value obtained for δ^{IS} and C with all the optical parameters of the DWBA analyses taken at their globally prescribed [13] values, except for the mentioned 2.0% increase in r_I and r_R. A similar figure constructed for the results displayed in the left part of Figs. 4(a)–4(c) contains no additional information of physical interest, except that the trajectory in the (δ^{IS},C) plane for varying W_D has a still smaller slope, the point of intercept corresponding to $\delta^{IS}=0.78$ fm and $C=1.15$.

The behavior of the trajectories in the (δ^{IS},C) plane is in accordance with the *a priori* known effects of the optical parameters on DWBA-DOMP predictions. In fact, W_D is known to affect the "peak" to "valley" ratio of the diffractive oscillations, higher values of W_D filling in the valleys progressively and washing the peaks out, resulting in higher δ^{IS} values, while the interference minimum remains about the same for constant C. On the other hand, the radii, particularly the real one, modify the proper diffraction pattern with respect to the angular scale, affecting especially the value of C. It is seen, through Figs. 4 and 5, that the enormous increase of a factor of 4 in the $\chi^2_{\min}$ values corresponds, in total, to a variability interval of no more than $\pm 10\%$ in the relevant physical quantities δ^{IS} and C. It seems, thus, qualitatively justified that significant physical information can be extracted, even if the optical model parameters are put under restricted doubt.

The Monte Carlo choosing applied here to three of the optical parameters is part of a study, which is still under way, to associate a total model uncertainty to the deformation lengths, and will be the subject of a forthcoming publication [16]. In fact, it is our intention, in the long run, to be able to extract a kind of error belt around the theoretical predictions, reflecting the analysis of the several theoretical shortcomings, with a hopefully increasing degree of completeness.

B. Uncertainties of the deformation lengths due to experimental errors

This section is devoted to discussing the influence of the experimental errors on the derived quantities of physical interest and their uncertainties. A systematic error on the absolute cross section scale, estimated to be less than 5%, affects exclusively δ^{IS} and not the ratio C and will not be considered in this section. The statistical errors, on the other hand, affect both parameters of interest. The error bars shown in Fig. 3 are representative of standard deviations on the data points. In the extraction of confidence intervals for the fitted parameters, the nuclear physics literature frequently registers the application of two misused recipes: the simple addition of 1 to the value $\chi^2_{\min}$, with all, but the one parameter under consideration, fixed at the values of the best fit or, worse, the increase of 10% to $\chi^2_{\min}$, both thought as defining the confidence interval of each parameter, for 68.3% of expectation. The first recipe is adequate only if a single free parameter is considered [9], while the second one is at best an approximation to the first, when about ten data points are available and agreement with the theoretical prediction is statistically perfect.

The statistically recommended procedure depends on the number of free parameters. Furthermore, if the parameters are correlated and/or if the model predictions are not linear in the parameters, as is the case for δ^{IS} and C, special care must be taken if any numerical manipulation involving both is to be done and the stability of the results is to be investigated. In particular, if δ^C is to be determined, the correlation has to be explicitly taken into account. For this purpose, general techniques have been brought forward by Cline and co-workers [17], in the extraction of electromagnetic matrix elements in multiple Coulomb excitation of nuclei, and by Lampton, Margon, and Bowyer [18], in a more detailed form, within their astrophysical research projects, the last being systematized only recently, among other issues, by Press *et al.* [9], in a successful book. The recommended procedure is to define the hypervolumes in the space of the interesting parameters which contain the expected amounts of events. The contours of these volumes are obtained by specifying predetermined values for $\Delta\chi^2$ to be added to $\chi^2_{\min}$, all the parameters being allowed to vary freely. The values of $\Delta\chi^2$ depend on the statistical confidence level (for instance 68.3%, 99.7%, etc.) and on the number of parameters. For two parameters, which is the case of the present example, the contour lines are not exactly elliptical curves in the plane (δ^{IS},C), since the model is not linear in both parameters. Another critical point is that $\chi^2_{\min}=51.5$, for the 17 experimental points of the example, leads to $\chi^2_{\text{red}}=3.43$,

clearly indicating differences between data and model prediction in excess of the statistical expectation for normally distributed data, although these values of χ^2_{red} may be considered typical for DWBA-DOMP fits with global parameters. These facts point to the convenience of a thorougher investigation of the statistical procedures.

Entering in detail, when two parameters are considered, the Lampton, Margon, and Bowyer recipe, as cited by Press *et al.* [9], specifies that the regions which should contain 68.3 and 99.7% of the statistically expected events for normal data and perfect fit are bounded by the approximately elliptical contour lines obtained considering $\Delta\chi^2$ of 2.3 and 11.8, respectively. In Fig. 6(a) these contour lines, obtained for the example under discussion, are represented by the two outermost solid curves. Focusing on the 68.3% region, it follows that the projections of this contour on each axis corresponds to approximately two times 1.5σ [18] of the respective parameter. That is, if both parameters are looked upon jointly, the projection of the 68.3% region exceeds necessarily the value of 2σ. If, on the other hand, the information needed refers to the uncertainty in one parameter of the fit, whatsoever the value of the other (which is thereby relaxed), slices of widths $\sim 2\sigma$ are defined in the plane (δ^{IS}, C) corresponding to the projection of the contour line of $\chi^2_{min}+1$ (represented in the figure by the inner solid almost elliptical curve). The referred slices are limited in Fig. 6(a) through small-dotted vertical and horizontal lines.

A frequently employed χ^2 minimizing procedure is the Gauss-Marquardt method, due to its rapid convergence properties. This method was, in fact, applied to obtain χ^2_{min} and the uncertainties of the parameters in the form of a covariance matrix, which contains all the relevant information, as long as the linear approximation is adequate. In this case, exact ellipses of constant χ^2 are defined around χ^2_{min}, which are function solely of the values of the standard deviations of the parameters and their correlation. These are shown as dotted curves in Fig. 6(a) and, for the relatively well-behaved case taken as example, they are seen to be very similar to the contour lines with the same $\Delta\chi^2$ values. Within the linear approximation, it may be shown [18] that the projections of the two inner ellipses on each parameter axis correspond exactly to twice 1.515σ and 1.000σ, respectively.

Now, as already stated, perfect fit of the CNI data is not expected nor obtained with DWBA-DOMP and global optical parameters. However, if the aim is on comparative studies of collective properties of nuclei, as will be further justified in the discussion, it is this kind of global analysis which is deemed as the most appropriate fit to CNI data. Furthermore, the most interesting parameter for these studies, C, is derived almost exclusively from the forward angle data points and may, in other situations, have an expressive nonlinear effect on the fit. It is, therefore, important to bear in mind that the linearization procedure employed in the Gauss-Marquardt approach may under circumstances not be the best method to trust. The Lampton, Margon, and Bowyer procedure [18], which is not restricted to linear dependence on the parameters, is clearly to be preferred. The general techniques discussed so far do, however, not address the issue for model and data in poor statistical accord. In order to verify the validity, of these techniques [9,17,18] for the CNI data under study, a direct statistical test was decided upon,

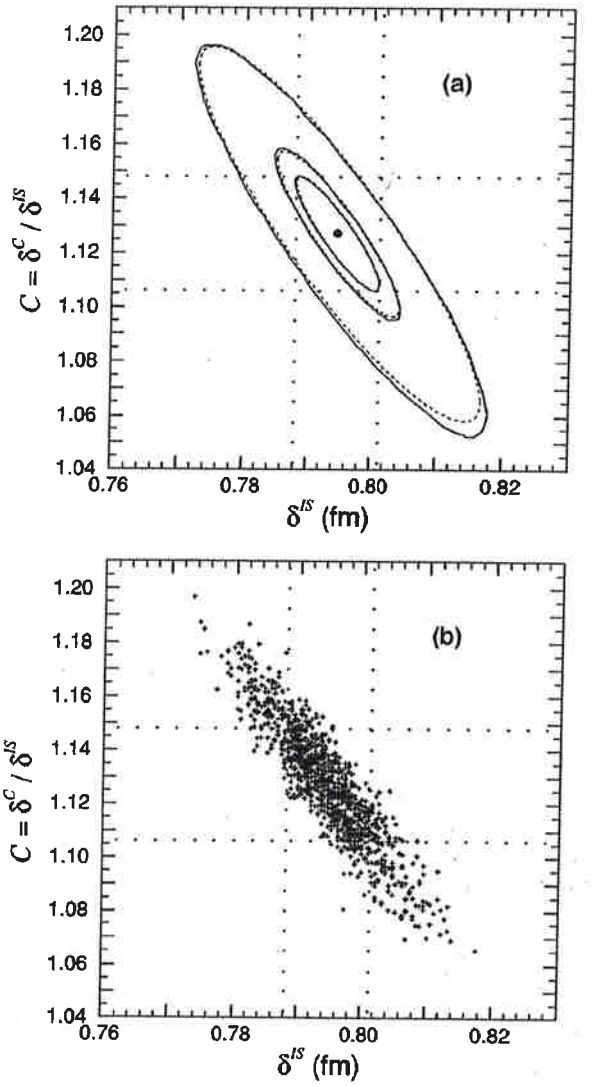

FIG. 6. (a) Best fit values of δ^{IS} and C for the experimental results presented in Fig. 3, with confidence region contours and ellipses: the solid curves are the constant χ^2 contour lines [9], while the dotted ones correspond to equivalent ellipses calculated from the Gauss-Marquardt parameters, both corresponding to statistical expectations of, respectively, 39.3% ($\chi^2_{min}+1$), 68.3% ($\chi^2_{min}+2.3$), and 99.7% ($\chi^2_{min}+11.8$) of the events. (b) Monte Carlo simulated results with 1002 trials on 17 fictitious "data" points, produced starting from the 17 actual experimental points. For each simulated "angular distribution" the minimum χ^2 was found and the corresponding values of δ^{IS} and C are represented as crosses in the (δ^{IS}, C) plane. Small-dotted vertical and horizontal lines in both (a) and (b) limit the slices which correspond, respectively, to 2σ of δ^{IS} and C.

through Monte Carlo simulations of "new" data. This statistical procedure is mathematically known to provide equivalent results, for Gaussian data distributions and perfect model fit. It is not *a priori* evident, on the other hand, if this property is maintained for the case under study, in particular, if any idiosyncrasy should be present in the experimental points. Figure 6(b) is the representation of the 1002 results obtained by Monte Carlo simulations of, each time, a "new angular distribution" containing 17 fictitious "data" points,

TABLE II. Results of the statistical analysis of DWBA-DOMP fits to the angular distribution of ^{94}Mo(d,d') presented in Fig. 3. The second and third columns contain numerical information associated with Fig. 6(a) and the last two columns with Fig. 6(b).

Parameters of physical interest	Experimental best fit		Monte Carlo simulation[a]	
	Gauss-Marquardt method	Contour line method	m	s
δ^{IS} (fm)	0.7947(64)	0.7947(66)	0.7942	0.0069
C	1.127 (20)	1.127 (21)	1.129	0.022
δ^{C} (fm)	0.896 (10)	0.896 (11)	0.896	0.011
r	−0.899	−0.904	−0.910	
$P(A_1)$	64.9%	66.7%	68.7%	
$P(A_2)$	93.1%	95.1%	95.5%	
$P(A_3)$	99.6%	99.7%	99.9%	

[a] m: mean value; s: standard deviation.

produced starting from the actual 17 experimental points, and choosing in accordance with Gaussian distributions defined by the experimental standard deviation of each point. For each simulated "angular distribution" the $\chi^2_{\min}$ was found and the corresponding values of δ^{IS} and C are represented as crosses in Fig. 6(b). It may be qualitatively appreciated that the crosses are distributed in the manner expected in behalf of the ellipses of Fig. 6(a), that is, almost all are contained within the outer ellipse, while about 2/3 are inside the middle one. Figure 6(b) also helps in making the meaning of the 2σ slices clear. Take, for instance, the horizontal slice which defines the 2σ interval for the C parameter. Comparing Fig. 6(a) with 6(b), it is seen that, since no restriction is made to δ^{IS}, crosses outside the 68.3% ellipse, but within this slice, are counted to complete the 68.3% expectation for C.

Table II presents in the first three lines the parameters of physical interest, as determined from the Gauss-Marquardt and contour line methods, also in comparison with the mean values (m) of the 1002 Monte Carlo results. The standard deviations, $\sigma_{\delta^{IS}}$ and σ_C, associated to the best fit values are given in parentheses, while the corresponding values (s) obtained from the Monte Carlo distribution are shown in the last column of Table II. In the present well-behaved example, where the data are good enough to restrict the parameters of the fit to only small variations around the "best values," the dependence may be considered as almost linear and the values came out very similar.

With the intention of better appreciating the quantitative statistical content of Fig. 6, a counting procedure of the crosses was executed, as a first step considering ellipses constructed with the proper mean values, standard deviations and correlation coefficient from the Monte Carlo simulations. A convenient way to represent the ellipses of constant probability density, for two correlated parameters obeying a Gaussian distribution, is through the constant A, given by

$$A^2=\left[\frac{\delta^{IS}-\langle\delta^{IS}\rangle}{\sigma_{\delta^{IS}}}\right]^2-2r\left[\frac{\delta^{IS}-\langle\delta^{IS}\rangle}{\sigma_{\delta^{IS}}}\right]\times\left[\frac{C-\langle C\rangle}{\sigma_C}\right]+\left[\frac{C-\langle C\rangle}{\sigma_C}\right]^2,$$

where $\langle\delta^{IS}\rangle$ and $\langle C\rangle$ are the mean (m) or the best fit values, $\sigma_{\delta^{IS}}$ and σ_C (standing also for s) are the standard deviations and r is the Pearson correlation coefficient between δ^{IS} and C. Figure 7 represents, as a function of A (calculated with the values of the two last columns of Table II), through a histogram, the relative frequency of crosses, per unit area (in each of the successive elliptical crowns), which is the physical approximation to the probability density dP/dS. Also shown in the figure is the expected probability density distribution. The good accordance lends support to the statistical assumptions made and demonstrates the internal consistency of the Monte Carlo procedure. The three last lines in the fourth column of Table II show the summed relative

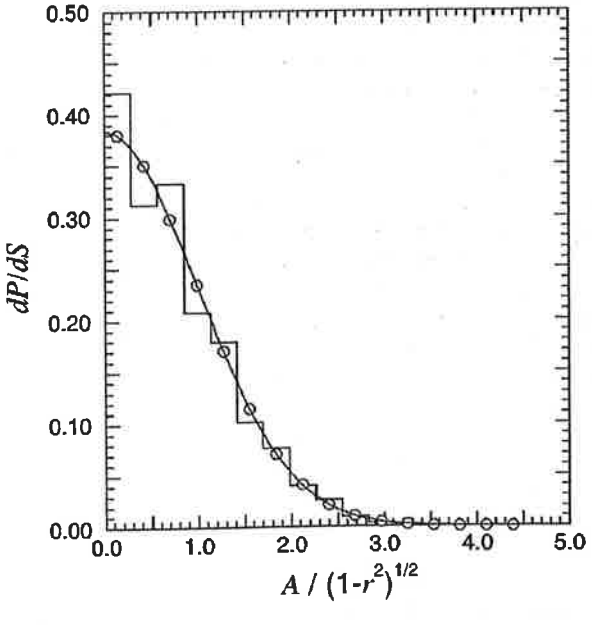

FIG. 7. Histogram of the probability density distribution as a function of the parameter A defined in the text, extracted for the Monte Carlo simulations presented in Fig. 6(b). The relative frequency was obtained counting the number of crosses contained in each of the successive elliptical crowns and normalizing per unit area and total number of events. In comparison, a Gaussian with $\sigma_0=1$ in the units of the horizontal axis, corresponding to the statistical expectation for a correlation coefficient of $r=-0.910$, is also shown as solid curve.

frequencies, $P(A)$, for the Monte Carlo results, up to values A_1, A_2, and A_3, which should theoretically correspond to probability contents of respectively 68.3, 95.4, and 99.7%, and are seen to be in extremely good agreement with these expectations. To complete the quantitative analysis, the counting procedure of the Monte Carlo results was also undertaken considering the Gauss-Marquardt ellipses and contour lines of interest, registering the crosses inside the respective curves characterized by the A_1, A_2, and A_3 values. It is to be remembered that two of these ellipses and contour lines, corresponding to A_1 and A_3, are shown as, respectively, dotted and solid lines in Fig. 6(a). The last three lines, in the second and third columns in Table II, present the statistical content $P(A)$ for the three ellipses and contour lines and it may be appreciated that the simulation came, within the statistical uncertainty inherent to determinations which start from only 17 experimental points, very close to the expected values [19]. It may, however, also be appreciated that the Gauss-Marquardt results are, in particular for the 68.7% ellipse, some 6% lower than the expectation. This situation will be intensified when data with larger error bars, or with insufficient definition of the crucial minimum, allow for farther excursions with respect to the "best" fit values, evidencing, thus, the known nonlinearities of the fitting function. In all, the comparative analysis of the physical information contained in Table II definitely shows, for the present example, the very good quantitative agreement of the three statistical procedures here adopted, demonstrating the basic equivalence of them. The adequacy of the Press *et al.* [9] recipe seems thus established also for the here considered CNI measurements with DWBA-DOMP fits. Whenever the constant χ^2 contour lines prove adequate resemblance with the corresponding ellipses characterized by A_1, A_2, and A_3 of the Gauss-Marquardt result, the uncertainties may be extracted directly from the covariance matrix. If, in other experimental situations, important differences between the two representations should show up, indicating perceptible influences of the nonlinearity, the contour line method [9] is recommended and comparison between experimental results can, in principle, only be made through direct inspection of the confidence regions in parameter space. In very suspect cases, other Monte Carlo simulations may be in order. Any important differences of these with respect to the contours may be indicative of trouble with the best fit.

Two more Monte Carlo simulations performed (with $N = 999$ and 1000) confirm, in the present test case, besides the expected stability of the results, that the fluctuations, measured through the standard deviations s, are systematically about 10% larger for the simulations in comparison with the Gauss-Marquardt values.

The statistical analysis instills confidence on the experimentally attributed uncertainties up to two significant figures. Therefore, from this point of view, the ratio C, in an experimental situation like that of Fig. 3, can be determined on a 2% precision level (see Table II). The nuclear deformation length, on the other hand, can through inelastic deuteron scattering be obtained with an about 1% statistical uncertainty, as can be also appreciated in Table II. The value of $\delta^C = C\delta^{IS}$ is accompanied by an statistical uncertainty smaller than that of the C value, since the negative covariance was taken into due account in the error propagation. The quadratic relationship reflects the quoted experimental (only statistical) uncertainties as $\pm 1.6\%$ in $B(IS2)$ and $\pm 2.2\%$ in $B(E2)$.

IV. DISCUSSION AND CONCLUSIONS

The statistical analysis applied in Sec. III has demonstrated that inelastic scattering studies with deuterons of ~ 13 MeV, on intermediate mass nuclei, may result, for the 2_1^+ excitations, in $B(IS2)$ and $B(E2)$ values on the few percent precision level. The accuracy, on the other hand, should be examined from a complementary perspective. The quantity of primary interest for several nuclear structure interpretations is the ratio of the reduced transition probabilities $B(E2)$ and $B(IS2)$, which, for CNI data, is more accurate than either quantity separately, since obtained from the same measurement. In fact, in this experimental situation, the cross section scale errors are canceled and some of the model errors in the analysis are diluted, in particular, those associated with known limitations of the distorted waves in the DWBA analysis.

In the ratio

$$\frac{B(E2)}{B(IS2)} = e^2\left(\frac{\delta^C}{\delta^{IS}}\right)^2\left[\frac{R_c}{R_m}\right]^2 = e^2\left(C\,\frac{r_c}{r_m}\right)^2,$$

besides the uncertainty in C, only the uncertainties in the reduced charge r_c and mass r_m radii have to be considered, if absolute values of the ratio are needed. In the present method of analysis, a reduced charge radius of $r_c = 1.22$ fm was used for the sharp cutoff spherical charge distribution, in accord with electron inelastic scattering and muonic atom data, as catalogued by Elton [20], Barret and Jackson [21], and de Vries *et al.* [22], when reduced to sharp-edge distributions. The reduced radius of the mass distribution is suggested to be taken as $r_m = 1.16$ fm, which is obtained from the value of Chung and Myers [23], also transformed to a sharp edge interpretation. Should the reduced radii be uncertain by as much as 5% each, a less than 15% systematic uncertainty would result on the ratio of the two reduced transition probabilities of interest. Otherwise, if chains of nuclei are studied in a comparative way, only the relative values of $B(E2)$ and $B(IS2)$ may be of importance and thus systematic errors such as those on the radii are irrelevant. It suffices, then, to be sure that the quantities C, for the several nuclei to be compared, were extracted in a consistent way. As formerly stated, optical parameters influence DWBA-DOMP results in a twofold manner, being responsible for the distorted waves and for the nuclear form factor of the transition. Whenever the experimental findings are not frontally misrepresented by the parameters of a global prescription, these are felt to provide the best choice for systematic spectroscopic analyses, since in this case the chain of nuclei is represented on the same footing. Comparison can thus be made, as is necessary, on the few percent level, due only to the statistical uncertainty in C, which was shown, in Sec. III B, to be determinable within 2%, under the present experimental conditions. It is to be remembered that C gives direct information on the ratio of proton to neutron quadrupolar moments of the 2_1^+ excitation, $C = 1.00$ being the limiting value between proton/neutron contributions exceeding ($C > 1.00$) or lacking (C

TABLE III. Results of the experimental best fit and the fit obtained with δ^C fixed at the Raman *et al.* [5] value.

Fit[a]	δ^{IS} (fm)	C	δ^C (fm)	χ^2_{min}	χ^2_{red}
Experimental best fit	0.7947(66)	1.127(21)	0.896(11)	51.51	3.43[c]
Fixed δ^C	0.8345(57)	0.971(14)	0.810(8)[b]	102.20	6.39[d]

[a] $r_R = 1.173$ fm and $r_I = 1.367$ fm; all other optical parameters at their prescribed [13] values.
[b] Deduced from the value adopted for $B(E2)$ by Raman *et al.* [5].
[c] Degrees of freedom $= 17 - 2 = 15$.
[d] Degrees of freedom $= 17 - 1 = 16$.

<1.00) with respect to the homogeneous Z/N value, expected for purely collective states [4].

Finally, what further concerns the accuracy of the absolute values of $B(E2)$ and $B(IS2)$ separately, from an experimental point of view not more that about 5% of absolute error is estimated on the cross sections and, if we stick to the chosen theoretical description and globally prescribed parameters, the preliminary analysis of the influence of some model parameters, presented in Sec. III A, is also not indicative of great variability. Of course, nothing can, for now, be said about systematic errors due to any fault in the representation of the reaction mechanism through the chosen DWBA-DOMP approach. Data taken at other incident deuteron energies and also with other projectiles may, in the future, offer clues on that.

Table III summarizes the results derived from the contour line recipe, taken as the final values of the analysis effectuated on the ^{94}Mo$(d,d')^{94}$Mo(2_1^+) reaction at 13.2 MeV. Also shown in Table III, for the sake of completeness, are the results of calculations (see Fig. 8), which tried to force, within the adopted methodology, a fit on the data taking the prefixed value of $\delta^C = 0.810$ fm, in correspondence to the adopted $B(E2)$ for ^{94}Mo of the Raman *et al.* [5] compilation. As may be seen in Fig. 8 and through the χ^2_{min} values of Table III, a considerably worse description of the experimental data is thereby obtained, in particular, in the interference region. This is not to be taken as implying that our value for δ^C is to be preferred to the one adopted [5], since, as stated, systematic errors may intervene, but in our view confirms the

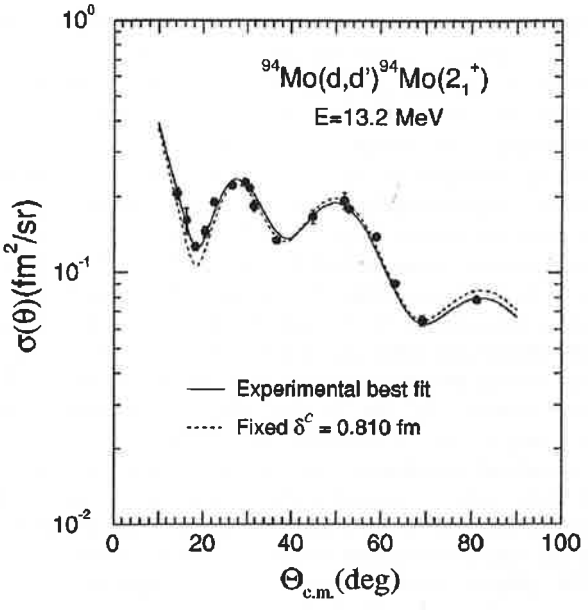

FIG. 8. Comparison between experimental best fit and a fit obtained with δ^C fixed at the Raman *et al.* [5] value.

value of $C \sim 1.1$. The analysis of data obtained for the same scattering at 16.0 MeV incident energy gives results which are basically consistent with the information here presented for 13.2 MeV. It is, therefore, argued that the CNI measurements, through the value of C, disclose the proton contribution to 2_1^+ excitation to be slightly more important than the neutron one in the case of the first quadrupolar excitation of ^{94}Mo, in the very contrast to what was observed [7] for its isotone, ^{92}Zr, where $Z = 40$ acts as if closed, resulting in a clear predominance of the neutrons in the 2_1^+ excitation.

ACKNOWLEDGMENTS

The authors are indebted to M. D. L. Barbosa for his contributions during several phases of the present work. Financial support by CNPq (Conselho Nacional de Desenvolvimento Científico e Tecnológico), FINEP (Financiadora de Estudos e Projetos), and FAPESP (Fundação de Amparo à Pesquisa do Estado de S. Paulo) is gratefully acknowledged.

[1] A. Bohr and B. R. Mottelson, *Nuclear Structure* (Benjamin, New York, 1975).
[2] M. M. Gazzaly, N. M. Hintz, G. S. Kyle, R. K. Owen, G. W. Hoffmann, M. Barlett, and G. Blanpied, Phys. Rev. C **25**, 408 (1982).
[3] A. M. Bernstein, V. R. Brown, and V. A. Madsen, Phys. Lett. **71B**, 48 (1977); **103B**, 255 (1981).
[4] G. R. Satchler, *Direct Nuclear Reactions* (Claredon, Oxford, 1983).
[5] S. Raman, C. H. Malarkey, W. T. Milner, C. W. Nestor, and P. H. Stelson, At. Data Nucl. Data Tables **36**, 1 (1987).
[6] L. C. Gomes, L. B. Horodynski-Matsushigue, G. M. Ukita, J. L. M. Duarte, and T. Borello-Lewin, XV Reunião de Trabalho em Física Nuclear no Brasil, Caxambu, 1992 (unpublished), p. 69; L. C. Gomes, L. B. Horodynski-Matsushigue, T. Borello-Lewin, J. L. M. Duarte, and G. M. Ukita (unpublished).
[7] L. B. Horodynski-Matsushigue, T. Borello-Lewin, and J. L. M. Duarte, XVI Reunião de Trabalho em Física Nuclear no Brasil, Serra Negra, 1993 (unpublished), p. 61; Proceedings of the International Nuclear Physics Conference, São Paulo, Brazil, 1989 (unpublished), Vol. I, p. 309.
[8] G. M. Ukita, L. C. Gomes, J. L. M. Duarte, L. B. Horodynski-Matsushigue, M. D. L. Barbosa, and T. Borello-Lewin, XVII Reunião de Trabalho em Física Nuclear no Brasil, Angra dos Reis, 1994 (unpublished), p. 48; T. Borello-Lewin, G. M. Ukita, J. L. M. Duarte, L. B. Horodynski-Matsushigue, L. C.

Gomes, and M. D. L. Barbosa, International Conference on Nuclear Dynamics at Long and Short Distances, Angra dos Reis, Brasil, 1996 (unpublished), p. 19.

[9] W. H. Press, B. P. Flannery, S. A. Teukolsky, and W. T. Vetterling, *Numerical Recipes* (Cambridge, New York, 1990).

[10] D. Pulino, G. M. Sipahi, G. M. Ukita, T. Borello-Lewin, L. B. Horodynski-Matsushigue, J. L. M. Duarte, W. G. P. Engel, and J. C. de Abreu, Rev. Bras. Aplicações Vácuo **10**, 87 (1991).

[11] J. K. Tuli, Nucl. Data Sheets **66**, 1 (1992).

[12] T. W. Burrows, Nucl. Data Sheets **68**, 635 (1993).

[13] C. M. Perey and F. G. Perey, At. Data Nucl. Data Tables **17**, 1 (1976).

[14] P. D. Kunz, computer code DWUCK4 version, Colorado University, 1974 (private communication).

[15] G. M. Ukita *et al.* (unpublished).

[16] J. L. M. Duarte *et al.* (unpublished).

[17] D. Cline, Annu. Rev. Nucl. Part. Sci. **36**, 683 (1986); D. Cline and P. M. S. Lesser, Nucl. Instrum. Methods **82**, 291 (1970); T. Czosnyka, D. Cline, L. Hasselgren, C. Y. Wu, R. M. Diamond, H. Kluge, C. Roulet, E. K. Hulet, R. W. Lougheed, and C. Baktash, Nucl. Phys. **A458**, 123 (1986).

[18] M. Lampton, B. Margon, and S. Bowyer, Astrophys. J. **208**, 177 (1976).

[19] A. Stuart, J. K. Ord, and M. Kendall, *Advanced Theory of Statistics* (Griffin, London, 1987).

[20] L. R. B. Elton, *Nuclear Sizes* (Oxford University Press, New York, 1961).

[21] R. Barret and D. F. Jackson, *Nuclear Sizes and Structure* (Claredon, Oxford, 1979).

[22] H. de Vries, C. W. de Jager, and C. de Vries, At. Data Nucl. Data Tables **36**, 495 (1987).

[23] H. S. Chung and W. D. Myers, Nucl. Phys. **A451**, 283 (1990).

Anexo 2.5

5_1^- excitations in the $40 \leqslant Z \leqslant 50$ region

L. B. Horodynski-Matsushigue, G. M. Ukita, T. Borello-Lewin, and J. L. M. Duarte
Instituto de Física da Universidade de São Paulo, Caixa Postal 66318, 05315-970 São Paulo, São Paulo, Brazil
(Received 24 February 1999; published 9 September 1999)

Triggered by experimental evidence formerly obtained for Zr and Mo isotopes, a survey of the literature in the $A \sim 100$ region was undertaken and revealed that 5_1^- states exist in even-even nuclei throughout the $40 \leqslant Z \leqslant 50$ region. They appear at an almost constant excitation energy of (2.4 ± 0.2) MeV and have, where studied in inelastic scattering, characteristics of one-step collective excitations. Angular distributions for ^{94,98}Mo(d,d') are presented for states at 2.611 MeV in ^{94}Mo and 2.622 MeV in ^{98}Mo and β_5 values were extracted. The β_5 value for ^{94}Mo is new in the literature and was obtained consistently for two incident energies. The β_5 value for ^{98}Mo is higher than a former result, where a two-phonon interpretation was considered. [S0556-2813(99)01810-5]

PACS number(s): 21.10.Re, 24.50.+g, 27.60.+j

Historically, the experimental uncovering of collective features has given rise to fruitfull interpretations of nuclear structure [1]. Thus, quadrupolar and octupolar excitations present, along the periodic table, certain common characteristics which have been taken as descriptive of a class of nucleon motions, which have, by now, accepted theoretical interpretations [1]. The authors of the present Brief Report have extensively worked on Zr, Mo, and Ru isotopes [2–6] and a singular pattern of $L=5$ excitations, in inelastic scattering, came to their attention. Extending the survey throughout the $Z=40-50$ region, it was observed that, in every isotope chain with even Z, first excited 5^- states with a rather distinct behavior exist. This survey employed as data base always the most recent Nuclear Data Sheets (NDS) compilations, unless otherwise stated. The 5_1^- levels appear, in this mass region, in the even-even nuclei at an almost constant excitation energy $E_{exc}=(2.4 \pm 0.2)$ MeV. Where observed in inelastic scattering, those levels show excitation characteristics which can most easily be interpreted if they are considered as collective excitations, corresponding then to several Weisskopf units. In fact, these 5_1^- states are normally characterized in inelastic scattering through angular distributions with features of a direct $L=5$ transfer. As the NDS compilations show, most 5_1^- states are excited through many different reactions, as are the 2_1^+ and 3_1^- states, in particular also in one-proton transfer, in one and two neutron transfers, in α transfer, and in several fusion reactions, demonstrating the complexity of their wave functions, in terms of their microscopic structure. Furthermore, they also may survive in neighboring odd nuclei, giving rise to a multiplet of levels with weak-coupling characteristics, as was shown at least in ^{91}Zr [2].

Figure 1 displays the regularity of the 5_1^- states in the $40 \leqslant Z \leqslant 50$ region, while Figs. 2(a) and 2(b) show the known characteristics of the 2_1^+ and 3_1^- states in the same region. The values of the excitation energy of the 2_1^+ levels reflect, in particular, the abrupt shape transition of the Zr nuclei between $A=98$ and $A=100$ and the semi-magic behavior of ^{90}Zr, ^{96}Zr, and the Sn isotopes. In contrast, Fig. 1 shows that, even for ^{90}Zr, as well as ^{100}Zr, the 5_1^- remains rather constant. Only the Zr isotopes with $N=56$, 58, and, to a lesser extent, also those of Mo with the same A, have 5_1^- which lie above the 2.6 MeV line, as also do the three lightest Sn isotopes, which correspond to $N=60-64$. Thus, of 39 levels with $J^\pi=5^-$ (only nine of them with doubtful spin

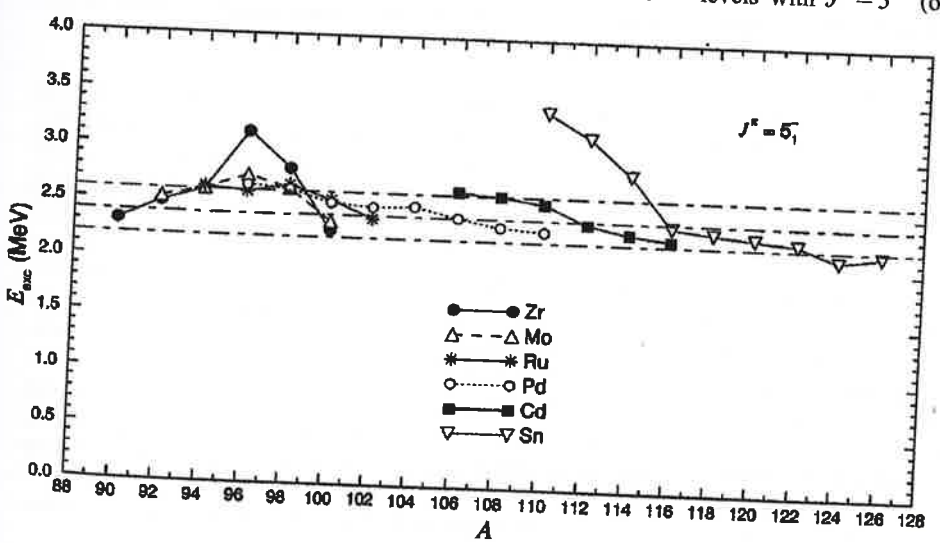

FIG. 1. Systematics of 5_1^- levels as reported by Nuclear Data Sheets (levels with doubtful spin attributions, in ^{98,100}Zr, ^{100}Mo, ^{94,98}Ru, ^{98,100,106}Pd, and ^{114}Cd, are also included). The (2.4 ± 0.2) MeV interval is indicated through dash-dotted lines.

0556-2813/99/60(4)/047301(4)/$15.00

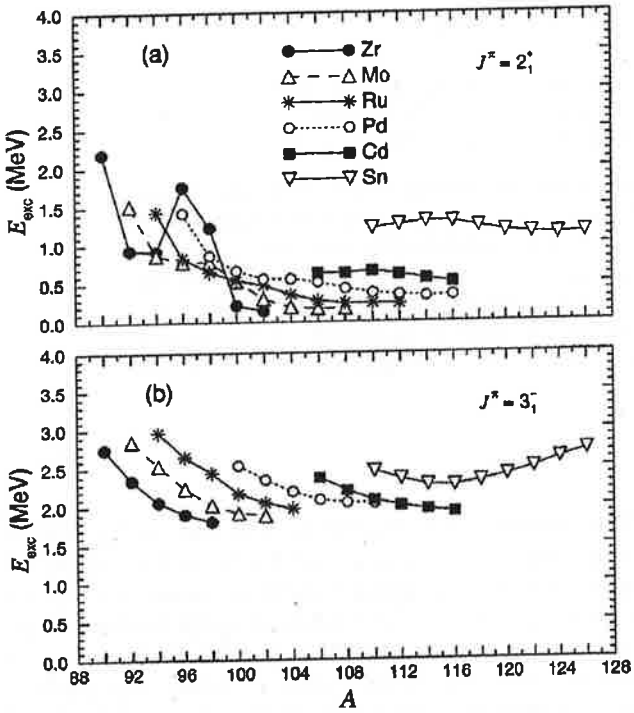

FIG. 2. (a) Systematics of 2_1^+ levels as reported by Nuclear Data Sheets. (b) Systematics of 3_1^- levels (levels with doubtful spin attributions, in ^{96}Ru and ^{100}Pd, are also included).

attribution, fitting, however, nicely into the trend), not more than five lie clearly above $E_{exc}=2.6$ MeV. This constancy (see Fig. 1) is remarkable, also in view of the 3_1^- systematics [see Fig. 2(b)], showing a behavior which is rather unaffected by the filling of the valence orbitals, being thus indicative of effects which are usually taken as "collective," involving more than one major shell.

The difference between the sum of the excitation energies of the 2_1^+ and 3_1^- states (which, in the harmonic vibrational model for both, should be the energy centroid of the corresponding two-phonon states) and the here cited 5_1^- levels is always positive, being largest for the light Zr, Mo, Ru, and for the heaviest Sn isotopes. For the $N=50$ isotones the 5_1^- states lie in fact below the proper 3_1^- ones and the sum exceeds the excitation energy of those by ≥ 2 MeV. The six heaviest Sn isotopes (116–126) also present sums which are ~ 1.5 MeV above the 5_1^- levels. Taken globally, the features seem to exclude one of the possible interpretations for the 5_1^- states, which considers them simply to be built through the coupling of the lowest quadrupolar and octupolar excitations. Unfortunately, up to now, there is not much detailed information available for these states. However, where analyzed as two-step excitations in inelastic scattering, the fit to the angular distributions of the 5_1^- states requires an important direct contribution to reproduce the experimental shape [7]. This is also true in other mass regions, as shown by Cottle *et al.* [8] for ^{146,148}Nd and ^{148}Sm. If analyzed as direct excitation, a value of the order of $\beta_5 \simeq 0.05$ turns out for several 5_1^- levels, but not many angular distributions were presented.

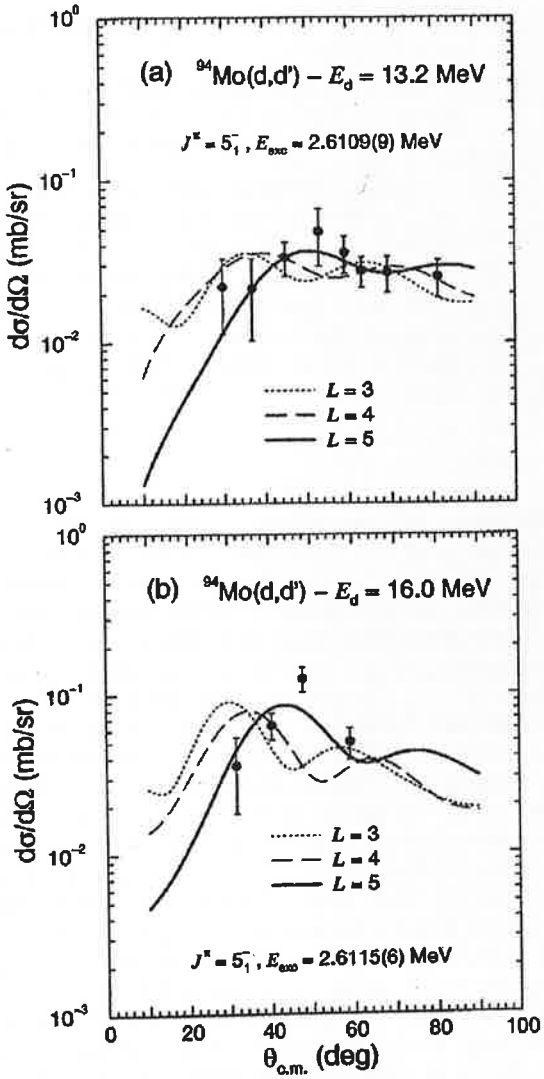

FIG. 3. Angular distributions for the 5_1^- state of ^{94}Mo at (a) $E_d=13.2$ MeV [$\beta_5=0.044(2)$] and (b) $E_d=16.0$ MeV [$\beta_5=0.048(3)$]. The solid curves represent cross sections calculated using DWBA, within a deformed optical model description, in one-step analyses. The uncertainties quoted are of statistical nature only.

Another description, found in the literature, in particular near closed shells, is to take a simple shell model interpretation for the 5_1^- states, involving protons in the $\pi 1g_{9/2}$ and $\pi 2p_{1/2}$ orbitals [9,10]. Such a component probably exists in most levels, since some of them (^{90}Zr, ^{94}Mo, ^{108,110,114}Cd) were shown to be populated through $l=4$ or $l=1$ one proton transfer from the $\frac{1}{2}^-$ or $\frac{9}{2}^+$ g.s. in odd proton neighbors. However, the rather strong excitation of the 5_1^- states through other reactions, in particular neutron tranfers, demonstrates that it does not exhaust the complete wave function. In fact, the 5_1^- states were almost always revealed through two-neutron transfer, inelastic scattering, and/or (HI, $xn\gamma$), which characterizes a greater complexity of their structure.

In our recent research work, which focused on the collec-

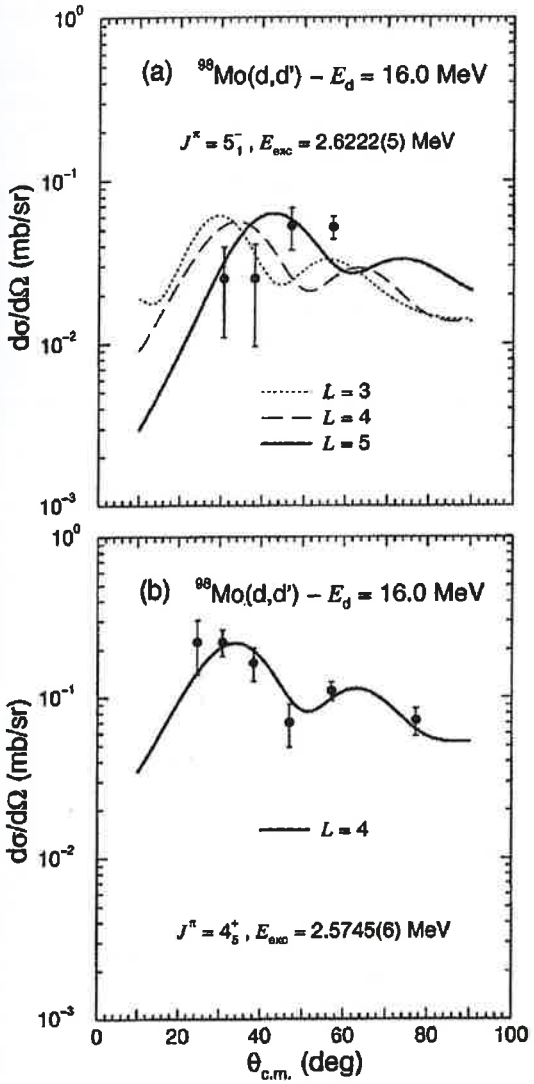

FIG. 4. Angular distributions at 16.0 MeV incident deuteron energy for (a) ^{98}Mo(5_1^-) and (b) ^{98}Mo(4_5^+). The values $\beta_5 = 0.040(3)$ and $\beta_4 = 0.061(3)$ are obtained in the one-step DWBA analyses. The uncertainties quoted are of statistical nature only.

tive characteristics of the 2_1^+ and 3_1^- excitations in ^{94,98}Mo [4,5], the 5_1^- states were observed in both isotopes, respectively at 2.6113(5) (^{94}Mo) and 2.6222(5) MeV (^{98}Mo), where the here quoted uncertainties are of statistical nature only. The measurements were made at the São Paulo Pelletron-Enge spectrograph facility [4], through the inelastic scattering of deuterons, with a detection limit of about 10 μb/sr in the excitation energy region of interest. For ^{94}Mo, data were taken at two incident energies and give consistent results. The energy resolution corresponds to 12 keV for 16.0 MeV of incident deuteron energy, for both isotopes, and to 8 keV at 13.2 MeV. Figures 3 and 4 show the experimental angular distributions, also in comparison with a nearby 4^+ level [11] seen in ^{98}Mo. Although hampered by the relatively low cross sections, the angular distributions discriminate $L = 5$ against lower L values, the corresponding χ^2 value being in all cases lower by a factor of ~ 2.

The energies obtained in this work for the 5_1^- states of ^{94,98}Mo, employing the known [12] calibration of the spectrograph and taking the respective 3_1^- levels as references, are in excellent agreement with the energies presented by the NDS compilations [13,14] for levels quoted as $(5)^-$ and (5^-). The uncertainties stated in the present work, for both, the excitation energies and the β_5 values, reflect only known statistical fluctuations. For the energies, an additional calibration uncertainty of ≤ 2 keV should be considered [12]. The β_5 values are affected by systematic uncertainties which are difficult to specify [15], but are estimated to be $\leq 20\%$.

The β_5 value extracted for ^{94}Mo is totally new in the literature. For ^{94}Mo only an old (p,p') study [16], with FWHM of 50 keV, exists, which saw a multiplet, at a somewhat lower energy, with $\beta_L = 0.07$. Pignanelli *et al.* [7] studied, in ^{98}Mo, $L = 3$ excitations and, as a by-product, also $L = 5$ ones (with a detection limit similar to the present work), but report a lower β_5 value for the 5_1^- state, since they used a predominant $2_1^+ \otimes 3_1^-$ interpretation on the angular distribution. No reanalysis is possible, since no angular distribution is presented in Ref. [7].

Both, the energy values of these 5_1^- states, as well as the deformation parameters extracted in the present work, for ^{94,98}Mo, fit into the systematics of the region. In conclusion, the 5_1^- levels, whose excitation energy and, where known, excitation characteristics were compiled for the whole of the $40 \leq Z \leq 50$ region, present systematic features which seem to indicate collectivity of the excitation, which is not explained through a pure two-step mechanism, pointing thus to a duotriacontapolar character.

Financial support by CNPq (Conselho Nacional de Desenvolvimento Científico e Tecnológico), CAPES (Coordenação do Aperfeiçoamento de Pessoal de Nível Superior), FINEP (Financiadora de Estudos e Projetos), and FAPESP (Fundação de Amparo à Pesquisa do Estado de São Paulo) is gratefully acknowledged.

[1] A. Bohr and B. R. Mottelson, *Nuclear Structure* (Benjamin, New York, 1975).
[2] L. B. Horodynski-Matsushigue, T. Borello-Lewin, and O. Dietzsch, Phys. Rev. C **33**, 1594 (1986).
[3] L. B. Horodynski-Matsushigue, T. Borello-Lewin, and J. L. M. Duarte, *XVI Reunião de Trabalho em Física Nuclear no Brasil*, Serra Negra, 1993 (unpublished), p. 61; *Proceedings of the International Nuclear Physics Conference*, São Paulo, Brasil, 1989 (unpublished), Vol. I, p. 307.
[4] J. L. M. Duarte, G. M. Ukita, T. Borello-Lewin, L. B.

Horodynski-Matsushigue, and L. C. Gomes, Phys. Rev. C **56**, 1855 (1997).

[5] G. M. Ukita, Ph.D. thesis, Universidade de São Paulo, 1998; G. M. Ukita, T. Borello-Lewin, L. B. Horodynski-Matsushigue, J. L. M. Duarte, and L. C. Gomes (unpublished).

[6] L. C. Gomes, Ph.D. thesis, Universidade de São Paulo, 1993; L. C. Gomes, L. B. Horodynski-Matsushigue, T. Borello-Lewin, J. L. M. Duarte, J. H. Hirata, S. Salém-Vasconcelos, and O. Dietzsch, Phys. Rev. C **54**, 2296 (1996).

[7] M. Pignanelli, N. Blasi, S. Micheletti, R. De Leo, M. A. Hofstee, J. M. Schippers, S. Y. Van Der Werf, and M. H. Harakeh, Nucl. Phys. **A519**, 567 (1990).

[8] P. D. Cottle, K. W. Kemper, and M. A. Kennedy, Phys. Rev. C **47**, 1048 (1993).

[9] M. R. Cates, J. B. Ball, and E. Newman, Phys. Rev. **187**, 1682 (1969).

[10] B. F. Bayman, A. S. Reiner, and R. K. Sheline, Phys. Rev. **115**, 1627 (1959).

[11] M. Pignanelli, N. Blasi, S. Micheletti, R. De Leo, L. LaGamba, R. Perrino, J. A. Bordewijk, M. A. Hofstee, J. M. Schippers, S. Y. van der Werf, J. Wesseling, and M. H. Harakeh, Nucl. Phys. **A540**, 27 (1992).

[12] M. D. L. Barbosa, T. Borello-Lewin, L. B. Horodynski-Matsushigue, J. L. M. Duarte, G. M. Ukita, and L. C. Gomes, Phys. Rev. C **58**, 2689 (1998).

[13] J. K. Tuli, Nucl. Data Sheets **66**, 1 (1992).

[14] B. Singh, Nucl. Data Sheets **84**, 565 (1998).

[15] G. R. Satchler, *Direct Nuclear Reactions* (Claredon, Oxford, 1983).

[16] H. F. Lutz, D. W. Heikkinen, and W. Bartolini, Phys. Rev. C **4**, 934 (1971).

Anexo 2.6

Coulomb-nuclear interference with deuterons: Isospin character of the 2_1^+ and 3_1^- excitations in ^{94,98}Mo

G. M. Ukita,[1,2] T. Borello-Lewin,[1] L. B. Horodynski-Matsushigue,[1] J. L. M. Duarte,[1] and L. C. Gomes[1]
[1]*Instituto de Física, Universidade de São Paulo, C.P. 66318, 05315-970 São Paulo, SP, Brazil*
[2]*Faculdade de Psicologia, Universidade de Santo Amaro, Rua Professor Enéas de Siqueira Neto, 340, 04829-300 São Paulo, SP, Brazil*
(Received 27 November 2000; published 19 June 2001)

Angular distributions of inelastic-scattering cross sections were measured for deuterons of 13.2 and 16.0 MeV, exciting the 2_1^+ and 3_1^- states of ^{94}Mo and ^{98}Mo. The analysis of the Coulomb-nuclear interference patterns displayed by these angular distributions was favored by the quality of the data obtained with the S. Paulo Pelletron-Enge-Spectrograph facility. The distorted-wave Born approximation–deformed-optical-model analysis with global parameters yielded values for the ratio $C_L = \delta_L^C/\delta_L^N$ and for δ_L^N (where δ_L^C and δ_L^N are, respectively, the charge and isoscalar deformation lengths), which inform the reader about the isospin character of the excitations. A reduced isoscalar transition probability, $B(ISL)$, was defined, in analogy to $B(EL)$, the ratio $B(EL)/B(ISL)$ being proportional to the square of C_L. The latter quantity is, however, experimentally better determined. The results obtained for C_2, C_3, δ_2^N, and δ_3^N at the two incident energies, 13.2 and 16.0 MeV, are consistent for each ^{94}Mo and ^{98}Mo. The values of C_L reveal a slight predominance of the protons in the quadrupolar transitions, in both ^{94}Mo and ^{98}Mo. The 2_1^+ and the 3_1^- states are more collective in ^{98}Mo than in ^{94}Mo, both with respect to the protons (charge) and with respect to protons and neutrons (mass).

DOI: 10.1103/PhysRevC.64.014316 PACS number(s): 21.10.Re, 25.45.De, 27.60.+j

I. INTRODUCTION

The Mo isotopes are of special interest for a comparative study of the collective properties of low-lying excitations, as they are neighbors, just one proton pair above the challenging $_{40}$Zr chain, where extremely rapid modifications occur as neutrons are added to the semimagic ^{90}Zr nucleus or, with still more dramatic consequences, to ^{96}Zr [1,2]. Indeed, if characterized, as usual, by the excitation energy E_{exc} and by the reduced electric transition probability $B(E2)$ to the first quadrupolar excitation, ^{90}Zr behaves almost like a doubly magic nucleus. The neighbors ^{92,94}Zr present intermediate values for these structure characteristics, but in ^{96}Zr, both $Z=40$ and $N=56$, seem well-closed subshells. This pattern is suddenly disrupted and ^{100}Zr presents several features of a well-deformed shape, such as a very low $E_{exc}(2_1^+)$ and a high $B(E2)$. Each isotopic chain in this region, up to $_{46}$Pd, shows some kind of transition around $N=56$ being washed out as Z is increased. The addition of neutrons, above this critical value, seemingly polarizes the proton distribution, enhancing the collectivity, which is taken as prolate deformed for the heavier Zr nuclei [2,3], γ soft, or even triaxial for Ru or Pd [3–5].

The characteristics of the first excited 2^+ states have, for a long time, been extensively used as nuclear structure indicators in comparison between experiment and model expectations, but they are usually inferred through $B(E2)$ values, which, in principle, are related only to the charge contributions to the excitation. Since it is clear that neutrons play, in this part of the nuclear chart, a primordial role in defining the collective behavior, it is important to assess also the reduced isoscalar transition probability $B(IS2)$. This is conveniently done through the study of inelastic scattering of isoscalarly interacting projectiles with incident energies such as to enhance Coulomb-nuclear interference [6], which allows for the simultaneous extraction of $B(ISL)$ and $B(EL)$ values for those excitations for which a predominant multipolarity L can be defined.

This paper presents a study of Coulomb-nuclear interference (CNI) in the inelastic scattering of deuterons on ^{94}Mo, an isotone of ^{92}Zr, and also on ^{98}Mo, which is an isotone of both ^{96}Zr and ^{100}Ru, for which quite different isospin characteristics of the low-lying quadrupolar excitations have been previously verified [7,8]. Coulomb-nuclear interference results have, to our knowledge, not been formerly reported for deuterons, due to experimental difficulties associated with the beam, in spite of this projectile being, in principle, a convenient choice for these studies. In fact, the huge amount of experimental information collected for deuteron reactions contributes to the pinning down of the parameters needed to phenomenologically describe the interaction of this projectile with the nuclei of interest. Therefore, the use of deuterons helps to keep the free parameters in the analysis under control, which is especially important if comparative conclusions, in the study of several isotopic chains, are to be drawn.

In the present work, besides analyzing the transitions to the 2_1^+ states in ^{94,98}Mo, $B(IS3)$ and $B(E3)$ values for the first octupolar excitations could also be extracted, since their angular distributions showed enough of the interference pattern to discriminate a value for their ratio, although with much lower precision.

II. EXPERIMENTAL PROCEDURE

For deuterons of some 10 to 20 MeV on medium mass nuclei, the interference minimum between the Coulomb and nuclear excitations appears at relatively forward angles. Detection techniques employing nuclear emulsions at the focal surface of the Enge spectrograph, in association with the excellent beam profile and energy characteristics provided by the São Paulo Pelletron facility, are, therefore, important

TABLE I. Isotopic composition of the molibdenum targets (Oak Ridge Separated Isotopes Division).

	Abundance (%)						
Target	^{92}Mo	^{94}Mo	^{95}Mo	^{96}Mo	^{97}Mo	^{98}Mo	^{100}Mo
^{94}Mo	0.87	93.90	2.85	1.04	0.40	0.75	0.22
^{98}Mo	0.32	0.22	0.45	0.59	0.69	97.18	0.55

means for obtaining the necessary quality of the data for these CNI studies. Additional care must be applied to the focusing conditions. Current intensity ratios of 1:30 and 1:100, in comparison between slits and beam, were achieved in the present experiment, respectively, on the defining slits before the target (1.0×2.0 mm^2) and on a circular slit of $\phi\sim6$ mm (situated approximately half a meter upstream). The deuteron beams of 13.2 MeV, or alternatively 16.0 MeV, impinged on uniform and thin (~30 μg/cm^2) enriched targets of ^{94}Mo or ^{98}Mo. Targets were made by a well-controlled electron bombardment evaporation technique [9] of metallic Mo (^{94}Mo targets) and MoO_3 (^{98}Mo targets), both in powder form, onto thin carbon backings (~10 μg/cm^2). Table I presents the isotopic composition of the material employed in the fabrication of the targets. The scattered deuterons were momentum analyzed by the S. Paulo Enge split-pole spectrograph and detected in nuclear emulsion (in the present study, Ilford G5 or equivalent, 50 μm thick). Aluminum foils, thick enough to absorb heavier reaction products, covered the emulsion. The use of nuclear emulsion enormously reduces the background associated with deuteron beams, since these detectors do not respond to the abundant neutron, γ, and x ray radiations that are produced, in particular, in the presence of the iron core of the spectrograph. In fact, the background observed in the spectra is mostly due to the tail of the elastic peak and is therefore extremely dependent on beam focusing.

In the present work, inelastic-scattering spectra were measured, for both isotopes, at 18 scattering angles from $\theta_{lab}=12.5°$ to 80° for the incident energy of 13.2 MeV and at eight angles between $\theta_{lab}=14°$ and 76° for 16.0 MeV. The solid angle of admittance to the spectrograph was maintained fixed, corresponding to $\Delta\theta_{lab}=\pm1.9°$. The emulsion plates were scanned, after processing, in strips of 200 μm across the plates and energy resolutions of ~8 and ~12 keV, full width at half maximum (FWHM), were achieved, respectively, in the spectra corresponding to 13.2 and 16.0 MeV incident energies.

Typical examples of the complete spectra of inelastic deuteron scattering obtained with the emulsion technique, on ^{94}Mo at $\theta_{lab}=58°$ and on ^{98}Mo at $\theta_{lab}=60°$, both for the incident energy of 13.2 MeV, are presented in Fig. 1. To illustrate the quality of the data, Fig. 2 shows part of four further spectra, displaying the peak associated with the first quadrupolar excitation in ^{98}Mo at 13.2 and 16.0 MeV incident energies. Figure 3, in a similar way, shows examples of the relevant part of the spectra for the octupolar excitation, observed for the same isotope at 16.0 MeV. As put into evidence by the spectra at forward angles, the good energy resolution of ~8 keV is essential to enhance the peak with respect to the background. This background, mainly associated with the elastic tail, drops with increasing scattering angle, as can be seen in the spectra at $\theta_{lab}=16°$ and $\theta_{lab}=26°$ [Figs. 2(a) and 2(b)]. Figure 2(d) also illustrates the judicious choice of the scattering angles, made to avoid that the peak of interest be hidden by the broad peaks associated with the presence of known contaminants in the target (which are, in general, not focused).

For the relative normalization of the spectra, the total number of incident deuterons was determined by a current integrator, which measured the charge collected in a Faraday cup (with electron suppression), while the direction of the beam was continuously monitored. Absolute normalization of the cross sections was referred to optical-model predictions for elastic-scattering of deuterons on the same target,

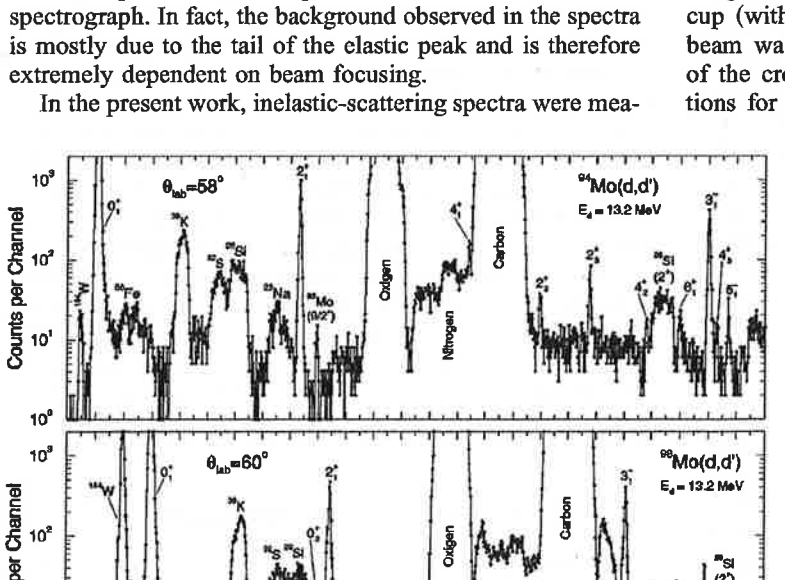

FIG. 1. Examples of spectra of ^{94}Mo(d,d') and ^{98}Mo(d,d') at 13.2 MeV, taken, respectively, at $\theta_{lab}=58°$ and $\theta_{lab}=60°$.

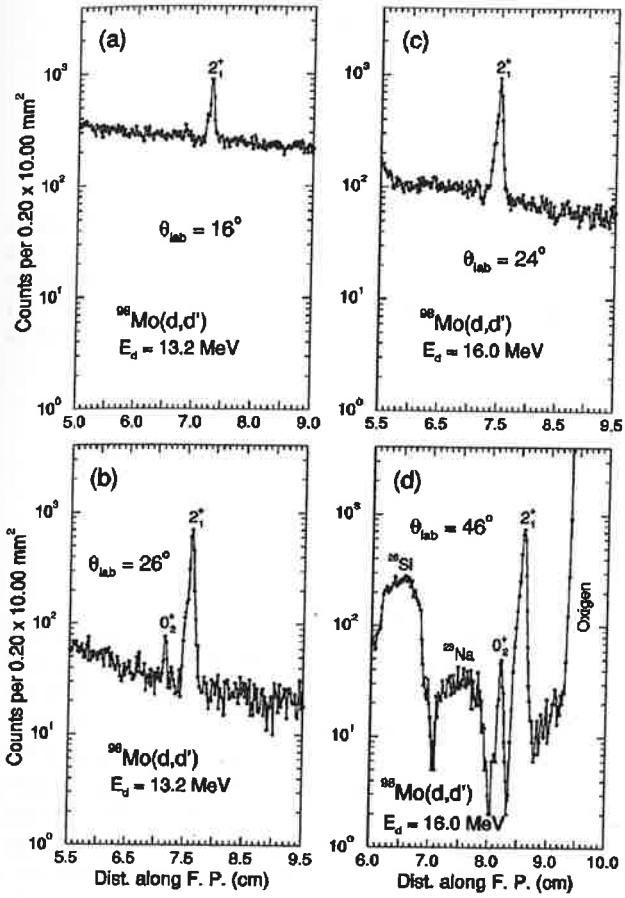

FIG. 2. Portions of the spectra of ^{98}Mo(d,d') for the 2_1^+ state, taken at 13.2 MeV, for (a) $\theta_{lab}=16°$ and (b) $\theta_{lab}=26°$, and at 16.0 MeV, for (c) $\theta_{lab}=24°$ and (d) $\theta_{lab}=46°$. Observe the very compressed log scale for the y coordinate.

measured under similar conditions. Figure 4 displays the elastic-scattering angular distributions for ^{94,98}Mo, measured at 13.2 and 16.0 MeV, in comparison with the optical-model predictions. The parameters of the systematics of Perey and Perey for deuterons [10] are employed in the normalization (see Table II). A maximum scale change of ~3% would be produced if the global optical-model predictions of Daehnick *et al.* [11], were taken. Due, furthermore, to target nonuniformity, plate scanning, and statistics in the elastic data, a maximum uncertainty of $\sim\pm5\%$, for 13.2 MeV incident energy measurements, and $\sim\pm7\%$, for 16.0 MeV, is estimated in the absolute cross section scale, for both isotopes.

III. ANALYSIS

Due to the relatively high excitation energies of the 2_1^+ states (871 keV for ^{94}Mo and 787 keV for ^{98}Mo) and not so high values of the deformation lengths, no appreciable coupling between ground and excited states has to be taken into acount in the reaction analysis. Thus, the well-established distorted-wave Born approximation (DWBA) could be employed. Incomplete information on the relevant aspects of the nuclear structure, beside the well-known difficulty to describe microscopically the imaginary part of the potential [12], point to the use of a macroscopic description of the excitation, in terms of what is usually called a deformed optical-model potential (DOMP), since the priority is on a comparative analysis throughout the region.

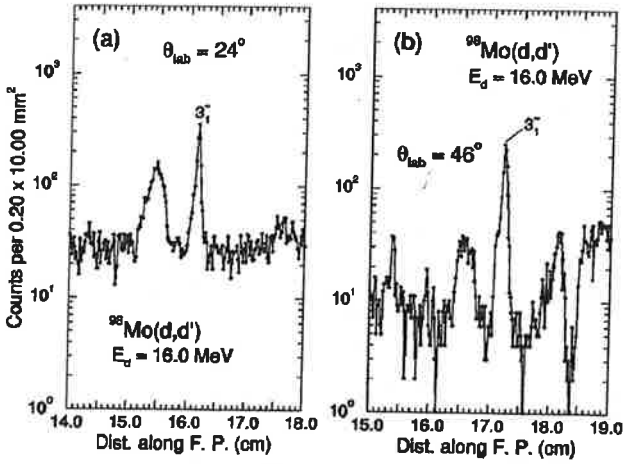

FIG. 3. Portions of the spectra of ^{98}Mo(d,d') for the 3_1^- state, taken at 16.0 MeV, for (a) $\theta_{lab}=24°$ and (b) $\theta_{lab}=46°$. Observe the very compressed log scale for the y coordinate.

In the DWBA-DOMP approach, the same phenomenological optical model describes both, the distorted waves in incident and exit channels and the transition potential to the collective state. The intensity of the excitation characterized by the deformation length extracted [12].

The DWBA-DOMP angular distributions were calculated by means of the code DWUCK4 [13], considering the influence of Coulomb excitation up to distances of 80 fm from the nuclear center. The macroscopic collective form factors [12], responsible, respectively, for the nuclear $F_L^N(r)$, and Coulomb $F_L^C(r)$ excitation processes, were taken as

$$F_L^N(r) = -\delta_{R,L}^N(U)\frac{dV(r)}{dr} - i\delta_{I,L}^N(U)\frac{dW_D(r)}{dr}, \qquad (1)$$

where V and W_D are the real and surface imaginary depths of the optical potential U, with the standard Woods-Saxon and derivative Woods-Saxon dependencies, with given geometrical parameters (r_R, a_R and r_I, a_I), and

$$F_L^C(r) = \begin{cases} \dfrac{4\pi Z_a e}{2L+1}[B(EL)]^{1/2}\dfrac{1}{r^{L+1}}, & \text{for } r \geq R_c \\ 0, & \text{for } r < R_c, \end{cases}$$

where $R_c = r_c A^{1/3}$ is the characteristic radius of the charge distribution. To take the Coulomb form factor as zero inside the charge distribution does not affect the results, since for the deuteron energies considered in this work, the reaction proceeds peripherically.

A charge deformation length $\delta_L^C = \beta_L^C R_c$, where β_L^C is the known deformation parameter [1], may be defined

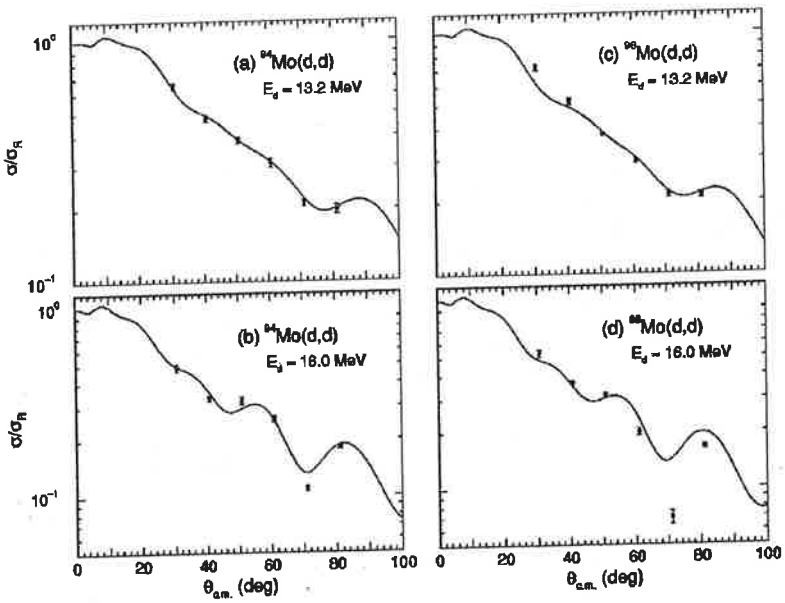

FIG. 4. Angular distributions for the elastic scattering of deuterons, in comparison with optical-model predictions [10]: (a) ^{94}Mo(d,d) at 13.2 MeV, (b) ^{94}Mo(d,d) at 16.0 MeV, (c) ^{98}Mo(d,d) at 13.2 MeV, and (d) ^{98}Mo(d,d) at 16.0 MeV.

$$\delta_L^C = \left(\frac{4\pi}{3ZR_c^{L-1}}\right)\frac{[B(EL)]^{1/2}}{e}. \tag{2}$$

The isoscalar deformation length $\delta_{R,L}^N(U) = \delta_{I,L}^N(U) = \delta_L^N$ may similarly be related to $B(ISL)$, through the following expression:

$$B(ISL) = (\delta_L^N)^2\left[\frac{3ZR_m^{L-1}}{4\pi}\right]^2, \tag{3}$$

where $R_m = r_m A^{1/3}$ is the characteristic radius of the mass distribution. Normalization to Z is preferred to the normalization to A employed by some authors [14].

For convenience of analysis, the parameters δ_L^N and $C_L = \delta_L^C/\delta_L^N$ were chosen to describe the collective excitations. Thus,

$$\frac{B(EL)}{B(ISL)} = e^2\left(\frac{\delta_L^C}{\delta_L^N}\right)^2\left[\frac{R_c^{L-1}}{R_m^{L-1}}\right]^2 = e^2C_L^2\left(\frac{r_c}{r_m}\right)^{2L-2}. \tag{4}$$

TABLE II. Global optical-model parameters for elastic deuteron scattering prescribed by Perey and Perey [10]. A Coulomb reduced radius of $r_c = 1.22$ fm was utilized.

A	E_d (MeV)	V (MeV)	r_R (fm)	a_R (fm)	W_D (MeV)	r_I (fm)	a_I (fm)
94	13.2	96.6	1.15	0.81	17.6	1.34	0.68
98	13.2	96.3	1.15	0.81	17.6	1.34	0.68
94	16.0	96.0	1.15	0.81	18.3	1.34	0.68
98	16.0	95.7	1.15	0.81	18.3	1.34	0.68

It is, therefore, seen that the parameter C_L contains the relevant information about the ratio of the charge (protons) with respect to the mass (protons + neutrons) contributions to the excitation of the particular state under observation. Grossly speaking, a value of $C_L = 1.0$ characterizes an excitation for which $B(EL)/e^2$ is, within the definition adopted, numerically equal to $B(ISL)$, implying that protons and neutrons contribute to it in the ratio of Z/N, that is an excitation usually referred to as being of homogeneous collective nature.

In the analysis, the distorted waves play an important role in defining the structures of the angular distributions. To make significant comparisons of CNI results, it is, therefore, convenient to maintain the optical-model parameters within a globally established systematics, as far as allowed by the data. The Perey and Perey [10] parameters (see Table II) have the best experimental basis in this deuteron energy region and have been adopted.

Inspection of Fig. 5, where DWBA-DOMP predictions are displayed for three values of incident deuteron energies, demonstrates the discriminative power of the CNI method, in the mass region of interest. The predicted angular distributions were calculated with global optical parameters taken from the systematics of Perey and Perey [10], for typical values of C_2 and δ_2^N, taking the ^{94}Mo$(0_1^+ \rightarrow 2_1^+)$ excitation as an example. It may be seen that an interference minimum develops for all incident energies: at $\theta_{c.m.} \sim 30°$ for $E_d = 10.0$ MeV and $\theta_{c.m.} \sim 15°$ for $E_d = 16.0$ MeV. On the other hand, the typical "diffractive" oscillations, due to the nuclear excitation, practically determine the shape of the angular distribution for the more backward angles. Therefore, good data around the interference minimum are essential for the extraction of C_2, while the larger angle data mostly give the global normalization constant $(\delta_2^N)^2$. At $E_d = 10.0$ MeV, discrimination of C_2 in the interval $0.8 \leq C_2 \leq 1.2$ depends on the possibility of taking data with very small statistical errors in the angular region $25° \leq \theta_{c.m.} \leq 35°$. It is clear that the incident energy region of about 13

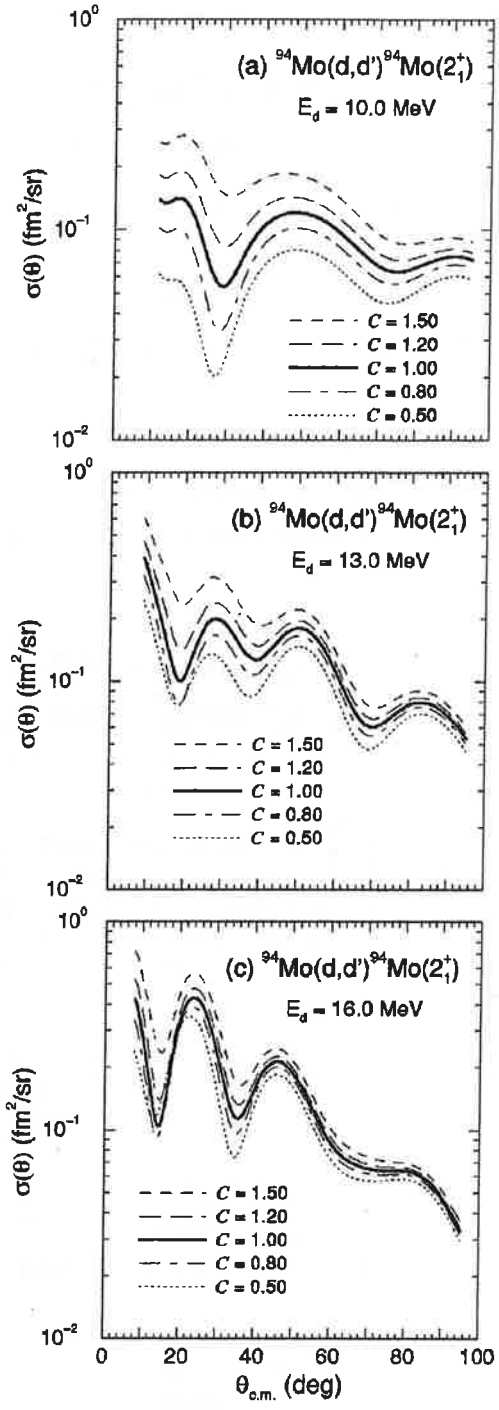

FIG. 5. DWBA-DOMP predictions for the quadrupolar excitation of ^{94}Mo(d,d'), for three incident deuteron energies and several values of $C=C_2=\delta_2^C/\delta_2^N$. A typical value of $\delta_2^N=0.8$ fm was employed.

MeV presents the best discrimination for the parameters of interest. In fact, it is for this incident energy region that the value of C_2, besides the minimum, also substantially affects the ratio of the heights of the two subsequent maxima of the angular distribution. The nonlinearity of the predictions as function of C_2 is also evident at $E_d=16.0$ MeV, with attention being called especially to the shape of the curves for the outmost values of $C_2=0.5$ and $C_2=1.5$, the former ones crossing those for $C_2=0.8$–1.2 near the interference minimum, rendering discrimination of C_2 much more difficult than at 13 MeV. To examine the consistency of the values extracted for the parameters of interest, it was decided to take detailed data at 13.2 MeV and complementary ones at 16.0 MeV.

If the relations

$$B(ISL)=\left|\frac{Z}{A}(\mathbf{M}_n+\mathbf{M}_p)\right|^2 \tag{5}$$

and

$$B(EL)=e^2|\mathbf{M}_p|^2, \tag{6}$$

consistent with the here adopted definition of $B(ISL)$, are employed, the assumption of proportionality of neutron and proton transition densities leads to the following equation for the multipolar moments of the neutron and proton distributions:

$$\frac{M_n}{M_p}=\left|\frac{\mathbf{M}_n}{\mathbf{M}_p}\right|=\frac{A}{Z}\left|\frac{B(ISL)}{B(EL)/e^2}\right|^{1/2}-1=\frac{A}{Z}\left(\frac{r_m}{r_c}\right)^{L-1}C_L^{-1}-1. \tag{7}$$

The experimentally well-determined parameter C_L informs, thus, about the isospin character of the excitation with multipolarity L.

A. Quadrupolar excitations

As previously discussed, the characterization of the CNI for the quadrupolar excitations is favored at the lower energy of 13.2 MeV, while the data at 16.0 MeV are mostly employed to check the consistency of the δ^N results. The DWBA-DOMP predictions, with global optical potential parameters, were fitted to the data [6] through the Gauss-Marquardt procedure, searching simultaneously on the values of three parameters, C_2, δ_2^N (13.2 MeV), and δ_2^N (16.0 MeV), which result in a minimum for χ^2. Thus, data at both energies were considered in the fit, constraining for the same value of C_2. The resulting fits to the angular distributions associated with the first 2^+ excitation in ^{94,98}Mo, at 13.2 and 16.0 MeV incident deuteron energies, are shown in Fig. 6. Solid lines refer to the results obtained if r_R and r_I are increased by 2% above the values of Table II. Also shown, as dashed lines, are the fits corresponding to the unmodified global parameters. The reduction of about a factor of 2 in the minimum χ^2 values of the simultaneous fit of the angular distributions, at the two incident energies for both isotopes, points possibly to a physical significance of the increased radii. In the inelastic scattering of deuterons, those nuclei seem, thus, to be represented by a somewhat larger object than in elastic scattering. The rather good stability of the resulting values (with and without the modification of the radii) for δ_2^N and C_2, for both isotopes, as may be appreci-

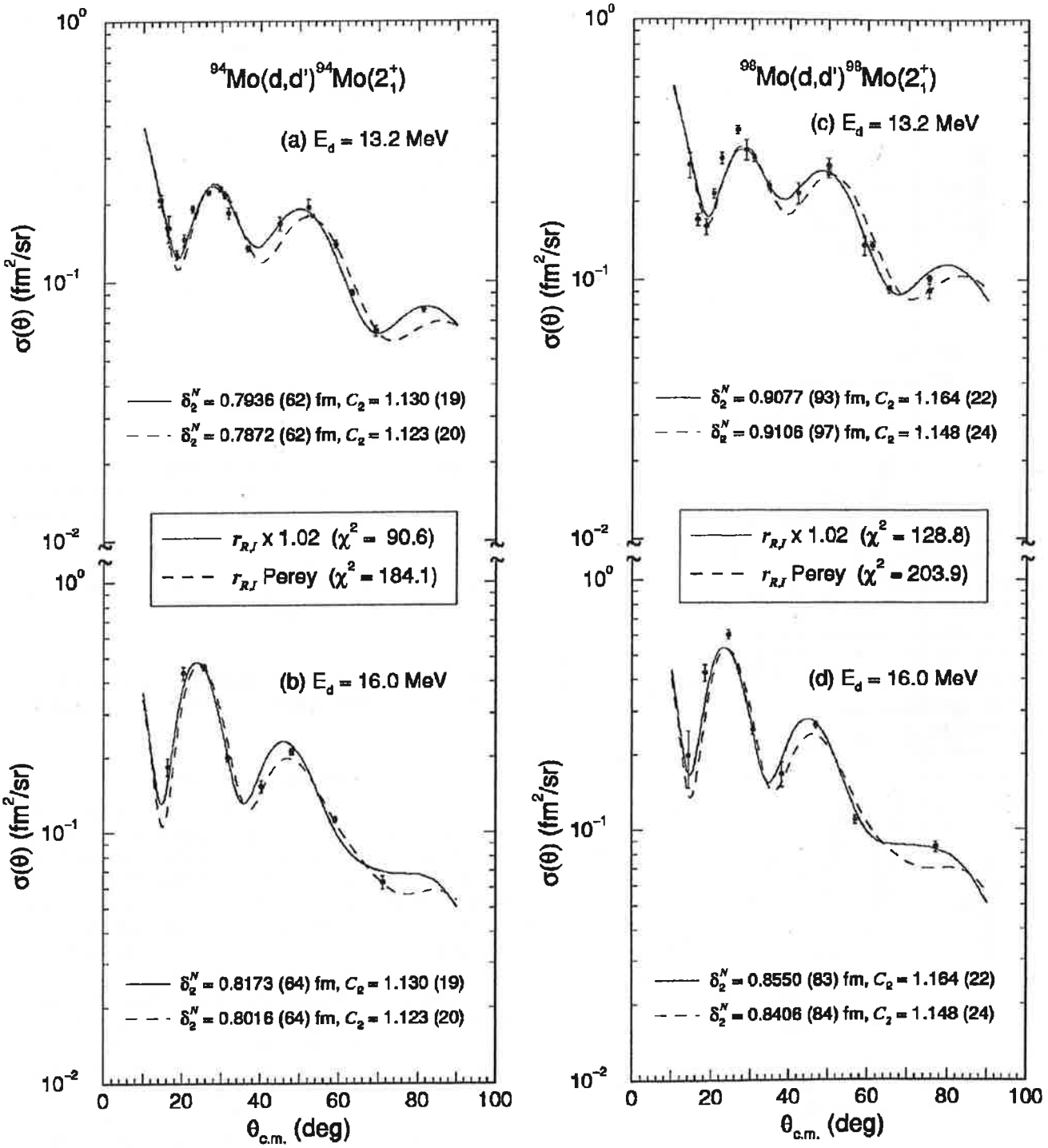

FIG. 6. Experimental angular distributions for the quadrupolar excitations in ^{94}Mo and ^{98}Mo, at two incident deuteron energies, in comparison with DWBA-DOMP best fits, for which the same value of C_2 was imposed. Solid lines correspond to the predictions for increased radii (+2%), while broken lines correspond to the predictions with the original Perey-Perey parameters. The χ^2 values characterize the quality of the constrained simultaneous fit to both angular distributions, for each isotope.

ated by comparing the values in the captions of Fig. 6, supports the confidence in the method of analysis employed here.

It is seen that for ^{94}Mo, the fit of the DWBA-DOMP predictions to the data reproduces the experimental shape very well, if the 2% increase of the real and imaginary radii is applied to the global optical parameters. On the other hand, the angular distributions for ^{98}Mo are, at both energies, somewhat more structured at the first maximum displayed than is predicted by the interpretation at hand. No possible

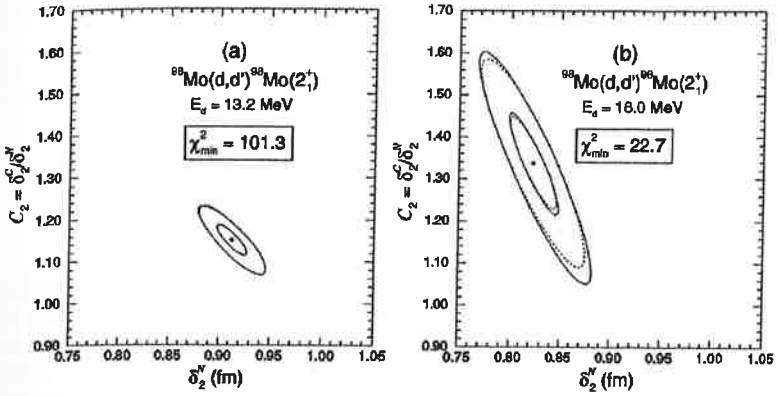

FIG. 7. Comparison of the contour lines for constant χ^2 (solid lines) with the ellipses, which result from the Gauss-Marquardt method (broken lines) for intervals corresponding to, respectively, 68.3% ($\Delta\chi^2=2.3$) and 99.7% ($\Delta\chi^2=11.8$), of statistical confidence, in the representation of individual fits to the ^{98}Mo(2_1^+) data at (a) 13.2 MeV and (b) 16.0 MeV.

variation of the parameters C_2 and δ_2^N contemplates this discrepancy, which probably contains physical information outside the proposed reaction model. This fact is illustrated through Fig. 7, which presents the constant χ^2 contour lines [6] corresponding to alternative individual (unconstrained) best fits to each, the angular distribution at 13.2 MeV and that at 16.0 MeV, for ^{98}Mo, where both C_2 and δ_2^N were allowed to vary, at each energy. The contour lines are approximately elliptical and, at 13.2 MeV, centered at about the same values of C_2 and δ_2^N, as formerly obtained in the constrained analysis. On the other hand, the results of an unconstrained analysis at 16.0 MeV show, as could be expected, C_2 to be rather poorly defined at this energy. Furthermore, since the value of C_2 affects δ_2^N in a covariant manner, this last value also wanders outside the regions defined by the better data at 13.2 MeV. It is, however, to be remembered that when comparison between the values of δ_2^N, extracted at both incident energies, is to be done, the scale uncertainties in the cross sections have to be included. The sum of the minimum χ^2 values obtained in the individual fits performed at the two energies, which equals 124.0, is only somewhat lower than that resulting from the constrained analysis and, even with the opportunity of varying the parameters freely, no fit to the discrepancy at the first maximum of either of the angular distributions was achieved.

B. Octupolar excitations

Due to their much reduced Coulomb excitation probability, the transition to the 3_1^- states is strongly dominated by the nuclear interaction. Nevertheless, as Fig. 8 reveals, at 13.2 MeV enough structure change remains at the forward angles of the predicted angular distribution to obtain some information on C_3. In Fig. 8 the separate contributions of the Coulomb and nuclear interactions to the excitation of the octupolar states are represented, respectively, as dotted and dashed lines, at both deuteron energies. For comparison, similar information is also presented for the quadrupolar excitations. In all instances, the most prominent change resulting from the inclusion of the Coulomb excitation is the development of an interference minimum at forward angles.

Constrained (same C_3) analyses of the first octupolar excitations in ^{94,98}Mo at 13.2 and 16.0 MeV incident deuteron energy were performed employing the same statistical analysis as for the quadrupolar ones. The results are shown in Fig. 9, again for increased radii (solid lines) and for the original global parameters (dashed lines). Data for the 3_1^- excitations are affected, for a considerable range of detection angles, $\theta_{lab} \geq 60°$, by the unavoidable presence of contaminant elastic peaks associated with carbon and oxygen (see Fig. 1).

The contour lines for constant χ^2, associated with the alternative unconstrained best fits at 13.2 MeV and at 16.0 MeV, are presented in Fig. 10, for the octupolar excitation in ^{94}Mo. It is clear that the data at 16.0 MeV are almost useless to define C_3. Since the contour lines are not ellipses, being, in fact, rather asymmetric with respect to χ^2_{min}, it is possible

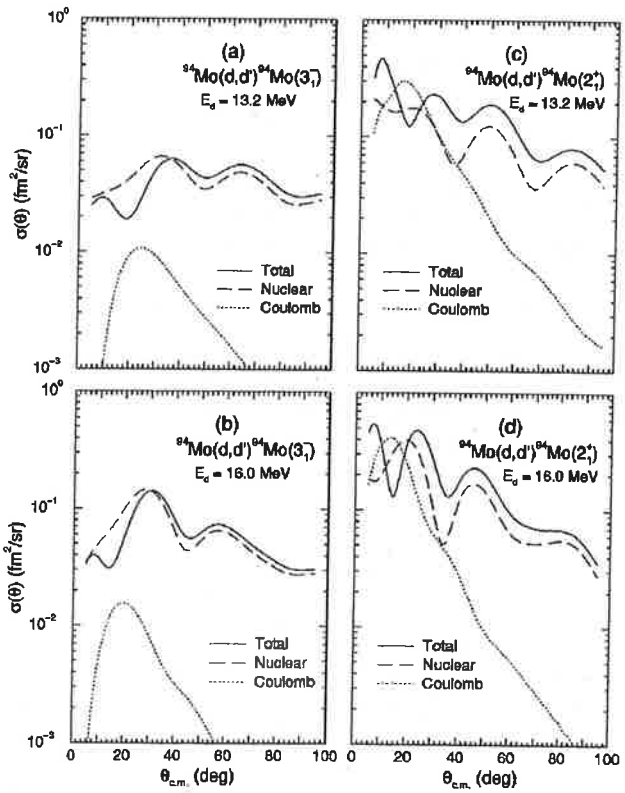

FIG. 8. The influence of Coulomb excitation on DWBA-DOMP predictions for the angular distributions in the excitation of, respectively, the 3_1^- state [(a) and (b)] and the 2_1^+ state [(c) and (d)], for both deuteron energies employed. The values for ^{94}Mo are taken as an example, but no essential difference is verified for ^{98}Mo.

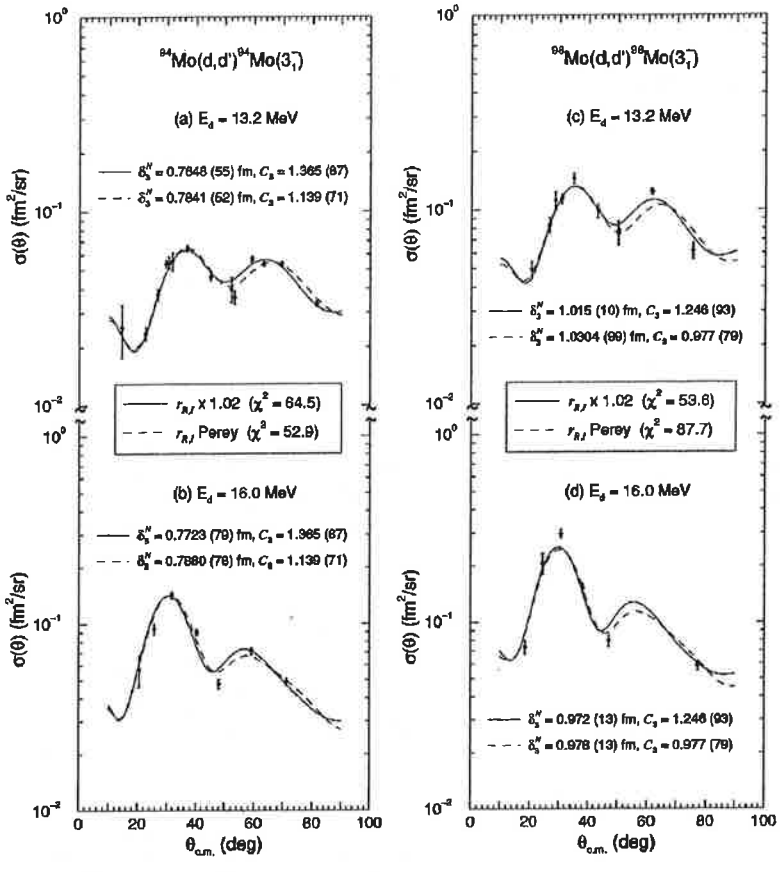

FIG. 9. Experimental angular distributions for the octupolar excitations in ^{94}Mo and ^{98}Mo, at two incident deuteron energies, in comparison with DWBA-DOMP best fits, for which the same value of C_3 was imposed. Solid lines correspond to the predictions for increased radii (+2%), while broken lines correspond to the predictions with the original Perey-Perey parameters. The χ^2 values characterize the quality of the constrained simultaneous fit to both angular distributions, for each isotope.

that C_3 is affected [6] by somewhat greater uncertainties than stated. Even so, as indicated in Fig. 9, the values obtained in the constrained analysis for the parameters δ_3^N and C_3, with and without the 2% increase in the radii, are almost compatible within the attributed uncertainties.

IV. DISCUSSION AND CONCLUSIONS

The results of the present experiment for the quadrupolar and octupolar excitations in ^{94,98}Mo, obtained within the adopted analysis (DWBA-DOMP with global optical parameters) are compiled in Table III. The values presented for δ_L^N are, for both isotopes, a weighted mean of the two informations, at 13.2 and 16.0 MeV, including the scale uncertainty in the cross sections of, respectively, $\pm 5\%$ and $\pm 7\%$. The ratios $B(EL)/B(ISL)$ are also presented in Table III. Values of $r_C = 1.22$ fm and $r_m = 1.16$ fm were employed for the reduced radii of the equivalent sharp cutoff uniform charge and, respectively, mass distributions [6]. An uncertainty of $\pm 5\%$ was associated with r_m in the ratios $B(EL)/B(ISL)$. The values extracted for M_n/M_p, in comparison with the values of N/Z, expected for a homogeneous collective excitation of the mass distributions, are also shown. It is, however, to be stressed, that the ratios M_n/M_p are affected, not only by rather important propagated experimental uncertainties [verify expression (7)], but also by uncertainties due to the underlying theoretical hypotheses, which are difficult to specify, but should preserve at least one significant figure.

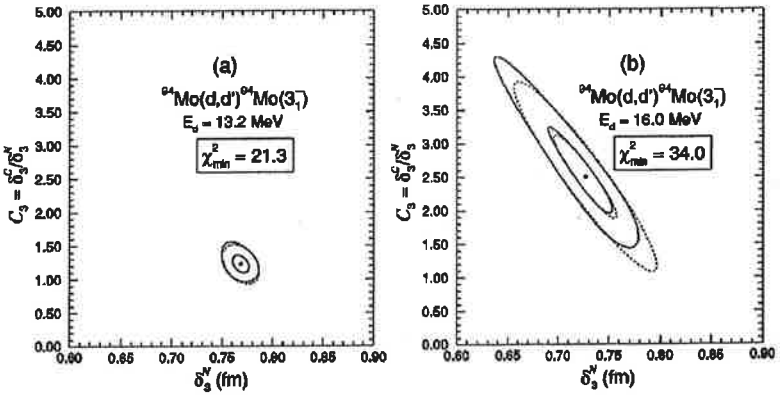

FIG. 10. Comparison of the contour lines for constant χ^2 (solid lines) with the ellipses that result from the Gauss-Marquardt method (broken lines) for intervals corresponding to, respectively, 68.3% ($\Delta\chi^2 = 2.3$) and 99.7% ($\Delta\chi^2 = 11.8$) of statistical confidence, in the representation of individual fits to the ^{94}Mo(3$_1^-$) data at (a) 13.2 MeV and (b) 16.0 MeV.

TABLE III. Parameters C_L and δ_L^N extracted in the present paper. Also indicated are the values of the ratios $B(EL)/B(ISL)$, M_n/M_p, and N/Z.

A	State	C_L	$\overline{\delta_L^N}$ (fm)	$\overline{\beta_L^N}$ [a]	$B(EL)/B(ISL)$ (e^2)	M_n/M_p	N/Z
94	2_1^+	1.123(20)	0.792 (17)	0.152 (3)	1.39(15)	0.89	1.24
98	2_1^+	1.148(24)	0.883 (19)	0.167 (4)	1.46(16)	0.93	1.33
94	3_1^-	1.14 (7)	0.785 (17)	0.150 (3)	1.6 (4)	0.8	1.24
98	3_1^-	0.98 (8)	1.011 (22)	0.191 (4)	1.2 (3)	1.2	1.33

[a] $\overline{\beta_L^N} = \overline{\delta_L^N}/1.15A^{1/3}$.

The uncertainties extracted through the statistical method of analysis employed [6], reflect (through a factor of about 4) the lower sensitivity of the data to the ratio C_3, in comparison with what is verified for C_2, while the deformation length δ_3^N is approximately as well determined as δ_2^N. The deformation parameters β_L^N calculated from the experimental mean values of δ_L^N, agree with β_L values formerly obtained in proton inelastic scattering [15,16] and in the 21.5 MeV deuteron inelastic experiment [17], both of which are influenced predominantly by the nuclear excitation. Incidentally, the experimental angular distributions of these older studies also indicate that a small increase in the radii of the optical potentials could provide a better fit to the inelastic results.

The values of $C_2 > 1.0$ and $C_3 \geq 1.0$, extracted in the present CNI studies for ^{94}Mo and ^{98}Mo, indicate that the protons contribute more than the neutrons to both the 2_1^+ and the 3_1^- excitations. The values $M_n/M_p \sim 0.9$ obtained for the quadrupolar excitations in ^{94}Mo and ^{98}Mo, being smaller than the $N/Z = 1.2$–1.3 expected from the homogeneous collective model, are another way to characterize the role played by the protons relative to the neutrons in these excitations.

The values $C_2 = 1.123(20)$ and $C_2 = 1.148(24)$ are about the same for ^{94}Mo and ^{98}Mo and, as a consequence, so are also the ratios $B(E2)/B(IS2)$. In a previous CNI study of inelastic scattering of alpha particles on ^{100,102,104}Ru [8], values of C_2 increasing from 1.04 to 1.22, had been found for that isotopic chain, demonstrating, also for Ru, a slight predominance of the protons. On the contrary, neutrons contribute more than protons to the first quadrupolar excitations in the isotones ^{92}Zr and ^{96}Zr. Values of M_n/M_p close to 2, for ^{92}Zr [7,18,19], and to 4, for ^{96}Zr [7,19], were reported in inelastic-scattering studies with alpha particles and ^{6}Li.

The evolution of the $B(ISL)$ and $B(EL)$ values between ^{94}Mo and ^{98}Mo, considering also the $B(EL)$ values adopted in the literature [1,20], may be examined through the ratios given in Table IV. These show the 2_1^+ excitation to be somewhat more collective in ^{98}Mo than in ^{94}Mo, for both mass and charge contributions. The parallel evolution of the $B(ISL)$ and the $B(EL)$ from ^{94}Mo to ^{98}Mo (compare values in columns 2 and 3 of Table IV, and note their compatibility) for the first collective 2^+ states, shows again that the isospin characteristics of these excitations do not change drastically, in contrast to what happens in the Zr isotopes. The agreement of the relative values of the $B(E2)$ with those resulting from the adopted ones [1] is good, although the absolute values determined in the present paper are higher, for both ^{94,98}Mo. It is to be noted that for $B(E2)$ the adopted values [1] are heavily based on the results of one laboratory; furthermore, for ^{94}Mo, there are several experimental results, spread over a considerable range. The octupolar excitation is also more collective in ^{98}Mo than in ^{94}Mo, the agreement with published $B(E3)$ values occuring within 2 standard deviations.

Summarizing, inelastic scattering of deuterons is presented as a convenient means of conveying information on the isospin character of collective excitations of low multipolarity, especially of the important 2_1^+ state, in the mass region of $A \sim 100$. For this purpose, the parameter $C_2 = \delta_2^C/\delta_2^N$ is defined (where the $\delta_2^{C,N}$ are the quadrupolar deformation lengths corresponding, respectively, to the charge and the mass excitations), as a measure of the relative contribution of protons (charge) and of protons plus neutrons (mass). The value of $C_2 = 1.0$ corresponds to the expectation of a homogeneous collective model. It is felt [6] that, when considering CNI results with a macroscopic description, C_2 is a better representation for any predominance of protons or neutrons in a particular 2_1^+ excitation than, for instance, M_n/M_p or either $B(E2)$ or $B(IS2)$ separately, since in the extraction of the C_L parameter, several systematic uncertainties of experimental and/or theoretical nature are cancelled. The values of C_2 may be directly translated into ratios of $B(E2)/B(IS2)$ and/or M_n/M_p, but the first ones are, additionally, affected by choices of reduced charge and mass

TABLE IV. Evolution of $B(ISL)$ and $B(EL)$ values between ^{94}Mo and ^{98}Mo.

	Present work		Literature
State	$B(ISL)_{(98)}/B(ISL)_{(94)}$	$B(EL)_{(98)}/B(EL)_{(94)}$	$B(EL)_{(98)}/B(EL)_{(94)}$
2_1^+	1.28 (8)	1.34 (8)	1.32(4)[a]
3_1^-	1.75(11)	1.29(26)	2.2 (5)[b]

[a] Reference [1].
[b] Reference [20].

radii, while in the extraction of the latter, further theoretical hypotheses are made.

The values of C_2 obtained in the present work reveal the 2_1^+ excitations in ^{94}Mo and ^{98}Mo to be not homogeneous, but with only a slight predominance of the protons. This is in marked contrast with what was observed for the isotones ^{92,96}Zr where neutrons strongly dominate the transitions [7,18,19]. For the other isotone of ^{98}Mo, ^{100}Ru, the first quadrupolar excitation had been previously characterized as almost homogeneous [8]. The quadrupolar excitation in ^{98}Mo is somewhat more collective than the corresponding one in ^{94}Mo, so no depression of collectivity due to a $N=56$ subshell closure is apparent for ^{98}Mo. In fact, the excitation energies of the 2_1^+ states in the sequence $^{94-98}$Mo are, accordingly, decreasing.

ACKNOWLEDGMENTS

Financial support by CAPES (Coordenação de Aperfeiçoamento de Pessoal de Nível Superior), CNPq (Conselho Nacional de Desenvolvimento Científico e Tecnológico), FINEP (Financiadora de Estudos e Projetos), and FAPESP (Fundação de Amparo à Pesquisa do Estado de São Paulo) is gratefully acknowledged.

[1] S. Raman, C. H. Malarkey, W. T. Milner, C. W. Nestor, and P. H. Stelson, At. Data Nucl. Data Tables **36**, 1 (1987).

[2] T. R. Werner, J. Dobaczewski, M. W. Guidry, W. Nazarewicz, and J. A. Sheikh, Nucl. Phys. **A578**, 1 (1994).

[3] J. Skalski, S. Mizutori, and W. Nazarewicz, Nucl. Phys. **A617**, 282 (1997).

[4] S. Åberg, H. Flocard, and W. Nazarewicz, Annu. Rev. Nucl. Part. Sci. **40**, 439 (1990).

[5] J. L. M. Duarte, T. Borello-Lewin, G. Maino, and L. Zuffi, Phys. Rev. C **57**, 1539 (1998).

[6] J. L. M. Duarte, G. M. Ukita, T. Borello-Lewin, L. B. Horodynski-Matsushigue, and L. C. Gomes, Phys. Rev. C **56**, 1855 (1997).

[7] D. Rychel, R. Gyufko, B. van Kruchten, M. Lahanas, P. Singh, and C. A. Wiedner, Z. Phys. A **326**, 455 (1987).

[8] L. C. Gomes, L. B. Horodynski-Matsushigue, T. Borello-Lewin, J. L. M. Duarte, J. H. Hirata, S. Salém-Vasconcelos, and O. Dietzsch, Phys. Rev. C **54**, 2296 (1996).

[9] D. Pulino, G. M. Sipahi, G. M. Ukita, T. Borello-Lewin, L. B. Horodynski-Matsushigue, J. L. M. Duarte, W. G. P. Engel, and J. C. de Abreu, Rev. Bras. Aplicações Vácuo **10**, 87 (1991).

[10] C. M. Perey and F. G. Perey, At. Data Nucl. Data Tables **17**, 1 (1976).

[11] W. W. Daehnick, J. D. Childs, and Z. Vrcelj, Phys. Rev. C **21**, 2253 (1980).

[12] G. R. Satchler, *Direct Nuclear Reactions* (Clarendon, Oxford, 1983).

[13] P. D. Kunz, computer code DWUCK4 version, Colorado University, 1974 (private communication).

[14] D. J. Horen *et al.*, Phys. Rev. C **44**, 128 (1991).

[15] H. F. Lutz, D. W. Heikkinen, and W. Bartolini, Phys. Rev. C **4**, 934 (1971).

[16] Y. Awaya, K. Matsuda, T. Wada, N. Nakanishi, S. Takeda, and S. Yamaji, J. Phys. Soc. Jpn. **33**, 881 (1972).

[17] T. Wada, Nucl. Phys. **A307**, 425 (1978).

[18] L. B. Horodynski-Matsushigue, T. Borello-Lewin, and J. L. M. Duarte, Proceedings of the International Nuclear Physics Conference, Universidade de São Paulo, Brazil, 1989 (unpublished), Vol. I, p. 307.

[19] D. J. Horen, G. R. Satchler, S. A. Fayans, and E. L. Trykov, Nucl. Phys. **A600**, 193 (1996).

[20] R. H. Spear, At. Data Nucl. Data Tables **42**, 55 (1989).